

Open Research Online

The Open University's repository of research publications and other research outputs

Optimization of Gold Nanoparticles for Radiotherapy

Thesis

How to cite:

Grellet, Sophie (2018). Optimization of Gold Nanoparticles for Radiotherapy. PhD thesis The Open University.

For guidance on citations see [FAQs](#).

© 2018 The Author



<https://creativecommons.org/licenses/by-nc-nd/4.0/>

Version: Version of Record

Link(s) to article on publisher's website:

<http://dx.doi.org/doi:10.21954/ou.ro.0000dfee>

Copyright and Moral Rights for the articles on this site are retained by the individual authors and/or other copyright owners. For more information on Open Research Online's data [policy](#) on reuse of materials please consult the policies page.

oro.open.ac.uk

School of Life, Health and Chemical Sciences

The Open University

Walton Hall

Milton Keynes

MK7 6AA



The Open
University

Optimization of gold nanoparticles for radiotherapy

A thesis submission to The Open University for the degree
of Doctor of Philosophy

February 2018



C'était comme un monde nouveau ouvert à moi, le monde de la science, que je pouvais enfin
connaître en toute liberté,

Marie Curie

It was like a new world open to me, the world of science which I could finally know quite freely

ABSTRACT

Radiotherapy is currently used in around 50% of cancer treatments. Although highly effective it is also damaging to surrounding healthy tissues and needs to be improved by better targeting of cancer cells. Improved radiotherapy outcomes can be achieved by using nanoparticles, especially those with high atomic number (Z), that interact with ionising radiation to generate secondary electrons and reactive species that increase cellular damage. One of the most promising elements to use is gold, in the form of gold nanoparticles (AuNPs) because of its biocompatibility and amenability to surface modification. For example, surface modification of AuNPs with simple sugars can improve their solubility and cellular uptake. Furthermore, positively charged AuNPs are thought to have an improved cellular uptake because of their interactions with negatively charged cell membranes.

This thesis is focussed on two research areas: (1) the development of dual action chemo-radiosensitising AuNPs and (2) the development of oligonucleotide-AuNPs for radiosensitisation.

(1) It is shown that sugar-PEGamine coated AuNPs demonstrate selective uptake and toxicity toward skin cancer cells with an IC₅₀ of 1 µg/ml [Au], without damaging normal skin cells at this concentration. Oxidative stress and caspase-dependent apoptosis both play a key role in the toxicity of these AuNPs. Moreover, AuNPs coated with sugar and PEGamine show a strong radiosensitisation effect in combination with kilovoltage X-rays and a smaller effect with megavoltage X-rays.

(2) Oligonucleotide-phosphine-coated AuNPs are shown to demonstrate a limited uptake in the cellular cytoplasm compared to the previous AuNPs but increase AuNPs uptake into the cell nucleus. The limited uptake into the cells, as well as the DNA triplex forming oligonucleotides (TFOs) attached to the AuNPs, is still responsible for a radiosensitisation effect, although smaller than with sugar:PEGamine AuNPs. In the future, the uptake of the oligonucleotides AuNPs may possibly be improved by varying their size (from 3.5 to 2 nm) and/or adding a spacer between the NP and the TFO.

ACKNOWLEDGMENTS

The work presented in this thesis, and the achievements it represents, would not have been possible without the support from so many people around me. It is very important for me to spend some time thanking the kind people who helped me during this journey. First, I would like to thank all the team within the Open University, starting with the LHCS department, where the people welcomed me and helped me find my place at the beginning of this project. Very special thanks to Tala and her beautiful family, who were always there for me, as well as Gaurav, Said, Sarah, Radka, Conor, Zerine, but also Nayab, Sonia, Perla, Emily, Laura, Shereen, Alex, Ester, Edu, Alexandra, Nadia, George, Brett, David, Nacho, Robert, Ilona, Julia. I would like to thank also friends from other departments, such as David, Germain, Brigitte from the math department, a special thanks to Anas and Safaa, Rahul, Rahul, Yadu from the engineering department, and finally friends from the DPS department, with a special attention to Telma, who was the support I needed at the end of my PhD and who found the words I needed to hear.

I would like also to thank all the people from the ARGENT team, who made this PhD experience unforgettable and with whom I enjoyed every event and training workshop across Europe. Very special thanks to the three musketeers Pablo, Kaspar and Lily.

This PhD would not have been possible without the supervision of my three supervisors Jon, Nigel, and Gosia, who believed in me, helped me from beginning to end, and were very supportive. A special thanks to Gosia who believed in me more than I believed in myself, welcomed me to her beautiful home, and to whom I wish the best of luck in the future.

Finally, I would like to thank those most important to me, who have enabled me to fulfil my dream; my family. They have believed in me since I was a little girl, and I would like to dedicate this thesis particularly to my mum, my dad and my brother, who have made me the person I am today.

ABBREVIATIONS

αGal: alpha galactose

βGlc: beta-D-glucose

¹O₂: singlet oxygen

A: Adenine

AA: Ascorbic acid

ACE: angiotensin-converting-enzyme

AET: Cysteamine

AFM: Atomic force microscopy

AL: Amino-linker

AMA: Antimycin A

AuMS NPs: gold nanoparticles coated with triphenylphosphine monosulfonate

AuTS NPs: gold nanoparticles coated with triphenylphosphine trisulfonate

AuNPs: gold nanoparticles

BSA: bovine serum albumin

C: Cytosine

Carboxy-DCFDA: 5-(and-6)-Carboxy-2',7'-Dichlorofluorescein Diacetate

CeO₂ NPs: Cerium Oxide NPs

CMFDA: green 5-chloromethylfluorescein diacetate

COX-2: cyclooxygenase 2

CPPs: Cell-penetrating peptides

CPS: counts per second

CT: computed tomography

CTAB: cetyl trimethylammonium bromide

Da: Dalton (unit of molecular weight)

DCFDA: 2', 7'-dichlorofluorescein diacetate

DEF: Dose enhancement factor

DFT: Density functional theory

DHR: Dihydrorhodamine 123

DNA: Deoxyribonucleic acid

DSBs: Double strand breaks

DPTA: Diethylenetriaminepentaacetic acid

DTT: Dithiothreitol

EDTA: Ethylenediaminetetraacetic acid

EGFR: Epidermal growth factor receptor

ER: Endoplasmic reticulum

EPR: Enhanced permeation and retention

EtOH: Ethanol

FACS: Fluorescence-activated cell sorting

FCCP: Carbonyl cyanide 4-(trifluoromethoxy)phenylhydrazone

FITC: Fluorescein isothiocyanate

G: Guanine

G-CSF: Granulocyte colony-stimulating-factor

GlcNAc: N-acetylglucosamine

GSH: glutathione

HaCaT: Spontaneously immortalized human keratinocyte cell line

HIF-1: Hypoxia Inducible Factor 1

HR: Homologous recombination

HSC-3: Human oral squamous carcinoma cell line with high metastatic potential

H₂O₂: Hydrogen peroxide

IC 50: Inhibition concentration 50% (Half maximal inhibitory concentration)

ICP-MS: inductively-coupled plasma mass spectrometry

ICP-AES: inductively-coupled plasma atomic emission spectrometry

IgG: immunoglobulin G

IEP: Isoelectric point

kVp: peak kilovoltage

LB: Luria-Bertani broth

L-DLPC: L- α -dilauroyl phosphatidylcholine

LHCS: Life, Heath and Chemical Sciences

LQ: Linear Quadratic

MAPK: mitogen-activated protein kinase

MCF-7: Human breast cancer cell line, acronym for Michigan Cancer Foundation-7

MCF-10: non tumorigenic Human breast epithelial cell line, acronym for Michigan Cancer Foundation-10

MD: Molecular dynamics

MDDC: dendritic cells

MDM: Human blood derived monocyte macrophage

MEEE: 2,2-mercaptoethoxyethoxyethanol

MeOH: Methanol

MES: 2-mercaptoethanesulfonate

miRNA: micro-RNA

MMPC: Mixed monolayer protected gold clusters

MRI: magnetic resonance imaging

NaP: Sodium pyruvate

NAC: N-acetyl-L-cysteine

NaCl: Sodium chloride

N-aglu: N-acetylglucosamine

NHEJ: Non-homologous end joining

NPs: Nanoparticles

Nrf2: nuclear factor (erythroid-derived 2)-like 2

$\cdot\text{O}_2$: Superoxide radical

$\cdot\text{OH}$: Hydroxyl radical

OU: Open University

PAA: poly(acrylic acid)

PAH: poly(allylamine hydrochloride)

PARP: Poly (ADP-ribose) polymerase

PBS: Phosphate buffered saline

PBvluc del-6: Plasmid DNA designed by Dr Massague which contains the insert c-myc promoter

PCR: Polymerase chain reaction

PC-3: Human prostate cancer cell line

PDADMAC: poly(diallyldimethylammonium chloride)

PEG: polyethylene glycol

pH: potential of Hydrogen

PI: propidium iodide

PSS: poly (sodium 4-styrenesulfonate)

PVA: poly(vinyl alcohol)

P/S: Penicillin/streptomycin

QDs: Quantum dots

RBE: Relative Biological Effectiveness

RNA: ribonucleic acid

RNAi: RNA interference

RNS: Reactive nitrite species

ROS: Reactive oxygen species

RT: Room temperature

RT-qPCR: Quantitative reverse transcription PCR

SD: Standard deviation

SEM: Standard error of the mean

SER: Sensitizer enhancement ratio

SiO₂ NPs: Silica NPs

siRNA: small interfering RNA

SOSG: single oxygen sensor green

SPIOs: Superparamagnetic iron oxides

SPR: Surface plasmon resonance

SSBs: Single strand breaks

T: Thymine

TB: Tris-borate

TBE: Tris-borate-EDTA

TBHP: Terbutyl hydroperoxyde

TBM: Tris-borate-MgCl₂

TE: Trypsin/EDTA
TEAA: Tris ethylammonium acetate
TEM: Transmission electron microscopy
TEMED: Tetramethylethylenediamine
TFO: Triplex forming oligonucleotides
TGF- β : Transforming growth factor
TMAT: N,N,N-trimethylammoniummethanethiol
TMRE: Tetramethylrhodamine ethyl ester
TPPMS: triphenylphosphine monosulfonate
TPTS: triphenylphosphine trisulfonate
UHP: Ultra high purity
VEGF: vascular endothelial growth factor
 α -gal: α -galactose
 β -glu: β -glucose
3-CCA: coumarin-3-carboxylic acid
7-OH-CCA: 7-hydroxycoumarin-3-carboxylic acid

CONTENTS

CHAPTER 1: INTRODUCTION	13
1.1. Cancer	14
1.2. Radiotherapy	15
1.2.1. Conventional Radiotherapy	15
1.2.2. Radiotherapy improvement	18
1.3. Nanoparticles: their use in radiotherapy	25
1.3.1 Nanoparticles definition and their different applications	25
1.3.2. NPs for radiotherapy	27
1.3.3. Role of oxidative stress in the combination of NPs with radiotherapy	30
1.4. Physical processes involved in the interaction between NPs and radiation	31
1.5. Different NPs composition used in radiotherapy	33
1.5.1 High atomic number NPs	33
1.6. NPs size used in radiotherapy	36
1.7. NPs charge used in radiotherapy	37
1.8. NPs surface coating used in radiotherapy	38
1.9. NPs uptake by cancer tissues	41
1.10. Gold NPs	42
1.10.1. AuNPs fabrication	42
1.10.2. AuNPs characterisation	43
1.10.3. AuNPs Uptake	44
1.10.4. AuNPs charge impacts on cellular uptake and toxicity	46
1.11. What are the risks of using AuNPs?	47
1.12. AuNPs mechanism of toxicity	51
1.13. Parameterisation of the radiosensitisation effect of NPs	52
1.14. Biological consequences of AuNPs radiosensitisation	54
1.15. Improvement of the radiosensitisation effect by targeted AuNPs	63
1.16. Aim/Goals of the research undertaken in this thesis	64
 CHAPTER 2: MATERIALS AND METHODS	 67
2.1. Different AuNPs used in this project	67
2.1.1. Nanoparticles coated with sugar and PEGamine	67
2.1.2. Nanoparticles coated with oligonucleotides	68
2.1.3. Non-coated nanoparticles of 2 nm diameter size	70

2.1.4. Characterisation of the different AuNPs	70
2.1.5. Description of the different oligonucleotide sequences used.....	72
2.2 Gel electrophoresis for DNA sequences interaction experiments	74
2.2.1 Agarose gel	74
2.2.2. Polyacrylamide gel	74
2.3. Oligonucleotide/DNA triplex formation.....	75
2.4. Coated AuNPs characterisation and oligonucleotide interaction	75
2.4.1. Characterisation of the AuNPs using agarose gel electrophoresis.....	75
2.4.2. Characterisation of the oligonucleotide attachment with electrophoretic mobility shift assay (EMSA)	76
2.4.3. Characterisation of the triplex formation with the AuNPs with polyacrylamide gel	76
2.5. Plasmid culture and modification.....	77
2.5.1. Preparation of petri dishes and bacteria culture	77
2.5.2. Incubate single colonies of bacteria	77
2.5.3. Drying bacteria and DNA extraction.....	77
2.5.4. Plasmid endonuclease digestion	78
2.6. Plasmid experiments.....	79
2.6.1. Characterisation of the different forms of the plasmid.....	79
2.6.2. Irradiation experiments of the plasmid	80
2.7. Cell lines used during the project	80
2.8. Cell culture.....	81
2.9. NPs adhesion tests	81
2.10. AuNPs exposure and clonogenic assay.....	82
2.11. Acute toxicity evaluation	83
2.12. Apoptosis related cell death measurements	83
2.13. Amount of AuNPs inside cells by ICP-MS	84
2.14. Localization of AuNPs in cells by TEM	84
2.15. Oxidative stress measurements	85
2.15.1. Antioxidant experiment.....	85
2.15.2. Fluorescence-activated cell sorting (FACS) analysis.....	86
2.15.3. Cell-free hydroxyl radical assay	86
2.16. Irradiation protocols of the different cell lines.....	87
2.17. Data reductions	89

CHAPTER 3: STUDIES WITH SUGAR:PEGAMINE COATED AuNPs	90
3.1. Physiochemical characterisation of the AuNPs coated with equal amount of sugar and PEGamine using TEM	91
3.2. Skin cells exposed to AuNPs, the role of the sugar onto the AuNPs	93
3.2.1. AuNPs toxicity related to the time of exposure and the type of sugar	94
3.2.2. The influence of water on toxicity	96
3.3. Physiochemical characterisation of the AuNPs coated with different amount of sugar and PEGamine	98
3.3.1. AuNPs characterisation using TEM	98
3.3.2. AuNPs characterisation by DLS	99
3.4. Skin cells exposed to AuNPs, the role of the coating and its ratio onto the AuNPs ...	101
3.5. Skin cells exposed to the ligands only are unaffected	103
3.6. AuNPs binding properties to culture plastic	104
3.6.1. Possible electrostatic interaction between AuNPs and surfaces	105
3.6.2. Effect on AuNP attachment of washing after loading.	106
3.7. Attachment of AuNPs to substrates and their toxicity under cell culture conditions	107
3.8. AuNP toxicity is related to cellular uptake	109
3.8.1. Amount of gold per cell	109
3.8.2. Where do AuNPs accumulate inside cells?	111
3.9. AuNPs toxicity on cells, role of oxidative stress and caspase dependent apoptosis ..	114
3.9.1. Role of oxidative stress in AuNP toxicity	114
3.9.2. ROS measurement in cells	117
3.9.3. Is caspase dependent death involved in AuNPs toxicity?	119
3.10. AuNPs interaction with irradiation	120
3.10.1. Intrinsic properties of AuNPs to interact with irradiation	120
3.10.2. Radiosensitisation of AuNPs on skin cells	124
3.10.3. Toxicity and radiosensitisation of AuNPs on breast cells	132
3.11. Conclusion of Chapter 3: galactose:PEGamine coated AuNPs	138
 CHAPTER 4: OLIGONUCLEOTIDES COATED AuNPs	 140
4.1. Oligonucleotide binding with its target	142
4.1.1. Oligonucleotide sequence selection	142
4.1.2. Duplex formation	145
4.1.3. Triplex formation	147
4.1.4. Triplex formation with plasmid	152
4.2. Oligonucleotide coated AuNPs characterization	155

4.2.1. AuNPs size characterised by TEM analysis	155
4.2.2. AuNPs concentration measurements.....	157
4.2.3. Oligonucleotide attachment to AuNPs and characterisation	158
4.3. Oligonucleotide coated AuNPs effect on cell survival	165
4.3.1. Cell proliferation and survival.....	165
4.3.2. Cell proliferation	166
4.4. Oligonucleotides coated AuNPs and cellular uptake	167
4.5. Oligonucleotide coated AuNPs and their effect with radiotherapy.....	172
4.5.1. Coumarin assay	172
4.5.2. Radiosensitisation effect on plasmid DNA.....	174
4.5.3. Radiosensitisation effect on cells	177
4.6. Conclusions of Chapter 4: oligonucleotide-coated AuNPs	182
CHAPTER 5: PRELIMINARY WORK WITH METAL OXIDE NPs.....	185
5.1. EM microscopy of commercial cerium oxide NPs	186
5.2. SEM-EDX composition.....	186
5.3. Cell exposure to commercial cerium oxide	187
5.4. Cell exposure to ceria and interaction with radiation	188
CHAPTER 6: CONCLUSION AND FUTURE WORK	191
6.1. General conclusion	191
6.2. Future works.....	195
6.2.1. Oligonucleotide coated AuNPs	195
6.4.2. Radiosensitisation effects of the NPs	195
6.4.3. Theoretical work and simulations	196
6.4.3. Cerium oxide NPs	196
6.4.4. Alternative strategies.....	197
LIST OF PUBLICATIONS AND POSTER/ORAL CONFERENCE PRESENTATIONS.....	198
Journal publications	198
Poster and oral conference presentations	199
BIBLIOGRAPHY.....	201

ANNEXES	219
1. Annexes related to Chapter 2	219
1.1. αGal :PEGamine AuNPs concentration	219
1.2. Consumables	219
2. Annexes related to Chapter 3	220
2.1. Statistical difference between AuNPs coated with different sugars	220
2.2. Dose response for each ratio of αGal:PEGamine AuNP exposed to adherent cells	222
2.3. Dose response for each ratio of αGal:PEGamine AuNP exposed to floating cells..	224
3. Annexes related to Chapter 4	226
3.1. Duplex formation with the DNA sequences of 23 bp and 70 bp	226
3.2. Triplex formation with the two duplexes of DNA	226
3.3. Triplex formation within the plasmid and the TFOs DY3 and PR	229
3.4. Oligonucleotides coated AuNPs characterisation by XPS analysis	229
3.5. Statistical differences in dose responses for the different oligo coated AuNPs exposure on cells analysed by one way Anova followed by a Dunnett's multiple comparisons test.	238
3.6. Oligonucleotide coated AuNPs and cellular uptake using TEM	239
3.7. Relaxed plasmid irradiated with or without the different AuNPs	240
3.8. Relaxed plasmid irradiated with or without the different AuNPs and PCR amplicon of the sequence of interest	240

LIST OF FIGURES

Figure 1.1: Different types of radiation used in radiotherapy and their penetration into matter. a) Particle track structure depending on the LET.	17
Figure 1.2: Different approaches for enhancing the radiosensitisation of cancer cells.	18
Figure 1.3: Different DNA repair mechanisms.....	23
Figure 1.4: schematic view of the interaction between X-ray radiation and NPs, the radiosensitisation effect.	25
Figure 1.5: Schematic representation of NP-mediated drug delivery, via active and passive targeting.....	26
Figure 1.6: Average tumour growth after different treatment.	28
Figure 1.7: Tumour-growth in nude mouse with and without treatment with coated gold nanorods (gAuNR).....	29
Figure 1.8: A) SSBs and B) DSBs observed in Plasmid DNA exposed with Platinum NPs and proton therapy, and without.	29
Figure 1.9: Possible emission pathways after photon irradiation of high-Z metal NPs.....	32
Figure 1.10: Distribution of energy deposited within 1 μm of a 20 nm size NP as a function of its atomic number.....	32
Figure 1.11: Different characteristics influencing NPs behaviour.	33
Figure 1.12: Canonical base triplexes helix formation.....	40
Figure 1.13: Natural size rules and gatekeepers within a mammalian cell	42
Figure 1.14: Toxicity of different size of AuMS NPs on four different cell lines	51
Figure 1.15: Survival curve and linear quadratic model of different human cancer cells irradiated at high dose rate	52
Figure 1.16: Exploration of tracks of ejected electrons on the surface (solid lines) or in the bulk (dashed lines) of a 20 nm AuNPs interacting with 50 keV photon (green line).....	55
Figure 1.17: Comparison of experimentally collected Xray dose modification from different experiments and predicted dose increase for AuNPs interaction with kilovoltage and megavoltage irradiation (.....	56
Figure 2.1: Diagram of the ligands on the AuNPs.	67
Figure 2.2: Curve representing the extinction coefficient versus the NPs diameter size.....	68
Figure 2.3: UV-VIS spectrum of 3.7 nm citrate (BBi) AuNPs sample.....	69
Figure 2.4: Transmission electron microscope (TEM) used in the experiments.....	71
Figure 2.5: Map of pBV-Luc/Del-6 plasmid and schematic view of the insertion del6	78

Figure 2.6: a) Schematic difference in topological forms of plasmid DNA, b) Migration difference of the topological forms of plasmid DNA on an agarose gel	79
Figure 2.7: Gulmay Xstrahl 200 clinical orthovoltage system.....	88
Figure 2.8: a) Clinical linear accelerator (Versa HD [®] , Elekta) and culture plate set up, b) treatment plan for the irradiation.....	88
Figure 3.1: Size histograms and TEM images of different NPs.	92
Figure 3.2: Bright field images of a) HSC-3 cells; b) HaCaT cells.	93
Figure 3.3: Clonogenic assay of HSC-3 and HaCaT cells exposed to α Gal:PEGamine (50:50) AuNPs for 3 hr.	93
Figure 3.4 Clonogenic assay after AuNPs exposure for different concentrations and different loading times.....	95
Figure 3.5: Dose response curve after a clonogenic assay where both HSC-3 and HaCaT cells were exposed to 3 different AuNPs.....	95
Figure 3.6: Effect of different concentrations of sterilized water on a) HSC-3 and b) HaCaT cultures..	97
Figure 3.7: TEM images of the AuNPs with different ratios of α Gal:PEGamine and their size histograms. a)100:0; b)80:20; c)60:40; d)40:60; e)20:80; f)0:100.....	99
Figure 3.8: TEM size comparison of the different AuNPs \pm SD.	100
Figure 3.9: Clonogenic assay after AuNPs exposure for different concentrations and various ratios of α Gal:PEGamine. a) HaCaT cells, b) HSC-3 cells.....	101
Figure 3.10: Skin cells exposed to different concentration of the molecules coating the AuNPs. a) PEGamine exposure, b) α Galactose, c) 50:50 α Gal:PEGamine exposure.....	103
Figure 3.11: Silver staining of HSC-3 cells exposed to 50:50 α Gal:PEGamine on culture plastic plates.....	104
Figure 3.12: silver staining observation of AuNPs loading for 3 hours in 50 μ l (glass) or 500 μ l (plastic) of a) Hank's solution, b) medium without serum, c) medium + serum.	105
Figure 3.13: schematic view of placement of AuNP drops in a culture plate well	105
Figure 3.14: Silver staining of AuNPs loaded in a) medium + serum, 1 h, b) medium + serum, 3 h, c) distilled water, 3 h, d) ethanol, 3 h, e) 5 M NaCl, 3 h, f) Hank's solution, 3 h.....	106
Figure 3.15: Silver staining observation of AuNPs loading for 3 h in 50 μ l (glass) or 500 μ l (plastic) of medium.....	106
Figure 3.16: Silver staining observations, after 3h of AuNPs diluted in medium with serum and loaded in 15 ml falcon tubes.....	107
Figure 3.17: Clonogenic assay of cells loaded in adherent conditions or in suspension	107

Figure 3.18: Clonogenic assay after AuNPs exposure on cells in suspension at different concentrations and different ratios of α Gal:PEGamine.....	108
Figure 3.19: IC50 values for HSC-3 cultivated on plates or in suspension arranged in ascending order of zeta potential.....	109
Figure 3.20: Amount of gold per cells. IC50 plotted as a line.....	110
Figure 3.21: Observation by transmission electron microscopy (TEM) of both a;d) HaCaT and b,c,e,f) HSC-3 exposed for 3 h to 10 μ g/ml of either 50:50 α Gal:PEGamine on top line or 0:100 α Gal:PEGamine AuNPs on bottom line.....	112
Figure 3.22: a) Clonogenic assay of HSC-3 cells exposed to H ₂ O ₂ in presence or in absence of antioxidants (1 mM NAC, or 0.25 mM GSH, or 0.1 mM NaP). b) Clonogenic assay of HSC-3 cells exposed to AuNPs in presence or in absence of antioxidants (1 mM NAC, or 0.25 mM GSH, or 0.1 mM NaP).	115
Figure 3.23: Fluorescence measurement of DCFH-DA or its oxidised form DCF, diluted in medium in presence or absence of AuNPs..	118
Figure 3.24: Response of HSC-3 exposed to 50:50 α Gal:PEGamine AuNPs at a concentration of 1 μ g/ml, with or without caspase inhibitor.	119
Figure 3.25: Coumarin assay in PBS after AuNPs incubation. 3-CCA was used at a concentration of 1 mM and 0.5 mM and was irradiated with 10 Gy of 6MeV X-rays.	121
Figure 3.26: Coumarin assay in PBS. 3-CCA was used at a concentration of 1 mM and the samples were irradiated with 10 Gy of 6MeV X-ray photon and without.....	122
Figure 3.27: Coumarin assay in PBS after citrate AuNPs incubation..	123
Figure 3.28: Coumarin assay with or without irradiation, with different AuNPs..	124
Figure 3.29: HSC-3 and HaCaT cells irradiated with 220 kV X-ray irradiation and exposed to a, b) 50:50 α Gal:PEGamine and c, d) 0:100 α Gal:PEGamine AuNPs.....	125
Figure 3.30: HSC-3 and HaCaT cells irradiated to 220 kV X-ray irradiation and exposed to citrate AuNPs.....	127
Figure 3.31: HSC-3 and HaCaT cells irradiated to 6 MeV X-ray irradiation and exposed to a, b) 50:50 α Gal:PEGamine AuNPs and c, d) 0:100 α Gal:PEGamine AuNPs.....	129
Figure 3.32: Bright field images of a) MCF-7; b) MCF-10.....	133
Figure 3.33: Clonogenic assay after AuNPs exposure on breast cells.....	133
Figure 3.34: MCF-7 and MCF-10 cells irradiated to 220 kV X-ray irradiation and exposed to a, b) 50:50 α Gal:PEGamine AuNPs and c, d) 0:100 α Gal:PEGamine AuNPs.	134
Figure 3.35: MCF-7 and MCF-10 cells irradiated to 6MeV X-ray irradiation and exposed to a, b) 50:50 α Gal:PEGamine AuNPs and c, d) 0:100 α Gal:PEGamine AuNPs.	135

Figure 4.1: Plasmid pBV-Luc/Del-6, a) map of the plasmid (from: www.addgene.com), b) nucleotide sequence of the <i>c-myc</i> P2 promoter region of the plasmid.	143
Figure 4.2: Triplex binding between the TFO and the DNA duplex. a) dY3 pairing, b) PR pairing. The loops highlight the triplex structure G(GC), T(AT), A(AT) and G(CG) as examples.	144
Figure 4.3: 20% PAGE representing the duplex formation.	146
Figure 4.4: 20% PAGE representing the triplex formation between the duplex of DNA and the dY3 sequence incubated overnight at different conditions.	148
Figure 4.5: 20% PAGE representing the triplex formation with PR sequence incubated overnight at different conditions.	149
Figure 4.6: 20% PAGE representing the triplex formation with dY3 sequence incubated overnight at RT.	150
Figure 4.7: 20% PAGE representing the triplex formation with PR sequence incubated overnight at RT.	151
Figure 4.8: 20% PAGE representing triplex formation with PR and dY2 sequence incubated overnight at RT.....	152
Figure 4.9: 1.2% AGE showing a) Incubation of plasmid pBV-Luc/Del6 with 2 endonucleases; b) mixtures of plasmid pBV-Luc/Del6 with PR or dY3 TFO sequences at a 10/1 ratio of TFO/plasmid incubated overnight at RT.....	153
Figure 4.10: 20% PAGE showing mixtures of plasmid pBV-Luc/Del6 with PR or dY3 TFO sequences incubated overnight at RT.....	154
Figure 4.11: Observation of the core size of the different AuNPs under the TEM. a) citrate AuNPs; b) PN AuNPs; c) oligonucleotides -PN-AuNPs; d) citrate-oligonucleotides-AuNPs.....	156
Figure 4.12: 1% AGE representing the AuNPs coated with different molecules.....	161
Figure 4.13: 15% PAGE representing the interaction between the TFO coating the AuNPs and its complementary sequence incubated overnight at RT, followed by an EMSA	162
Figure 4.14: 20% PAGE showing mixtures of D23 with PR or dY3 TFO coated AuNPs incubated overnight at RT.....	164
Figure 4.15: Clonogenic assay after AuNPs exposure at different concentrations.	165
Figure 4.16: Effect of the different AuNPs on the cell proliferation and survival. CyQuant assay.	167
Figure 4.17: Observation by TEM of HSC-3 cells exposed to a) no AuNPs, b) citrate AuNPs, c) PN AuNPs, d) citrate dY3 AuNPs, e) citrate PR AuNPs, f) citrate GFP AuNPs, g) PN-dY3 AuNPs, h) PN-PR AuNPs, i) PN-GFP AuNPs.	168
Figure 4.18: Observation by TEM of HaCaT cells exposed to a) no AuNPs, b) citrate AuNPs, c) PN AuNPs, d) citrate dY3 AuNPs, e) citrate PR AuNPs, f) citrate GFP AuNPs, g) PN-Y3 AuNPs, h) PN-PR AuNPs, i) PN-GFP AuNPs.	169

Figure 4.19: TEM analysis of AuNPs/area of the cells after exposure	170
a) citrate AuNPs, b) PN AuNPs, c) citrate dY3 AuNPs, d) citrate PR AuNPs, e) citrate GFP AuNPs, f) PN dY3 AuNPs, g) PN PR AuNPs, h) PN GFP AuNPs.	171
Figure 4.20: Coumarin assay of the different citrate, PN or oligo coated AuNPs in PBS, with or without irradiation.....	173
Figure 4.21: 2% AGE showing the relaxed plasmid pBV-Luc/Del6 incubated with different AuNPs for 3 hours and then irradiated with 220 kV X-rays at 20 Gy.	174
Figure 4.22: 2% AGE showing a 700 bp PCR amplicon, derived from the c-myc promoter region of plasmid pBV-Luc/Del6.....	176
Figure 4.23: HSC-3 and HaCaT cells irradiated with 220 kV X-ray irradiation and exposed to a) citrate AuNPs, b) PN AuNPs or c) oligonucleotide coated AuNPs.	178
Figure 5.1: Geometrical form of a) Ce^{4+} and b) Ce^{3+}	185
Figure 5.2: Size histogram and TEM image of CeO_2 NPs pH 8..	186
Figure 5.3: SEM-EDX spectrum of CeO_2 NPs showing their elemental composition.....	186
Figure 5.4: Toxicity of CeO_2 NPs on HSC-3 and HaCaT cells.....	187
Figure 5.5: Coumarin assay with or without irradiation, with different CeO_2 NPs.....	188
Figure 5.6: Radiosensitisation of CeO_2 NPs on HSC-3 and HaCaT cells exposed to kilovoltage radiotherapy.	189

LIST OF TABLES

Table 1.1: Different radiation characteristics and their use in cancer radiotherapy.....	17
Table 1.2: Summary of chemotherapeutic strategies used in combination with radiotherapy.	24
Table 1.3: Toxicology studies on cancer <i>in vitro</i> models of different spherical AuNPs exposure	48
Table 1.4: Toxicology studies on cancer <i>in vitro</i> models of different rods AuNPs exposure.....	49
Table 1.5: Toxicology studies on normal <i>in vitro</i> models of different spherical AuNPs exposure	50
Table 1.6: Summary of <i>in vitro</i> experiment on human cells exposed to AuNPs (below 10 nm) and radiotherapy	58
Table 1.7: Summary of <i>in vitro</i> experiment on human cells exposed to AuNPs (above 10 nm) and radiotherapy	59
Table 3.1: Summary of the experiments reported in Chapter 3.....	90
Table 3.2: Summary of AuNPs diameter from TEM, hydrodynamic diameter from DLS in water and zeta potential measured in 3.2% PBS pH 7.4.....	100
Table 3.3: Chemotoxicity of different AuNPs on HSC-3 adherent cells	103
Table 3.4: Toxicity of different AuNPs on HSC-3 loaded in suspension culture..	108
Table 3.5a: Approximation of the number of AuNPs per region of the cell, measured from TEM images of cells exposed to the AuNPs for 3 hours at 10 µg/ml concentration	112
Table 3.5b: Average surface area of the cell, its nucleus and its cytoplasm..	113
Table 3.6a: Sensitivity Enhancement Ratios and Dose Enhancement Factors calculated for skin cells	130
Table 3.6b: linear quadratic factor for skin cells.....	130
Table 3.7a: Sensitivity Enhancement Ratios and Dose Enhancement Factors calculated for breast cells	136
Table 3.7b: Linear quadratic parameters for breast cells.....	136
Table 4.1: Summary of the experiments done in Chapter 4.....	141
Table 4.2: Different DNA sequences used in the Chapter 4.	144
Table 4.3: UV-VIS absorption characteristics of the different oligonucleotide samples.	145
Table 4.4: Concentration of the different AuNPs.	157
Table 4.5: Dynamic Light scattering analysis	158
Table 4.6: XPS analysis, characteristics of the different peaks.....	159

Table 4.7a: Sensitivity Enhancement Ratios and Dose Enhancement Factors calculated for skin cells	179
Table 4.7b: Linear quadratic parameters of oligonucleotides AuNPs calculated for skin cells irradiated with 220 kV X-rays.....	180

CHAPTER 1: INTRODUCTION

Cancer is one of the major diseases of the 21st century and one of the leading causes of non-communicable death in developed countries worldwide (McMullin, 2016). In 2012 the World Health Organization (WHO) reported 14 million of new cases of cancer and 8.2 million cancer related deaths worldwide (McMullin, 2016). Cancer can potentially affect any part of the body, expand quickly locally and spread throughout the body (McMullin, 2016) often leading to rapid and irreversible deterioration in the patient. Accordingly, the study of causes and mechanisms of cancer and the development of new treatment methods is one of the major research topics in modern human health.

Radiotherapy e.g by X-rays (Zolotoyabko, 2014) provides one of the major treatment methods for cancer but is limited by the need to restrict radiation doses such that healthy tissue is not damaged by incident radiation (Zolotoyabko, 2014). One method for increasing the effectiveness of the radiation without damaging healthy tissue is to add a radiosensitiser to the tumour. The work presented in this thesis focuses on the potential of nanoparticles (NPs), made of gold, to act as radiosensitizers.(Burger et al., 2014a). The main aims of this project were:

- 1) To investigate, cellular uptake, intracellular localisation and toxicity of both bare and coated AuNPs in cancer and normal cell lines.
- 2) To characterise, understand, and improve the radiosensitisation potential of such AuNPs using clinical X-ray sources at different energies.

NPs composed of many different materials have been exploited in radiotherapy (Zolotoyabko, 2014) but NPs made of gold have been chosen in these studies because of their significantly high atomic number, their biocompatibility and amenity to surface modification (Kwatra *et al.*, 2013).

Specifically two types of AuNPs coated with sugar:PEGamine or oligonucleotides were used in this work.

Both of these AuNP types have a core size below 5 nm in diameter, so they can be quickly cleared from the body via kidneys and so avoid long term toxicity (Longmire *et al.*, 2008), but their small size can also allow them to pass through nuclear pores and enter the cell nucleus (Kodiha et al., 2015). Two types of coating have also been considered, one being positively charged, containing a PEGamine and a sugar group, in order to look at the cellular effect of different AuNPs charge (Haume *et al.*, 2016b); the other coating employs oligonucleotides which are negatively charged and thought to improve the deoxyribonucleic acid (DNA) targeting (Huo *et al.*, 2014, Tkachenko *et al.*, 2003) and possibly the radiosensitisation improvement. The DNA sequence chosen is a single stranded DNA, which is able to specifically form a triplex with part of the *c-myc* promoter

sequence. Another type of NP (ceria) has also been considered for possible radiosensitisation improvement and some preliminary studies are presented in Chapter 5.

In this introductory chapter the mechanisms and use of several agents to improve radiotherapy efficiency is summarised beginning with a review of radiotherapy treatment and its various strategies, followed by a description of the different NPs currently used in therapeutic irradiation. Details on the characteristics of the AuNPs used in our experiments will be provided followed by a review of the potential effect of AuNPs in cells, as well as their interaction with radiation.

1.1. Cancer

The origin of the word cancer comes from the Greek physician Hippocrates. He used the word *carcinos*, which in Greek, refer to a crab, imaging the cancer spreading by its claws. It is Celsus who later translated the word into *cancer-*, the Latin word for crab.(2014).

Cancer is defined as a population of cells whose cell cycle is dysregulated and their proliferation and division are faster than under physiological conditions (2001). This dysregulation is the consequence of an alteration of several genes, such as downregulation of tumour suppressor genes, upregulation of oncogenes, or loss-of-function of genes involved in DNA repair and proliferation (Hanahan and Weinberg, 2000, Patel *et al.*, 2014, Schwab, 2008). For example, EGF is involved in the growth stimulus of many epithelial cells and is up-regulated in squamous cell carcinoma (Weber, 2007). However, p53, which is the most important protein for maintaining cell-cycle control, is suppressed in 50% of all cancers, resulting in uncontrolled and rapid cell proliferation (Weber, 2007).

Early stage cancer is localised to the tissue where it formed, but can subsequently mutate further and spread anywhere in the body when in an advanced stage (Schwab, 2008). When it forms a solid mass, it is called a tumour. However, some cancers, such as leukaemia affect blood cells and do not necessarily form a solid mass (Schwab, 2008).

Cancer is a major health concern of the 21st century but is not a new disease, since it can be traced back many millennia. Metastatic osteosarcoma has been detected in an ancient Egyptian skeleton dated to 3200 years ago (Binder *et al.*, 2014). It is thought to be originally nasopharyngeal, which can spread to different organs such as thyroid, kidneys and bones (Binder *et al.*, 2014).

Several factors are associated with the development of cancer such as primarily aging, followed by genetic susceptibility such as BRCA1 mutation and breast cancer predisposition (Weber, 2007), and lifestyle (Ferlay *et al.*, 2007). For example, there is a positive association between lung cancer and tobacco or particles coming from diesel fumes (2014).

Moreover, infection by viruses such as papilloma viruses, hepatitis B and C, and HIV can lead to cancer development (2014).

1.2. Radiotherapy

1.2.1. Conventional Radiotherapy

Radiotherapy is a major methodology for treatment and about 50% of cancer patients will receive radiotherapy at some point in their treatment (Burger et al., 2014a). Radiotherapy represents the use of ionising radiation, such as photons (X-rays and gamma rays) or particles (electrons and ions) to kill cancer cells, or the vasculature that feed them. Radiotherapy can be used on its own during a cancer treatment but is more often combined with chemotherapy as adjuvant therapy to complement the effect of the drug. Radiotherapy can be also used as a remission treatment, following another treatment, to make sure that all the cancer cells were eradicated from the body (Tubiana *et al.*, 1990).

Radiation induced damage targets different biomolecules and organelles in cells and particularly the DNA which may be present breaks or modifications by both direct and indirect processes with the most important of the latter processes being the production of reactive oxygen species (ROS). ROS are defined as chemically unstable molecules or free radicals that have an unpaired electron and are highly reactive with the environment (Roesslein *et al.*, 2013). They derive from molecular oxygen and can be produced via numerous pathways (e.g. mitochondrial respiration, nanomaterials, radiotherapy) (Fu *et al.*, 2014). They are formed upon irradiation of water. Water radiolysis is the decomposition of water molecules into different ROS, such as hydrogen radical (H^{\bullet}) and hydroxyl radical ($\bullet OH$) due to ionising radiation (Le Caër, 2011). After a cascade of events, such as relaxation and solvated electron formation, other molecules can be produced such as dihydrogen (H_2), hydrogen peroxide (H_2O_2), hydronium ions (H_3O^+) and hydroperoxyl radicals (HO_2^{\bullet}) (Le Caër, 2011).

The most commonly used radiotherapy employs X-rays in the energy range from 80 kV to 25 MV, which causes ionization of atoms and molecules in the irradiated tissues (Dendy P.P and Heaton B, 1999). X-rays have been used to treat cancer and other medical conditions for over a century (Mozumder and Hatano, 2003).

Various energies of X-rays are used in radiotherapy. Kilovoltage X-rays (10-400 kV) were the first to be used in radiotherapy (Mayles *et al.*, 2007). Their use has gradually decreased due to their limited penetration into tissues and with the increased availability of high energy photons, but they are still used for superficial cancer treatment, such as basal and squamous

cell carcinoma, where the radiation beam is deposited on the surface of the patient skin and does not need to travel deep into tissues (Mayles *et al.*, 2007).

In contrast, megavoltage X-rays (typically 6 MV or above) have the advantage of deeper penetration in tissues and deliver the majority of the applied radiation dose below the skin surface, decreasing any adverse effects on the skin and superficial tissues (Mayles *et al.*, 2007) (Figure 1.1b). Linear accelerators (LINAC) are commonly used to produce high energy electrons. These electrons are converted into megavoltage X-rays by bombarding a high atomic number target (Mayles *et al.*, 2007).

One of the main limitations of X-ray radiotherapy is its damage to tissues all along the beam track, including above and below the intended target tissues (Chauhan *et al.*, 2011). This can be explained by low Linear Energy Transfer (LET) for these type of energies (50kV and above) (Mayles *et al.*, 2007). The LET is the average energy released per unit path length due to ionization and excitation processes (Becker *et al.*, 2007, Hatano *et al.*, 2010) and describes the density of ionization in the particle tracks (Joiner and Van der Kogel, 2009). A low LET corresponds to a relatively low ionisation density of the secondary charged particles (Mayles *et al.*, 2007). Low LET radiation cannot therefore travel long distances but can deposit their energy everywhere along the track (Figure 1a). By contrast, beams of heavy ions (such as carbon), due to their high LET, deposit most of their energies at the end of the track and can lead to a potential increase of the biological effectiveness. Indeed, as the LET increases, the cell death increases (Niemantsverdriet *et al.*, Mayles *et al.*, 2007).

γ -rays are also used for the treatment of malignant diseases, with the advantage that they penetrate deeply into the tissue, allowing treatment of deeply sited tumours, such as pancreas, brain, or prostate cancers (Porcel *et al.*, 2010c). Megavoltage γ -rays can be produced using different sources, including Cobalt-60, which produces two well-defined photon energies of 1.173 MV and 1.332 MV. The main differences between X-ray and gamma rays are their wavelength, which is shorter for gamma rays, and their generation, which is made via atomic energy level excitations for X-rays and nuclear interaction and transformations for γ -rays (Mozumder and Hatano, 2003).

Electron radiotherapy can also be used for superficial lesions as the dose deposited by an electron beam is very sharp and constant, due to the high LET, but decreases rapidly at the end of their track (Raju, 2012). LINAC can increase the energy of electrons for a deeper penetration within the tissues.

New strategies of cancer treatment include radiation delivery by charged particles such as protons and heavy ions (e.g. carbon) (Mayles *et al.*, 2007). Both protons and heavy ions confer the improvement of dose delivery to the tumour by controlling the dose distribution. Indeed, since heavy ions are characterised by a high LET, their ionisation capacities increases at the end

of their track. Therefore, the depth-dose curve characterising heavy ions irradiation will give rise to a Bragg peak, due to an increase of energy deposition with depth penetration (Mayles *et al.*, 2007). The large cross section of their interaction with matter increases the efficiency of ion radiotherapy by a factor of three times compared to X-rays (Figure 1.1 b). The advantages of therapies using ions, also known as hadrontherapy, explains the fast expansion of therapy centres (especially proton) in the world (Porcel *et al.*, 2010c). However, these new methods of radiotherapy are limited due to the complexity and cost of such techniques (Niemantsverdriet *et al.*). All these different radiotherapies are summarised in the Table 1.1.

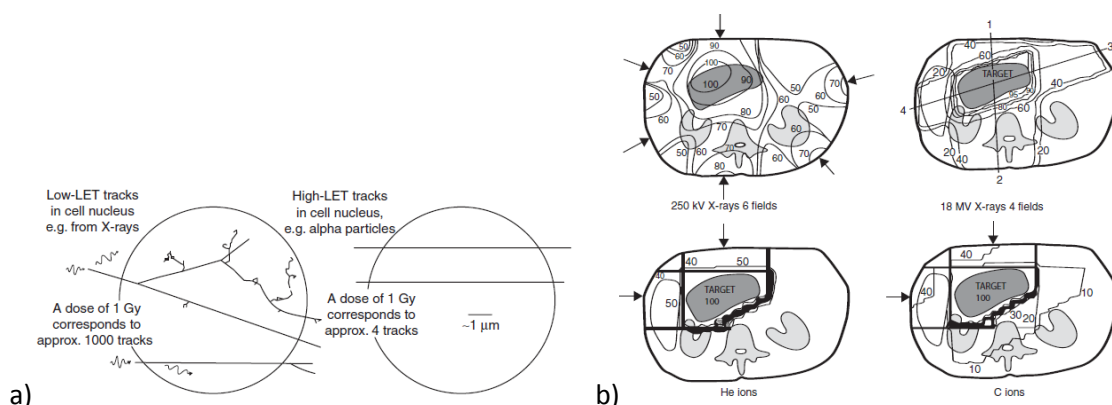


Figure 1.1: Different types of radiation used in radiotherapy and their penetration into matter. a) Particle track structure depending on the LET, b) treatment plans of the same pancreas carcinoma (Joiner and Van der Kogel, 2009).

Table 1.1: Different radiation characteristics and their use in cancer radiotherapy (Ma, 2013, Mayles *et al.*, 2007, Raju, 2012).

Type of radiation	energy	LET	Tissue penetration	Cancer treated
X-rays kilovoltage	$\sim 220 \text{ kV}$	$<1 \text{ keV}/\mu\text{m}$	Maximum dose at 0.5 cm	Skin lesions
X-rays megavoltage	6-10 MV	$<1 \text{ keV}/\mu\text{m}$	Maximum dose at 1.5 cm	Breast, brain, pancreas, prostate
γ -rays, Co^{60}	1.173, 1.332 MV	$<1 \text{ keV}/\mu\text{m}$	Maximum dose at 0.5 cm	Pancreas, prostate
Protons	200-250 MV	$100 \text{ keV}/\mu\text{m}$	Maximum dose between 20 and 30 cm	ophthalmic and intracranial tumours
Carbon ions	300 MV	$13 \text{ keV}/\mu\text{m}$, bragg peak up to 200 $\text{keV}/\mu\text{m}$	10 cm	ophthalmic and intracranial tumours

1.2.2. Radiotherapy improvement

Throughout the latter part of the 20th and the first decades of the 21st century there have been many attempts to improve radiotherapy treatment. These different methods may be summarised as either increasing the damage induced by radiation in the tumour or preventing damage to healthy tissue allowing larger doses to be applied to the tumour. These two approaches will be summarised below. An alternative approach is to limit or slow the repair of DNA damaged during irradiation, which is a method for enhancing net radiation damage in the complete radiotherapy cycle.

Increased damage in tumour

Conventional radiotherapy delivers fractionated doses of radiation in order to limit toxicity to surrounding normal tissues (Moding *et al.*, 2013). The advantages of fractionation of radiotherapy was established more than 30 years ago, through the observation that administering small but frequent radiation doses over a period of weeks gave better results in cancer killing and less side effects than when using single-dose treatments (Mayles *et al.*, 2007).

Radiotherapy side effects include fibrosis and secondary tumours appearing due to non-selective DNA damage in healthy tissues. These are critical problems in clinical delivery and need to be resolved (Chauhan *et al.*, 2011). In the field of cancer treatment research, different strategies are being developed in order to avoid these problems (Kwatra *et al.*, 2013); either by: (1) radioprotecting the healthy tissues surrounding the tumour, (2) by suppressing radioresistance, or (3) by radiosensitising the tumour to radiotherapy. These three strategies can be used separately or in combination and will be described below (Chauhan *et al.*, 2011) (Figure 1.2).

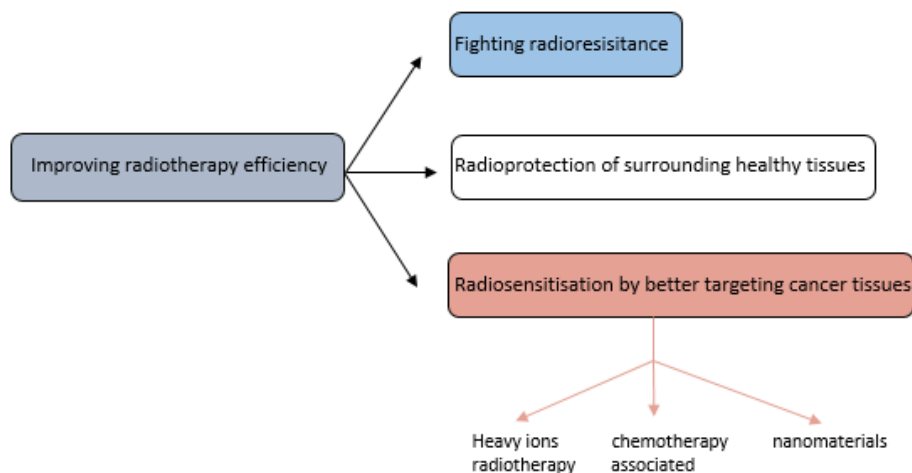


Figure 1.2: Different approaches for enhancing the radiosensitisation of cancer cells.

Radioprotection of healthy tissue

In order to improve the efficiency of radiotherapy treatment, it is possible to protect adjacent healthy tissues from radiotherapy toxicity (Kwatra *et al.*, 2013). Compounds such as the amino acid cysteine have shown radioprotective effects *in vivo*. A possible mechanism for such radioprotectors could be free radical trapping by sulfhydryl groups (Bari, 1968). However, their potential as radioprotective agents is limited by the high toxicity, defined as a negative effect decreasing the viability of an organism or a cell after a specific treatment, of the drug dose required to have a biological antioxidant effect.

Antioxidants such as vitamin E have also been explored for radioprotection given after radiotherapy. They protect especially from ROS induced damage (Kumar, 2002). ROS can directly cause damage via the oxidation of DNA, lipids, proteins, or indirectly by activating intracellular signalling, such as mitogen-activated protein kinase (MAPK) signal, for which a cascade of activation is seen in the presence of ROS (Shen *et al.*, 2013), with implication of extracellular signal related kinase (ERK), c-jun-N-terminal kinase (JNK) signal and p38-MAPK (Torres and Forman, 2003). Their activation require the phosphorylation of a tyrosine and threonine. Amifostine is a phosphorylated aminothiol prodrug compound than can selectively radioprotect normal tissues. The prodrug amifostine becomes active after alkaline phosphatase dephosphorylation, which is enriched in the environment of healthy cells, where its free thiol is capable of scavenging free-radicals (Kouvaris *et al.*, 2007). Recently, amifostine showed clinical improvement in radiation therapy and was approved by the US Food and Drug Administration (FDA) for head and neck cancer radiotherapy (Kouvaris *et al.*, 2007). However, some cancers, such as breast cancer and choriocarcinoma up-regulate alkaline phosphatase, limiting the utility of amifostine in these cases (Sharma *et al.*, 2014). Nitroxides, such as Tempol, have been explored as radioprotectors as they can easily enter cells and act as antioxidants, reacting with free radicals or mimicking the enzyme superoxide dismutase, responsible for detoxification of superoxide ions (Hahn *et al.*, 1994). Tempol has been tested clinically and it can not only selectively protect normal tissues from radiotoxicity but is non-toxic by itself (Davis *et al.*, 2011, Davda *et al.*, 2016, Metz *et al.*, 2004). Finally melatonin hormone has been explored as a radioprotector in preclinical and clinical studies as it can act as an antioxidant and also mimics the activity of glutathione peroxidase and superoxide dismutase; two antioxidant defences (Citrin *et al.*, 2010).

Suppressing radioresistance

A cascade of events, such as cytokine production, vascular damage and hypoxia can lead to late damage of healthy tissue after radiotherapy and this can result in increased radioresistance. Radioresistance is defined as the maximal dose of radiation for which an

organism is still able to survive. Different characteristics such as differences in cell cycle, repair mechanisms and growth factors can predict the sensitivity of a tissue to radiotherapy (2001). Cancer cells can develop resistance to radiotherapy, especially under hypoxia, where the low amount of oxygen is linked to a low ability to generate free radicals responsible for cellular damage, resulting in sub-lethal damage. Radiation mitigators are molecules generally used to limit the toxicity of radiation, even after the treatment. They can have an impact on oxidative stress phenomenon and thus decrease the late toxicity after radiation (Citrin *et al.*, 2010). Different molecules such as inhibitors of: cyclooxygenase 2 (COX-2), angiotensin-converting-enzyme (ACE) and Transforming growth factor (TGF- β) can be used to reduce acute radiotoxicity (Citrin *et al.*, 2010). TGF- β inhibitors are particularly used to protect tissues against fibrosis (Xavier *et al.*, 2004). Granulocyte colony-stimulating-factor (G-CSF) can reduce the radiation toxicity on healthy tissues by enhancing the cell differentiation and development (Bertho *et al.*, 2005, Finch and Rubin, 2004). Palifermin in particular is a recombinant keratinocyte growth factor used clinically to help reduce oral mucositis, adverse effects defined as inflammation and ulceration of the mucous membrane in the digestive tract, in patients receiving radiotherapy (Brizel *et al.*, 2008, Finch and Rubin, 2004).

One of the main strategies in overcoming radioresistance of cancer cells consists of inhibiting specific proteins that are overexpressed in tumour cells (Kwatra *et al.*, 2013). This is the case for example with survivin; which is an important regulator of cell division, apoptosis, cell migration and metastasis and is overexpressed in most tumours, while it is barely detectable in normal tissues (Zaffaroni *et al.*, 2005, Grdina *et al.*, 2013).

In addition, the transmembrane glycoprotein epidermal growth factor receptor (EGFR) regulates cell proliferation and the overexpression of EGFR can be associated with cancer invasion and resistance to various treatments (Small Jr, 2008). Inhibiting EGFR signalling can prevent accelerated repopulation of cancer tissues (Small Jr, 2008).

Radiosensitisers and modifying DNA damage

Radiosensitisation, which is designed to increase the sensitivity of cells to radiation by better targeting of cancer tissues, is central to radiotherapy research and can be achieved using different molecules and technologies. The combination of radiotherapy and chemotherapy has been widely used clinically to improve cancer treatment efficiency. In this area, various drugs have been designed which can cause intracellular suppression of radioprotection, can be oxygen-mimetics in the cells, can increase of the production of toxic substances intra or extracellularly, or can inhibit the repair mechanisms in the cells (Lehnert, 2014).

Nucleoside analogues, such as gemcitabine or clofarabine, can inhibit DNA polymerase and ribonucleotide reductase, thus inhibiting DNA repair (Cariveau *et al.*, 2008). Particularly, the

nucleoside analogue halogenated pyrimidine, 5-Fluorouracil, can inhibit thymidylate synthase and thus inhibit the production of thymidine, but also can be incorporated into the DNA of cancer cells during proliferation and therefore can increase the DNA damage by interfering with the duplication of the DNA (Koutcher *et al.*, 1997). Cisplatin can have the same effect by interacting with DNA and creating more damage during irradiation through the generation of secondary electrons, especially if it is close to the source of radiation (Zhang *et al.*, 2011). However, the specificity of these molecules is limited and can damage the DNA of normal tissues as well (Zhang *et al.*, 2011). To overpass cisplatin toxicity, new molecules were designed, such as oxaliplatin, which contains an oxalate group, which is supposed to protect health tissue by interacting with the platinum group until displaced in physiological environment. Although less toxic compared to cisplatin, oxiplatin still presents some unwanted toxicity in clinics, such as ototoxicity (Mehmood, 2014, Montagnani *et al.*, 2011).

Taxanes, such as paclitaxel, are a new generation of radiosensitisers. They derive from the Yew tree *Taxus brevifolia* and their main mechanism of action is to stabilise microtubules, thereby preventing metaphase spindle formation, resulting in G2/M cell cycle arrest, which is the most sensitive cell cycle phase to radiation, due to the DNA duplication (Joseph *et al.*, 2014).

Doxorubicin is a well-known cancer chemotherapeutic. Its mechanism of action involves the formation of complexes with DNA, interfering with the DNA polymerase and thus inhibiting the DNA repair (Costantini *et al.*, 2010). Camptothecin is a plant alkaloid obtained from the "happy tree" *Camptotheca acuminata* and is used in cancer therapy as an inhibitor of topoisomerase I, a nuclear enzyme important for DNA replication (Zhu and Willett, 2003). Irinotecan is part of the same family as camptothecin and has the same mechanism of action (Saijo, 2002). Its particularity is to be a precursor of the active product SN-38, improving its biocompatibility and life time (Saijo, 2002).

Since 2000, many groups have used different agents to enhance the susceptibility of tumour tissue to radiation exposure damage (Kwatra *et al.*, 2013). The application of poly (ADP-ribose) polymerase (PARP) inhibitors in cancer treatments has shown it can lead to selective cancer cell damage (Kouvaris *et al.*, 2007). For example, Shelton *et al.* studied the enhancement of radiotherapy in *in vitro* models of colorectal cancer combined with chemotherapeutic molecules such as 5-Fluorouracil, irinotecan, or oxiplatin and in addition with PARP inhibitors (Shelton *et al.*, 2013). They have shown that the PARP inhibitors significantly increases the radiosensitisation both with and without chemotherapeutics by increasing the number of double strand breaks (DSBs) in DNA, which corresponds to breakage of both strands of the DNA helix (Shelton *et al.*, 2013). By contrast, single strand breaks (SSBs) correspond to breaks only to one strand of the DNA helix.

There are two main mechanisms of SSB and DSB repairs in eukaryotes. Base excision repair (BER) is the main repair mechanism of SSBs (Clancy, 2008). Glycosylases play important roles in this process and are able to recognise specific base damage such as uracil containing DNA, or base oxidation. The DNA glycosylase cleaves the damaged or abnormal base from its sugar-phosphate bond, leaving a free base and a free sugar. Thereafter, endonucleases can cleave the free sugar and leave the place for the DNA polymerase to replace the missing base and the DNA ligase to seal the DNA (Figure 1.3 a) (Clancy, 2008, Cooper and Ganem, 1997). Nucleotide excision repair (NER) is mainly responsible for DNA repair following UV radiation, and damage which are not recognised by the glycosylases. NER acts via DNA polymerase and DNA helicase, by removing a group of bases containing the damage (oligonucleotide), and then as before, DNA polymerase and DNA ligase replace the missing bases and seal the DNA strand (Figure 1.3 b) (Clancy, 2008). By blocking the BER mechanism, PARP 1 inhibitors can increase the number of both SSBs and DSBs in the DNA of cancer cells (Powell et al., 2010a) This is due to the fact that cancer cells seem to be more susceptible to DNA repair pathways modulation than normal cells (Powell et al., 2010a). DSBs are more complex to repair due to the effect on the double stranded DNA and are mostly repair through homologous recombination (HR) and non-homologous end joining (NHEJ) repair mechanisms (Figure 1.3 c) (Raleigh and Haas-Kogan, 2013). The mechanism of choice will depend of the nature of the damage. Indeed, HR needs the homologous chromosome to be damage free. It uses the homologous chromosome as a template to repair the DSB and is also responsible for the DNA crossover and genetic information exchange during meiosis. In contrast, NHEJ, uses DNA ligase in order to take pieces of DNA adjacent to the break and fill it, which can lead to additional errors, depending on the cell cycle, especially if the cell has not completed its DNA replication (Clancy, 2008, Cooper and Ganem, 1997).

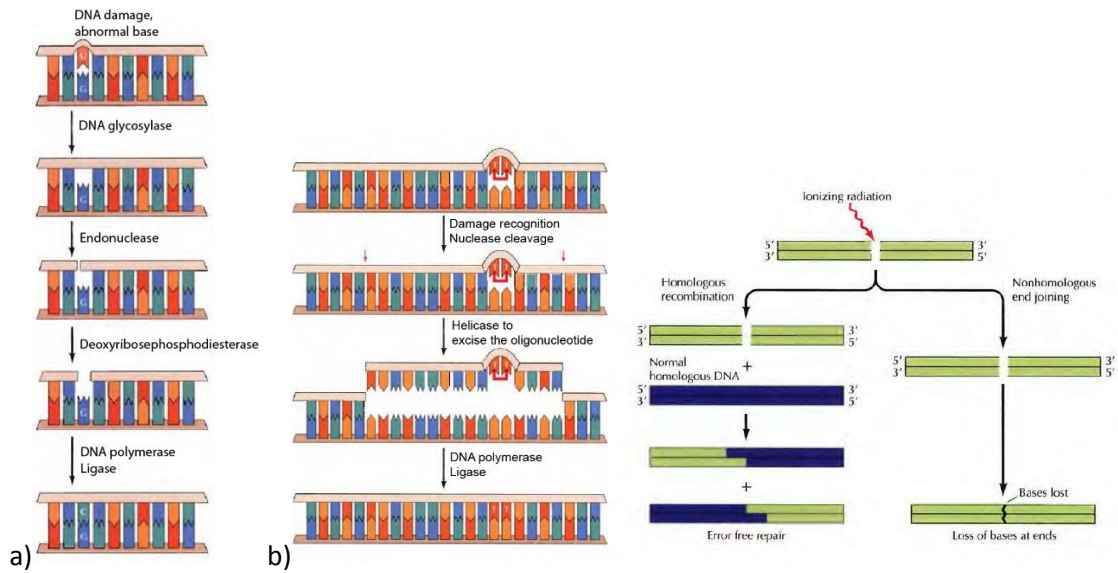


Figure 1.3: Different DNA repair mechanisms. a) Base excision repair, b) nucleotide excision repair, c) DSBs repair, covered by homologous recombination and non-homologous end joining (Cooper and Ganem, 1997).

Table 1.2 summarises the different chemotherapeutic strategies used in combination with radiotherapy.

Table 1.2: Summary of chemotherapeutic strategies used in combination with radiotherapy

Drug	mechanism	Clinical trials
Vitamin E (Kumar, 2002, Singh <i>et al.</i> , 2013)	Tocopherol and tocotrienol family Antioxidant Good biodistribution	Phase II clinical trials, oral administration to prevent diarrhoea and nausea after radio- and chemotherapy
Amifostine (Kouvaris <i>et al.</i> , 2007)	Reduced in an active product by alkaline phosphatase, scavenging free radicals	Food and Drug Administration approval for reducing xerostomia after post-operative radiotherapy (head and neck,
Tempol (Davis <i>et al.</i> , 2011, Davda <i>et al.</i> , 2016, Metz <i>et al.</i> , 2004)	Radioprotective and contrast product on magnetic resonance	Exploration on phase I clinical trials to reduce alopecia
Cox-2 inhibitors (Citrin <i>et al.</i> , 2010)	Counterbalance increase of COX-2 and prostaglandin expression Promotion of apoptosis, radiosensitiser	On-going and phase III completed trials as radiosensitiser
ACE (Citrin <i>et al.</i> , 2010)	Inhibition of angiotensin II production, decrease of proliferation and oxidative stress	On-going and final phase III of clinical trials, prevention of radiation-induced nephrotoxicity
G-CSF, palifermin (Brizel <i>et al.</i> , 2008, Finch and Rubin, 2004)	Favour cell differentiation and proliferation	Phase II of clinical trials for radioprotector
VEGF inhibitors (Small Jr, 2008)	Reduce tumour vascularisation	Phase I clinical trials in combination with 5-fluorouracil
5-fluorouracil (Koutcher <i>et al.</i> , 1997)	Pyrimidine analogue, inhibition of DNA synthesis	phase II clinical trials as radiosensitisers
Cisplatin, oxaliplatin (Zhu and Willett, 2003)	Integrating on DNA, between two guanines or a guanine and adenine, decreasing the DNA synthesis	phase II clinical trials as radiosensitisers in rectal cancers
Clofarabine, Gemcitabine (Metro <i>et al.</i> , 2010, Ogawa <i>et al.</i> , 2012)	Purine (Clofarabine) and pyrimidine (Gemcitabine) nucleoside analogue, DNA polymerase and Ribonucleotide reductase inhibitors	Phase III of clinical trials as chemotherapeutic, adjuvant of radiotherapy treatment of pancreatic cancer
Paclitaxel (Joseph <i>et al.</i> , 2014)	G2/M blocker, metabolised by cytochrome P450 Bind beta tubulin to stabilise microtubule	Already established as radiomodulator (head and neck), blocking the cell cycle Paclitaxel coating NPs is FDA approved
Irinotecan (Zhu and Willett, 2003)	Inhibition of DNA polymerase I, decrease of DNA synthesis	phase II clinical studies as radiosensitisers on colorectal cancer
PARP inhibitors (Powell <i>et al.</i> , 2010a)	Decrease of DNA SSB repair, radiosensitiser	On-going phase I and II clinical trials in BRCA-1 deficient patient and metastatic melanoma

Nanomaterials

Finally, nanomaterials can be used as radiosensitisers. They are of interest due to the physical interaction happening between, for example, the photon produced by X-ray radiation and the high element surface of the NPs (Retif *et al.*, 2015). Due to their high atomic number, specific NPs have a high density of electrons, which promote such photon interaction and therefore can release different species after interacting with radiation (Kwatra *et al.*, 2013).

Different physical processes can happen between the NPs and the photon interacting, depending on its energy and therefore, electrons of different energies will be produced (Mesbahi, 2010). These electrons will be able to directly damage the DNA of the cells, or indirectly by reacting with the water and oxygen within the environment and creating radicals, such as hydroxyl ($\cdot\text{OH}$) And superoxide ($\cdot\text{O}_2^-$) (Boudaiffa B *et al.*, 2000) (Figure 1.4). The use of NPs as radiotherapy agents and in particular as radiosensitisers is the main topic of this thesis.

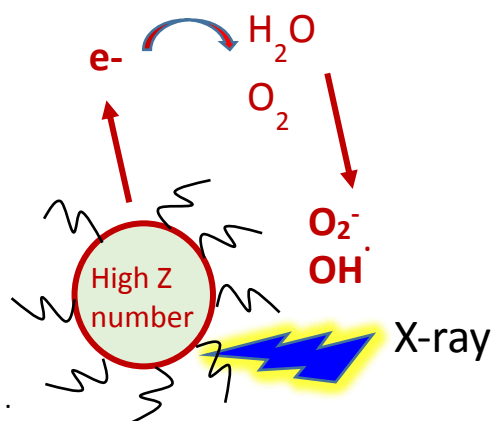


Figure 1.4: schematic view of the interaction between X-ray radiation and NPs, the radiosensitisation effect.

1.3. Nanoparticles: their use in radiotherapy

1.3.1 Nanoparticles definition and their different applications

Nanoparticles are defined as atomic structures, generally spherical but not always, and whose diameter lies within the range of 4-100 nm, while a nanocluster refers to such structures with a diameter below 4 nm (Tan *et al.*, 2004).

“Nano” size technologies are interesting in many different disciplines, such as engineering and biomedicine. Due to their small size, their behaviour is different and particularly, they are characterised by a large surface area. They exhibit catalytic properties and are also interesting for cell penetration (Hebié *et al.*, 2013) (Figure 1.5). The potential use of NPs includes the delivery of attached drugs such as chemotherapeutics, whose efficiency is limited by their poor targeting (Cui *et al.*, 2014, Zheng *et al.*, 2015). As an example, many studies have satisfactory shown doxorubicin encapsulation in nanomaterials, such as liposomes or PGLA polymeric NPs, and improved delivery to cells (Piktel *et al.*, 2016, Zheng *et al.*, 2015, Madhankumar *et al.*, 2006). NPs have also been used as drug delivery in combination with radiotherapy. In this area, Cui *et al.* have shown an improvement of radiotherapy efficiency when using NPs consisting of polylactone based structure with gelatinase and PEG coating as delivery for docetaxel in gastric cancer cells (Cui *et al.*, 2014).

Moreover, gene therapy, which consists of introducing NPs with attached DNA sequences and derivatives to promote or suppress protein production is particularly of interest nowadays with the development of personalised therapy (Muddineti O.S et al., 2015). NPs (such as gold) can also be used in medical imaging (Adler et al., 2008, El-Sayed et al., 2005). Indeed, AuNPs have the ability to scatter visible light due to the delocalised electron oscillations that exist at the surface of this material (El-Sayed *et al.*, 2005). The term Plasmon resonance refers to the interaction of electrons inside the metallic NPs with the electric field vector of the incident light causing an oscillation of free electrons at the surface of AuNPs (Boisselier and Astruc, 2009, Louis and Pluchery, 2012). The Localized Surface Plasmon Resonance (LSPR) is responsible for the red-purple colour of the spherical AuNPs and comes from the confinement of the electric field within the small spherical NP, where the radius is smaller than the wavelength of light (Pluchery, 2012).

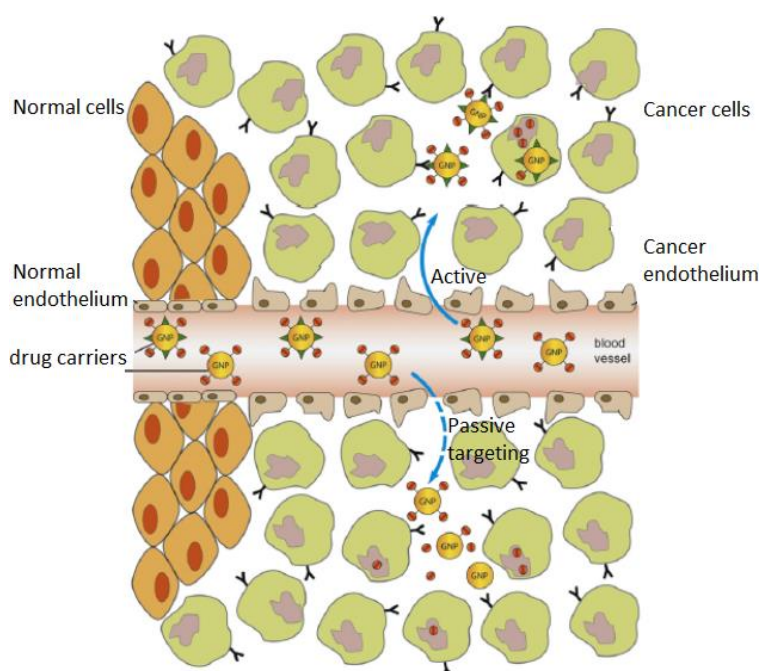


Figure 1.5: Schematic representation of NP-mediated drug delivery, via active and passive targeting (Ghosh P *et al.*, 2008).

Although nanoparticles are widely used as drug delivery agents in order to improve the biocompatibility or selectivity of different drugs, and to deliver molecules such as proteins, DNA or RNA to their target, they can also be used on their own in combination with radiotherapy (Barkalina *et al.*, 2014, Ghosh P *et al.*, 2008). Indeed, by interacting with x-ray or gamma-ray photons, or heavy protons, different physical processes lead to the formation of reactive oxygen species (ROS) and/or electrons, as described soon in Section 1.4 (Muddineti O.S *et al.*, 2015).

1.3.2. NPs for radiotherapy

Targeted radiotherapy can be achieved by using nanoparticles (NPs) (Porcel *et al.*, 2010b), which act to increase the dose of radiation deposited in the vicinity of the NP (Dendy and Heaton, 1999, Kwatra *et al.*, 2013). Hainfield *et al.* (2004) were the first to show an improvement of cancer cell killing when AuNPs were combined with kilovoltage radiotherapy *in vivo* (Figure 1.6) (Hainfeld *et al.*, 2004, Haume *et al.*, 2016b). The radiosensitisation effect of NPs used with radiotherapy involves different processes such as physical, chemical and biological. The physical processes involved when the beam of radiotherapy interacts with the NPs are described in section 1.4 and will be linked with the potential attenuation of particles (e.g photons) with matter. Depending on the energy of the particles used in radiotherapy, different processes will take place such as the photoelectric effect, Compton effect and pair production and secondary electrons will be produced. The electrons can react with the environment (e.g water) to produce reactive species in the vicinity of the NPs. The interaction of these species with the environment will depend on their half-life and the distance they can travel (Havaki *et al.*, 2015). Electron are the most common secondary species produced and can react with the environment and subsequently produce a cascade of reaction including the production and transformation of radicals (Leroy C, 2009).

In addition, the surface of NPs, such as gold, can be electronically active and catalyse chemical reaction, especially if the NPs have a small size/high surface area (Rosa *et al.*, 2017). Different reaction such as water radiolysis or reaction between energised molecules can be catalysed at the NP surface (Le Caër, 2011) and will depend on the composition, the size, the charge and the surface coating of the NPs (Kwatra *et al.*, 2013). These parameters are described further in section 1.5 to 1.9.

Finally, the radiosensitisation effect on the cellular level is described in section 1.14. The different species produced around the NPs will interact with the biological environment within the cell, having a potential impact on different organelles and on the cell DNA (Jeynes *et al.*, 2014, Kong *et al.*, 2008). Indeed, the biological effects can be due to radical species formed from the reaction between electron produced and water molecules or from radicals formed with biological molecules (e.g DNA, proteins). Some NPs can also have a direct toxic effect on the cells due to chemical reaction or release of metal ions for example and engender a synergistic effect when combined with radiotherapy (Grellet *et al.*, 2017, Kong *et al.*, 2008).

When considering the NPs composition, NPs various materials such as silicon, fullerenes, or metallic NPs can be used (Kwatra *et al.*, 2013). Heavy elements (with an atomic number above 50) such as gold, gadolinium, platinum or silver, were found to increase the level of damage

caused by X-ray radiotherapy. This phenomenon is known as radiation sensitisation or nanoparticle enhanced X-ray therapy (NEXT) (Kwatra *et al.*, 2013). Such heavy elements are characterized by a high density of electrons which increase the probability of interaction with the X-ray photon beam. They can selectively scatter or absorb high energy gamma/X-ray photons (Kwatra *et al.*, 2013).

The interesting properties of gadolinium, gold and high atomic number elements come not only from their radiosensitisation effect, but also due to their contrast agent's properties in presence of magnetic field such as magnetic resonance imaging (MRI) and computed tomography (CT). CT scanners are used as standard imaging technique for diagnosis and radiotherapy treatment planning (Smith *et al.*, 2012).

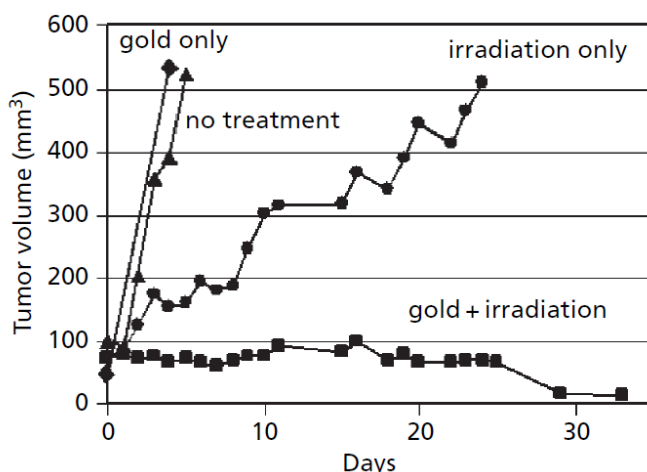


Figure 1.6: Average tumour growth after different treatment (Hainfeld *et al.*, 2004). (▲, n = 12); gold only (◆, n = 4); irradiation only (30 Gy, 250 kVp, ●, n = 11); intravenous gold injection (1.35 gAukg⁻¹) followed by irradiation (■, n = 10).

Radiotherapy leads to cell death mainly by damaging the DNA. The most common types of DNA damage are the SSBs, DSBs or sugar and base modifications (Hein *et al.*). SSBs are the most common and are generally rapidly repaired by DNA repair pathways but if not, SSBs can lead to DSBs (Powell *et al.*, 2010b). DSBs are the less common but are most important because they are much more difficult to repair correctly.

An enhancement in cancer cell death when NPs were combined to radiotherapy has been shown with X-rays at kilovoltage energies (Hainfeld *et al.*, 2004, Haume *et al.*, 2016b) and megavoltage energies. Indeed, Figure 1.7 shows tumour volume in mouse after different treatment using gold nanorods goserein acetate coating (gAuNPs), a synthetic analogue of the LHRH that can binds to the overexpressed LHRH receptors on pancreas cancer cells and lead to the reduction of testosterone secretion (Wolfe *et al.*, 2015). Before in vivo experiment, Wolfe *et al* explored the effect of these AuNPs on PC-3 pancreas cancer cells and showed a pick of uptake in cells and particularly in vesicles after 24h exposure (exposure time between 15 min and 72 hours). They

further showed that this exposure for 24 h was responsible for a radiosensitisation effect on cells with a radio enhancement factor at 20% of 1.36 (Wolfe *et al.*, 2015).

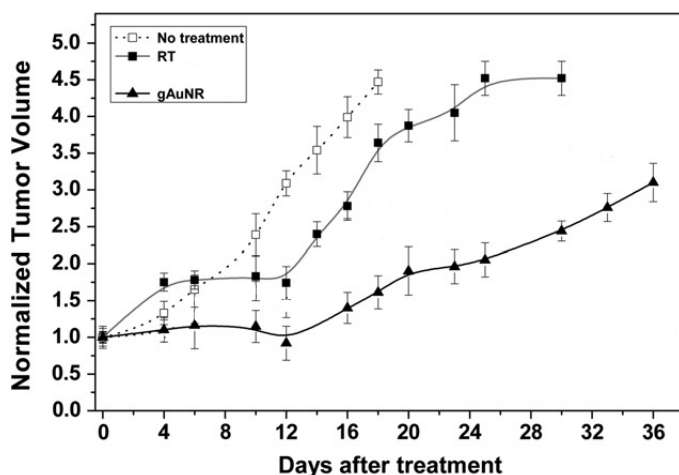


Figure 1.7: Tumour-growth in nude mouse with and without treatment with coated gold nanorods (gAuNR). The mice were irradiated with a dose of 5 Gy X-rays at 6 MV, 24h post AuNPs intravenous injection (1.35 mg of gold per gram of body weight) (Wolfe *et al.*, 2015).

Moreover, with the increasing use of heavy ions therapy, such as proton therapy, considerable research has been undertaken to explore and understand the combination of proton therapy with NPs. Schlatholter *et al.* (2016) have shown that platinum NPs combined with 150 MeV protons increase the amount of SSBs and DSBs on plasmid DNA (Figure 1.8). They observed that an increase of DSBs was related to an increase of LET. Indeed, the ratio of SSBs/DSBs was higher at the entrance of the track (low LET) than at the end of the Bragg peak (high LET). This indicated that the damage was more complex at the Bragg peak (Schlathölter *et al.*, 2016).

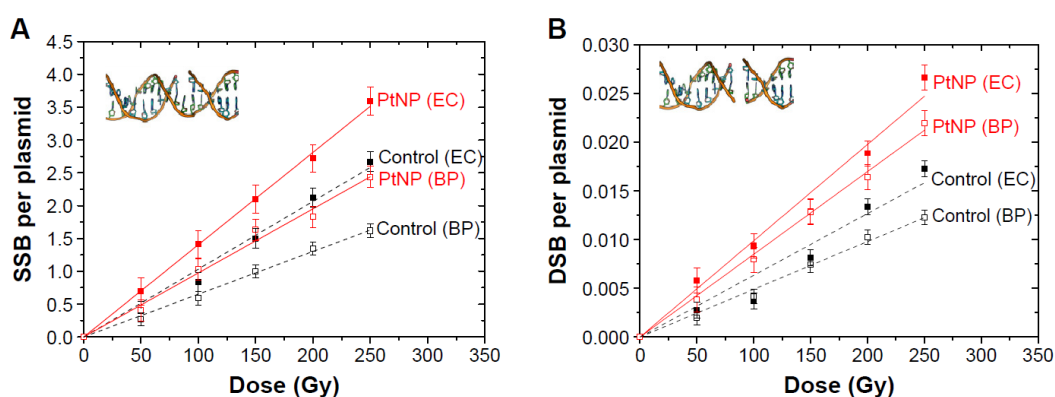


Figure 1.8: A) SSBs and B) DSBs observed in Plasmid DNA exposed with Platinum NPs and proton therapy, and without. EC stands for entrance channel and represents proton beam therapy with low LET, mimicking the entrance of the ion track, while BP stands for Bragg peak and represents therapy with high LET, mimicking the end of the track (Schlathölter *et al.*, 2016).

In order for the irradiated NPs to demonstrate robust DNA damage, they need to be able to enter cells (Jain *et al.*, 2011, Kong *et al.*, 2008, Retif *et al.*, 2015). Indeed, NP uptake plays a major role in the radiosensitisation effect, as the localisation of the NPs will determine the effects on the cell. The cellular uptake of the NPs will be described further in this chapter, in Section 1.10 and its impact on radiosensitisation will be mentioned in Section 1.14.

1.3.3. Role of oxidative stress in the combination of NPs with radiotherapy

Oxidative stress plays a key role in radiotherapy and the radiosensitisation effect (Kryston *et al.*, 2011). For example, in addition to the direct effect of radiation, ROS are implicated in bystander effects via the induction of different molecules such as MAPK and p53 and inflammatory processes (Azzam *et al.*, 2003). Bystander cells are cells which are not directly irradiated, but in the vicinity of targeted irradiated cells also respond to the radiation exposure (Azzam *et al.*, 2003). NAD(P)H oxidase and cyclooxygenase 2 are key factors in the production of further ROS by these bystander cells (Havaki *et al.*, 2015).

Among the different ROS species responsible for DNA damage, H₂O₂ is stable and characterised by a long lifetime (miliseconds until it is dissociated) and can therefore cause damage at a distances from the radiation site (Havaki *et al.*, 2015). Conversely, superoxide ion ($^{\bullet}\text{O}_2^-$) has a shorter lifetime (microseconds) and therefore has a more limited range of possible damage (Mikkelsen and Wardman, 2003). The hydroxyl radical, $^{\bullet}\text{OH}$ is the most reactive ROS species (nanosecond lifetime) and can therefore only travel few nanometres (Mikkelsen and Wardman, 2003). All of these ROS species can react with DNA, proteins and lipids, causing changes to cell function and further damage (Havaki *et al.*, 2015).

The prediction of direct or indirect effects of free radicals produced after radiation on DNA is dependent upon different factors, such as the energy of irradiation, the amount of water and oxygen. Without water and oxygen, no indirect effect of irradiation would be observed (Ogawa *et al.*, 2016). Moreover, the distance from the radical production to the DNA molecule impacts also on the damage and it is estimated that free radicals produced at a distance of 5 nm or less from the DNA helix will be most likely to create a damage (Ogawa *et al.*, 2016).

ROS production may be influenced by the presence of NPs. Misawa *et al.* have shown an enhancement of ROS generation (by a factor of 7.68 for $^{\bullet}\text{O}_2^-$ and 1.46 for $^{\bullet}\text{OH}$) when using 5 and 20 nm AuNPs combined with kilovoltage X-ray (100 kV) in water (Misawa M and Takahashi J, 2011). They observed that the production of $^{\bullet}\text{O}_2^-$ was proportional to the NPs characteristics such as an increase of surface area and therefore decrease of size, while $^{\bullet}\text{OH}$ related to its volume (Misawa M and Takahashi J, 2011).

Several studies have tried to improve ROS production during irradiation by using catalytic materials (such as ceria (Wason *et al.*, 2013)) which can capture molecules of oxygen depending on their oxidative state and can act as antioxidants, radioprotectors or radiosensitisers (Sun *et al.*, 2012, Colon *et al.*, 2010, Wason *et al.*, 2013). Previous work has shown their potential as adjuvant with radiotherapy (Shcherbakov *et al.*, 2014).

1.4. Physical processes involved in the interaction between NPs and radiation

Depending on the energy of incident photons, various processes may take place when NPs are irradiated. These include (in order of increasing photon energy): the photoelectric effect, fluorescence, Auger electron emission, Compton scattering, and electron-positron pair production (Figure 1.9).

At low energies the photoelectric effect is prominent. The photoelectric effect was one of the first examples of the quantum nature of matter and light explaining how photons can liberate electrons from a metallic surface if they have an energy ($h\nu$) greater than the 'work function' of the metal W , the residual energy of the absorbed photon may then be released as kinetic energy of the ejected electron (Jeynes *et al.*, 2014, Mesbahi, 2010). Typical values of W are 4-6 eV and thus short-wavelength visible or ultraviolet light is required to liberate electrons from most metals. Higher energy photons may liberate electrons from inner shells (K, L etc) of an atom creating a 'hole' valence electrons may decay into the hole releasing energy in form of fluorescence (Hobbie and Roth, 2007). The photoelectric effect probability is a function of the atomic number (Z) of the NPs. The higher is the Z number, the higher the probability of the Auger effect. In the solid state, metal, the core levels of atoms are little perturbed and essentially remain as discrete, localised (i.e. atomic-like) levels, and thus electrons are released from the metal by high energy photons, X-rays with few hundred eV to keV energy (Leroy C, 2009, Mesbahi, 2010). In X-ray Photoelectron Spectroscopy (XPS) the absorbed X-ray energy ejects a core level electron directly whilst in Auger Electron Spectroscopy (AES) as one electron falls from a higher level to fill an initial core hole in the inner-shell the energy liberated in this process is simultaneously transferred to a second (Auger) electron ; a fraction of whose energy is required to overcome the binding energy of this second electron, the remainder being retained by this emitted Auger electron as kinetic energy (Hobbie and Roth, 2007). Both XPS and AES are relevant for electron liberation from nanoparticles and give rise to a continuum of secondary electrons worth energies from 10 eV to keV (Pradhan *et al.*, 2009).

At higher energies (> 500 keV), incident photons scatter off electrons within the atoms of the NP. the Compton effect leads to the production of a recoil electron and a photon of lower energy than the one interacting (Leroy C, 2009).

Finally, electron-positron pair production takes place for incident photons with energies higher than 1.02 MeV and comes from the interaction between a photon and an atomic nucleus inducing an electron and a positron (positive electron) formation (Leroy C, 2009).

All of these different photon interactions can produce secondary energetic photons, electrons, and ions, which can interact with oxygen and water or can directly interact with DNA and cause cellular damage in the vicinity of the NP (Mayles *et al.*, 2007, Retif *et al.*, 2015).

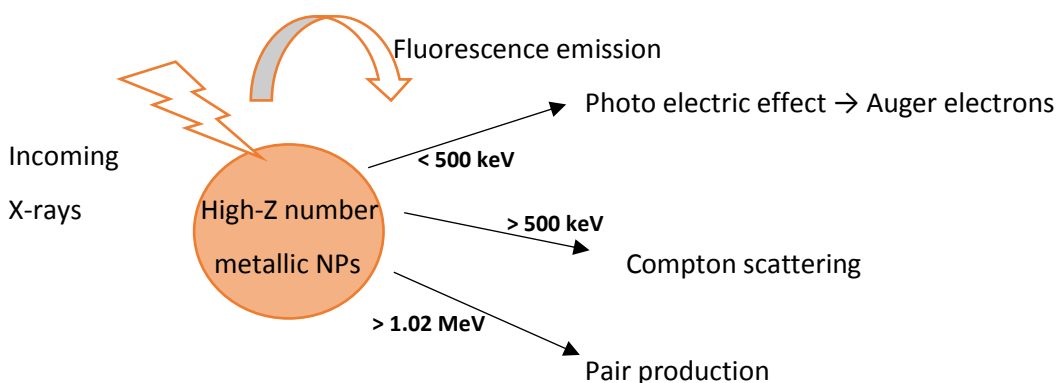


Figure 1.9: Possible emission pathways after photon irradiation of high-Z metal NPs (Kwatra *et al.*, 2013).

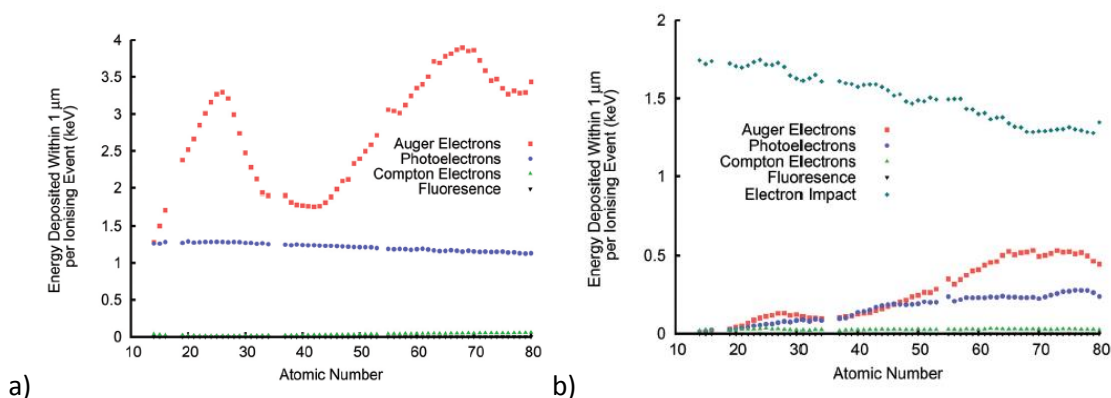


Figure 1.10: Distribution of energy deposited within 1 μm of a 20 nm size NP as a function of its atomic number. a) energy deposited for kilovoltage X-rays, b) energy deposited for megavoltage X-rays (McMahon *et al.*, 2015).

However, MacMahon *et al.* found that high atomic number does not always correlate with enhanced radiosensitisation effects (McMahon *et al.*, 2015). They have shown, using Monte Carlo simulations that, when kilovoltage x-rays interact with the NPs, Auger electrons are the main source of energy deposition at the vicinity of the NPs. Monte Carlo simulations are often used to calculate and follow the probability for numerous photons to be scattered after

interacting with a substance (Hobbie and Roth, 2007). The spectra for these electrons is dependent on the NPs elemental composition and gives an indication of the “radiosensitisation potential”, although it has a multi-peaked dependence (Figure 1.10 a). When considering megavoltage energies, Auger electron production, although still present, is reduced, and the main energy deposition comes from secondary electrons produced by the primary beam of radiation. The total energy deposition at the vicinity of the tumour is constant, with a weak dependence on atomic number (Figure 1.10 b). In consequence, megavoltage X-rays are predicted to give a radiosensitisation effect independent of the element the NPs are made from (McMahon *et al.*, 2015).

In this thesis, gold was chosen as the main constituent of the NPs to be used for cancer radiotherapy. However, different elements can be used as radiosensitisers and will be described below. In addition, since different characteristics of the NPs play a role in the radiosensitisation potential, the effect of NPs size, charge and surface coating will be also considered (Figure 1.11)

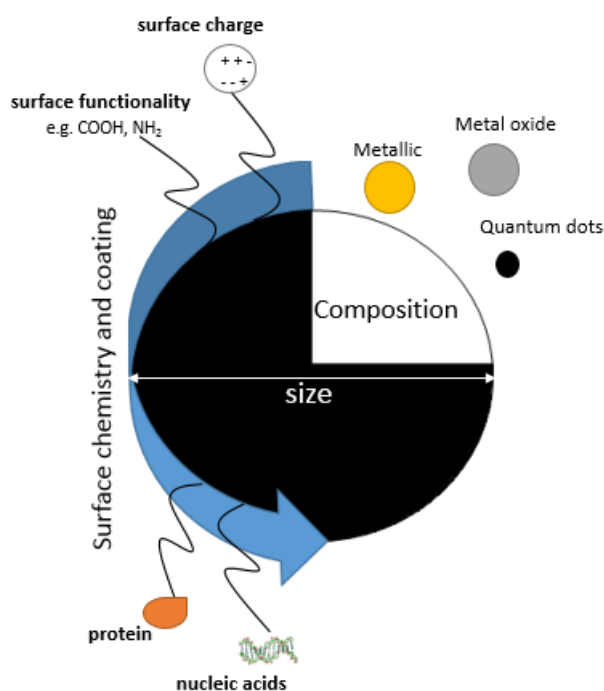


Figure 1.11: Different characteristics influencing NPs behaviour (Chou *et al.*, 2011).

1.5. Different NPs composition used in radiotherapy

1.5.1 High atomic number NPs

As discussed previously, nanomaterials characterised by a high Z number are good candidates for radiosensitisation and several NPs have already been used in radiotherapy.

Metallic NPs

The first material explored as a radiosensitiser was gold. A radiosensitisation effect was shown by Hainfeld *et al.* using 2nm diameter AuNPs. After injecting the AuNPs into mice, they noticed a decrease in tumour growth when X-ray irradiation treatment was combined with NP injection, as compared to irradiation alone (Hainfeld *et al.*, 2004) (Figure 1.6). Gold is therefore the most used in radiosensitisation applications and many studies have been undertaken to characterise AuNPs and explore how they may be used in radiotherapy (Haume *et al.*, 2016b).

Gadolinium, due to its high X-ray photon interaction cross section, has also been adopted as a radiosensitiser (Townley *et al.*, 2012). In addition, it is often used as a chelated compound in combination with magnetic resonance imaging, due to its paramagnetic properties, to enhance the quality of the images, making it a theranostic material (Kwatra *et al.*, 2013). However, gadolinium ions Gd^{3+} can cause toxicity in different organs by oxidative stress and chelation of Ca^{2+} , such that it needs to be handled carefully (Rogosnitzky and Branch, 2016) and is often being encapsulated/chelated by other molecules such as silica, in order to control its toxicity.

Various teams have exploited gadolinium in radiosensitisation experiments, such as a 5 nm size NPs, consisting of a polysiloxine core with a shell of diethylenetriaminepentaacetic acid (DTPA), forming the gadolinium chelates. These experiments have shown for example that the NPs are capable of efficient radiosensitisation *in vitro* in head and neck squamous cell carcinoma cells with a SER of 2.00 (corresponding to 50 % decrease) after incubation for 1h at a concentration of 0.6 mM and an irradiation with a dose of 2 Gy with 250 kV X-rays (Miladi *et al.*, 2015) in squamous cell carcinoma (Sancey *et al.*, 2014), as well as in brain cancer cells U87 with a 37% decrease of viability thanks to the sensitizing effect of the NPs after exposure for 3 h with 0.5 mM NPs and an irradiation of 8 Gy with 6 MV X-rays (Mowat *et al.*, 2011). A radiosensitization effect has also been shown *in vivo* with an increase of animal survival treated by Gd-NP (20 min or 24h incubation at 40 μ g per gram of weight) and microbeam radiotherapy irradiation by 2 compared to irradiation alone in rats brain with gliosarcoma (Sancey *et al.*, 2014). It is difficult however to compare the effect of the NPs on different models as the different papers published use generally different outcome measures (SER, decrease of viability and DEF) at different doses of radiation and using different NPs concentration and exposure time.

Platinum NPs have often been explored in cancer treatment strategies. Porcel *et al.* have shown the potential of platinum nanoparticles as radiosensitisers. By using *in vitro* plasmid DNA, they have shown that the combination of Pt-NPs with hadron therapy (carbon) can enhance DNA strand breakage. Indeed, they have shown that an incubation of 1 NP of 3 nm per 2 plasmid PbR322 1h before irradiation with a dose up to 360 Gy with 276 MV Carbon irradiation was

responsible for a 2-fold increase of SSB and 1.3 increase of DSB (Porcel *et al.*, 2010a). They hypothesised that it was the Pt²⁺ ions released from the Pt-NP that causes significant DNA damage and cellular apoptosis. These Pt²⁺ ions form a complex with DNA which seems to be similar to that of cisplatin, which is commonly used as radiotherapy agent (Porcel *et al.*, 2010a).

Metallic oxides NPs

Metallic oxide NPs have the advantage of providing NPs with well-controlled size, shape and structure when synthesized (Jolivet *et al.*, 2010). They offer interesting properties in radiotherapy since they can promote the formation of ROS by catalysis of radicals' production from the surrounding water. Their limitations are in the active sites which are weak by themselves. Some authors have shown that the catalytic properties of these types of NPs are enhanced when they are formed with another high element metal such as gold around it, forming a core shell structure with the catalytic part on the core and the other element constituting the shell (Mitsudome *et al.*, 2015).

Titanium oxide (TiO₂) is a photocatalytic metallic oxide that can react with water to produce ROS when irradiated with UV (Smith *et al.*, 2012, Sotter *et al.*, 2005). Radiosensitisation has been shown for example with breast cancer (MCF-7) and gastric cancer (MKN-45) cells using TiO₂ NPs and gamma irradiation, with a 15% and 10 % survival with NPs and radiation compared to 30 % and 15 % for radiation only after irradiation with a dose of 2 Gy and exposure with a NP concentration of 30 µg/ml for MCF-7 and MKN-45 respectively (Rezaei-Tavirani *et al.*, 2013). The NPs therefore seem to be responsible for an enhancement between 5-15% for these particular conditions (Rezaei-Tavirani *et al.*, 2013). Mirjolet *et al.* have also shown that 10 nm TiO₂ nanotubes were able to radiosensitise both U87MG and SNB-19 cell lines after an exposure of 1 µg/ml for 24h and an irradiation with a dose of 2 Gy using a LINAC leading to a survival fraction of 0,18 for SNB-19 cells compared to 0,36 for the control and a survival fraction of 0,43 compared to 0,60 for the control for U87MG cells (Mirjolet *et al.*, 2013). However, TiO₂ NPs aggregate easily due to their isoelectric point (IEP) which is close to neutral pH, and therefore will have a poor solubility in neutral medium (Townley *et al.*, 2012). The IEP represents the pH at which a specific molecule will carry no net electric charge. One way to avoid this problem is to coat the NPs with, for example, silica group (Townley *et al.*, 2012).

Hafnium oxide NPs are interesting due to their high electron density (Zarschler *et al.*, 2016). They are also quite inert, and demonstrate selective toxicity toward cancer tissues (Maggiorella *et al.*, 2012). They can produce cellular stress damage when irradiated due to their high atomic number (Maggiorella *et al.*, 2012). This effect has been shown both *in vitro* in HCT116 cells with a DEF superior to 1.10 after a dose of 4 Gy with 6 MV X-rays and *in vivo* using xenograft mice models with a DEF superior to 1.5 and irradiated with a dose of 8 Gy with 6 MV

Co-60 gamma rays (Maggiorella *et al.*, 2012). Moreover, hafnium oxide NPs have been now in phase II clinical trials as adjuvant therapy with radiation for the treatment of hepatocellular cancer and liver metastases (2015).

Zinc oxide and iron oxide could be suitable radiosensitisers but their application is limited due to their potential dissolution in cellular media, which is responsible for their high toxicity (Nel *et al.*, 2009). Ceria (cerium oxide, CeO₂) is a cubic fluorite-type oxide, in which each cerium site is surrounded by 8 oxygen sites, allowing it to store and transport oxygen. Cerium oxide can act as radiosensitiser (Briggs *et al.*, 2013, Cheng *et al.*, 2013, Park *et al.*, 2008) or radioprotector (Arya *et al.*, 2016) depending on its redox state, and the pH of the environment.

Magnetic NPs

Magnetic properties of matter are defined by the orbital and spin motions of electrons, whose spin and angular momentum are associated with a magnetic moment (Colombo *et al.*, 2012). Magnetic properties are used for electricity, mechanic, optic, bio-separation properties, but also contrast enhancement agents for magnetic resonance imaging in particular (Yu *et al.*, 2008).

Superparamagnetic iron oxide nanoparticles (SPIONs) have been used due to their ability to catalyse ROS formation. Their superparamagnetic properties allow better targeted therapy, by directing and localising them into organs using an external magnetic field (Klein *et al.*, 2014, S Wadajkar *et al.*, 2013). Superparamagnetic iron oxide nanoparticles refer mainly to magnetite (Fe₃O₄) (S Wadajkar *et al.*, 2013). Recently, superparamagnetic NPs have been used in combination with doxorubicin and antibody targeting endothelium growth factor receptor (EGFR) for magnetic resonance imaging applications and as an anti-cancer drug in addition to photothermal therapy using an in vitro model of cancer cells (DLD-1) where a 60 nm size NPs have shown more than 80 % of cell viability after 24h of NP exposure and then photothermal therapy compared to the control (Mu *et al.*, 2017).

Cobalt NPs are metallic NPs and can reach a higher state in magnetisation than iron oxides or other metallic oxides NPs, and so are of interest in magnetic resonance imaging. However, their toxicity limits their use in patients. Silica coatings can reduce their toxicity (Zarschler *et al.*, 2016).

1.6. NPs size used in radiotherapy

The size of the NPs also plays a crucial role in its biodistribution and elimination (Zarschler *et al.*, 2016). The surface area and the number of atoms present at the surface,

relative to non-surface atoms, increase when the NPs size decreases, hence, an ultras-small NP of 2 nm size will have 70% of its atoms at the surface (Zarschler *et al.*, 2016).

The size of the NPs regulates its clearance from the body via the kidneys. It is well known that NPs below 5 nm are preferentially cleared from the body via kidney clearance and so, avoid long term exposure at the whole-body level (Alric *et al.*, 2013, Sancey *et al.*, 2014). The NPs size also impacts on their uptake in cells and will be discussed in Section 1.10.

NP size is also important for the interaction with the beam of radiation. As the NPs size increases, the ionization event from the interaction with radiation may occur within the bulk of the NP, reducing the dose deposited on its surface (Haume *et al.*, 2016b, McMahon *et al.*, 2011). The size of NP plays a role on the course of the species produced and the distance they have to travel in order to reach the surface. Indeed, the catalytic abilities of the NPs depend on having excited electrons as its surface. Bigger is the NP and bigger are the chances that the electrons recombine in the bulk of the NPs before reaching the surface. Therefore, the physical dose enhancement can be different as for smaller NP most of the atoms are at the surface and for bigger NP, long distance between the bulk and the surface (Haume *et al.*, 2016b).

1.7. NPs charge used in radiotherapy

The charge on the surface of the NPs plays an important role in its interaction with the environment and especially the cells. Positively charged NPs are known to be able to interact with the cellular membrane which is negatively charged by creating pores and disrupting its integrity, and thus engenders toxicity (Beddoes *et al.*, 2015a, Goodman *et al.*, 2004).

Simulations of NP entry through the cellular membrane have been made by Rocha *et al.*, who analysed NP behaviour as a function of charge density and interestingly found that a small amount (20% of positive coating interacting with the membrane) of positive charge improved the uptake, while a large amount (100% of positive coating) favoured the membrane dysfunction (Da Rocha *et al.*, 2013).

Whether the charge on a NP causes toxicity is still controversial, Bannunah *et al.* found that positively charged AuNPs (50 and 100 nm) cause strong toxicity to CaCo-2 cells while negatively charged NPs were not toxic (Bannunah *et al.*, 2011b). On the other hand, Schaeublin *et al.* have shown that both positive and negatively charged AuNPs (1.5 nm) were more toxic on HaCaT cells than neutral ones, and contribute to different cell death pathways (Schaeublin *et al.*, 2011b).

It is important to point out that the surface charge of the NPs can be modified when loaded in cellular medium, forming a protein corona around the NP (Yonamine *et al.*, 2013).

1.8. NPs surface coating used in radiotherapy

The coating placed upon NP is a very important characteristic for the stability of that NP in solution and may be used to avoid aggregation and agglomeration. The coating influences the interaction between the NP and the environment and can regulate the solubility of the NP and its interaction with molecules around it (Pavlin and Bregar, 2012). The NP coating and its charge can therefore be modified during the exposure by interacting with either the extracellular or intracellular environment (Hirsch et al., 2013a, Lv et al., 2014, Zhu et al., 2012, Schollbach M et al., 2014). The surface charge can also play a major role in AuNPs stabilization and interaction in aqueous solution (Alkilany and Murphy, 2010a). For example, cell exposures to NPs are generally conducted through dilution in culture medium and because NPs can interact with serum proteins, surface functionalization with polyethylene glycol (PEG) is often used in order to prevent interactions of serum proteins with NPs (Damodaran et al., 2010, Pissuwan *et al.*, 2011).

The number of ligand vacancies on a NP surface depends on their diameter (Babaei and Ganjalikhani, 2014a). For example, 2 nm AuNPs can have, on average 100 ligand sites when considering molecules such as PEG, proteins or derivative molecules, whereas 100 nm NPs can have around 4000 (Babaei and Ganjalikhani, 2014a).

The pH of the environment is also important for the biomolecule behaviour coating the NPs. Indeed, a pH above the IEP makes the molecule negatively charged, while at pH below the IEP is positively charged (Yu *et al.*, 2008). This is particularly important when the NPs are localised in specific organelles such as the lysosomes which have a more acidic environment (Drescher and Kneipp, 2012).

Different types of forces can bind the NP to its coating. Non-covalent binding is based on electrostatic interaction between a molecule and the NPs. Non-covalent binding has the advantage that there is an absence of any toxic chemical during the NPs production and therefore the biomolecule is coated in its native and unchanged form. The disadvantage is its weak interaction with the NP surface, which can be easily broken (Yu *et al.*, 2008). For example, the citrate group on AuNPs is attached via weak ionic interactions and therefore will be easily and rapidly replaced by other groups such as antioxidants, proteins, antibodies or DNA of interest on the AuNPs (Kalimuthu and John, 2010). One of the most interesting coatings uses the covalent Au-S bond and is composed of thiolates (Boisselier and Astruc, 2009, Häkkinen, 2012). In this way, coating exchange from a phosphorous coated group to a thiol coated group has been demonstrated and produces a precursor with a mixture of phosphorous and sulphur groups onto the AuNPs (Warner *et al.*, 2000).

Covalent interactions between molecules and NPs provide strong and stable binding which can be used for specific applications, such as drug delivery.

The NP coating and particularly its net charge also plays a role in cancer cell targeting and particularly the uptake of NPs (Schaeublin *et al.*, 2011a, Yah, 2013). Positively charged NPs are thought to improve the uptake by interacting with the negatively charge membrane of the cells (Bannunah *et al.*, 2011b, Kralj *et al.*, 2012).

As mentioned above, one coating than can often be used to improve the biocompatibility of NPs is the PEG group. Its amphiphilic characteristics can improve the cellular uptake by interacting with the cell membrane (Pissuwan *et al.*, 2011). It can also improve the circulation time of NPs in the blood stream (Pissuwan *et al.*, 2011). The PEGamine group, with an amine group at the end of the carbon chain, provides a positive charge on the NPs.

Alternatively, since sugar, and especially glucose, is a primary source of metabolic energy for cells, and cancer cells especially need and use significantly more glucose compared to normal cells, sugar coated NPs can be an effective way to facilitate the entry of NPs into cancer cells (Hu C *et al.*, 2015).

Oligonucleotides have been widely used for drug delivery and targeting of cancer cells (Asthana *et al.*, 2014, Carbone *et al.*, 2004, Huo *et al.*, 2014, Tkachenko *et al.*, 2003, Zeller *et al.*, 2006). Different strategies can be used in order to regulate non-physiologically a gene and achieve a better cancer cell killing (Malvy *et al.*, 1999). RNA interference (RNAi) for example is a sequence-specific gene silencing. It is mediated by small interfering RNA (siRNA) and can decrease the translation of a gene, and therefore the protein level (Huang *et al.*, 2008, Wang *et al.*, 2005). Wang *et al.*, in 2005, were able to suppress by more than 75 % the expression of c-myc protein in MCF-7, and decrease its growth rate 5 days after a transfection for 2 days with an RNA silencing sequence that targeted c-Myc production (Wang *et al.*, 2005). Anti-micro RNAs (miRNA) have also been used for gene silencing by interacting with the messenger RNAs. Indeed, miRNA act as post-transcriptional genes in physiological processes (Kim *et al.*, 2011), thus, anti-miRNA can help understanding gene regulation (Kim *et al.*, 2011).

The possibility of targeting a particular DNA sequence in the genome via the triplex forming oligonucleotides (TFOs) strategy is of interest and can be used to inhibit the expression of this particular gene (Vasquez and Glazer, 2002). TFOs were discovered for the first time in 1957 by Felsenfeld and Rich, when they noticed whilst looking at the binding characteristics of the DNA, a strand composed of polyuridylic and polyadenylic acid able to create a complex with the double stranded DNA via a Hoogsteen pairing (Vasquez and Glazer, 2002). TFOs are able to bind directly and specifically to the gene of interest in a stable conformation (McGuffie *et al.*,

2000). Natural triple helix, such as H-DNA exist in living organisms and seem to play a role as gene modulator (Malvy *et al.*, 1999).

In the Hoogsteen mode, the third strand runs parallel to the oligopurine sequence of the double helix, whereas in the reverse Hoogsteen configuration, it adopts an antiparallel orientation. Oligonucleotides containing C and T form Hoogsteen hydrogen bonds (Figure 1.12.a) whereas oligonucleotides containing G, A, and possibly T form reverse Hoogsteen hydrogen bonds (Figure 1.12.b) (Malvy *et al.*, 1999). The limitation of the structure C⁺G:C is that a protonation of the cytosine is required for the structure to be formed and therefore the environment need to be at an acidic pH (Malvy *et al.*, 1999).

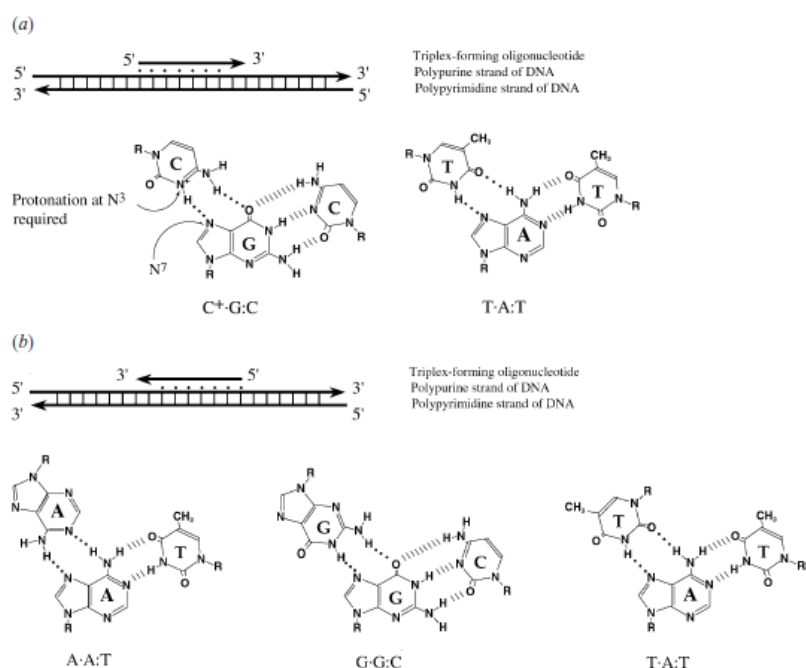


Figure 1.12: Canonical base triplexes helix formation. a) When the third strand binds to the pyrimidine motif, it is parallel to the purine strand; while b) when it binds to the purine motif, it is anti-parallel (Vasquez and Glazer, 2002).

TFOs needs optimum conditions, such as specific pH and magnesium presence, in order to bind to the duplex sequence of interest DNA. Once formed, this structure is fairly stable with half-lives observed *in vitro* of several hours, up to days (Carbone *et al.*, 2004).

In the gene-targeting strategy of treatment, one should try to target a gene which is involved in several types of cancer or which causes severe dysregulation of the cell modulation (Hanahan and Weinberg, 2000). Two types of genes are involved in tumour development; proto-oncogenes and tumour suppressor genes. *C-Myc* is a proto-oncogene that promotes cell division and an undifferentiated state in cancer cells. Many strategies have been developed in order to inactivate or decrease its activity using for example plasmid DNA and T7 RNA polymerase via triplex/quadruplex formation (Belotserkovskii *et al.*, 2007) or *in vitro* cell models (Colo 320) using shRNA (Huang *et al.*, 2008). *C-Myc* is a transcription factor, highly expressed in stem cells and

deregulated in many cancer cells. It is involved in maintaining pluripotency and cell proliferation. *C-Myc* is defined as a pro-oncogene as it is up-regulated in many different types of cancers and is often targeted for cancer treatment to decrease the abnormal cell proliferation (Carbone et al., 2004, Huo et al., 2014, McGuffie et al., 2000). C

TFOs targeting the *c-myc* gene have already been designed, but have never been used in combination with radiotherapy (McGuffie et al., 2000), and therefore will be one of the focus of this thesis.

1.9. NPs uptake by cancer tissues

NPs are a new method proposed for improving radiotherapy efficiency (Burger et al., 2014a). Due to the enhanced permeation and retention (EPR) effect, NPs can be better absorbed into the tumour tissues. The permeation effect is the cause of cancerous tissues developing a rapid vascularisation to compensate the lack of resources, secreting growth factor such as VEGF. This rapid vascular development leads to irregular blood vessels with discontinuous epithelium, easily permeable and favouring extravasation to the tumour environment (Kwatra *et al.*, 2013). The retention effect comes from a defective lymphatic function, resulting in poor drainage (Kwatra *et al.*, 2013).

As mentioned earlier in this chapter, NPs uptake is an important criterion determining the radiosensitisation effect. Kong *et al.* showed that NPs localised in the cell cytoplasm decreased the cell viability more than when they are at the membrane surface (Kong *et al.*, 2008). Furthermore, they showed that glucose coated NPs improve cellular uptake and radiosensitisation, compared to non-coated ones (Kong *et al.*, 2008).

NP interaction with cells are determined by the different characteristics presented above, such as their size, shape, or coating (Mao *et al.*, 2007, Zhu *et al.*, 2012). Some of the main pathways of cellular uptake are phagocytosis and endocytosis. Phagocytosis generally involves the uptake of particles larger than 100 nm, whereas endocytosis takes place for NPs of smaller sizes (Mao *et al.*, 2007, Shukla *et al.*, 2005). If the NPs are small enough (below 10 nm), they can enter directly by diffusion through the membrane (Zhu *et al.*, 2012); however, they can be toxic by generating holes in the membrane if they have positive surface charge (Zhu *et al.*, 2012). Figure 1.13 illustrates different mechanisms of NPs cellular uptake. Nevertheless there are still questions about the mechanism of uptake of NPs and different characteristics such as their size, shape or their coating are linked to their therapeutic properties (Alkilany and Murphy, 2010b, Kwatra et al., 2013) and these will now be discussed in the case of AuNPs as used in this work.

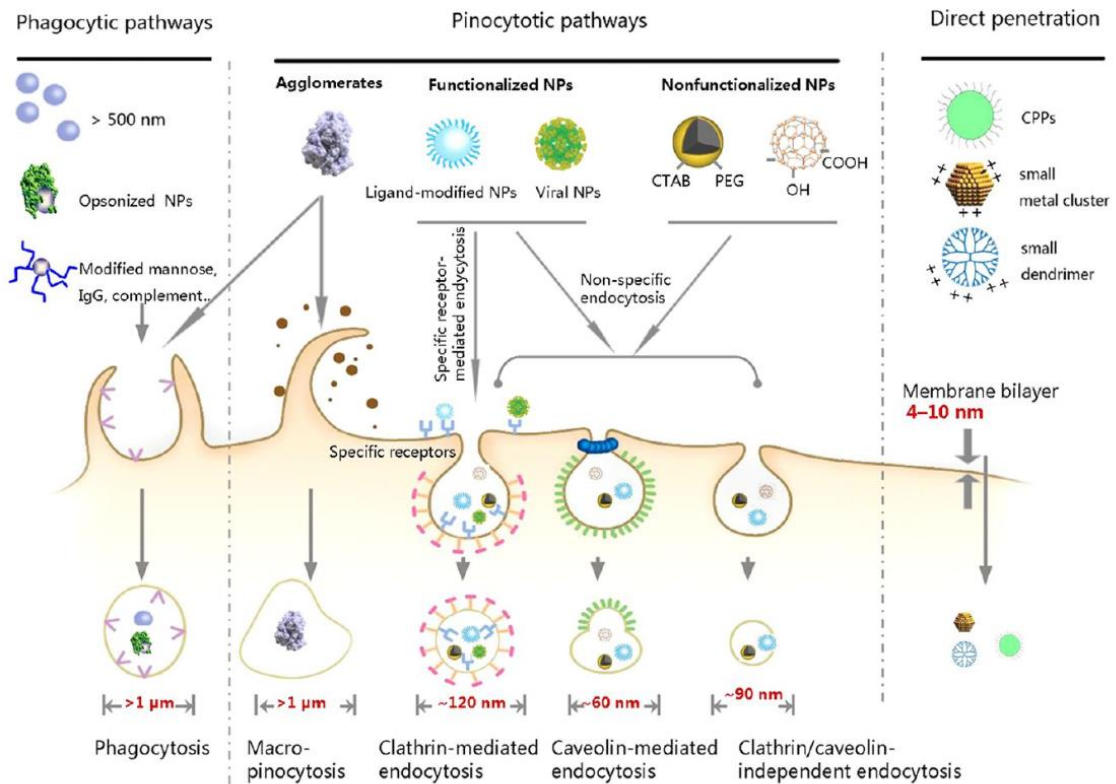


Figure 1.13: Natural size rules and gatekeepers within a mammalian cell (Zhu *et al.*, 2012, Mao *et al.*, 2007).

1.10. Gold NPs

Having discussed the properties of NPs in general and how they influence their properties as radiosensitisers, a specific case study will be discussed, that of gold which was used in the work presented in this thesis.

1.10.1. AuNPs fabrication

Gold colloid NPs have been known for a long time. Indeed, Michael Faraday in 1857 was the first to define the colloid solution as “finely dispersed metal” (Tan *et al.*, 2004). AuNPs have been often used, due to their optical properties, biocompatibility and easiness of surface modification. AuNPs can be made in a variety of sizes and shapes, which are known to play a significant role in the uptake by cells, and in the radiosensitisation effect (Kwatra *et al.*, 2013). AuNPs can be produced by many different techniques. The two most advanced reactions to produce a gold colloid are the aqueous Turkevich method and the “phase transfer catalyst” method. The Turkevich method can produce gold nanoparticles around 12 nm by reducing an

aqueous solution of HAuCl_4 with citric acid or trisodium citrate. On the other hand, the phase transfer catalyst method can produce smaller NPs about 4 nm (Tan *et al.*, 2004).

Using various reducing agents such as sodium borohydride in the presence of HAuCl_4 ; Au^{3+} can be reduced to neutral gold atoms (Au^0) (Yah, 2013). UV or microwave radiation can be used also to make AuNPs via a photochemical reduction technique (Khan *et al.*, 2014), with high purity and a relatively uniform size. Alternatively, green methods have been used to make AuNPs without using strong and toxic reductants (Nazir S *et al.*, 2014); these include the use of microbial enzymes, microorganisms or plant extracts (Yah, 2013).

1.10.2. AuNPs characterisation

When using AuNPs for radiotherapy treatment, it is crucial to determine their size, as well as their coating (surface density and ligand).

AuNPs in solution can have a different colour linked to their plasmon resonance. This localized surface plasmon resonance depends on the size of the AuNPs and will occur especially if the AuNPs size is above 2 nm (Alkilany *et al.*, 2009, Kelly *et al.*, 2003). This plasmon resonance can be of interest when characterising the AuNPs and for better visualisation due to their colour in solution.

Different techniques can be used in order to characterise AuNPs. X-ray diffraction spectroscopy (XRD) and electron microscopy are both sensitive to the shape and the electron density of the AuNPs (Fleury *et al.*, 2015, Tan *et al.*, 2004). X-ray diffraction (XRD) and transmission electron microscopy (TEM) are both techniques to study the size and elemental structure of the NPs.

TEM allows the size, morphology and element analysis of an isolated AuNPs to be determined, while Scanning Electron Microscopy (SEM) can define the AuNP microstructural characterisation but only of a thin layer. However, neither SEM nor TEM are accurate for analysis of aggregated AuNPs. In contrast, XRD can overcome these limitations and can be used for exploring the composition of various samples (Lee *et al.*, 2012, Zolotoyabko, 2014).

X-ray absorption occurs via the photoelectric effect, the X-ray photon is absorbed by the AuNPs and a free electron is released. The resonant nature of the X-ray absorption, which is characterised by a maxima depending on the X-ray energy, can be used to explore material chemistry (Zolotoyabko, 2014). X-rays have characteristic energies related to the element, both X-ray photoelectron spectroscopy (XPS) and X-ray diffraction use this phenomenon (Wagner, 2010).

XPS provides information on the electronic surface, its chemical composition and the oxidation state (Wagner, 2010).

Not only does the size of the NPs in vacuum needs to be determined but also their size in solution, in order to have information on their surface characteristics, as well as their charge and potential aggregation. Optical analysis techniques such as dynamic light scattering (DLS), single scattering angle and scattered light with polarisation parallel to the incident beam are effective techniques to study the size or hydrodynamic radius, and the potential aggregation of AuNPs (Tan *et al.*, 2004, Falabella *et al.*, 2010, Zimbone *et al.*, 2011). More specifically, the hydrodynamic size of AuNPs gives information on the inorganic layer on top of the AuNPs and therefore its coating.

1.10.3. AuNPs Uptake

The size of the AuNPs needs to be small enough (equal or below 50 nm) in order to cross the cell membrane without disrupting it and to enter the cell. Chitrani *et al.* in 2006 have shown that NPs of 50 nm in size were showing the best uptake compared to smaller and bigger size (14 nm and 74 nm) (Chithrani *et al.*, 2006). When the AuNPs enter the cells, they will follow a certain course before reaching the target of interest (Kodiha *et al.*, 2015). For example, AuNPs can be trapped in the lysosomes, before reaching a second target which could be the mitochondria or the nuclei (Chithrani *et al.*, 2006, Georgieva *et al.*, 2011, Gromnicova R *et al.*, 2013). In order to passively pass through the nuclear pore complex, the AuNPs need to have a diameter below 9 nm while the inner membrane of the mitochondria contains channels allowing only 2 nm size particle to cross the membrane (Kodiha *et al.*, 2015).

Cellular uptake depends not only on the characteristics of the AuNPs but also on the cell type, with tumour cells being known to be more sensitive to AuNPs entry, particularly regarding the nucleus uptake, where its homeostasis is often modified in cancer cells (Kodiha *et al.*, 2015). Indeed, cancer cells are generally defined with an increased proliferative rate and an accelerated cell cycle compared to normal cells. Moreover, the cell membrane can be different with less adhesion molecules and more collagenase for cancer cells (Cooper and Hausman, 2004)

As mentioned previously, the coating of the NP plays an important role on cellular uptake and various sugars, like glucose, are often used on top of AuNPs to target cancer cells. Cancer cells have generally a higher and faster proliferation than many normal cells, therefore they need greater amount of glucose for their metabolism (Babaei and Ganjalikhani, 2014a). Glucose-coated AuNPs can enter via GLUT receptors, particularly GLUT-1 (Calvaresia E.C and Hergenrother P.J, 2013), on the cancer cell membrane (Gromnicova R *et al.*, 2013, Hu C *et al.*, 2015). However, this is a challenging technique because it needs a specific recognition of AuNPs and its coating by the glucose receptor. This interaction needs to be very specific and as

previously mentioned, AuNPs surfaces can be modified in the blood circulation before reaching their target (Hirsch et al., 2013a, Zhu et al., 2012). Moreover, the interaction between transferrin (involved in iron transport) and its receptor is a useful tool for cellular uptake of drugs and genes and has been successfully applied for enhancing internalization of transferrin-coated 20 nm AuNPs (Levy *et al.*, 2010).

The uptake of AuNPs is an important criterion for the radiosensitisation effect. Several laboratories have used different ligands in order to allow the AuNPs to enter specifically into cancer cells, such as glucose which improve the uptake NP uptake in MCF-7 cells compared to no coating (Kong *et al.*, 2008) or peptides such as the combination of peptides targeting CRGDK and neuropillin-1, which shows a strong toxicity (70%) on MDA-MB-321 cells when coated on AuNPs compared to free (Kumar A et al., 2012). These ligands and the size of the AuNPs were modulated in order to target specifically organelles in the cells such as mitochondria, which is strongly linked to ROS production (Mkandawire *et al.*, 2015, Pan *et al.*, 2009).

Moreover, it was previously mentioned that the localisation of the AuNPs close to the DNA (eg. nucleus) impacts on its radiosensitisation effect (Kong *et al.*, 2008).

Nuclear uptake is a challenging target. It can be accessed via a non-targeting or passive pathway but can lead to organelle damage (Kodiha *et al.*, 2014, Kodiha *et al.*, 2015). Previous studies have shown a nuclear uptake with AuNPs specifically coated with target molecules such as Tat protein, a protein involved in nuclear localisation sequences (NLS) (de La Fuente *et al.*, 2006, Tkachenko *et al.*, 2003). Interestingly, Tkachenko *et al.* have shown that AuNPs of 20 nm size were able to enter the nucleus of HepG2 cells when coating with nuclear sequence localisation NLS and RME together but not separately (Tkachenko *et al.*, 2003). For example, 3 nm AuNPs functionalized with Tat peptide have been shown using electron microscopy to be localized both in the nucleus and in the cytoplasm (Levy et al., 2010). Recently, several groups have focused their attention on DNA to coat the AuNPs, such as oligonucleotides or aptamers, which can be used not only to improve the uptake, but also for drug delivery (Huo *et al.*, 2014, Patel *et al.*, 2014, Tkachenko *et al.*, 2003).

However, so far, very few experiments have successfully shown a nuclear uptake of the AuNPs associated with radiosensitisation. Indeed, to the best of our knowledge, only one experiment has successfully showed a nuclear targeting uptake of NPs associated with a radiosensitisation effect (Fan W *et al.*, 2015). Fan *et al* describe in their work novel mesoporous silica upconversion nanoparticles of 47 nm size coated with tat protein, a nuclear localisation sequence (NLS), which allows a nuclear targeting, and encapsulating mitomycin C, an anti-cancer drug which, all together were able to radiosensitise MCF-7 cells (Fan W *et al.*, 2015). They have shown more than 50 % decrease of cell number after X-ray irradiation (5Gy) in the presence of 10 µg/ml of NPs for 24h compared to irradiation alone (Fan W *et al.*, 2015).

To measure cellular uptake, TEM is a useful technique, as it takes advantage of the high electron density of AuNPs. TEM can have an image resolution of 1 nm. In addition, dark field optical microscopy can be performed on living cells to visualize the location of AuNPs using their elastic light scattering properties. Fluorescence microscopy can also be used on living cells to study AuNPs localization in specific organelles using fluorescent probes (Pernodet N *et al.*, 2006, Shukla *et al.*, 2005). Nonetheless, since AuNPs absorb light in the visible region, their interference with fluorescent assays has to be considered (Alkilany and Murphy, 2010a). All these techniques provide qualitative information about uptake of AuNPs. However, there is also a need to precisely quantify the number of NPs in cells, for which inductively coupled plasma mass spectrometry (ICP-MS) is the best semi-quantitative technique. In ICP-MS, the sample is ionized, separated and the ions produced quantified. This technique can give high specificity and excellent limits of detection (e.g. 18 parts per trillion for gold) and can be applied to quantify the cellular uptake by digesting the cells with strong acid (Alkilany and Murphy, 2010a). The number of AuNPs can therefore be approximated by the amount of gold and its mass found per cell.

1.10.4. AuNPs charge impacts on cellular uptake and toxicity

A positive charge on the AuNPs is thought to improve the uptake by cells due to their interaction with the lipid membrane, which is negatively charged (Hirsch *et al.*, 2013b, Kalay *et al.*, 2014, Yah, 2013). These positively charged AuNPs can also selectively target cancer cells because of the glycocalyx structure, which can be thicker in some cancer cells (Marquez *et al.*, 2004). Gromnicova *et al.* discussed the possibility that glucose-coated AuNPs can pass through the brain endothelium through glycocalyx, which appears to be more negatively charged when compared to endothelium of other tissues (Gromnicova R *et al.*, 2013). This glycocalyx is composed of different glycoproteins and glycosaminoglycans, which can influence the membrane organisation, signal transduction and possibly enhance endocytosis (Paszek M.J *et al.*, 2014). Some work has shown that negatively charged AuNPs may also lead to a better uptake in cells by having a longer life-time in the blood stream.

Nevertheless, there are still questions about the proper amount of charge to optimize AuNPs uptake. Previous work by Beddoes *et al.* has shown that the amount of charge on AuNPs is linked to their cell membrane penetration and an endocytosis pathway is observed with a 100 % cationic charge density of coating (Beddoes *et al.*, 2015b, Da Rocha *et al.*, 2013). Shaedlin *et al.* found that negatively charge AuNPs about 1.8 nm size gave a better uptake in HaCaT cells but the anionic AuNPs were more toxic than the cationic ones. Moreover, a theoretical study of AuNPs coated with alky thiol ligands suggests that AuNPs with low charge density penetrates

the lipid cell membrane more easily than those with high density surfaces charges, which interact with the membrane, causing a change in morphology and a wrapping of the AuNPs (Da Rocha *et al.*, 2013).

Finally, other parameters can influence and make it difficult to analyse the cellular uptake depending on the AuNPs charge, such as the degree of ionization of these charged AuNPs, the circulation time in the body and the potential formation of a protein corona onto the AuNPs (Bannunah *et al.*, 2011a, Bertrand N *et al.*, 2014, Calvaresia E.C and Hergenrother P.J, 2013).

1.11. What are the risks of using AuNPs?

Even if AuNPs are supposed to be inert and biocompatible, more information about their toxicological profile still needs to be provided (Kwatra *et al.*, 2013). The EPR effect is an advantage, considering the uptake in cancer tissues; however, it may not be beneficial when considering the long circulation time in the whole body. There have been several previous studies focused on the potential toxicity of AuNPs. Tables 1.3, 1.4 and 1.5 present a non-exhaustive list of the different toxicology studies conducted with different size of AuNPs, different cell types (Table 1.3 and 1.4 for cancer cells and Table 1.5 for normal ones) and different AuNPs concentrations. Most of the studies exploring the relationship between AuNPs characteristics and their uptake and toxicity on cancer tissues involve *in vitro* models. *In vitro* models include primary cells, normal cell lines and cancer cell lines. These models are easy to use, less expensive and more practical when compared with *in vivo* models (Mrakovcic M *et al.*, 2014), which involve animal studies. *In vivo* situation of a tumour and its characteristic is very complex. Cell communications play an important role in tumour development and differentiation and particularly the fibroblastic mesenchyme impacts on the cell morphology and differentiation (Kunz-Schughart *et al.*, 1998). Moreover, angiogenesis and neovascularism are important mechanism of the tumour development and are influenced by the cellular endothelium within the tumour environment (Kunz-Schughart *et al.*, 1998). *In vitro* models have limitation compared to *in vivo* models in this different mechanism of differentiation and for most of them, they do not take into account the communication between the cells and what is called the bastender effect (Kucinska *et al.*, 2017). Being a 2D model, they do not take into account the complexity of connection within the cancer tissue and for example the barrier and circulation which needs to be cross for the NPs before reaching their target. Moreover, it is critical for the derived cell line to retain the differentiated features of the tumour of origin. In this way some tumour models are more likely to adapt to cell culture such as sarcomas cells which have been widely used over the past 25 years (Masters and Palsson B, 1998). Moreover, some effort have

been done trying to combine different types of cells within a 3D *in vitro* models to mimic the interaction of NPs with a more complex model (Kucinska *et al.*, 2017). Although NPs must be studied on animals to be able to conduct any clinical trials, *in vitro* models are good tools to provide some new information on the selective uptake and toxicity on different types of cells.

Table 1.3: Toxicology studies on cancer *in vitro* models of different spherical AuNPs exposure

Reference	Size (nm)	Coating	Cancer cells	Exposure	Time	Toxicity
Tsoli <i>et al.</i> , 2005	1.4	Ph ₂ PC ₆ H ₄ SO ₃ H	MV3, BLM	< 0.4 mM	24h	IC50 0.24 μM IC50 0.30 μM
Pan <i>et al.</i> , 2007	0.8; 1.2; 1.4; 1.8; 15	TPPMS, TPTS	Hela, SK-mel-28	Up to 10000 μM	36h	1.4 AuNPs are the most toxic one with IC 50 for Hela cells of 30 μM and 46 μM for 1.4 MSAu NPs and 1.4TSAu NPs,
Pan <i>et al.</i> , 2009	1.1-1.4- 15	TPPMS, GSH	Hela	5.6 mM	48h	1.4 AuMS NPs (IC 50 48 μM) 1.1 AuGSH NPs (IC 50 31μM) 1.4 AuMS NPs with GSH (IC50 181 μM), 15 AuMS NPs less toxic NPs
Butterworth <i>et al.</i> , 2010	1.9	No coating	DU-145 PC-3 MCF-7 MDA-231-B T98G	200-2000 nM	1h	Clonogenic assays show a slight toxicity after 200 nM AuNPs exposure on MCF-7 (20%) and strong toxicity after 2000 nM exposure on PC-3 (60%)
Shukla <i>et al.</i> , 2005	3.5 ± 0.7	Lysine, poly(lysine)	RAW 264.7 mouse macrophage	10-100 μM	24h-72h	AuNPs not toxic up to 100 μM after 24h, slightly toxic after 72h, Decrease of ROS levels after 100 μM exposure for 48h
Gu <i>et al.</i> , 2009	3.7	PEG	Hela	0.08-100 μM	6-72h	Low toxicity (70% viability after 72h of up to 10 μM AuNPs exposure)
Connor <i>et al.</i> , 2005	4, 12, 18	CTAB, citrate, cysteine, glucose, biotin	K562 human leukemia	0.001-0.25 μM	72h	MTT assay, CTAB-NPs 18 nm not toxic up to 25 μM
Glazer <i>et al.</i> , 2010	35.9 ± 6.7	Cetuximab antibody	Panc-1 Cama-1	100 nM	Not mentione d	AuNPs not toxic for cama-1, cell death for Panc-1 (IC50 ~ 100 nM) and mostly via a necrosis pathway

Table 1.4: Toxicology studies on cancer *in vitro* models of different rods AuNPs exposure

Reference	Size (nm)	Coating	Cancer cells	Exposure	Time	Uptake	Toxicity
Cho <i>et al.</i> , 2014	50×20	CTAB, PEG, anti-HER ₂	SK-BR-3	0.06 nM	24h	ICP-MS, AuNPs/cell (8,000 for CTAB, 3,000 for PEG, 4,400 for anti-HER ₂)	Not measured
Hauck <i>et al.</i> , 2008	40×18	CTAB, PSS, PAH, PDADMAC	Hela	10-150 μM gold atoms 1 nM	6h	ICP-AES, AuNPs/cell (150,000 for PDADMAC, 12,000 for PAH and CTAB, 1,000 for PSS)	Slight toxicity at 150 μM for CTAB in serum free media (20.8 % cell death) and PDADMAC (11.7 %) in serum containing media
Alkilany <i>et al.</i> , 2009	65×15	CTAB, PAA, PAH	HT-29	up to 10 nM	96h	ICP-MS, AuNPs/cell (45 ± 6 for CTAB, 270 ± 20 for PAA, 2,320 ± 140 for PAH)	CTAB-AuNPs show cytotoxicity on cells (IC ₅₀ ~ 0.3 nM), as well as PAH-AuNPs (IC ₅₀ ~ 2 nM) but not with PAA negative coating CTAB in solution gives 50% of cell death at 0.4 nM while PAA and PAH are not toxic up to 1 nM
Cho <i>et al.</i> , 2014	50×20	CTAB, PEG, anti-HER ₂	SK-BR-3	0.06 nM	24h	ICP-MS, AuNPs/cell (8,000 for CTAB, 3,000 for PEG, 4,400 for anti-HER ₂)	Not measured

Table 1.5: Toxicology studies on normal *in vitro* models of different spherical AuNPs exposure

Reference	Size (nm)	Coating	Normal cells	Exposure	Time	Toxicity
Pan <i>et al.</i> , 2007	0.8; 1.2; 1.4; 1.8; 15	TPPMS, TPTS	L929, J774A1	up to 10000 μM	36h	1.4 AuNPs are toxic for both cell lines, with a IC50 for 1.4 MSAuNPs of 30 μM for J774A1 and 56 μM for L929, 15 nm is not toxic (up to 6300 μM) and the toxicity is cell line independent
Schaeublin <i>et al.</i> , 2011	1.5	MEEE, TMAT, MES)	HaCat	0-100 $\mu\text{g/ml}$ 25 $\mu\text{g/ml}$	6-24h 24h	IC50 < 10 $\mu\text{g/ml}$ for TMAT and MES and IC50 = 25 $\mu\text{g/ml}$ for MEEE
Rahman <i>et al.</i> , 2009	1.9	Not coated	BAECs	0.125- 1 mM	Not mentioned	~ 30% cell death at 1 mM AuNPs exposure AuNPs clustered in the cell cytoplasm
Butterworth <i>et al.</i> , 2010	1.9	Not coated	L132 Primary astrocytes AGO 1552	200-2000 nM	1h	Clonogenic assays show a slight decrease of viability after 200 nM AuNPs exposure on L132 (20%) and AGO 1552 (25%). Decrease of viability more important after 2000 nM on L132 (30%) and AGO 1552 (40%)
Goodman <i>et al.</i> , 2004	2	Quaternary ammonium, carboxylic acid	COS-1 Red blood cells	0.38-3 μM 0.27-833 μM	1-24h	IC50 MMPC1+ 1.0 μM IC50 MMPC2- > 7.37 μM IC50 MMPC1+ 1.0 μM IC50 MMPC2- 72 μM
Mironava <i>et al.</i> , 2010	13 45	Not coated	CF-31 primary dermal human fibroblast	Up to 180 $\mu\text{g/ml}$	3; 6 days	75% and 100% cell death by apoptosis pathway after 45 nm AuNPs exposure at 25 $\mu\text{g/ml}$ for 3 days and from 20 $\mu\text{g/ml}$ for 6 days.
Hartono <i>et al.</i> , 2009	20 \pm 2	Citrate BSA-coated AuNPs Neutravidin-coated AuNPs Fibrinogen-coated AuNPs	L-DLPC	50 nM	1-40h	BSA-coated NPs can disrupt phospholipid monolayer in 40h, uncoated AuNPs are unable to disrupt with the same condition. A disruption occurs after 32h for neutravidin-coated AuNPs and for 1-2h for fibrinogen-coated AuNPs
Patra <i>et al.</i> , 2007	33	CTAB and citrate	A549, BHK21	0-120 nM	48h	Toxicity for A549, IC50 ~ 100 nM no toxicity observed for BHK21 up to these concentrations

It appears that the toxic potential of AuNPs can vary with their size, their coating but also differs for various cell types. For example, Pan *et al.* showed that the toxicity of coated AuNPs is size-dependent but does not depend on the type of coating as TPTS and TPPMS coatings have the same toxicity for different cell lines (Pan *et al.*, 2007). However, Tsoli *et al.* found that AuNPs can improve the toxicity for cancer cells compared to standard chemotherapy,

with a 50 % toxicity after exposure to 0.24 μM of 1.4 nm Au₅₅ NP clusters for 24 h (Tsoli *et al.*, 2005). Indeed, the 50 % toxicity (IC₅₀) on a melanoma cell line exposed to 1.4 nm Au₅₅ NPs clusters was 180 times lower than the IC₅₀ after exposure to cisplatin (Tsoli *et al.*, 2005).

To date, no work has demonstrated a toxicity of AuNPs for cancer cells only, compared to its relative normal model, also known as selective toxicity. Pan *et al.* showed a similar toxicity for both cancer and normal cell lines after exposure to 1.4 nm AuMS NPs exposed for 36 h (Figure 1.14) (Pan *et al.*, 2007). Promisingly, Butterworth *et al.* have shown a decrease in viability for PC-3 cells exposed to 1.9 nm AuNPs (more than 50 % decrease compared to the control) with less toxicity towards L132 fibroblasts (around 30 %) (Butterworth K.T *et al.*, 2010). Thus, more information about the difference in toxicity between cancer cells and the respective normal cells is required.

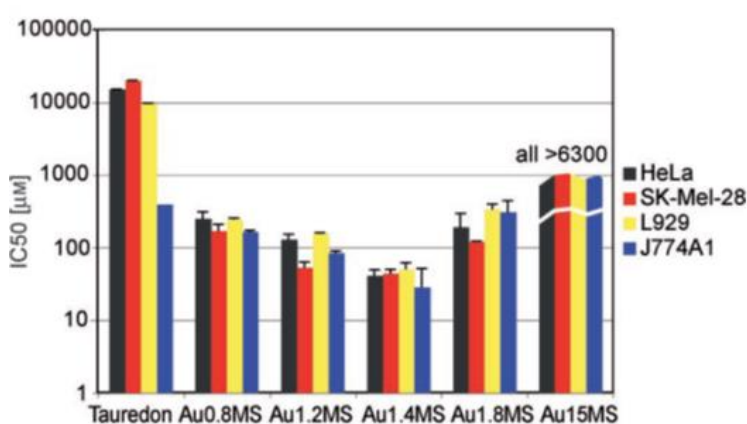


Figure 1.14: Toxicity of different size of AuMS NPs on four different cell lines (Pan *et al.*, 2009). Four different cell lines are presented, HeLa represent cervical cancer cells and SK-Mel-28 human melanoma cells, while L929 represent mouse fibroblast cells and J774A1 mouse macrophage cells.

1.12. AuNPs mechanism of toxicity

Does the toxicity appear directly after exposure? Is it a late process? Does it come from an apoptosis or necrosis death pathway? Does it depend upon the characteristics of the AuNPs, the cell types and the conditions of exposure? All these questions will try to be answered in this thesis.

Pernodet *et al.* have shown that NPs do not immediately cause cell damage but are linked to the formation of large vacuoles inside the cells, which may be the cause of toxicity (Pernodet N *et al.*, 2006). AuNPs can cause two types of cell deaths; apoptosis and necrosis. These two cell death pathways have different morphological and biochemical characteristics; however; they can occur simultaneously after a toxic exposure (Leist M *et al.*, 1997). Liu *et al.* showed that 13 nm AuNPs were toxic to lung cells, partially involving apoptosis but mostly a necrosis pathway (Liu M *et al.*, 2013).

One of the mechanisms of toxicity of AuNPs, or other high-Z metallic NPs is the involvement of oxidative stress induced by elevated ROS, or the depletion of antioxidants. This effect is both cancer cell-line and exposure time dependent (Cui *et al.*, 2013). ROS are generated during the cellular oxidative metabolism, which mostly occurs in the mitochondria (Fu *et al.*, 2014). The interaction of AuNPs with different cellular components can imbalance ROS production. (Li *et al.*, 2010). Cui *et al.* have shown an increase in ROS after exposure to Tiopronin AuNPs of 2.7 nm size at a concentration of 0,5 mg/ml for up to 24h, with a fourfold increase compared to the control. (Cui *et al.*, 2013). ROS dysregulation is related to the chemical and physical structures of the AuNPs, such as size, shape, surface area, coating or solubility (Fu *et al.*, 2014). For example, Shukla *et al.* found that high concentrations of AuNPs (100 μ M compared to 50 μ M) lead to a reduction of ROS after an exposure for 48h and is a time and dose-dependent effect (Shukla *et al.*, 2005).

1.13. Parameterisation of the radiosensitisation effect of NPs

The following section outlines the most common parameters used in radiotherapy efficiency and radiosensitisation measurement, such as the linear quadratic model (LQ), the sensitizer enhancement ratio (SER) and the dose enhancement factor (DEF).

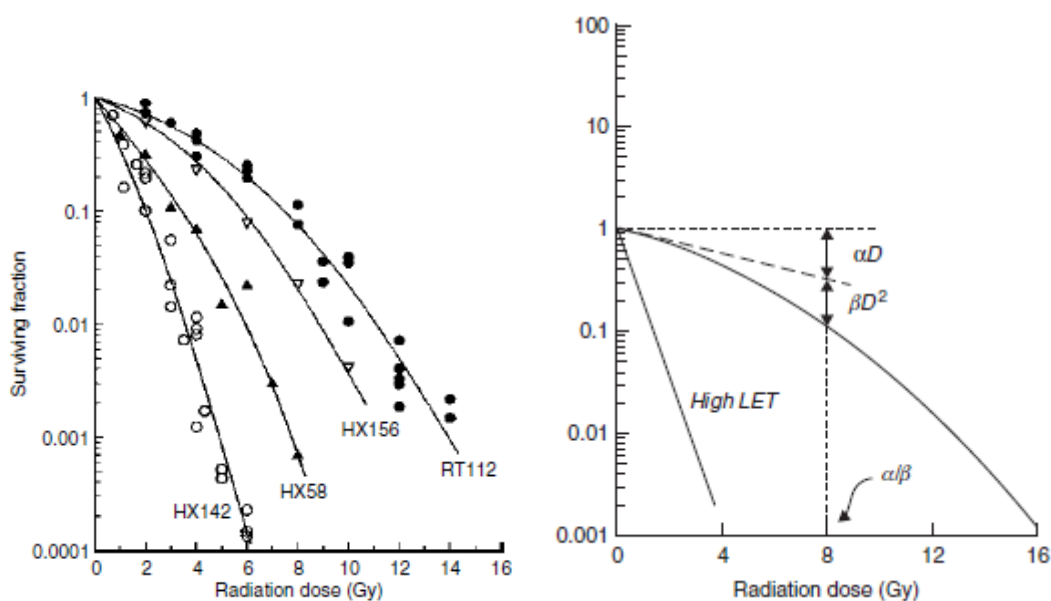


Figure 1.15: Survival curve and linear quadratic model of different human cancer cells irradiated at high dose rate (Mayles *et al.*, 2007, Taupin *et al.*, 2015).

Linear-quadratic (LQ) curves are useful tools to explore the survival fraction due to radiation. It is the model of choice for estimating biological effects after radiation and is used both experimentally and in the clinic to evaluate responses to radiation both *in vitro* and *in vivo*

(Joiner and Van der Kogel, 2009). As highlighted in Figure 1.15, fitting to the data are made via the equation:

$$\text{survival fraction} = e^{(-\alpha d - \beta d^2)},$$

where d is the radiation dose.

LQ model can also help to understand radiobiological mechanisms (Joiner and Van der Kogel, 2009). To explore the relative radiation contribution to cell killing, the two following parameters are separated:

$$\text{linear or alpha component} = e^{(-\alpha d)}$$

$$\text{quadratic or beta component} = e^{(-\beta d^2)}$$

The alpha component helps to characterise the first part of the cell survival curve and the radiobiological effectiveness after a single dose of radiation, while the beta component is used to represent the contribution from cumulative damage (Taupin *et al.*, 2015). The α/β ratio indicates the dose where linear and quadratic component contribute equally to the effect.

The linear-quadratic model can give indications of the mechanism of cell toxicity and especially on the effect of both acute and cumulative damage. NPs concentration can influence the radiosensitisation mechanism and therefore affect the alpha and beta contributions to the LQ graph (Butterworth K.T *et al.*, 2010, Taupin *et al.*, 2015).

The contribution of AuNPs in increasing the radiotherapy efficiency is measured by the DEF. DEF is defined by the radiation dose absorbed by the tumour cells in combination with AuNPs compared to the radiation dose absorbed by the cells without AuNPs (Muddineti O.S *et al.*, 2015). The radiation dose absorbed at a specific point in a tissue represents the quantity of energy deposited close to that point when the radiation passes through this tissue (Tubiana *et al.*, 1990). DEF may vary with the AuNPs characteristics (Coulter J.A *et al.*, 2012, Hossain M and Su M, 2012), their location inside the cell and especially the distance from the nucleus (Hossain M and Su M, 2012). The SER is similar to the DEF but is typically used to characterise radiosensitising drugs (Joiner and Van der Kogel, 2009). Large enhancement ratios (>2) can be found in animal models when the sensitisers are administered prior to radiation and in most cases, a radiosensitiser shows a SER >1 (Joiner and Van der Kogel, 2009).

$$DEF = \frac{\text{radiation dose without sensitizer}}{\text{radiation dose with sensitizer}}$$

1.14. Biological consequences of AuNPs radiosensitisation

AuNPs inside the cell can generate a large number of secondary low energy electrons when impacted by ionizing radiation. Such low energy electrons may be of importance in the process of DNA strand breakage, since they interact with neighbouring molecules, via a process called dissociative electron attachment, and leading to direct breakage of DNA (Boudaiffa B *et al.*, 2000), or $\cdot\text{OH}$ formation, that may lead further to DNA damage. This effect has been shown to take place inside the cells, causing cell death by damaging the DNA, specifically increasing the number of SSBs and more importantly DSBs (Rahman W.N *et al.*, 2009).

The exact region where electrons are produced may be important. Energetic electrons can travel long distances (microns), leading to a widely dispersed electron distribution throughout the target. This would suggest that it is not crucial where the AuNPs is located for this phenomenon. On the other hand, low energy secondary electrons, such as Auger electrons, that are produced by direct radiation interaction with the NPs do not travel far (e.g. 10 nm) and therefore such electrons have a more local effect and will depend on where AuNPs are within the cells (Davidson and Guo, 2014) (Figure 1.16).

Moreover, the radiation source also affects the secondary electrons produced, since kilovoltage photons produce long range dose enhancement in the cellular system, away from the AuNP surface, while this enhancement will be more limited due to targeted radiation on AuNPs in cells for proton therapy (Lin *et al.*, 2014).

AuNPs can also play a role on the cell cycle. During the G2/M phase of the cell cycle, the cells are sensitive to radiotherapy, as this phase corresponds to the division of the cells and the genetic material is sensitive to any changes, while they become more resistant during the G0/G1 phase (Iliakis and Nüsse, 1983, Parshad *et al.*, 1984). Roa *et al.* in 2009 demonstrated that glucose-coated AuNPs were able to arrest the cell cycle in G2/M phase by interfering and decreasing the expression of p53, cyclin E, cyclin A and cyclin B1 (Roa *et al.*, 2009).

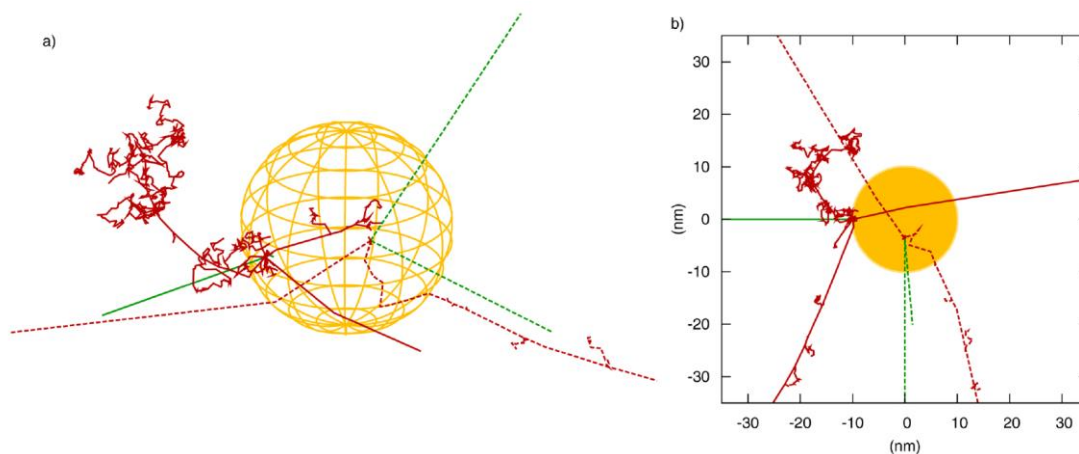


Figure 1.16: Exploration of tracks of ejected electrons on the surface (solid lines) or in the bulk (dashed lines) of a 20 nm AuNPs interacting with 50 keV photon (green line), plotted in a)3D, b)2D (McMahon *et al.*, 2011).

Several *in vitro* and *in vivo* studies have explored the biological basis of radiosensitisation (Butterworth *et al.*, 2012). In addition, isolated DNA has often been used in combination with radiotherapy as a proof of concept that AuNPs can enhance DNA damage (Śmialek *et al.*, 2008). In 1952, Joshua Lederberg defined a “Plasmid” as any extrachromosomal heritable determinant (Smalla *et al.*, 2015). Plasmids are double-stranded DNA that carry specific genes and can replicate them independently from chromosomal DNA (Smalla *et al.*, 2015). They are replicated upon cell division and are transmitted from one bacteria to another, creating numerous copies of the gene and therefore allow the study of damage upon radiation of a particular sequence in a gene of interest (Śmiałek 2007). A brief description of the work already been done in radiosensitisation effect using AuNPs is described below.

MacMahon *et al.* have shown in 2011 that small NPs, about 2 nm, deposit 2 to 3 times more energy in their vicinity compared to larger NPs (200 nm) due to the important surface/volume ratio of small NPs. This particular statement is true at the vicinity of the NPs but vanishes at longer distance as the dose deposited away from the NPs results from the photoelectrons and Auger electrons, escaping from all sizes of NPs (McMahon *et al.*, 2011).

It has already been shown that the closer the AuNPs to the DNA, the better radiosensitisation (Brun *et al.*, 2009a, Coulter J.A *et al.*, 2012, Hossain M and Su M, 2012). Additionally, Zhang *et al.* studied theoretically the benefit of 100 nm size AuNPs combined with Ir 192 source of radiotherapy using Geant 4. They found that after passing through AuNPs-containing region (in the tumour) (more than 20 nm away from the NP), the photon beam was responsible for a dose deposition much lower (similar to the one without NP) than within the

NPs region (28 % enhancement), which is important from a clinical perspective (Zhang *et al.*, 2009).

It is important to mention that although theoretical models in order to predict the dose enhancement when using NPs are developed but have limitation on the correlation between the predicted dose enhancement and the actual experimentally collected dose modifications as seen in Figure 1.17.

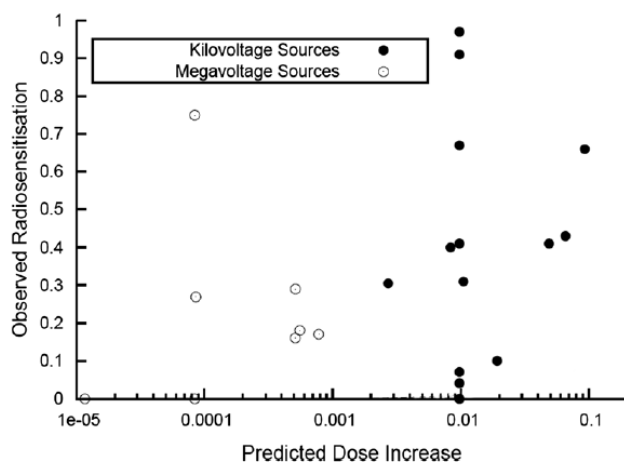


Figure 1.17: Comparison of experimentally collected Xray dose modification from different experiments and predicted dose increase for AuNPs interaction with kilovoltage and megavoltage irradiation (Butterworth *et al.*, 2012).

The type of radiation also plays a major role in the radiosensitisation effect. Rahman *et al.* found that low energy X-rays (80 peak kilovoltage, kVp) in combination with AuNPs were able to give a high DEF of 24 (Rahman W.N *et al.*, 2009). This DEF increased with increasing concentration of AuNPs. It is important to mention that low energy X-ray irradiation is used only for treating superficial tumours and cannot penetrate deeply inside the body. Such an effect was not observed with megavoltage radiation (6 MeV) (Butterworth *et al.*, 2012, Rahman *et al.*, 2009). So far, the average DEF obtained with combining AuNPs and radiotherapy is approximately 2 (Table 1.6 and 1.7).

Not only the type of radiation, but also the AuNP characteristics play a role in the radiosensitisation. It has been reported that concentration of AuNPs plays a bigger role on radiation dose enhancement rather than its size (Babaei and Ganjalikhani, 2014a, Mesbahi *et al.*, 2013). Indeed, a high concentration of AuNPs is related to high amount of gold atoms near the tumour and a better radiosensitisation (Chithrani *et al.*, 2009). Brun *et al.* tried to understand the relationship between the size and the molar ratio of AuNPs with X-ray radiotherapy using various photons energies (14.8-70 keV) (Brun *et al.*, 2009b). They found using plasmid DNA that the best radio-enhancement (6-fold improvement relative to the controls) was achieved with

large size AuNPs of 37.5 nm, high molar concentrations with a molar ratio of 1:1 DNA/AuNPs and an energy of 50-keV (Brun et al., 2009b). In addition, Zheng *et al.* have exposed plasmid DNA to AuNPs at a ratio of 1/1 or 1/2 DNA/AuNPs with energy of 60 keV electrons. In their work, the condition with 1/2 DNA/AuNPs lead to a 2.5 times increase of double strand breaks (Kwatra *et al.*, 2013).

Table 1.6 and 1.7 represent a non-exhaustive list of the different radiosensitisation obtained with AuNPs of various size and with different coatings.

Table 1.6: Summary of in vitro experiment on human cells exposed to AuNPs (below 10 nm) and radiotherapy

Reference	Size (nm)	Coating	Cells	NPs exposure	Radiation	Radiosensitisation	Uptake/comment
Rahman <i>et al.</i> , 2009	1.9	No coating	BAECs	0.125-1 mM	X-ray machine, 80-150 kV, 0-5 Gy 6 MeV-12 MeV	Enhancement concentration dependant. Maximum DEF of 24 with 80 kVp X-ray and 1 mM AuNPs	Not measured
Butterworth <i>et al.</i> , 2010	1.9	No coating	DU-145 and PC-3 MDA-231-B and MCF-7 L-132 (alveolar epithelial cell) T98G Human primary astrocytes AGO-1522B	10-100 $\mu\text{g}/\text{mL}$, 1h	160 kVp 0.625 Gy/min Dose between 0-10 gy	Highest DEF of 1.97 for AGO-1522B at 100 $\mu\text{g}/\text{ml}$ and lowest DEF of 1.04 for Astrocytes at 10 $\mu\text{g}/\text{ml}$	Du-145 show the highest toxicity after AuNPs exposure (more than 50 %). Toxicity observed also for primary cells (around 30 %)
Jain <i>et al.</i> , 2011	1.9	No coating	DU-145, MDA-MB-231, L132	12 μM , 24h	160 kVp x-rays 3Gy 6 MV X-rays 6 MV electrons (el) Dose of 0-2-4-6 Gy	MDA-MB-231, SERs 160 kV = 1.41 6 MV Xray = 1.29 6 MV el = 1.04 DU-145, SERs 160 kV = 0.92 6 MV Xray = 1.13 6 MV el = 1.12 L132, SERs 160 kV = 1.05 6 MV Xray = 1.08 6 MV el = 0.97	NPs accumulation in lysosomes Better uptake in MDA-MB-231 cells (4 $\mu\text{g}/\text{ml}$), compared to 2 $\mu\text{g}/\text{ml}$ for L132, linked to the better radiosensitisation
Bobyk <i>et al.</i> , 2013	1.9	No coating	F98 glioma cells	10 mg/ml, 15 min	50 keV, 6 Gy 0.5 Gy/min	SER 10% survival of 1.92	Not measured
Rashid <i>et al.</i> , 2018	1.9 nm	No coating	Hela	0.197 mg/ml 24 h	6; 10 MV X-ray 15 MV electron 100 MU/ml Dose 0-10 Gy	SER = 1.15 (6MV) SER = 1.05 (10 MV) (linear quadratic model) α parameter slightly higher (0,17 with NPs compared to 0.14 without)	NPs accumulation in endosome vesicles, no quantification studies

Reference	Size (nm)	Coating	Cells	NPs exposure	Radiation	Radiosensitisation	Uptake/comment
Zhang <i>et al.</i> , 2012	4.8,	PEG	Hela	0.05-0.1 mM overnight	137Cs with activity of 3600 Ci, 662 keV 1-2-4-6-8 Gy 6 dishes for each dose	SER 0.05 mM of 1.41, SER 0.1 mM of 1.46,	Cell death cause by both necrosis, followed by apoptosis
Cui <i>et al</i> 2017	5.81	PEG, peptide (RME)	MDA-MB 231 cells	0.5 mg/ml 24h	225 kV X-ray,, 3.47 Gy min and 13 mA with a dose up to 6 Gy.	In association with cisplatin 12 µM for 30 min or 0.5 µM for 48h, DEF = 1.14 for AuNPs-PEG DEF = 1.24 for AuNPs-RME and DEF= 1.39 for AuNPs-RME + cisplatin	AuNPs-RME concentration after 4 hours > 20 pg/cell and after 24 h > 40 pg/cell, concentration AuNPs-PEG inferior to 10 pg/cell in both cases.
Burger <i>et al.</i> , 2014	7.5	Citrate Transfection reagent DNA sequence	Hela	16h-48h concentration not mentioned	6 MV x-rays linear accelerator Dose rate 6.67 Gy/min Dose between 0-8 Gy Triplicate	DEF 4Gy = 1.25 ± 0.14	Better cellular uptake for NPs coated with DNA (semi-quantitative uptake: 100 % of strong fluorescence for cells exposed with AuNPs-DNA 20 % of cells with citrate AuNPs
Hanžić <i>et al.</i> 2018	8.8 nm 17 nm 30 nm	GSH Citrate diethylaminoethyl-dextran hydrochloride (DEX)	MDA-MB-231	10–50 µM 48h before irradiation	6 MV X-ray Dose of 4 Gy 4Gy/min	Increase amount of cell in S phase of the cell cycle 6 hours after irradiation (13.4 % for X-ray + AuNPs, 10.7 % for X-ray and 7.9 % for the control). G2/M arrest was observed 24 h after irradiation (40.5 % cells in G2/M compared to 33.2 % for the control)	Au-GSH Highest (> 1.10 ⁶ AuNPs/cell), while Au-Citrate and Au-DEX show a concentration < 1.10 ⁶ AuNPs/cell IC80 = 30 µM for GSH AuNPs IC80 = 50 µM for Au-Citrate and Au-DEX AuNPs

Table 1.7: Summary of *in vitro* experiment on human cells exposed to AuNPs (above 10 nm) and radiotherapy

Reference	Size (nm)	Coating	Cells	NPs exposure	Radiation	Radiosensitisation	Uptake/other
Kong <i>et al</i> 2008	10.8	Cysteamine (AET) Glucose (Glu)	MCF-7 ; MCF-10A	15 nM 3.85 nM 2 hours	200 kVp X-ray ;1.19 Gy/min, Dose of 10 Gy	63.5 % death after radiation (Glu-NPs) and 31.7 % (AET-NP) compared to the control, complete cell death after 5 days for Glu-NPs, compared to 13.8 % remaining for AET-NPs.	15 nM Glu NPs and 3.85 nM AET-NPs give the same cellular uptake of $2.96 \cdot 10^4$ AuNP/cell. 3 to fourfold uptake increase with AET coating
Wang <i>et al.</i> , 2013	13	Thio-glucose	A549	20 nM, 24h	6 MV X-rays Dose of 0-2-4-6-10 Gyc Triplicate	SER at 10 Gy = 1.49	AuNPs uptake maximum after 24 h with concentration of $6.51 \cdot 10^4$ and $(11.8 \cdot 10^4)$ per cell for coated AuNP and naked-AuNPs respectively.
Zhang <i>et al.</i> , 2012	12.1, 27.3, 46.6	PEG	Hela	0.05-0.1 mM overnight	137Cs with activity of 3600 Ci, 662 keV	12.1 nm NPs gives the strongest radioenhancement SER 0.05 mM 12.1 nm = 1.65, 27.3 nm = 1.58, 46.6 nm = 1.42. SER 0.1 mM 12.1 nm = 2.07, 27.3 nm = 1.86, 46.6 nm = 1.52.	Cell death cause by both necrosis, followed by apoptosis
Chithrani <i>et al.</i> , 2010	14, 50, 74	Anhydrous citric acid	Hela cells	24 H $7 \cdot 10^9$ NP/ml Triplicate	Gulmay 4.7 Gy/min 105 kVp 2.3 Gy/min 220 kVp. 137Cs irradiator 660 kV. 6 MV beam 600 MU/min, LINAC Dose of 2-4-6-8 Gy	SERs calculated at 10% survival SER 105kV = 1.66 SER 220 kV = 1.43 SER 660 kV = 1.18 SER 6 MV = 1.17 DSB observed after irradiation with 220 kV and 6 MV X-rays (75 foci per cells with NPs compared to less than 50 without).	50 nm AuNPs best effect with radiotherapy and best cellular uptake (6000 NPs/cell for 50 nm compared to less than 3000 for the others)

Reference	Size (nm)	Coating	Cells	NPs exposure	Radiation	Radiosensitisation	Uptake/other
Geng <i>et al.</i> , 2011	14.3 7 ± 2.49	Thio-glucose	SK-OV-3	5 nM, 24h	90 kVp x-rays (Faxitron x-rays); 6 MV photons, (linear accelerator)	SER 5Gy using 90 kV = 1.43 SER 5Gy using 6 MV =1.37	Better uptake for thio-glucose AuNPs (9.3.10 ³ NPs/cells) compared to naked AuNPs (8.0.10 ³ NPs/cell).
Zhu <i>et al.</i> , 2015	20	Galactose-PEG	HEP-G2	1 µg/ml, 24h TriPLICATE	6 MV X-ray LINAC 2-4-6-8 Gy	SER= 1.95	Best uptake in cells reached after 8h for Gal-PEG-NPs (30000 NPs/cell) and in a higher amount than non-coated AuNPs (<5000 NP/cell).
Joh <i>et al.</i> , 2013	23	PEG	U251 glioblastoma cell line	1 mM, 24h	4 Gy, 150 kVp	SER = 1.3	1.7 increase of Y-h2ax density for AuNPs+RT compared to RT alone
Ngwa <i>et al.</i> , 2013	50	Methyl polymer	Hela cells	0.2 mg/ml 24 H	Gamma photon, I-125 brachytherapy 2.1 cGy/hr to 4.5 cGy/hr	Biological effect 2.3 times greater when cells were irradiated with AuNPs than with radiation alone. DEF over 3.5	Not measured
Jeynes <i>et al.</i> , 2014	50	FBS TaT peptide	RT112	5.5 µg/ml 4 H TriPLICATE	3 MeV protons 250 kVp Gulmay X-ray machine	300 % decrease of survival after 5Gy of 250 KvP X-ray irradiation and TaT NPs present, compared to the control. No significant different after irradiation with 5 Gy of 3 MV proton irradiation.	NPs localised in the cytoplasm, close to the nucleus. TaT peptide increases the number of NPs/cell (5000 NP/cell with the peptide compared to 1000 NP/cell without)

Reference	Size (nm)	Coating	Cells	NPs exposure	Radiation	Radiosensitisation	Uptake/other
Khoshgard <i>et al.</i> , 2014	52 ± 11.5 47 ± 8.2	Folate-conjugated AuNPs, PEG-AuNPs	Hela	50 µM 6-12-24-48 h Triplicate groups	Co-60 γ-rays 2 Gy X-rays 120-250 kVp	Radiosensitisation better for X-rays than for γ-rays. The best DEF (1.67) is obtained with 180 kVp	The folate-AuNPs give a better cell targeting (35000 NPs/cell compared to less than 10 000 for PEG AuNPs).
Nicol <i>et al.</i> 2018	28.7 nm 45.9 nm	PEG (AuNP-P) PEG + peptide (RME ;H5 WYG) (Au-DP)	MCF-7 MCF-10A MDA-MB-231	25 µg/ml 24h	160 KvP X-rays 0-6 Gy	MCF-10A no radiation dose enhancement MDA-MB-231 cells SER = 1.19 for AuNP-DP. SER = 1.25 for AuNP-P SER = 3.19 for AuNP-DP at 4 Gy AuNP-DP significantly sensitized MCF-7 SER of 2.57 at 6 Gy.	AuNP-DP resulted in maximum nanoparticle internalization (10 times more than AuNPs P) and increase DNA damage (gamma H2AX) by 1.7 compared to radiation alone.
Ma <i>et al</i> 2017	50 nm	AuNPs, nanospikes and nanorod coated with PEGs (FITC labelled nano-materials for uptake)	KB cancer cells	50 µg/ml 24h	6 MV X-ray irradiation	1.62, 1.37, and 1.21 corresponding to the treatments of AuNPs, nanospikes and nanorods	AuNPs showed the best uptake after 24h compared to the other forms (side scatter intensity 1.2 higher for AuNPs compared to nanospikes and 1.5 higher compared to nanorods)

So far, clear enhancement ratios linked to radiosensitisation, have been shown for kilovoltage X-ray radiotherapy, where the photoelectric effect dominates (e.g Section 1.8). However, megavoltage irradiation gives much less of a radiosensitisation effect (Burger *et al.*, 2014b, Jain *et al.*, 2011, Wang *et al.*, 2013). There is a clear benefit of combining AuNPs with radiotherapy, nonetheless, it remains difficult to understand the best properties and concentration to obtain an efficient radiosensitisation effect on the cancer tissues.

1.15. Improvement of the radiosensitisation effect by targeted AuNPs

As mentioned before in Sections 1.3 and 1.11, NPs are interesting in combination with radiotherapy and many parameters impact on the radiosensitisation effect. The concentration of AuNPs in the cancer tissue plays an important role in radiotherapy improvement (Babaei and Ganjalikhani, 2014a, Mesbahi et al., 2013). Numerous strategies have been used to increase the concentration of AuNPs inside cells and one of them includes the use of coatings to improve biocompatibility and uptake (Babaei and Ganjalikhani, 2014b, Retif et al., 2015). With the proper coating, increasing the uptake, but not interfering with the release of secondary electrons, it is possible to improve the radiosensitisation effect (Gilles *et al.*, 2014, Zhu *et al.*, 2015).

AuNPs coated with sugar have already been shown to have a radiosensitisation effect (Geng et al., 2011, Babaei and Ganjalikhani, 2014b), using both kilovoltage and megavoltage X-ray radiotherapy. Kong *et al.* have shown that glucose AuNPs increased the radiotherapy effect, especially with 200 kV X-ray radiation, and more efficiently for breast cancer cells, where AuNP uptake is higher than for normal breast cells (Kong T *et al.*, 2008).

Among the different types of cancers, glioblastoma multiforme is the most common and aggressive brain cancer (Setua *et al.*, 2014). It is difficult to treat because of the blood brain barrier which protects the brain from any contamination and is therefore a barrier to numerous treatments. Joh *et al.* found that AuNPs in glioblastoma cells enhanced their radiation effect *in vitro* but also increase the survival rate in mice with glioblastoma tumours (Joh *et al.*, 2013). In addition, Setua *et al.* found that polyethylenimine AuNPs inside glioblastoma cells from patient samples were able to increase the radiotherapy cytotoxicity, shown by the increase of DSBs. However, when observing the cell viability 25 days post-irradiation, among the three samples of glioblastoma from different patients investigated, one developed resistance to the treatment. Their new strategy of treatment involved AuNPs functionalisation with cisplatin and this specific combination with radiotherapy resulted in a higher damage and toxicity, and abrogated radioresistance of the different glioblastoma cells explored (Setua *et al.*, 2014).

One promising strategy to improve AuNPs uptake specifically in cancer cells, and therefore increase the radiosensitisation effect, is to use active targeting, where AuNPs are coated with specific molecules that strongly bind to their target in the cells (Kodiha *et al.*, 2015). By using specific coatings such as DNA, it is possible to increase the amount of gold per cell, preferentially in the cancer cells and therefore to improve the effect of radiation (Burger *et al.*, 2014b).

Wolfe *et al.* in 2015 have shown a radiosensitisation effect of luteinizing hormone releasing hormone (LHRH) coated AuNPs combined with megavoltage X ray irradiation because of higher accumulation in PC-3 cells than non-coated AuNPs (Wolfe *et al.*, 2015).

Recently, improvements have been made on the NPs entrance in the cell nucleus, not only as a drug delivery vehicle but also to improve the radiosensitisation effect as, the closer the NPs to the DNA, the bigger the radiosensitisation effect (Brun *et al.*, 2009b). Several works have involved specific coating such as oligonucleotides, nuclear localisation sequence (Fan W *et al.*, 2015), nuclear membrane disruptors (Setua *et al.*, 2014) in order to target and enter the cell nucleus. As mentioned before, very few studies have been done on the radiosensitisation of nuclear targeted AuNPs (Fan W *et al.*, 2015). Specific signalling sequence were used to improve the uptake, however, targeted sequences allowing gene silencing, especially via a triplex sequence, have never been tested in addition to radiotherapy and could be of interest as novel radiotherapy strategies.

Moreover, additional coating on the NPs to aid the nucleus entry requires a careful design. Indeed, the coating can impact on the radiosensitisation effect by decreasing the release of the electrons from the bulk of the NPs to its surface (Haume *et al.*, 2016b). Not many studies take into account the chemistry of the AuNPs and its intrinsic properties to radiosensitise the cells.

1.16. Aim/Goals of the research undertaken in this thesis

As mentioned before, cancer is one of the major leading cause of non-communicable death in developed countries worldwide and a major health public concern (McMullin, 2016). Effort have been done trying to improve cancer treatment and nowadays, radiotherapy is one of the major treatment methods, but has limitation due to the potential damage to healthy tissue and the lack of tumour selectivity toxicity (Zolotoyabko, 2014). The work presented in this thesis focuses on the radiosensitisation potential of AuNPs, improving the selectivity of radiotherapy to cancer tissues, with main aims of investigating cellular uptake and localisation of coated AuNPs in cancer and normal cell lines, and better understand their radiosensitisation potential using clinical X-ray sources. Many studies presented use quite significant concentration of AuNPs (mM) (Joh *et al.*, 2013, Zhang *et al.*, 2012). However, for reproducibility and to be able to develop NPs at clinical level, it will be interesting to explore radiosensitisation effect using less material and many studies are going in this direction using nM concentration (Geng *et al.*, 2011, Wang *et al.*, 2013).

Moreover, very limited work have successfully shown a specific radiosensitisation effect toward cancer cells without affecting the healthy counter cells (Butterworth K.T *et al.*, 2010,

Kong *et al.*, 2008). It is critical to obtain more information on the selectively of effect between cancer cells and normal cells. However, this is difficult to achieve, especially as *in vitro* models have limitation in representing the tumour environment. Indeed, many criteria impact the development of a tumour such as the blood flow and microvessel development, the different cell type and their interconnections, the inflammation and oxidative stress (Wu and Swartz, 2014). These process such as blood flow, inflammation and interconnections between cells are difficult to mimic *in vitro* and need to be taken into account when interpreting radiosensitisation effect and NPs exposure (Wu and Swartz, 2014).

This thesis contains six different chapters, with the first one being the introductory chapter, which has presented several radiosensitisers to improve radiotherapy efficiency, as well as NPs characteristics used in radiotherapy and their effect on cells.

The second chapter of this thesis will detail the experimental plan followed to explore the AuNPs as radiosensitisers. After characterising the size, the charge, and the coating on top of each AuNPs, the toxicity toward different cell models was studied. Skin and breast models, including both cancer and normal cells were chosen to explore the radiosensitisation of both kilovoltage and megavoltage X-ray radiotherapy. Breast cancer is the most frequently diagnosed cancer and the leading cause of cancer death in women, with 1.7 million cases and 521,900 deaths in 2012 (Torre *et al.*, 2015), while squamous cell carcinoma is the second most leading cause of chronically sun exposed skin cancer, with more than 1 million cases diagnosed in United States each year (2014). Although very common, it is also treatable if diagnosed early (2014). Different *in vitro* assays, including the well-known clonogenic assay, were used to characterise the toxicity of the different AuNPs and their mechanism of action. Possible involvement of oxidative stress, as well as apoptosis related cell death were explored. Plasmid DNA and different associated sequences were also used to explore the mechanism of action and interaction of oligonucleotide coated AuNPs with the sequence targeted in the DNA of the cell. It is important for future radiotherapy and to obtain a better understanding of toxicity, to have information of the uptake of the different AuNPs and their localisation inside cells. Electron microscopy have been used in this thesis to provide information of the localisation of AuNPs inside cells, as well as mass spectrometry to provide the general amount of gold per cell. Finally, after acquiring all these information, the potential radiosensitisation of these AuNPs were observed, both outside cells, using the coumarin assay, which provide data on $\cdot\text{OH}$ production after irradiation in the presence of AuNPs in solution, and inside cells using linear quadratic models and measuring the survival fraction of the cells.

In the third chapter, the results of the exploration of αGal :PEGamine AuNPs will be presented. These AuNPs were coated with a sugar in order to selectively target the cancer cells as they generally need more nutrient than normal cells to survive (Hu C *et al.*, 2015). The

PEGamine group was used as a biocompatible to stabilise the NPs from aggregation and increase its lifetime in the circulation (Pissuwan *et al.*, 2011). Not only increasing the NPs stability, PEGamine is composed with an amine group, which brings a positive charge onto the AuNPs, known to potentially interact with the cell membrane and increasing the AuNPs uptake in cells (Marquez *et al.*, 2004). After exploring different coating on the AuNPs, in term of stability and toxicity, the ones which gave the best uptake and selective toxicity toward cancer cells only were chosen for radiosensitisation exploration. AuNPs were combined with radiation and the effect were measured outside and inside the cells.

In the fourth chapter, detailed about the TFOs used for coating the AuNPs will be presented. The interaction of the oligonucleotide only and the triplex formation with the sequence target was explored *ex vivo*, using designed sequences of DNA, as well as *in vitro* in plasmid DNA. The characterisation of the oligonucleotide sequences, as well as the AuNPs coated with these oligonucleotides, and their potential to interact and form a triplex will be presented *ex vivo* and *in vitro* in plasmid DNA and in cells. Then, the AuNPs potential toxicity and uptake in cells will be described, before looking at their radiosensitisation effect outside, and inside the cells.

In the fifth chapter, preliminary results of the use of cerium oxide NPs as radiosensitisers will be presented, with a brief description of the NPs characteristics and their effect of cells.

The final chapter of the thesis will present a general conclusion from the work described, and the future lines of experiment to complete this work.

CHAPTER 2: MATERIALS AND METHODS

In order to improve radiotherapy efficiency, various AuNPs have been developed to interact with the beam of X-rays. As discussed in the first chapter, depending on the size, surface charge and coating, the AuNPs can have different properties. Therefore, all these criteria were taken into account when designing the AuNPs.

The first type of AuNPs was designed in collaboration with Midatech Pharma[®] (Abingdon, UK). For simplification, the company will be called Midatech in the rest of the thesis. The AuNPs have a diameter size of 2 nm and are coated with various types of sugars and a PEGamine group. The second type of NPs was designed in the laboratory at the Open University, in collaboration with BBi[®] Company, having a diameter size of c.a. 3.7 nm and are coated with 4,4'- (Phenylphosphinidene)bis(benzenesulfonic acid) dipotassium salt hydrate, named phosphine (PN) for simplification, further in the thesis, and/or a short sequence of DNA.

The [®] sign indicating the trade mark of a company will be noted only once after each introduction of a new product. Moreover, all the consumables used for the experiments are listed in Annex 1.2.

2.1. Different AuNPs used in this project

2.1.1. Nanoparticles coated with sugar and PEGamine

In order to explore the effect of the coating and the charge of the AuNPs on cells, (the results are described in Chapter 3), different AuNPs coated with either a sugar or a PEGamine were designed, in collaboration with Midatech, with different input ratios (100:0, 80:20, 60:40, 50:50, 40:60, 20:80, 0:100) of HS-C2-sugar (α -galactose derivative, β -glucose derivative, or N-acetyl glucosamine derivative) and 1-amino-6-mercapto-hexaethyleneglycol (PEGamine), as described previously (Lund *et al.*, 2011). All AuNPs concentrations can be found in Annex 1.1 recorded as the gold mass in water. A schematic view of coated AuNPs can be found in Figure 2.1.

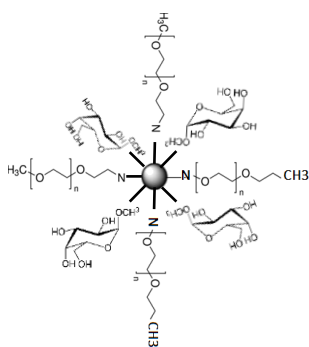


Figure 2.1: Diagram of the ligands on the AuNPs.

2.1.2. Nanoparticles coated with oligonucleotides

Triplex forming oligonucleotide coating was chosen to improve the cancer cell targeting and bring a dual action of gene-silencing on top of radiotherapy, which have never been done before. In order to prepare AuNPs coated with oligonucleotides, described (for experiments described in Chapter 4), gold colloid NPs of 3.7 nm were used, specially made by BBi company (CC.T00543.5NM). 3.7 nm was chosen as an average size between 2 and 5 nm, in order to visualise them for characterisation and to optimise the oligonucleotides attachment on the AuNPs. They are composed of approximately 1,547 gold atoms per NP and have a mass of 5.12×10^{-19} g (308.3 kDa).

The concentration of coated BBi NPs with different molecules was measured by absorbance using the Beer Lambert Law (Rahman, 2016, Taton, 2001):

$$c_n = \frac{A_{520} \times d}{\epsilon_n \times b}$$

where $\epsilon_n = 4.7 \times 10^6 \text{ M}^{-1} \cdot \text{cm}^{-1}$ is the molar extinction coefficient measured at 520 nm, d the dilution factor, b is the path length of the cuvette and is in our case $b = 1 \text{ cm}$.

The molar extinction coefficient value described in Section 4.2.2 was predicted from the estimated extinction coefficients of other sizes of AuNPs size (Figure 2.2).

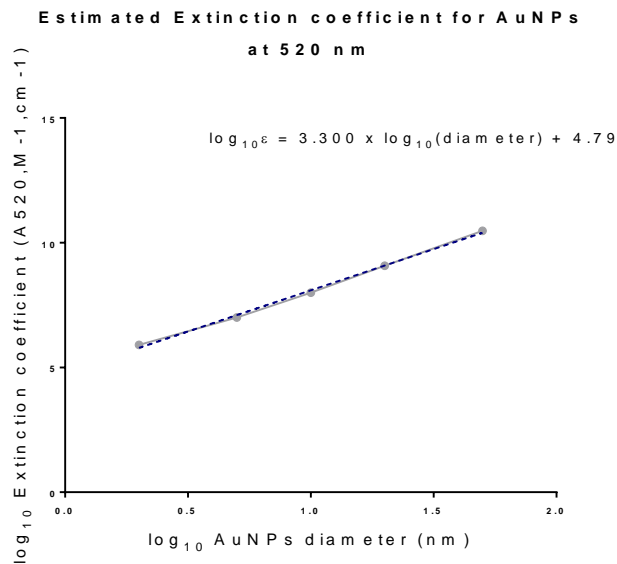


Figure 2.2: Curve representing the extinction coefficient versus the NPs diameter size.

Estimated value for 3.7 nm size: $\log_{10}(3.7) = 0.568$

$$\log_{10}(\epsilon(0.568)) = 6.667$$

$$\epsilon = 10^{6.667}$$

$$\epsilon = 4.7 \times 10^6 \text{ M}^{-1} \cdot \text{cm}^{-1}$$

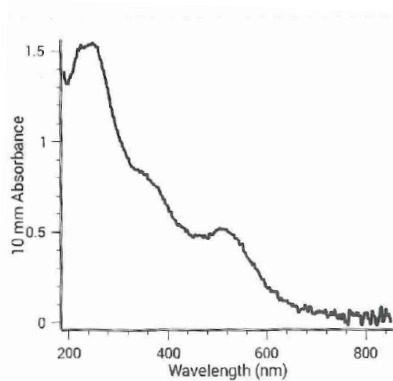


Figure 2.3: UV-VIS spectrum of 3.7 nm citrate (BBi) AuNPs sample. The Surface Plasmon resonance (SPR) peak occurs at 512 nm.

As well as measuring the concentration of the AuNPs by absorbance (Figure 2.3), the AuNPs were also characterised by measuring the gold content in each sample. In order to measure the concentration in g/L, a gold assay was set up using different volumes (up to 10 μ l) of gold standard for AAS (Sigma Aldrich[®], 08269-100 ml) and the different samples, diluted in 20 μ l of water. The gold samples were then incubated in 30 μ l of 50 % HCL/50 % nitric acid, diluted in water, in order to fully dissolve gold. After adding 150 μ l of 2M sodium bromide (NaBr, Sigma, 229881-10G) solution, the absorbance at 390nm of each sample (triplicate) was measured using the Microplate reader (BMG Labtech[®], FLUOstar Optima) and the concentration of each sample determined using a gold standard curve. The results of these AuNPs characterisation is described in Section 4.2.3.

Oligonucleotide-coated NPs were made following the protocol from Taton, 2001 (Taton, 2001) and described in Section 4.2.1. First, 4ml of citrate AuNPs provided by BBi were concentrated using a 10 kDa molecular weight cutoff centrifugal filter (Merck Millipore[®], UFC801008) at 4400 rpm for 20 min. After measuring their concentration by UV-Vis absorbance, the AuNPs were then incubated with 0.1 M phosphine (PN) (4,4'-(Phenylphosphinidene)bis(benzenesulfonic acid) dipotassium salt hydrate (Sigma, 479497-1G) solution, at a molar ratio of 2:1 for 14 h at 25 °C in order to exchange the ligand on the AuNPs. PN, due to its size and charge, restricts the number of DNA attachment sites and can therefore be used to control the DNA ligand coating density (Taton, 2001). In order to remove PN excess, the AuNPs were spin washed in a 10 kDa molecular weight cut-off spin filter (Merck Millipore, UFC201024) at 3000 rpm for 45 min. Oligonucleotides containing a 5'-trityl group on a 6-carbon spacer (detailed in Section 4.1), were deprotected (detached from the spacer), in order to activate the thiol group and allowed to form a strong covalent bond with the AuNPs, following the protocol of Storhoff *et al.*, 1998 (Storhoff *et al.*, 1998). Since the thiol group is highly reactive,

the deprotection needs to be performed immediately before incubation of the oligo of interest with the AuNPs. Briefly, the oligonucleotide sequence of interest was diluted in 100 μ l of 0.1 M triethylammonium acetate buffer (TEAA, Fluka analytical[®], 90357-100ml). Then, in order to cleave the protecting group from the thiol, 15 μ l of 1 M silver nitrate (AgNO_3 , Sigma[®], S6506-25g), was added (the solution turns white), and the mixture was incubated for 30 min at room temperature (RT). To remove the excess of AgNO_3 after reaction, 20 μ l of 1 M DL-dithiothreitol (DTT, Sigma, 43816-50ml) was added and incubated for 5 min at RT (the solution turns yellow). The solution was then centrifuged to wash away the protecting group, and the remaining oligonucleotide-containing solution was purified on a NapTM-5 Column Sephadex[®] G-25 DNA grade (GE healthcare illustra[®], 17-0853-01) via elution with ultrapure water (UHP water). The purified oligo was then used to coat the AuNPs. The amount of oligo to add to the AuNPs solution was calculated by multiplying the surface area of the AuNPs available for the conjugation by the expected surface density of AuNPs-bound oligonucleotide, which is around 35 pmol/ Au^2 (Taton, 2001). A different quantity of oligonucleotides excess in molar concentration (1-10 excess) to the one calculated previously were incubated with the AuNPs for 20 h and described in Section 4.2. The final AuNPs were then washed by mixing UHP water and filtered using Amicon Ultra-2 (10K) centrifugal filter at 3000 rpm for 45 min. For each step, the concentration of each different AuNPs was measured using a NanoDrop 1000 Spectrophotometer (Thermo fisher[®]).

2.1.3. Non-coated nanoparticles of 2 nm diameter size

2 nm size AuNPs are often used to explore the radiosensitisation effect in cells (Bobyk *et al.*, 2013, Butterworth *et al.*, 2010, Jain *et al.*, 2014). They are a standard size in radiosensitisation efficiency. Therefore, in order to compare the effect of the AuNPs with different coating, a control gold colloid NPs of 2 nm was selected, also purchased by BBi company (EM.GC2). They are composed of approximately 244 gold atoms per NP and have a mass of 8.08×10^{-20} g (48.7 kDa).

2.1.4. Characterisation of the different AuNPs

For characterising the different AuNPs in solution and defining their size, Transmission Electron Microscopy (TEM) was used. TEM was chosen as it allows to measure the core size of single NPs and give information of the NP distribution and potential aggregation, within a reasonable amount of time. Moreover, this technique, mentioned in Section 1.3, explores more precisely the uptake and localization of AuNPs inside the cells. The AuNPs were deposited either on carbon or copper grids, and 1 μ L of sample was used. The samples were left to dry overnight

before electron microscopy. AuNPs (triplicate samples) were analysed using a JEM-1400 microscope (JEOL[®], USA) (Figure 2.4) at an accelerating voltage of 80 kV and a magnification from x50 000 to x200 000. Nanoparticle size was measured from thresholded TEM images using ImageJ[®] software. ImageJ analysis give data on the area values of the NPs. The raw data were then extracted into an excel sheet and the average diameter of the AuNPs calculated from the area values from the 2D images, assuming that each AuNPs shape is a sphere, where the area is $A = \pi r^2$ and therefore the *diameter* = $(\sqrt{A/\pi}) \times 2$ (Gromnicova, 2017). These experiments are described in Sections 3.1, 3.3 and 4.2.1 of the result chapters.

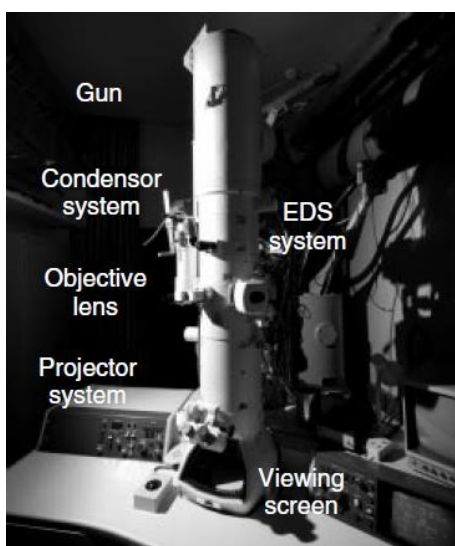


Figure 2.4: Transmission electron microscope (TEM) used in the experiments (Kleebe *et al.*, 2012).

Dynamic light scattering (DLS) was used to measure the hydrodynamic size of the nanoparticles ($\sim 100 \mu\text{g/ml}$), using a zetasizer (NanoZSP, Malvern Instruments, using a DTS1070 cell). This technique does not need using lots of material and can give information not only on the NP size but also its surface charge. Indeed, as well as the size, the zeta potential values of the different AuNPs were measured in 3.2% PBS pH 7.4 (for the sugar:PEGamine coated AuNPs) or in UHP water (for oligonucleotide coated AuNPs), using the same instrument. About $100 \mu\text{l}$ of each AuNP was diluted in 1 ml of solution and measured three times by the zetasizer. The results from these techniques are described in Sections 3.3 and 4.2.1.

In order to characterise the DNA and PN coated AuNPs, and especially looking at the different coatings, X-ray photoelectron spectroscopy (XPS) was used. XPS was chosen among other microscopy techniques (TEM, SEM) or infrared spectroscopy as it gives quantitative information on the elemental characterisation of an entire solution of NPs and with a very small quantity of material. These experiments were done only once, using about $10 \mu\text{l}$ of material, and give indication on the AuNPs composition.

XPS allows to determine the elemental composition of a sample, and for example the coating of AuNPs, as well as the chemical and electronic state of these elements. The different spectra of the samples were generated by irradiation with a beam of X-rays, which ejects photoelectrons of specific energies from the sample, which is further analysed using Casa XPS software[®]. The results from these techniques are described in Section 4.2.3.2 of the result chapter and in Annex 3.5.

2.1.5. Description of the different oligonucleotide sequences used

The different oligonucleotide sequences used in Chapter 4 were purchased from Sigma.

dR1 and dY2 are both *c-myc* promoter 2 sequences, complementary to each other and therefore can form a duplex. Both these sequences are used for the experiment described in Section 4.1. This specific part of the *c-myc* gene is known to be able to form a triplex structure, due to its high amount of purine groups (Huo *et al.*, 2014). They have a length of either 23 bp, which corresponds to the length of the TFOs sequences, or 70 bp in order to explore the potential triplex formation depending on bigger DNA length. These different sequences are used for the triplex characterisation in Section 4.1.3 and 4.1.4.

- dR1 (23): 5'-TCCCTCCCTCCGTTCTTTTCCC-3' and

- dR1 (70)

5'-AACCGGCTTTATACTCAGCGCATCCCTCCCTCCGTTCTTTTCCCGCCAAGCCTCTGAGAAGCCCTGC-3'

- dY2 (23): 5'-GGGAAAAAGAACGGAGGGAGGGA-3' and

- dY2 (70)

5'-GCAGGGCTTCTCAGAGGCTTGGCGGGAAAAAGAACGGAGGGAGGGAATCGCGCTGAGTATAAAAGCCGGTT-3'

Both dY3 and PR are sequences targeting *c-myc* sequence via a triplex formation. The dY3 sequence is designed to form a reverse Hoogsten pairing, described in Section 1.9, via guanosine-guanosine-cytosine (G(GC) and thymine-adenine-thymine (T(AT))) structure. The PR sequence is designed to form the same pairing via (G(GC) and (A(AT))) structure. The 5'-trityl group on the 6-carbon [ThioC₆] on the 5' end of the sequences is used for the attachment on the AuNPs, while the biotin molecule (fluorescence group), also on the 5' end is used to explore the interaction of the oligonucleotide to its complementary sequence (forming a duplex). The biotin group is used for the experiment described in Section 4.2.4 on the AuNPs characterisation. Below is a list of the different oligonucleotides used.

- dY3: 5'-TGGGTGGGTGGTTTGTTTTTGGG-3'
- dy3 modified with biotin molecule in the 5' side or with a thiol [ThiC₆]
- dY3 complementary: 5'-biotin-CCCAAAAACAAACCACCCACCCA-3'
- dY2: 3'-AGGGAGGGAGGCAAGAAAAAGGG-5'
- PR: 5'-AGGGAGGGAGGGAAGAAAAAGGG-3'
- PR modified with 5'-biotin or with 5' [ThiC₆]
- PR complementary: 5'-biotin-CCCTTTTCTTGCCTCCCTCCCT-3'
- GFP control: 5'-AATATCGCGACAGAAGACG-3' and modified with 5' [ThiC₆] or not.

Finally, GFP is a negative control sequence, of similar length to the other oligonucleotides, which is not present in the human genome. It was used to explore the effect of the different oligonucleotides on cells, described in Section 4.4. It was chosen as already designed and well-characterised by another colleague from the Open University laboratory. The concentration and purity of each oligonucleotide sequence was assessed by UV-Vis absorption measurement (Table 2.1) using a NanoDrop 1000 Spectrophotometer. Once again, this technique allows with a very small amount of material (1 µl) determining the concentration of gold in solution. The absorbance at 260 nm is used to measure the concentration of DNA, while the absorbance at 280 nm is used to measure any impurities and at 230 nm any traces of salt in the solution. The two ratios:

$$Purity\ ratio = \frac{A_{260}}{A_{280}} \qquad \qquad \qquad Turbidity\ ratio = \frac{A_{260}}{A_{230}}$$

are used to evaluate the presence of any contaminants such as proteins or phenols, or to explore the presence of salt in the solution respectively.

A sample will be considered pure with a purity ratio around 1.8, while it will be considered exempt of any salt with a turbidity ratio > 1.5.

2.2 Gel electrophoresis for DNA sequences interaction experiments

2.2.1 Agarose gel

Agarose-gel electrophoresis is a useful technique to separate samples on the basis of their sizes and charges in an electric field. It is also efficient for samples with a molecular weight heavier than 100 kDa. Not only separating different samples, it can give semi-quantitative information using images software, and in small amount of times, compared to chromatography or immunoblotting. It was used principally in this work to explore plasmid DNA, described in Section 2.5. Since DNA is negatively charged, its migration through the gel is inversely proportional to the size of the sample. However, the electrophoretic mobility of DNA samples or molecules in the gel can be also modified by their shape, the agarose concentration, the electrophoresis buffer, the temperature and the applied voltage. In order to load the samples; this thesis work used a 6x loading dye made with 0.25g of xylene cyanol (Sigma, X4126-10g), 0.25g of bromophenol blue (Sigma, 114391-5g), 0.25g of cresol red (Sigma, 114472-5g), 30 g of glycerol (Sigma, G5516-100 ml), mixed with 100 ml of UPH water and autoclaved.

To analyse the different gels, Image J[®] software was used. Briefly, using digitised UV transilluminator images of the gels (Syngene[®], G:Box), the different bands were selected using rectangular marque tool and the intensity of each band recorded. Then the different band intensities for each sample were expressed as a percentage of the total intensity in order to quantify the different samples of DNA. The gel analyses are described in Sections 4.1.4, 4.5 and in Annex 3.

2.2.2. Polyacrylamide gel

Polyacrylamide gel (PAGE) electrophoresis is also a useful electrophoresis technique to separate samples on the basis of their charge and size. PAGE allows separating samples of much smaller size than the agarose gel and this will specifically depend on the percentage of the gel, which generally varies from 5 % (for separation of 100 bp) to 20 % (for separation of 10 bp). PAGE was therefore used for oligonucleotides explorations, described in Sections 4.1 and 4.2. A dilution of 30% Acrylamide/bis-acrylamide (Sigma, A2792-100 ml) was made in water and 5x Tris-Borate- MgCl₂ (TBM). After adding 20 mg of Ammonium persulfate (APS, Sigma, A3678-25g) and 10 ul of N,N,N',n'-Tetramethylethylenediamine (TEMED, Sigma,T7024-25ml), the solution was gently mixed and poured into empty cassettes mini-PROTEAN[®] (Bio-rad[®], 4560003) for

making cassette gel. To load the samples and analyse the gel, the same procedure as the one described in Section 2.2.1 was applied.

2.3. Oligonucleotide/DNA triplex formation

To explore and characterise the duplex and triplex formation described in Section 4.1, 20% polyacrylamide gels were used.

The two-single strands, designed to form a duplex of DNA were incubated at 1 μ g/ml, 20 μ l each, diluted in DNase free water for 5 min at 95°C and then for 1h at room temperature. In order to incubate the duplex sequences with the TFOs and run them onto the gel, the protocols from McGuffie *et al.*, 2000 (McGuffie *et al.*, 2000) and Sedelnikova *et al.* 2001 (Sedelnikova *et al.*, 2001) were followed.

The 23 bp oligonucleotide sequences dY3 or PR were loaded with either plasmid DNA or duplex sequences, containing 50% of incubation buffer (50 mM Tris,HCl, pH 8, 10 mM magnesium chloride (MgCl₂, Acros organics[®], 223210010), 50 mM NaCl). The samples were then run in 1x TBM buffer, from a 5x TBM stock solution, at pH8 plus 2-4 μ L of 6X loading dye (Thermofisher, R0611). The gel was pre-run for 1 h at 8 V/cm and then the samples run for 2-4h at 8 V/cm in 1x TBM buffer at 4°C. At the end of the migration, the gel was incubated with Ethidium Bromide (EB) (Fisher scientific[®], BP1302-10) (100 μ L in 100 ml of TBM buffer) just before revelation under UV illumination.

2.4. Coated AuNPs characterisation and oligonucleotide interaction

These experiments were based on the protocols of McGuffie *et al.*, 2000 and Huo *et al.*, 2014 (Huo *et al.*, 2014, McGuffie *et al.*, 2000) and described in Section 4.2.1.

2.4.1. Characterisation of the AuNPs using agarose gel electrophoresis

In order to explore and characterise the coating of the AuNPs, agarose gel electrophoresis was used. Tris-Borate-EDTA (TBE) 5x buffer stock was prepared, by adding 57 g of Trizma base, 27.5 g of Boric acid and 4.65 g of EDTA, in 1 L of UHP water and autoclaved. TBE buffer was used either at 0.5x dilution or 1x dilution. The agarose gel was used either at 1-1.4% agarose (for 1h to 3h migration at between 5-7 V/cm) or 1.4% agarose (for 16h migration at 0.95

V/cm) in 0.5x or 1x TBE. After putting the gel into the electrophoresis tank, the different samples were loaded into the gel in a loading buffer.

In some experiments, the AuNPs (about 20 μ l) were incubated in 1x Tris-Borate (TB), prepared in the same way as TBE buffer but without adding EDTA, with duplex sequences of interest of 23 bp, in the presence of 1 mM $MgCl_2$ for 3h, and single strand oligonucleotide complementary to the sequence of interest for 1 h, to explore any possible interaction.

The AuNP samples in the presence of DNA could migrate into the gel. For experimental with samples in the presence of DNA duplexes, the gel was incubated with Ethidium Bromide (100 μ L in 100 ml of TB buffer) just before revealing the gel under UV, or normal light for the one containing only coated AuNPs.

2.4.2. Characterisation of the oligonucleotide attachment with electrophoretic mobility shift assay (EMSA)

An EMSA assay was used to explore the oligonucleotide coating the AuNPs using the biotin probe (complementary to the sequence of interest), experiment described in Section 4.2.3. This technique is very sensitive and allows to detect the biotin recognition sequence. Compared to agarose gel, much less material was needed to obtain a response signal. The assay was made following the protocol from Male *et al*, 2017 (paper in preparation). Briefly, the samples containing oligonucleotide coated AuNPs and the oligonucleotides labelled with biotin were incubated for one hour allowing the duplex structure to form. Then the samples were diluted or not 100X in water and 1 μ l was mixed with 6 μ l of TB and 4 μ L of loading buffer. The samples were loaded into 5% acrylamide gel, pre-run at 7 V/cm and run for 50 min at 7 V/cm in 0.5 x TB. The gel was then transferred for blotting onto a membrane, at 100 V in 0.5x TB 1 h. Finally, the membrane was cross-linked under UV light and revealed with a chemiluminescence nucleic acid detection kit (Thermo scientific, 89880).

2.4.3. Characterisation of the triplex formation with the AuNPs with polyacrylamide gel

5% polyacrylamide gels were used to explore the duplex and triplex formation with the oligonucleotide sequence attached onto the NPs. As the triplex used in this work is a small sequence, it was difficult to observe any migration change using agarose gel and therefore, PAGE was prioritised for smaller sequences separation.

AuNPs coated with different ratios of dY3 sequence (about 2 μ l) were mixed with the D23 DNA duplex (about 1 μ l, ratio about 50 duplex/ 1 AuNP) in the in the presence of 1mM $MgCl_2$ in order to look at triplex formation. The gel was pre-run for 1 h at 7 V/cm and then the samples were

incubated with 4µL of loading buffer. They were run for 1h at 7 V/cm in 1x TB. At the end of the migration, the gel was incubated in EB (100 µL in 100 ml of TBM buffer) just before revelation under UV.

2.5. Plasmid culture and modification

2.5.1. Preparation of petri dishes and bacteria culture

Plasmid was prepared and used in Sections 4.1.5 and 4.5.2 of the results chapters. Two solutions of Luria-Bertani broth (LB Broth, Sigma, L3022-250g) were prepared at a concentration of 20 g/L and 7.5 g/L of agar was added into one. Both solutions were autoclaved (Meadowrose scientific LTD[®], serial n°1316). Ampicillin (Sigma, A9518-25g) antibiotic (50 µg/ml solution in ultrapure water) was sterilised with a Terumo[®] syringe without needle (Terumo, SS+01T1, 1ml) using a filter (Millex[®]HA, SLHA033SS) of 0.45 µm pore size. After sterilisation, Ampicillin was added to the warm temperature (below 36 °C) LB+agar (Sigma, A1296-1Kg) solution and poured into sterile petri dishes (Cellstar, greiner bio one[®], 628 160) to set at RT. Finally, the bacteria pBV-Luc/Del6 were streaked onto plates and incubated overnight at 37°C. All these steps were done near a flame to minimise any exterior contamination.

2.5.2. Incubate single colonies of bacteria

After the incubation, single colonies of bacteria were picked for amplification. Each colony was inoculated in LB solution containing ampicillin antibiotic for 4 h at 37°C while shaking at 1000 rpm. After 4 h, 1 ml of this solution was added to 100 ml of LB solution and the bacteria were incubated again for 14 h at 37°C while shaking.

2.5.3. Drying bacteria and DNA extraction

The amplified bacteria were centrifuged at 4°C for 30 min. The resulting bacterial pellet was dried for at least 1 h. The plasmid of interest was then extracted from the bacteria using a Qiagen plasmid mini kit (Qiagen[®], 12123) and cleaned. The collected DNA pellet was then air dried and dissolved again in water of pH 8, adjusted with NaOH. The concentration of DNA and its purity was measured on the nanodrop and the DNA samples aliquoted and kept in the freezer at -20°C.

2.5.4. Plasmid endonuclease digestion

Plasmid pBV-Luc/Del-6 (Addgene[®], 14969) is circular and double stranded and its size is about 4900 bp. It comes from the pBV-Luc plasmid (4867 bp) where the *c-myc* promoter (442 bp) was inserted between the cloning sites XhoI (which was destroyed) and PvuII (Figure 2.5).

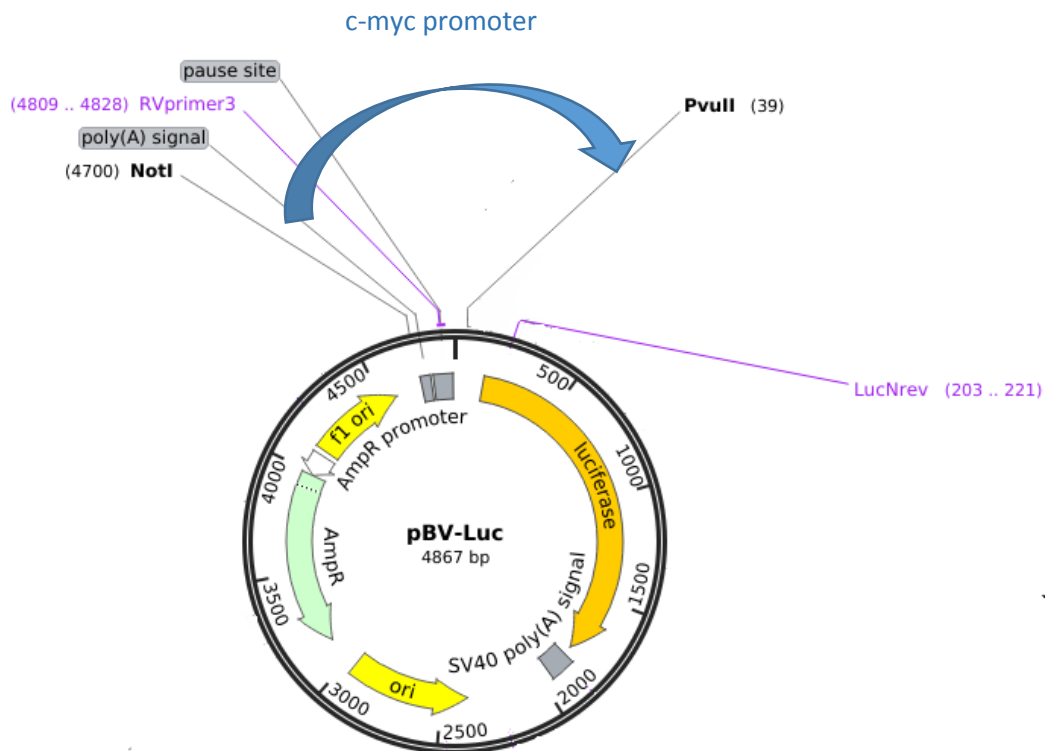


Figure 2.5: Map of pBV-Luc/Del-6 plasmid and schematic view of the insertion del6 (Addgene[®]).

Plasmid DNA can exist in different topological conformations, such as supercoiled, relaxed and linear (Figure 2.6 a). Supercoiled DNA must be relaxed in order for replication to occur (Bjornsti, 1999). This relaxation happens with just one break on one of the DNA strands. Linear plasmid, however, contains one double-strand cut. All these forms of plasmid DNA can be differentiated by their relative migration on an agarose gel; where the supercoiled DNA will migrate as a single band, migrating faster than the linear, migrating faster than the relaxed form (Figure 2.6 b).

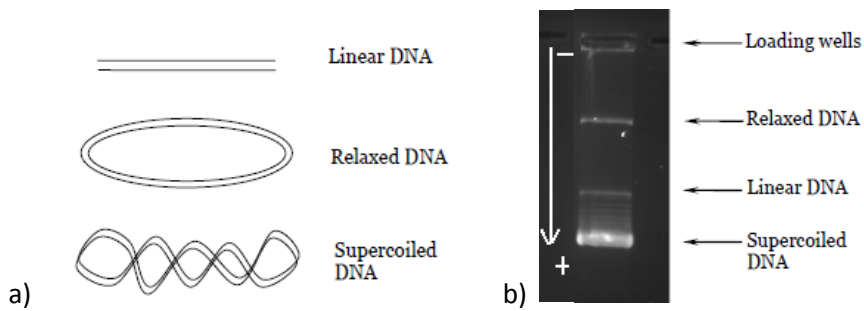
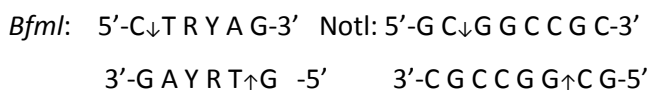


Figure 2.6: a) Schematic difference in topological forms of plasmid DNA, b) Migration difference of the topological forms of plasmid DNA on an agarose gel (Śmiałek 2007).

Each plasmid contains restriction sites that can be digested by specific endonuclease enzymes. These types of enzymes were used to try to cut the plasmid in strategic places where the TFO will get easier access to its targeted sequence. Here, the fragment of DNA including the P2 promoter of *c-myc*, which starts in position 504 and finishes in position 527 of the known *c-myc* sequence, was of interest. Therefore, two linear restriction enzymes were used, the first one, *Bfml* (*Bfml*, *Sfcl*, Thermo Scientific, ER11651, 200 U) cutting at position 454 and the second one, *NotI* (Thermo Scientific, ER0591) cutting at position 723. *Bfml* enzyme was incubated at a concentration of 10 UI/ μ g of plasmid in 1X buffer Tango for 1H at 37°C. Then *NotI* enzyme was added at an excess concentration of 40 UI/ μ g of plasmid in 2X Tango again for 1H at 37°C. Finally, the samples were heated up at 80°C for 20 min to inactivate the enzymes and stop the reaction. Through this procedure, the fragment of interest, containing the *c-myc* promoter sequence, will be about 269 base pairs long. The fragmented plasmid was used in Section 4.1.4.

The enzyme recognition sequences are, as follows:



2.6. Plasmid experiments

2.6.1. Characterisation of the different forms of the plasmid

To characterise the different forms of DNA plasmid, 1-1.4% agarose gel (for 1h to 3h migration at between 5-7 V/cm) or 1.4% agarose (Sigma, A9539-100 mg) (for 16h migration at 0.95 V/cm) were used. These experiments are presented in Section 4.1.4. The samples were run in 0.5 x TBE. Then, the gel was incubated with either SYBR Green (to detect double stranded DNA) (Sigma, S9430) (20 μ L in 150 ml of TBE buffer) or EB (to detect single or double stranded DNA) (100 μ L in 100 ml of TBE buffer) just before photographing it under UV to detect any possible DSBs.

2.6.2. Irradiation experiments of the plasmid

To explore the possible breaks on the plasmid after irradiation in the presence or absence of AuNPs, agarose gel electrophoresis was realised and presented in Section 4.5.2. Once again, this technique was chosen as, although less precise than immune-blotting or rt-qPCR, it gives in a very small amount of time a semi-quantitative information of any changes in the plasmid. Briefly, the AuNPs were incubated with the plasmid in water, at a concentration of 1/1 Plasmid/AuNPs, as described previously (Brun et al., 2009b). The samples were irradiated in collaboration with Northampton hospital with X-rays at 220 kV energies at a single dose of 10 Gy. The facilities are described in Section 2.16. After irradiation, the samples were run in a 2 % agarose gel for 1h at 7 V/cm in 0.5x TBE and the gel revealed with EB (100 µL in 100 ml of TBE buffer), to look at the possible SSBs and DSBs. The SSBs are more likely to happen on the targeted sequence of the *c-myc* promoter and were explored using polymerase chain reaction (PCR). PCR is used to amplify a DNA segment of interest to analyse a specific fragment. In this case, the *c-myc* promoter is the sequence of interest and is designed to be about 700 bp. Briefly, two primers have been chosen to amplify the *c-myc* promoter sequence, a forward primer 3'-5' RVprimer3 (CCCTGTCGGATAAAAACGATC, 409402, Tm 68°C, %GC 50, ThermoFisher) and a reverse primer 5'-3' LucNREV (CCTTATGCAGTTGCTCTCC, 409402, Tm 68°C, %GC 50, ThermoFisher). 50 ng of plasmid were incubated with 1 µL of both primer at a concentration of 10 µM, 0.2 µL of DNA polymerase, 1 µL of 10 mM deoxynucleotides (dNTP solution mix, N0447S, Biolabs®) and filled up to 20 µL with UHP water, following the protocol from Phusion High-Fidelity DNA polymerase (M0530S, BioLabs). The fragment of interest was amplified using the following thermocycling conditions: Initial denaturation at 98 °C for 30 secs, 15 cycles of: 98 °C for 10 sec, 60 °C for 30 sec, 72 °C for 15 sec, and a final extension of 72 °C for 5 min.

Finally, the different samples were run on a 2 % agarose gel for 1h at 7 V/cm in 0.5x TB and the gel revealed with EB (100 µL in 100 ml of TB buffer).

2.7. Cell lines used during the project

HSC-3 and HaCaT cells both derived from human epithelial skin tissues. They respectively represent human oral squamous carcinoma cells and keratinocytes. They were commonly used and very well characterised in the laboratory, therefore were chosen as primary model for the experiment in this work. Moreover, they can grow clonogenically which allows further exploration of the effect of radiotherapy. HaCaT cells were a gift of Erik Walbeehm, Erasmus Medical Centre, Rotterdam. HSC-3 cells were purchased from the American Type Culture Collection.

MCF-7 and MCF-10 cells are derived from human breast epithelial tissues. They are the second model used in this thesis as growing clonogenically but also widely used in combination with radiotherapy, they allow comparing effect of different NPs in previous work (Butterworth *et al.*, 2010, Kong *et al.*, 2008, Nicol *et al.*, 2018). MCF-7 cells derived from a human invasive breast ductal carcinoma. MCF-7 cells were a gift of Marilena Loizidou, University College London. MCF-10 are human non-tumorigenic mammary epithelial cell line.

MCF-10 cells were a gift of Kevin Prise, Queen's University Belfast.

2.8. Cell culture

HSC-3, HaCaT and MCF-7 cells were incubated in low glucose (1 g/l) DMEM (Gibco[®], 21885-108), supplemented with 10 % Fetal bovine serum (FBS) (Sigma Life Science[®], F9885), and 1% penicillin/streptomycin (P/S) (Gibco, 15140-122). Low glucose condition was chosen to simulate the glucose concentration of normal serum (0.7 – 1 g/l).

MCF-10 cells were incubated in DMEM/F-12, HEPES, no phenol red medium (Fisher scientific, 11039021), supplemented with 5% horse serum (Sigma, H1270-500 ml), 2.5 mM L-glutamine (Sigma, G7513), 15 mM HEPES, 1 ng/ml Cholera Toxin from *Vibrio cholera* (Sigma, C8052-5mg), 10 µg/ml insulin (Sigma, I1882-100mg), 50 µM hydrocortisone (Sigma, H0888-1 g), and 100 µM EGF recombinant human protein (Fisher scientific, PHG0311).

MCF-10 and MCF-7 were used for the experiments in Section 3.10.3. All the cells were cultivated in 75 cc culture flasks (Cellstar, Greiner bio one[®], 658170) in a CO₂ incubator (Binder[®], C150) at 37°C and 5% of CO₂. After 80% of confluence, the cells were washed with 5ml of Hank's balanced salt solution (HBSS) (Sigma, H6648), then trypsinised with 5ml of trypsin / EDTA (TE) 0.25% (Invitrogen[®], 25200056) and used for further experiments. The rest of the cells were frozen in cryotubes (Cryo.s, Greiner bio-one, 126280) containing FBS with 20% of Dimethylsulfoxide (DMSO, Sigma, D2438), and kept at -80°C in order to maintain frozen stocks.

2.9. NPs adhesion tests

These experiments are described in Section 3.6.

AuNPs were diluted to 10 µg/ml [Au] in either: low glucose DMEM (with or without serum), distilled water, ethanol (EtOH, Fisher scientific, BP28184), 5 M sodium chloride (NaCl), (Sigma, 57553-250g), or Hank's buffered saline solution. AuNPs were loaded either on glass coverslips (VWR[®], 631-0156), or directly in tissue culture plates, for 1 h or 3 h. Incubation was

performed at RT and the plates were kept humid to avoid evaporation by wrapping with a wet paper towel and aluminium foil.

Afterwards, the plates were washed with one of the previously mentioned solutions, fixed for 10 min with 4% paraformaldehyde plus 37% formaldehyde (Fisher scientific, F77-20) in 20 mM phosphate buffered saline (PBS) (Thermo Fisher, BR0014G) at pH 7.4, rinsed with water, and then 500 μ L of silver staining solution, prepared according to the silver stain enhancement kit (R-Gent, Aurion) for about 10 min in order to make the AuNPs large enough to become coloured.

2.10. AuNPs exposure and clonogenic assay

Cell proliferation and survival were quantified by clonogenic assay, which is described in the published paper Grellet *et al.* 2016 (Grellet *et al.*, 2017). Clonogenic assay is a standard assay to explore the cellular effect of radiotherapy as it allows to measure the effects on a long-term basis (days after radiotherapy), and does not need fluorescence microscopy like DSB measurements. The clonogenic assay was used in Sections 3.2, 3.4, 3.5, 3.7, 3.9, 3.10 and 4.3.1. HSC-3 and HaCaT skin cells were seeded at 300 cells/well on 24 well plates (Greiner bio one, 662160), or diluted in 500 μ L of cell medium at a concentration of 3600 cells/ml in a falcon tube for 3 hours. The cell density was evaluated using a Haemocytometer Bright-line (Sigma, Z359629-1EA) and optimized regarding the format of the plastic plates and wells used, and the well differentiated colonies obtained.

Different concentrations of AuNPs were prepared in 15 ml falcon tubes in serum containing medium. The solutions were vortexed just before exposure. Twenty-four hours after seeding the plates, the medium in contact with cells was removed and 250 μ L of the various concentrations (0.3; 1; 2; 3; 10; 20; 30; 200 μ g/ml Au) of AuNPs was added to both HSC-3 and HaCaT cells for 1, 3, 6 or 24 hours described in the section 3.2.1, and 3h for the rest of the experiments. Later, the cells were washed once with 500 μ L of cell medium and grown for 6 days in the incubator. Medium was changed every 2-3 days.

After 6 days of cultivating cells, they were rinsed once with UHP water and then stained with 500 μ L of 10 mg/ml methylene blue (Sigma, M9140,) in 50% EtOH for at least 3 h. Then, cells were washed with UHP water and immediately dried with a stream of hot air to prevent any loss of staining. Finally, colonies containing 50 cells or more were counted and colony formation expressed as a percentage compared to the control (without exposure to AuNPs).

For the exposure of floating cells, described in Section 3.7, AuNPs solutions were prepared as previously mentioned, in 15 ml falcon tubes but at double the concentration, then 250 μ L of cells in suspension was added and left in contact with AuNPs for 3 h in the incubator.

After exposure, the cells were washed twice with 5 ml cell medium and centrifuged for 5 min. Finally, the cells were seeded on plates as described and grown for 6 days. The breast cells MCF-7 and MCF-10 were seeded at 600 and 250 cells/well respectively on 24 well plates. The growth and incubation conditions remained the same as for HSC-3 and HaCaT cells.

2.11. Acute toxicity evaluation

Acute toxicity was measured in addition to the clonogenic assay to explore the effect of the NPs at different time points after exposure and the potential impact on cell cycle.

To evaluate the acute toxicity of the AuNPs, described in Section 3.9 and 4.3.2, cells were seeded at a density of 100 000 cells/well on 24 well plates or 2000 cells/well on 96 well cell culture plate, F-bottom, with lid (Cellstar, Greiner bio one, 655180). Both cancer and normal cells were then exposed to AuNPs, for 3h, and washed with medium. Thereafter, the cells were grown for 1-3 additional days before exploring the toxicity using CyQuant (Fisher Scientific, C7026) assay. CyQuant is a fluorescence assay which measures the amount of DNA in the samples, relating to the number of cells. The fluorescence of the CyQuant assay was measured at an excitation of 480 nm and emission of 520nm, using a Microplate reader (FLUOstar Optima, BMG Labtech).

2.12. Apoptosis related cell death measurements

To explore if caspase dependent apoptosis is linked to AuNPs exposure, described in Section 3.9, a general caspase inhibitor (Z-VAD-FMK) (BD Pharmingen[®], 550377) was used. This can irreversibly bind to catalytic sites of caspase proteases, especially caspase 1 and 3 and inhibits apoptosis. Once more, it can give in a small amount of time a semi-quantitative information on the apoptosis related death after NP exposure compared to blotting. HSC-3 and HaCaT cells were loaded on 24 well plates at 300 cells/well for a clonogenic assay. Antimycin A (AMA) (Sigma, A0149) was used as a positive control as this drug is known to induce apoptosis by dysregulation of the mitochondrial membrane potential (Park *et al.*, 2007).

After 24 h, cells were pre-loaded with 50 μ M of caspase inhibitor, before exposure to AuNPs at a concentration of 1 μ g/ml or AMA at a concentration of 10 μ M, in presence or absence of caspase inhibitor. After 3 h, cells were washed and let grow for 5 days. At the end of the clonogenic assay, the cell population exposed to various toxins were compared, in presence or absence of caspase inhibitor, to the relative controls.

2.13. Amount of AuNPs inside cells by ICP-MS

To quantify the AuNPs uptake into cells, described in Section 3.8.1, Inductively Coupled Plasma Mass Spectrometry (ICP-MS) was used, an analytical technique used for elemental characterisation, performed with the ICP-MS Perkin-Elmer NexION 300X[®] and analysing the data with NexION ICP-MS software version 1.4. ICP-MS was chosen as it gives information on the overall amount of NPs per cell, directly after exposure. To quantify the amount of gold inside the cells, HSC-3 and HaCaT were loaded in suspension at a density of 500 000 cells/15 ml falcon tube with different ratios of sugar coated-AuNPs for 3h. Cell were exposed in suspension and not in adherent conditions to avoid possible interaction with the plastic and falsely high gold concentration. The AuNPs concentration used were concentration which gave 50% of cell death (IC50) for HSC-3 cells. After exposure, cells were washed twice by centrifugation using a Centrifuge (DJB labcare[®], ALCPK121R) with 5 ml of serum containing medium and the cell density measured by haemocytometer. The cell pellet was dissolved in 2.5 ml of 3% tetramethylammonium hydroxide and 0.2% Triton X-100 (Acros Organics[®], 215682500). Then, 2.5 ml of 1% HCl with iridium as internal standard was added prior to the ICP-MS analysis. The amount of gold was calculated against a calibration curve ranging from 0.1 to 100 ng/ml of gold, including a blank (zero) point. ICP-MS analyses were performed in collaboration with Midatech in Bilbao, Spain and with Samantha Hammond, from the Open University.

2.14. Localization of AuNPs in cells by TEM

To complete the information given by ICP-MS on the average amount of gold content per cell, TEM was used to have information on the localization of the NPs within the cell. These experiments are described in Section 3.8.2 and 4.4 of the result chapters. To prepare the samples, the protocol from Gromnicova *et al.* (Gromnicova R *et al.*, 2013) was used. Cancer and normal cells were seeded onto Thincert cell culture insert 12 well (Cellstar, greiner bio one, 665641) at 150 000 cells per inset for overnight. The cells were then exposed to AuNPs at a concentration of 10 µg/ml for 3 h. Cells were then washed 3 times with sterile PBS, resuspended then fixed in 2.5% glutaraldehyde (25% Vacuum Distilled 100ml) (Agar scientific[®], AGR1311), in 0.2M Sorenson's phosphate buffer at pH 4 for 1.5 h. phosphate buffer was prepared by mixing 0.497g of sodium phosphate monobasic monohydrate (NaH₂PO₄.H₂O, Sigma, 71507) with 2.328 g of sodium phosphate dibasic (Na₂HPO₄, Sigma, 255793) in 100ml of UHP water. Finally, cells were washed 3 times with Sorenson's phosphate buffer, silver enhanced by freshly-prepared silver staining solution (RGENT SE-EM, Aurion, Netherlands) to stain AuNPs and processed by washes and cutting for transmission electron microscopy. Ultrathin sections were analysed at

magnifications of between x2000 and x20000. TEM tissue processing was done by the Open University Electron Microscopy Facility staff: Heather Davies, Dr Radka Gromnicova and Dr Igor Kraev. The microscopy images and their analysis were performed by myself.

In order to analyze the NPs/nm² cells within the different part of the cells, the protocol from Nadia Tzelepi has been used (paper in preparation). Briefly, 25 images of each samples were analyzed using Image J software, measuring the cytoplasm and nucleus area, and the cell perimeter. Then each NP localized in one of these cell compartments was recorded, and the NP number expressed as NP/ each nm² for each compartment of the cell.

2.15. Oxidative stress measurements

2.15.1. Antioxidant experiment

It was described previously that NPs can engender oxidative stress by themselves, without radiotherapy (Rosa *et al.*, 2017). This effect could be interesting in combination with radiotherapy. NPs exposure in the presence of antioxidants give information on this particular oxidative stress involvement.

This protocol was used in Section 3.9 of the results chapter.

HSC-3 and HaCaT cells were seeded at a density of 300 cells/well for a clonogenic experiment. After 24 h, cells were exposed to different concentration of sodium pyruvate (NaP) (Sigma, P5280-25g) (10 mM stock solution), N-acetyl cysteine (NAC) (Sigma, A9165-5g) (500 mM stock solution) and reduced glutathione (GSH, 25mM stock solution), adjusting the pH to 7.4 with sodium hydroxide (NaOH, Fisher scientific, 215-185-5), to explore the impact of these three antioxidants.

These three molecules were used at the optimum concentration determined by clonogenic assay, which gives rescue of the cells from oxidative stress and does not engender toxicity, in order to explore the potential oxidative stress related to AuNPs exposure. Hydrogen peroxide (H₂O₂, Sigma, H3410-500ml) was used as a positive control; at a concentration of 0.1 mM, which was shown previously to induce oxidative stress (Gülden *et al.*, 2010). Cells were seeded on 24 well plates at a density of 300 cells/well. After 24 h, cells were exposed to AuNPs at 1 µg/ml Au (IC50) for 3 h, with or without antioxidants. After washing the cells from the exposed chemicals, fresh medium was added, with and without antioxidants for 24 h. Finally, the cells were washed once more and grown for 6 more days. At the end of the clonogenic assay, the cell population exposed to different toxic, in the presence or absence of antioxidants, were compared to the relative controls.

2.15.2. Fluorescence-activated cell sorting (FACS) analysis

In the continuation of oxidative stress involvement, FACS is an interesting technique it gives semi-quantitative information on the amount of ROS produced and its intracellular characteristics. This method allows analysis of a heterogeneous population of cells by determining variations in fluorescence. Two fluorescence probes were used for these experiments, described in Section 3.9. Propidium iodide (PI) (Sigma, P4170), stains the DNA of permeable unhealthy cells, such as dead cells or dying cells. Carboxy-DCFH-DA (5-(and-6)-Carboxy-2',7'-Dichlorofluorescein Diacetate) (Life technologies, C-400), was used to quantify the amount of ROS following AuNPs exposure. DCFH-DA is hydrolyzed in DCFH by esterases inside the cells and can then be oxidized by ROS into the fluorescent product DCF. For these experiments, the cells were loaded and incubated with phenol red-free low glucose DMEM (Gibco, 21885-108). The cells were loaded at a density of 250 000 cells/well in 15 ml falcon tubes with 20 μ M of DCFDA probe diluted in phenol-red free medium with 10% serum. The cells were loaded for 30 min and then exposed to 1 μ g/ml AuNPs (IC50) for 3 h without washing. After exposure, fluorescence of 10 000 cells was analysed using flow cytometer BD Biosciences BD FACScalibur on the fluorescein isothiocyanate (FITC) channel. Cells in presence of the oxidizing agent Tert butyl hydroperoxide (TBHP) (Luperox, Sigma, 458139) (100 μ M) were used as a ROS positive control.

2.15.3. Cell-free hydroxyl radical assay

Furthermore, to have information on the potential effect of NPs with radiotherapy, before cell exposure which require times and more expenses, the hydroxyl radical production coming from the interaction of NPs and radiation was explored. X-ray induced hydroxyl radical production was determined by the hydroxylation of coumarin-3- carboxylic acid (3-CCA) to fluorescent 7-hydroxycoumarin-3-carboxylic acid (7-OHCCA) (Collins *et al.*, 1994, Manevich *et al.*, 1997). The assay was optimised for use with nanoparticle radiotherapy. The optimisation is described in Section 3.10.a, while the coumarin assay was used in Section 3.10.1 and 4.3.1. A 5 mM stock solution of 3-CCA (Sigma, C85603-25G) was prepared in 20 mM PBS buffer. The fully oxidised 7-OHCCA, called also Umbelliferone, (Sigma, H24003-10G), was used in order to set up the protocol to measure its fluorescence. The fluorescence of umbelliferone is pH dependent and reaches its maximum at pH 9, therefore, samples were adjusted to pH 9 before fluorescence measurements. Fifty microliter aliquots of water, or 12 μ g/ml AuNPs in water, were added to 50

μl of 5 mM 3-CCA in 3 kDa cutoff 96-well ultrafiltration plates (Acroprep Advance omega, Pall Life science[®], PN 8033).

Plates were irradiated with 10 Gy of 6 MV X-rays at a dose rate of 5 Gy/min. Control plates were not irradiated. Then, 100 μl ethanol was added per well to aid 7-OHCCA solubility, each plate was placed onto an empty receiving black, 96 well plate (Cellstar, greiner bio one, 655090), and the nanoparticle-free filtrate was collected by centrifugation at 1500 $\times g$ for 60 minutes. 100 μl of PBS pH 9 was added to each sample in order to increase the coumarin signal to its maximum. Quantification of 7-OHCCA fluorescence was performed with an excitation of 390 nm and emission maximum at 450 nm (Collins *et al.*, 1994) using a Microplate reader (FLUOstar Optima, BMG Labtech).

2.16. Irradiation protocols of the different cell lines

The radiosensitisation effect of the different NPs explored in this thesis was explored with the gracious collaboration from two medical centre. Irradiation experiments were performed in The Oncology Department of Northampton Hospital, using an Xstrahl 200 clinical orthovoltage system for the kilovoltage irradiation (Figure 2.7), in collaboration with Peter Goldie and Nicky Whilde, and described in Section 3.10 and 4.5.3. A second set of experiment was performed at Milton Keynes Genesis Care Medical Centre, using a linear accelerator (Versa HD[®], Elekta) (Figure 2.8 a) using 6 MV irradiation, in collaboration with Aquila Sharif and Richard Slade-Carter, and described in Section 3.10.2 and 3.10.3. This allowed exploring two range of energy of irradiation to compared radiosensitisation depending on energies. All the various cells were seeded on 24 well plates at between 300-1000 cells/well for skin cells, and 300-1800 cells/well for breast cells, 24 h before irradiation. On the day of experiment, cells were exposed to AuNPs and the plates heat sealed within plastic bags to maintain sterility, humidity and pH, and then transported in thermal boxes in order to maintain the temperature. Here again, the cell densities were optimised after irradiation to obtain well-separated colonies. Concentration which give 50% of toxicity (IC50) obtained for HSC-3 and MCF-7 were used in order to expose both cancer and normal cells with AuNPs for 3 h. This concentration was chosen as it is responsible for an uptake in cancer cells and does not affect the normal cell viability, therefore is hoped to show a selective radiosensitivity toward cancer cells. Cultures were then irradiated with 2-8 Gy of either kilovoltage or megavoltage X-rays. For megavoltage work, the plate was imaged in a CT scanner and a treatment plan was computed that involved solid water shielding (Gammex) to prevent backscatter build-up and the dose was delivered from below and from above the culture plate (50:50) (Figure 2.8 b). For kilovoltage work, the dose was delivered through the bottom of the culture plate (Figure 2.7).



Figure 2.7: Gulmay Xstrahl 200 clinical orthovoltage system.

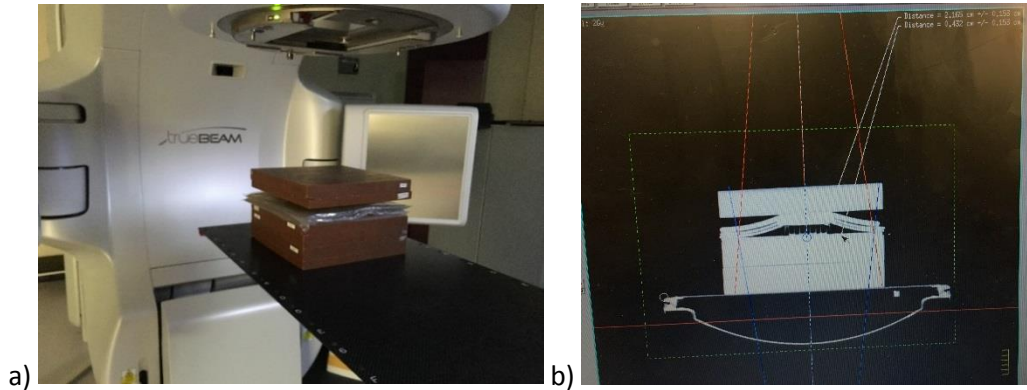


Figure 2.8: a) Clinical linear accelerator (Versa HD[®], Elekta) and culture plate set up, b) treatment plan for the irradiation.

Two hundred and twenty kV X-rays were delivered at 0.52 Gy/min for the kilovoltage experiment while 6 MV X-rays were delivered at a rate of 5 Gy/min for the megavoltage experiments. Control plates were transported to each facility but were not irradiated. Cell colonies were counted after 6 days and expressed as the surviving fraction (SF). The survival fraction represents the viability of cells exposed to a toxic compared to the control. Its value is comprised between 0 and 1.

A decrease in SF with AuNPs can be attributed to two reasons: an intrinsic chemotoxicity and local radiation enhancement. Accordingly, log-linear plots of SF versus radiation dose are presented in two ways: the raw data visualising the AuNPs toxicity in addition to the radiation one, and the data normalised for chemotoxicity by multiplying the SF data for each type of AuNP by 1/SF at 0 Gy. A linear-quadratic function was used to the normalized SF versus dose (D) data, in order to transform the data and calculate dose enhancement factors, in the form of:

$$SF = \exp(\alpha D + \beta D^2)$$

Radiation enhancement effects are reported as two measurements from normalized SF data. The Sensitivity Enhancement Ratio (SER_{4Gy}) is a measure of cell senescence or death enhancement by AuNPs at 4 Gy, calculated as the ratio of SF without and with AuNPs (Luchette et al., 2014). The Dose Enhancement Factor (DEF_{0.3}) is a measure of the gain in effective radiation

dose due to AuNPs, calculated as the ratio of the dose of radiation only with respect to the dose of radiation and AuNPs at a SF of 0.3.

$$DEF0.3 = \sqrt{(a^2 + (4b * \ln(SF0.3)))}$$

2.17. Data reductions

All the experiments on cell toxicity, described in Sections 3.2, 3.4, 3.5, 3.7, 3.9, 3.10 and 4.4.1 and 4.4.4. were performed in triplicate. Data regarding AuNPs toxicity was expressed as the mean of the percentage of viability as compared to the control. The standard error of the mean (SEM) was shown in order to quantify the precision of the mean value observed. It is calculated by dividing the standard deviation (SD) by the square root of the number of samples. Genetool and genesis software were used to count the cell colonies on the clonogenic plates. In order to explore statistically the effect of different exposure, Graph prism® software has been used (Watt *et al.*, 2007). These statistical tests were performed in order to determine if the differences between groups were significant and not due to random variability. When comparing a difference in two groups, an unpaired t-test was used. To compare a difference in more than two groups, a one-way ANOVA was used. In order to set multiple comparisons, a post-test was used (Tukey for comparing the difference between all the samples, Dunnett for comparing the differences to a control). If a difference due to two factors and between more than two groups needed to be explored, a two-way ANOVA was used. Differences with p-value <0.05 and lower were verified by multiple comparisons post-test (Bonferroni for comparing within each group, the difference between all the time points, Dunnett for comparing, within each group, the differences between the time points to a control and Sidak for comparing for each time point, the difference between the groups). IC50 values were calculated with Graph Prism software as well. A nonlinear regression analysis was designed and a logarithm versus normalized response equation with a normalised response was used:

$$Y = 100 / (1 + 10^{(X - \text{Log}(IC50))})$$

with X being the logarithm of the AuNPs concentration and Y the cell viability.

CHAPTER 3: STUDIES WITH SUGAR:PEGAMINE COATED AuNPs

The aim of this work was to explore the potential of different AuNPs to act as radiosensitisers.

The AuNPs uptake in the cells plays an important role on the radiosensitisation effect, as more gold inside the cells is linked to more interaction with the beam of radiation. The coating of the AuNPs plays a role on their uptake as the molecules around the AuNPs can improve their stability and biocompatibility (Gilles *et al.*, 2014). The experiments in this chapter are summarised in Table 3.1.

Table 3.1: Summary of the experiments reported in Chapter 3

EXPERIMENTS	RESULTS	CONCLUSION
TEM and DLS for AuNPs characterisation	AuNPs have an average size between 1.68 and 2.32 nm, AuNPs coated with high amount of sugar tend to aggregate	α Gal:PEGamine AuNPs seem more homogenous and stable than the other coated ones.
Clonogenic assay/toxicity	Specific sugars coating the AuNPs have different effects on toxicity. α -galactose coated AuNPs are more toxic than β -glucose and N-acetylglucosamine coatings	α -galactose gives the best selective toxicity toward cancer cells IC 50 of 1 μ g/ml, 3 h was chosen as a loading time
Clonogenic assay, different ratio of molecules coating the AuNP	A 50:50 ratio of α Gal:PEGamine gives an higher toxicity toward cancer cells than other ratios	The amount of α Galactose and PEGamine is linked to the toxicity and stability of AuNPs in solution
Mass spectrometry and TEM	Uptake in skin cancer and normal skin cells is different depending on the coating of the AuNPs	The toxicity of the AuNPs is linked, but not entirely, to their uptake in cells. AuNPs give a better uptake in cancer cells and the AuNPs localised in cytoplasm and vesicles
AuNPs sticking and interaction with plastic plates	AuNPs sticks to plastic, but less so when NaCl is present	The sticking does not affect the toxicity as even on floating conditions, the AuNPs are toxic for cells. This sticking seems to be related to electrostatic interaction between AuNPs and plastic.
Coumarin assay	The coumarin assays shows increase of fluorescence when the samples were irradiated and when the citrate AuNPs were present	The coumarin assay gives good indication of the hydroxyl radical production in water. Having coating present decreases the amount of \cdot OH radical produced.
Radiosensitisation effect	AuNPs decrease the survival fraction of cancer cells with radiotherapy, much more with skin cancer cells and much more with kilovoltage radiotherapy	The α Gal:PEGamine coated AuNPs have a higher effect inside cells than outside cells. They give an additive effect with both kilovoltage and megavoltage radiotherapy. Effect is more pronounced and more selective toward skin cancer cells than for breast cells

As mentioned in Section 1.3 of the introduction, Monte Carlo simulation, as well as experiment on plasmid DNA have shown that AuNPs of 2 nm size can have a radiosensitisation effect in combination with radiotherapy (Hainfeld *et al.*, 2004, Haume *et al.*, 2016b).

AuNPs 2nm in size were therefore selected for tumour radiosensitisation studies, also because of their biocompatibility and amenability to surface modification (Hainfeld *et al.*, 2008, McMahon *et al.*, 2011). The size of the AuNPs is also important for entering in cells and particularly for favouring renal clearance, avoiding long term exposure and potential toxicity (Alric *et al.*, 2013, Sancey *et al.*, 2014). AuNP toxicity is often unknown and depends on the coating surrounding the AuNPs. However, they are generally non-toxic, unless used at high concentrations (Fratoddi *et al.*, 2015, Haume *et al.*, 2016b). In order to better understand the role of AuNPs on the radiosensitisation effect, especially regarding the charge, the coating, and the localisation of AuNPs in cells, we explored the effect of 2 nm AuNPs coated with α galactose and PEGamine. These two molecules were used in order to improve the biocompatibility of the AuNPs and their selectivity toward cancer cells (Chhour *et al.*, 2016, Jokerst *et al.*, 2011). These AuNPs were initially tested as potential radiosensitizers but were found to have a selective toxicity toward cancer cells and therefore, the impact of the coating on its toxicity was explored.

This chapter will detail the characterisation of the AuNPs, looking at their potential aggregation and agglomeration in water and their size. Then, the toxicity of these AuNPs on 4 different cell lines will be detailed, looking at the mechanism of action, the potential selective toxicity toward cancer cells and their potential to act as radiosensitizers outside of the cells. This chapter will end with the potential use of these AuNPs to act as radiosensitisers in cells (Grellet *et al.*, 2017). This work has already been published in the Journal PLoS One in 2017 (Grellet *et al.*, 2017).

3.1. Physicochemical characterisation of the AuNPs coated with equal amount of sugar and PEGamine using TEM

The size of the AuNPs core was determined by transmission electron microscopy (TEM). This technique was detailed in sections 1.11.2 and 2.1.4.

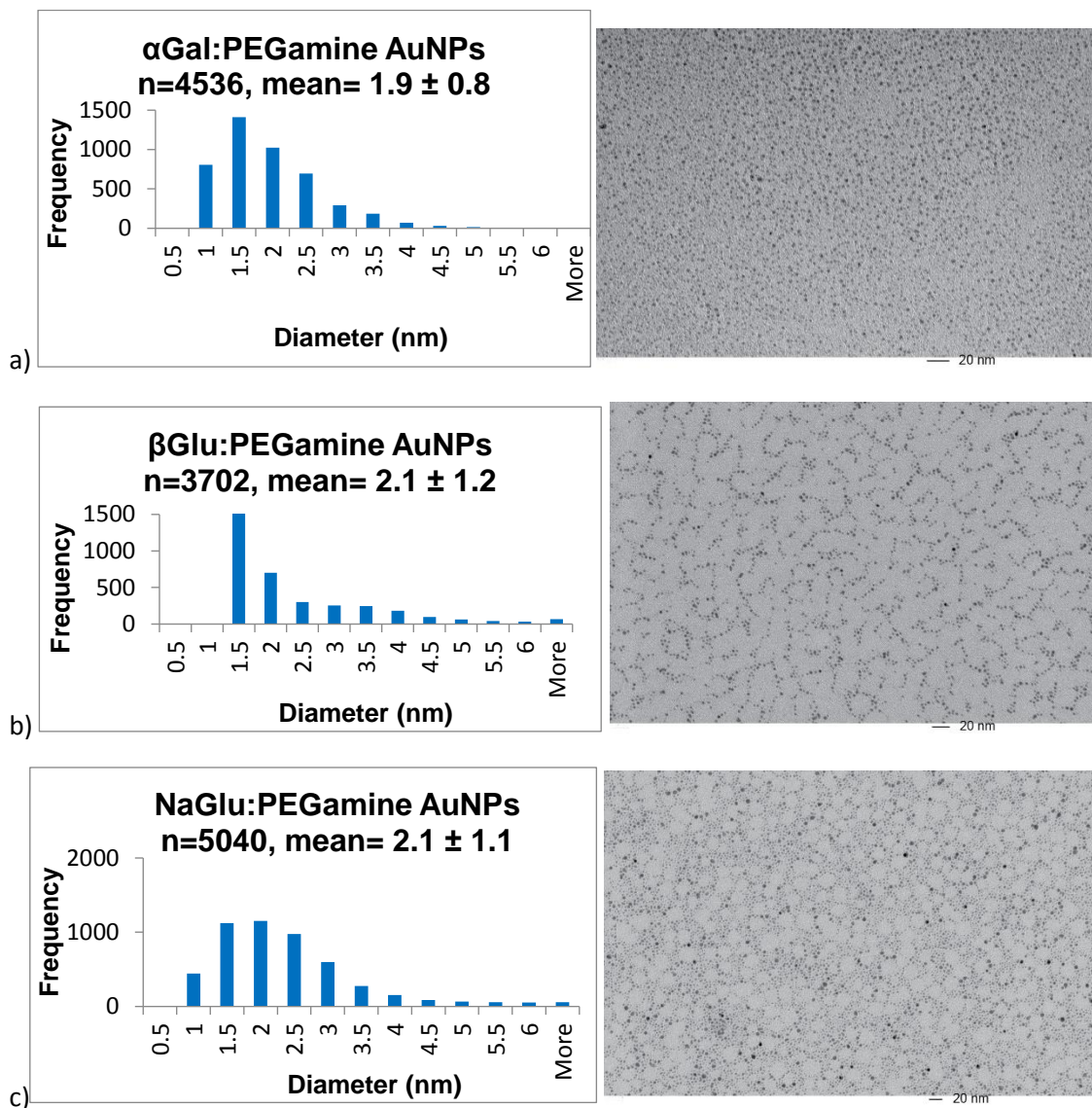


Figure 3.1: Size histograms and TEM images of different NPs. a) α Gal:PEGamine AuNPs; b) β Glu:PEGamine AuNPs; c) N-aGlu:PEGamine AuNPs. The data are presented as mean AuNP diameter \pm standard deviation.

The different sugar:PEGamine AuNPs, coated with an equal amount of each molecule, have an average core diameter between 1.9 and 2.1 nm (Figure 3.1). The α Gal:PEGamine NPs are homogeneously distributed on the TEM grids, with a standard deviation of 0.79 (40%) while the other AuNPs adhere to the grids in a more ordered and partially aggregated way, with a standard deviation superior or equal to 1.1 (50%) (Figure 3.1b, c). In addition, these same AuNPs have a tendency to contain a higher proportion of large sized AuNPs.

3.2. Skin cells exposed to AuNPs, the role of the sugar onto the AuNPs

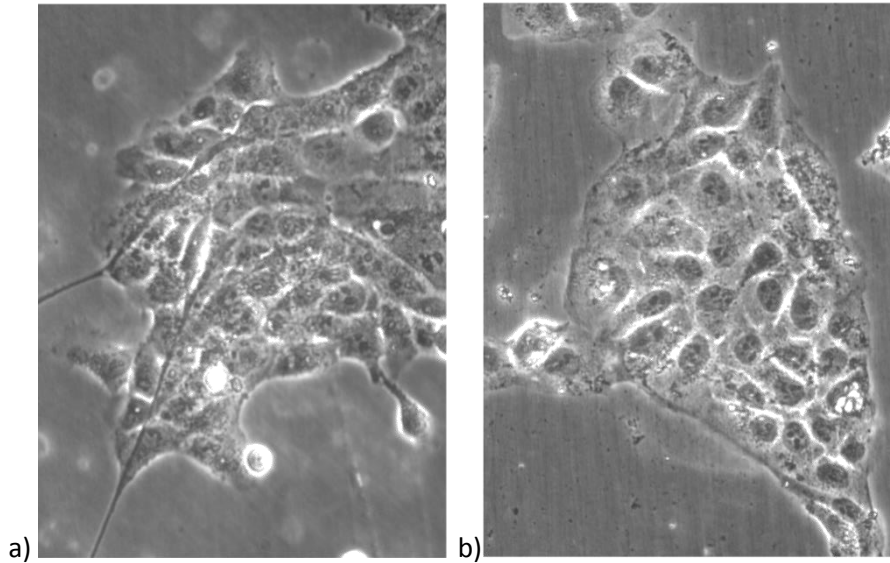


Figure 3.2: Bright field images of a) HSC-3 cells; b) HaCaT cells. Scale is unavailable.

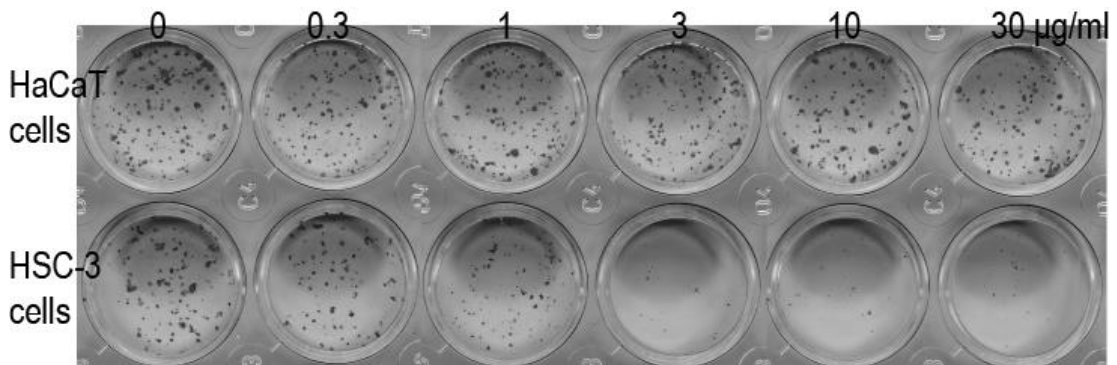


Figure 3.3: Clonogenic assay of HSC-3 and HaCaT cells exposed to α Gal:PEGamine (50:50) AuNPs for 3 hr.

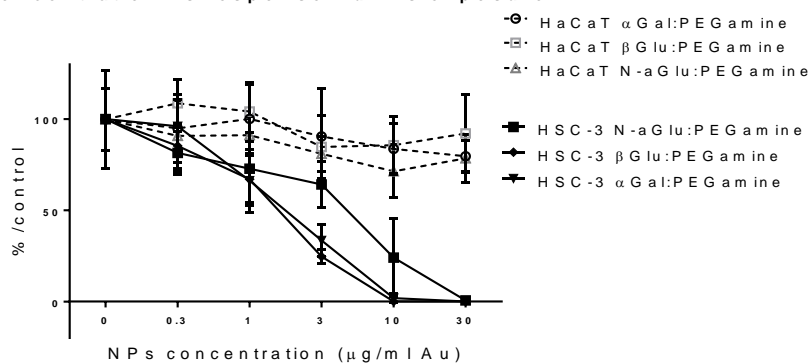
Two different cell lines, a squamous carcinoma cell line (HSC-3), and a normal keratinocyte cell line (HaCaT) were used for toxicity and radiosensitisation experiments (Figure 3.1). Both skin cancer and skin normal cells have similar cell morphology (Figure 3.2). HaCaT cells, were seeded at clonogenic density with the assay detailed in section 2.8, and exposed to 0.3, 1, 3, 10 or 30 μ g/ml Au of α Gal:PEGamine (50:50) or β Glc:PEGamine (50:50) or N-aGlu:PEGamine (50:50) AuNPs for 3 hours. The cells were then washed with medium and allowed to grow for 6 days before stopping the assay. Figure 3.3 shows a clonogenic assay. A decrease in cell colonies is linked to both toxicity and failure to proliferate, and the number of surviving colonies is compared to the control condition without AuNPs. Each AuNP demonstrated a dose-dependent cytotoxic/cytostatic effect that was selective for the HSC-3 cells, compared to HaCaT cells (Figure 3.3).

The data demonstrate that 50:50 α Gal:PEGamine (IC 50, concentration which give 50% of toxicity for HSC-3 cells, are between 1.7 and 0.24 μ g/ml) and 50:50 β Glc:PEGamine AuNPs (IC

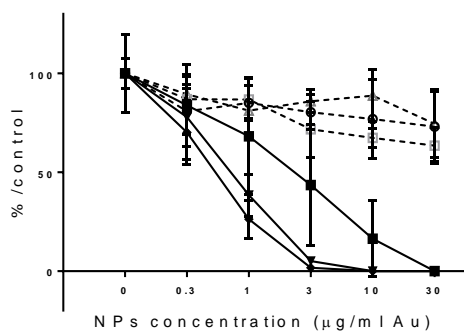
50 for HSC-3 cells between 1.4 and 0.33 $\mu\text{g}/\text{ml}$) have an equivalent effect on HSC-3 cells, while N-aGlu:PEGamine are less toxic/cytostatic (IC 50 between 3.5 and 0.78 $\mu\text{g}/\text{ml}$) (Figure 3.3). The IC50 were estimated using the data analysis software Graph prism and detailed in Section 2.17.

3.2.1. AuNPs toxicity related to the time of exposure and the type of sugar

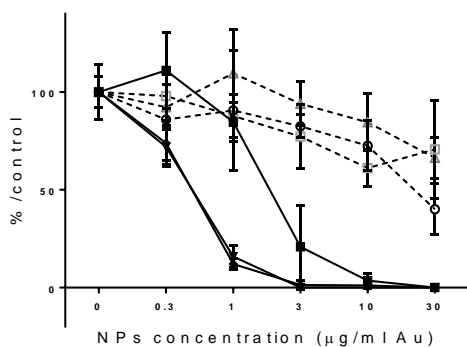
Concentration vs response AuNPs exposure 1H



Concentration vs response AuNPs exposure 3H



Concentration vs response AuNPs exposure 6H



Concentration vs response AuNPs exposure 24 H

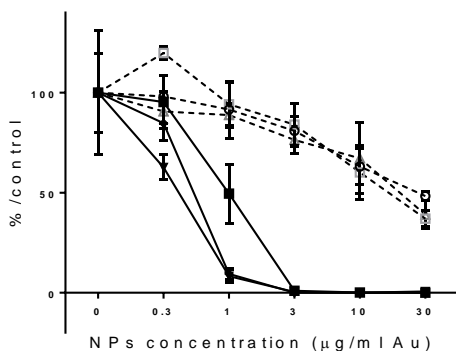


Figure 3.4 Clonogenic assay after AuNPs exposure for different concentrations and different loading times. The graphs represent the percentage viability compared to the control. Data are presented as mean percentage survival \pm standard deviation.

Exposure to AuNPs for different time periods shows clear differences in the HSC-3 cells but smaller effects in HaCaT cells that only become apparent above 10 $\mu\text{g/ml}$ following 6 hr or 24 hr exposure (Figure 3.4). Based on these data, three hours of AuNPs exposure time was routinely used as it demonstrated the greatest difference in toxicity between normal and cancer cells.

Concentration vs response AuNPs exposure 3 H

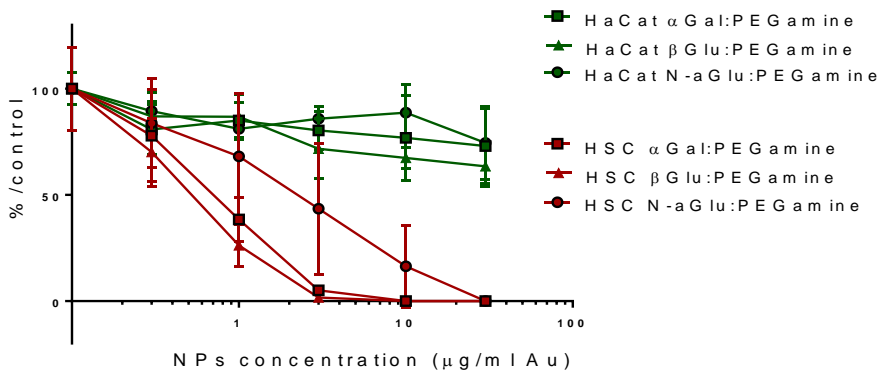


Figure 3.5: Dose response curve after a clonogenic assay where both HSC-3 and HaCaT cells were exposed to 3 different AuNPs. The graphs represent the percentage of cell colonies compared to the control, with increasing AuNPs concentration.

Data are presented as mean percentage colonies \pm standard deviation. Statistical differences in dose responses for each AuNPs on each cell line were analysed by two-way Anova followed by a Dunnett's multiple comparisons test, while statistical differences in dose responses for each AuNPs comparing both cell line was determined by oneway Anova followed by a Sidak's multiple comparisons tests.

From Figure 3.5, it is shown that all the AuNPs have a more significant impact on HSC-3 than on HaCaT cells (Annex 2.1.1). The difference in viability compared to the control for HSC-3

cells is statistically significant at an exposure of 1 $\mu\text{g}/\text{ml}$ for each AuNPs ($p < 0.001$), and even at 0.3 $\mu\text{g}/\text{ml}$ for 50:50 $\alpha\text{Gal}:\text{PEGamine}$ and 50:50 $\beta\text{Glu}:\text{PEGamine}$ AuNPs ($p < 0.01$). The different IC₅₀ after exposure of HSC-3 cells are respectively, 0.8, 0.45 and 2 $\mu\text{g}/\text{ml}$ after exposure to $\alpha\text{Gal}:\text{PEGamine}$, $\beta\text{Glu}:\text{PEGamine}$ and N-aGlu: PEGamine AuNPs. 50:50 $\alpha\text{Gal}:\text{PEGamine}$ and 50:50 $\beta\text{Glu}:\text{PEGamine}$ AuNPs are responsible for a statistically significant difference compared to the control for HaCaT cells at 3 $\mu\text{g}/\text{ml}$ ($p < 0.0001$) but not below, while N-aGlu: PEGamine AuNPs exposure do not significantly decrease the viability for HaCaT cells at any concentration used ($p > 0.05$) (Annex 2.1.1).

Finally, when comparing the difference in toxicity between HSC-3 and HaCaT cells exposed to these three AuNPs, it is possible to note a statistically significant difference between cancer and normal cells already at a concentration of 1 $\mu\text{g}/\text{ml}$ for $\alpha\text{Gal}:\text{PEGamine}$, $\beta\text{Glu}:\text{PEGamine}$ AuNPs, and at 3 $\mu\text{g}/\text{ml}$ for N-aGlu: PEGamine AuNPs (Annex 2.1.2). The difference in toxicity between the two types of cells exposed to AuNPs confirms the selective toxicity of all AuNPs toward cancer cells.

However, it is important to note that in addition to their toxicity, $\alpha\text{Gal}:\text{PEGamine}$ AuNPs have been tested by Midatech in phase I and phase II clinical trials as vectors for drug delivery and therefore, have been very well characterised. Following these first results, the following work is focused on the optimum $\alpha\text{Gal}:\text{PEGamine}$ coated AuNPs.

3.2.2. The influence of water on toxicity

Stock solution of AuNPs are in water and at concentrations around 1 mg/ml . Therefore, the highest concentrations of AuNPs used also contain the highest proportion of water and this may provide an additional osmotic stress to the cells. To quantify any contribution from osmotic stress, HSC-3 and HaCaT cells were exposed to media containing different volumes of water (as if AuNPs were present) for 3 hours.

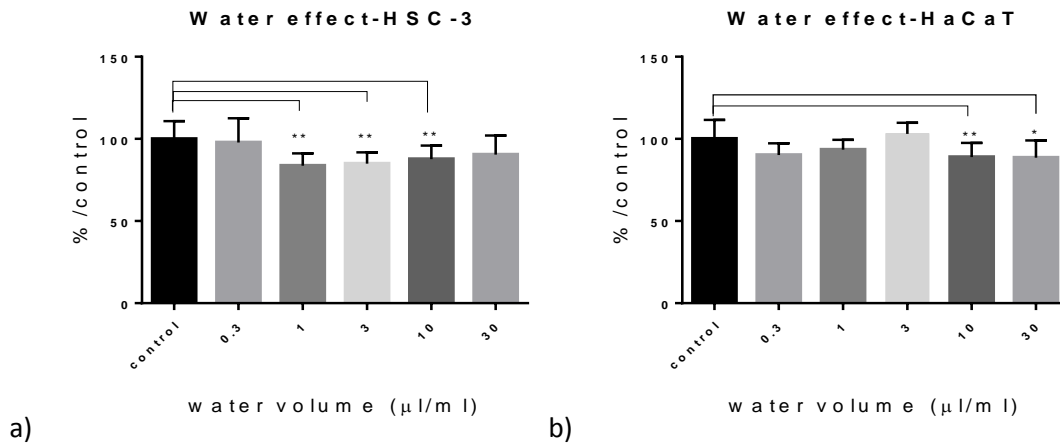


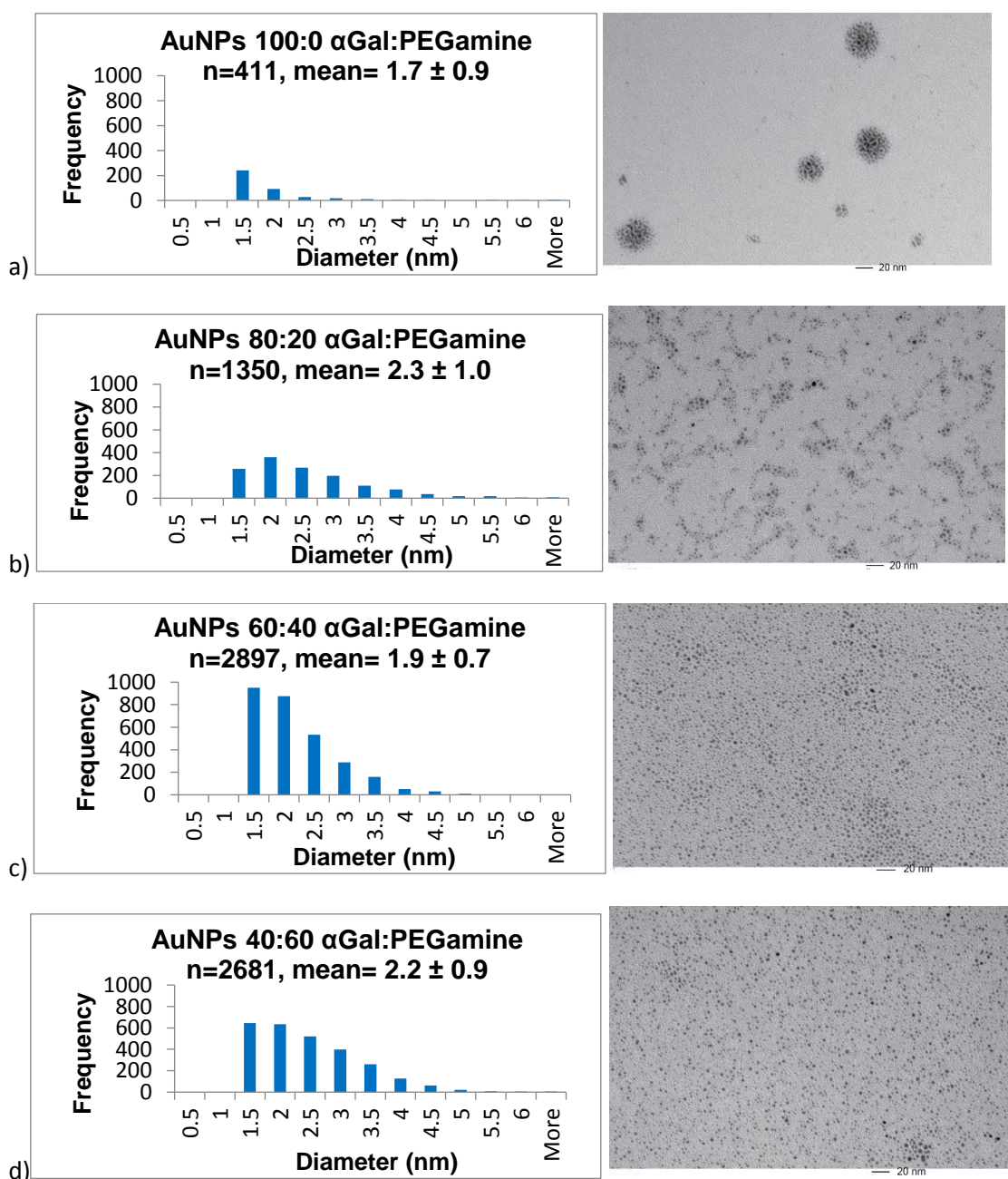
Figure 3.6: Effect of different concentrations of sterilized water on a) HSC-3 and b) HaCaT cultures. The graphs represent the percentage of viability compared to the control as a function of water volume. The data is expressed as an average with their standard deviation. A one-way ANOVA test was used to investigate any significant differences between exposures. The different asterisks show a significant difference compared to the control.

Having water present in the cell medium decreases colony number, in both cancer and normal cells (Figure 3.6). This effect is statistically significant from 1 to 10 µl/ml for HSC-3 cells ($p < 0.001$) and at 10 µl/ml for HaCaT cells ($p < 0.001$) (Figure 3.6). It is important to note that the decrease of cell survival is much less pronounced than that one observed with AuNPs exposure, with water contributing at most 15% reduction in colony number.

3.3. Physiochemical characterisation of the AuNPs coated with different amount of sugar and PEGamine

After determining the optimum sugar coating on the AuNPs for selective cancer cell toxicity, the impact of different sugar:PEGamine ratios on cell toxicity was explored. Seven different AuNPs with the following ratios of α Gal:PEGamine coating the AuNPs were used: 0:100; 20:80; 40:60; 50:50; 60:40; 80:20; 100:0 . Together they represent a broad range of different charge and molecular coatings.

3.3.1. AuNPs characterisation using TEM



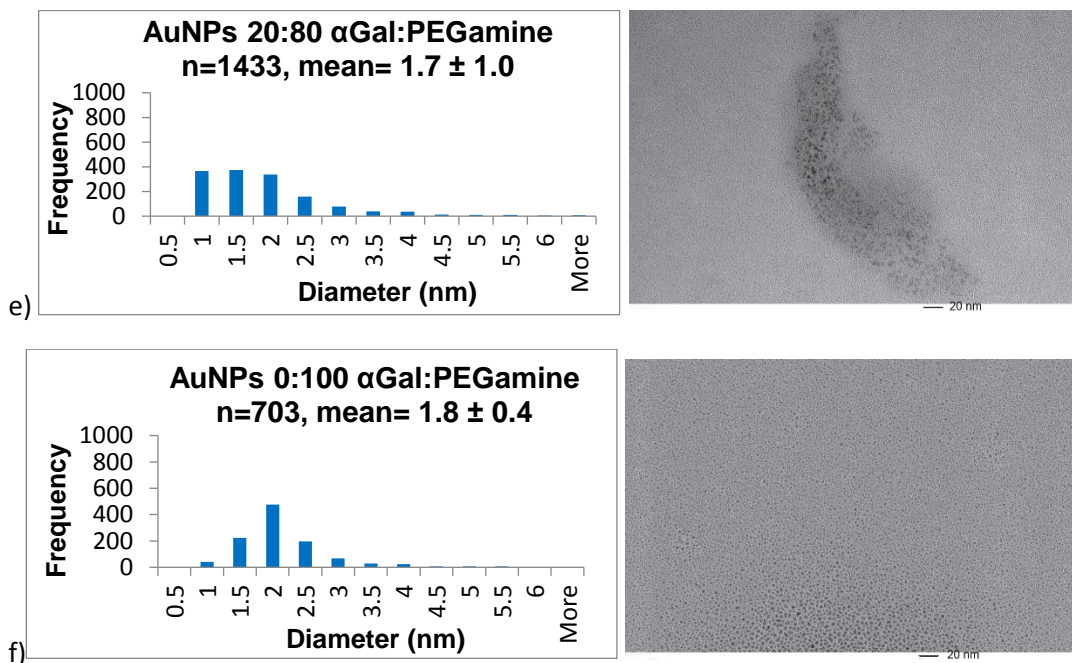


Figure 3.7: TEM images of the AuNPs with different ratios of α Gal:PEGamine and their size histograms. a)100:0; b)80:20; c)60:40; d)40:60; e)20:80; f)0:100. The data are presented as mean AuNP diameter \pm standard deviation.

The AuNPs vary in average diameter value between 1.7 and 2.3 nm. Some of the AuNPs are homogeneously distributed, while others (100:0, 80:20, 20:80) form clumps (Figure 3.7 a,b,e).

3.3.2. AuNPs characterisation by DLS

It is possible to relate the size of the AuNPs obtained by TEM with those obtained by DLS, which measures the hydrodynamic size of the AuNPs, as well as the zeta potential, representing its surface charge, as discussed in Section 1.11.2 and Section 2.1.4. When looking at Table 3.2, it is possible to note a trend that the larger the AuNPs measured by TEM, the larger it is by DLS.

Table 3.2: Summary of AuNPs diameter from TEM, hydrodynamic diameter from DLS in water and zeta potential measured in 3.2% PBS pH 7.4.

AuNPs	TEM diameter (nm) ±SD	DLS diameter (nm) ±SD	Zeta potential (mV) ±SD
100:0 αGal:PEGamine	1.68 ± 0.90	5.13 ± 1.28	-16.0 ± 6.3
80:20 αGal:PEGamine	2.32 ± 0.95	3.37 ± 2.66	+26.7 ± 4.2
60:40 αGal:PEGamine	1.94 ± 0.69	5.27 ± 2.31	+24.5 ± 7.2
50:50 αGal:PEGamine	1.86 ± 0.79	6.29 ± 2.17	+45.4 ± 7.6
40:60 αGal:PEGamine	2.23 ± 0.87	4.45 ± 2.35	+21.8 ± 5.7
20:80 αGal:PEGamine	1.69 ± 0.97	8.76 ± 5.03	+27.4 ± 7.8
0:100 αGal:PEGamine	1.79 ± 0.39	5.08 ± 3.31	+43.0 ± 5.7
50:50 βGlc:PEGamine	2.10 ± 1.21	6.15 ± 1.76	+24.1 ± 5.1
50:50 NaGlu:PEGamine	2.13 ± 1.09	6.11 ± 1.59	+30.9 ± 7.7
Citrate AuNP	2.04 ± 0.98	6.64 ± 2.17	-45.1 ± 13.9

Moreover, when looking at the charge of the AuNPs, they all have a positive surface charge, except the one coated with 100:0 αGal:PEGamine (-16 mV) and the citrate AuNPs (-45 mV) (Table 3.2). There is no linear trend between the zeta potential NPs and its ratio of αGal:PEGamine. Neither is there a linear trend in the mean size of the AuNPs.

It is also important to note that there is no statistically significant differences in mean core size depending on the coating of the AuNPs as shown in Figure 3.8, when comparing all the AuNPs to the one coated with 50:50 αGal:PEGamine.

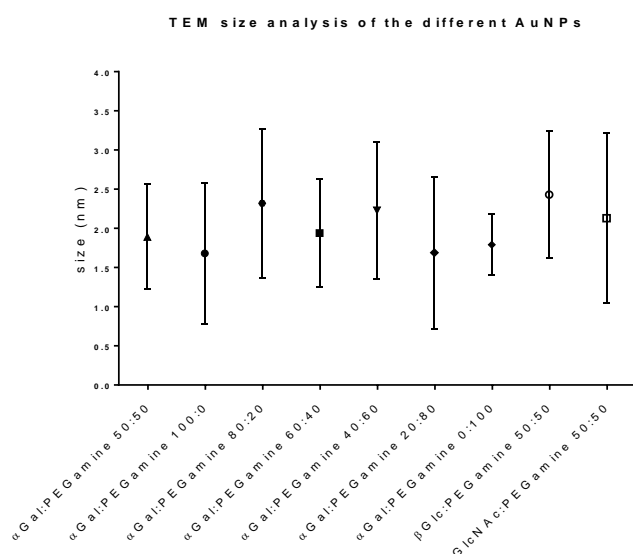


Figure 3.8: TEM size comparison of the different AuNPs ±SD.

3.4. Skin cells exposed to AuNPs, the role of the coating and its ratio onto the AuNPs

In order to explore the potential effect of different coatings on the AuNPs, both cancer and normal cells were exposed for 3 hours to each of these seven different α Gal:PEGamine coated AuNPs at concentrations of 0.3, 1, 3, 10 or 30 $\mu\text{g}/\text{ml}$ Au. The cells were then washed and grown for 7 days before stopping the clonogenic assay.

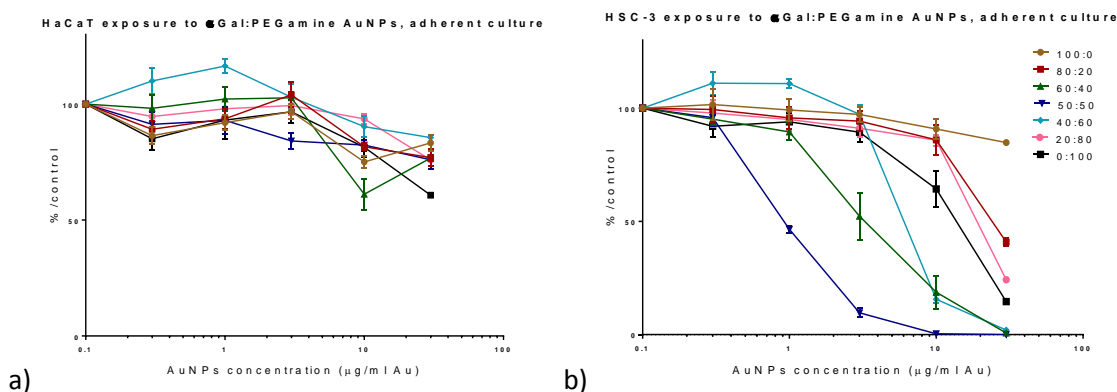


Figure 3.9: Clonogenic assay after AuNPs exposure for different concentrations and various ratios of α Gal:PEGamine. a) HaCaT cells, b) HSC-3 cells. The graphs represent the percentage of colonies compared to the untreated control. Data are presented as mean percentage colonies \pm standard deviation. Statistical differences in the dose responses for each AuNPs on each cell line were analysed by two way Anova followed by a Dunnett's multiple comparisons test.

HaCaT cells are largely unaffected by any of the different AuNP ratios (Figure 3.9.a) especially at low concentrations. However, there is a statistically significant decrease in viability compared to the control at 10 $\mu\text{g}/\text{ml}$ ($p < 0.001$) for all AuNPs except for the 40:60 ($p < 0.01$) and 20:80 α Gal:PEGamine ($p < 0.0001$) where this decrease is significant at 30 $\mu\text{g}/\text{ml}$. Interestingly, dose-dependent toxicity is seen with two AuNPs in HSC-3 cells. (Figure 3.9 b), with a statistically significant toxicity compared to the control at 1 $\mu\text{g}/\text{ml}$ for the 50:50 α Gal:PEGamine and at 3 $\mu\text{g}/\text{ml}$ for the 60:40 α Gal:PEGamine (Annex 2.2.1). These two AuNPs show a strong toxicity on HSC-3 cancer cells but not on HaCaT normal cells. All the AuNPs appear to have a strong toxicity for HSC-3 cells at 10 $\mu\text{g}/\text{ml}$ ($p < 0.01$) compared with AuNPs coated with a ratio 100:0 α Gal:PEGamine, which have a statistical effect at 30 $\mu\text{g}/\text{ml}$ (Figure 3.9 a). AuNPs coated with ratios 80:20 and 100:0 are less toxic for HSC-3 cells than the other ones (Figure 3.9 a) ($p < 0.01$). Moreover, these AuNPs have a higher toxicity for HaCaT cells than for HSC-3 cells (Figure 3.9 b) (Annex 2.2.2).

After exploring the dose response relationship with AuNPs exposure, it was possible to estimate, with Graph prism® software, the IC50 values (the concentration which gives 50 % of reduction in colony numbers) for each ratio.

The 50:50 α Gal:PEGamine AuNPs were the most toxic for cancer cells (IC50 = 0.8 μ g/ml), just ahead of the 60:40 α Gal:PEGamine coated ones (IC50 = 4.2 μ g/ml), (Figure 3.9, Table 3.2).

The charge is known to have an influence on toxicity. In the particular case of α Gal:PEGamine coated AuNPs, negative charged AuNPs did not cause toxicity on the cells, while high positively charged AuNPs did cause a strong toxicity (Table 3.2). Indeed, AuNPs coated with almost only α Galactose or almost only PEGamine are less toxic than the ones which have equal amount of both molecule (Table 3.3). In particular, the 100:0 α Gal:PEGamine AuNPs, which are negatively charged, have a very high IC50, which indicates a small effect on the cancer cells (Table 3.3, Figure 3.8). It is important to mention that the toxicity observed here on skin cells occurs at a very low AuNP concentration (nM), much lower than in any previous study published (μ M) (reviewed in (Haume *et al.*, 2016b)) and that this toxicity is highly selective, with a factor of 100 in IC50 between the cancer cells and the normal cells. Patra *et al.* have shown that 30 nm AuNPs were able to cause toxicity at a concentration of 100 nM and for 48 h exposure on A549 lung cancer cells but did not affect HepG2 liver cancer cells (Patra *et al.*, 2007). Demonstrating selective toxicity after only 3 h of exposure, the α Gal:PEGamine coated AuNPs are a promising tool in cancer treatment.

Table 3.3: Chemotoxicity of different AuNPs on HSC-3 adherent cells

HSC-3 exposure for 3 hours to the different AuNPs	100:0	80:20	60:40	50:50	40:60	20:80	0:100
IC50 (µg/ml)	>100	23	4.2	0.8	6.8	20	13

3.5. Skin cells exposed to the ligands only are unaffected

In order to explore if the coating ligands are directly toxic, HSC-3 and HaCaT cells were exposed to different concentrations of α Galactose or PEGamine or a 50:50 mixture of both, at the same concentration as the AuNPs exposure.

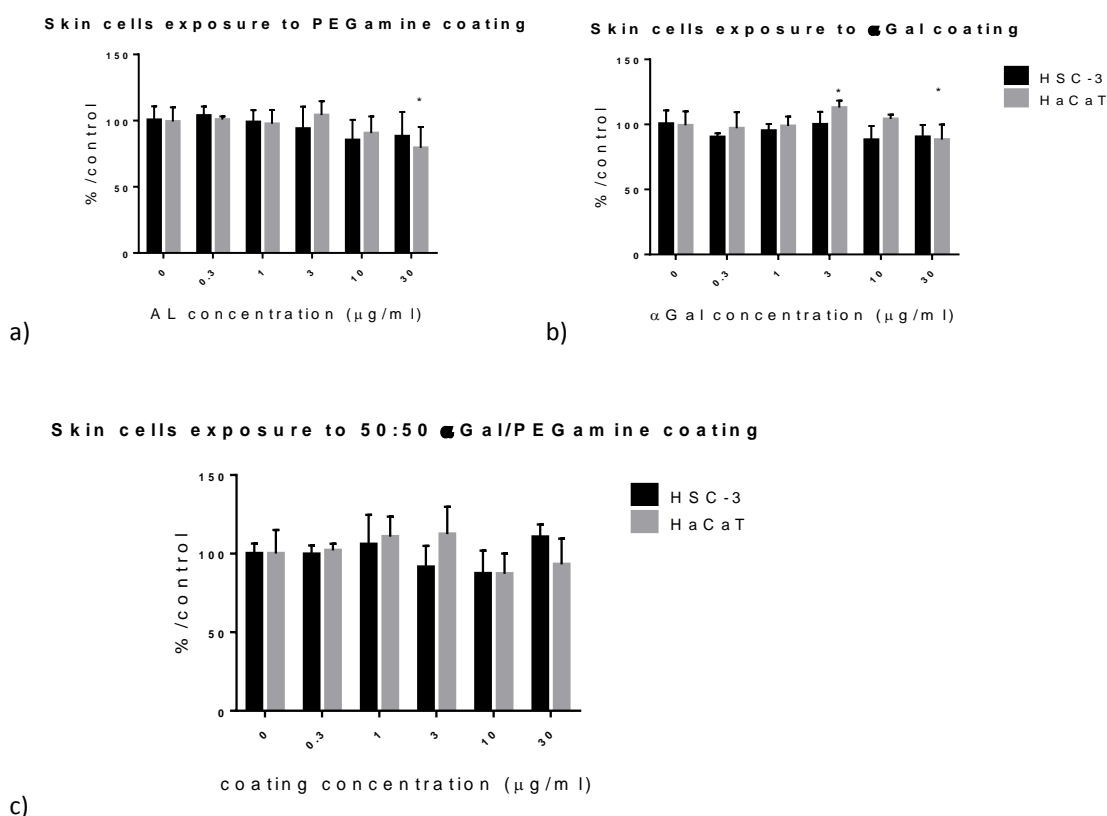


Figure 3.10: Skin cells exposed to different concentration of the molecules coating the AuNPs. a) PEGamine exposure, b) α Galactose, c) 50:50 α Gal:PEGamine exposure. The graphs represent the percentage of viability compared to the control. Data are presented as mean colonies \pm standard deviation. Statistical comparisons with no-ligand controls was done by two-way ANOVA with Dunett post-test.

When looking at the response of both HSC-3 and HaCaT exposed to PEGamine only, the molecule itself does not have any statistically significant effect on the HSC-3 cells as the viability

remains constant, whereas it is responsible for a small statistically significant effect for HaCaT cells only at 30 $\mu\text{g/ml}$ ($p < 0.05$) (Figure 3.10 a). The same result was seen when the cells were exposed to $\alpha\text{Galactose}$, with no obvious toxicity (Figure 3.10 b) being reported for HSC-3 and again a small statistical difference for HaCaT at 30 $\mu\text{g/ml}$ ($p < 0.05$). Finally, when looking at the cell viability after exposure of a mixture of $\alpha\text{Galactose}$ and PEGamine, no significant difference where observed for HSC-3 or HaCaT (Figure 3.9 c). These data indicate that the ligands are not appreciably toxic by themselves. However, the intracellular concentration of ligands was not assessed, and it could be that the combination of ligands with AuNPs acts as a delivery vector to greatly increase intracellular ligand uptake.

3.6. AuNPs binding properties to culture plastic

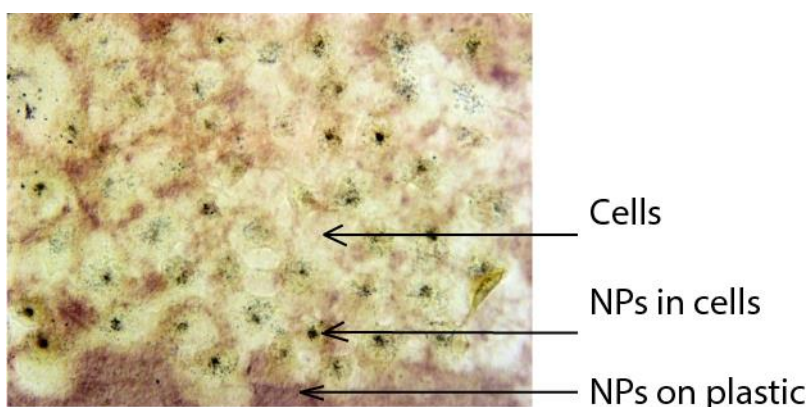


Figure 3.11: Silver staining of HSC-3 cells exposed to 50:50 αGal :PEGamine on culture plastic plates.

All the toxicity studies are made on *in vitro* models, using plastic plates to cultivate and expose cell models to AuNPs. Unfortunately, as well as entering into cells, these AuNPs also demonstrate some adherence to the plastic (Figure 3.11). For these specific experiments, the cells were over-exposed with the AuNPs, and over-silver stained in order to accentuate the background of the AuNPs. These experiments are detailed in Section 2.9. The mechanisms of AuNPs sticking to the culture plate is unknown, although an electrostatic interaction with the negative plastic surface could be a hypothesis. The substrate used to perform the AuNPs exposure might have an effect on this sticking. Incubation with different solvents could give information on the types of forces that cause this interaction. Moreover, different types of washes could help to limit or reduce this sticking. Several pilot experiments were performed to investigate AuNP binding to various substrates that could be used for cell culture.

3.6.1. Possible electrostatic interaction between AuNPs and surfaces

50:50 α Gal:PEGamine AuNPs NPs were diluted in medium with or without 10 % foetal calf serum, or in Hank's solution, and were seeded on 24 well plates for 3 h in the incubator to replicate cell culture conditions.

These same AuNPs were diluted in 15 ml falcon tubes and then were put on glass coverslips and culture plastic to examine adhesion to different substrates.

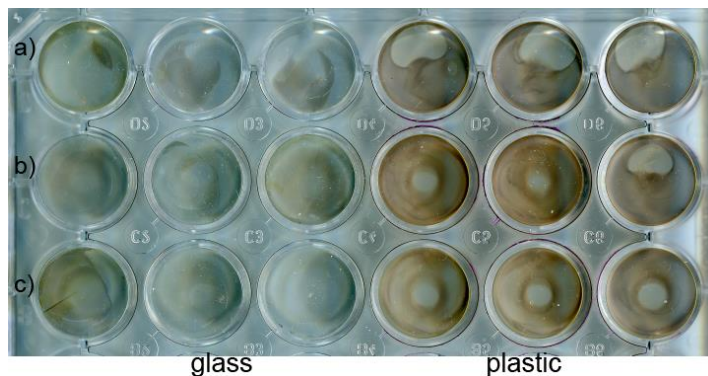


Figure 3.12: silver staining observation of AuNPs loading for 3 hours in 50 μ l (glass) or 500 μ l (plastic) of a) Hank's solution, b) medium without serum, c) medium + serum.

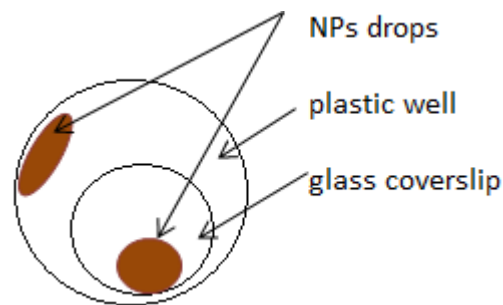


Figure 3.13: schematic view of placement of AuNP drops in a culture plate well

No obvious differences in adhesion were detected using either specific cell medium DMEM with or without serum, or Hank's solution (figure 3.12a, b, c), while the amount of AuNPs adhering to plastic is higher than the one observed on glass surfaces (Figure 3.12 and 3.13).

The PEGamine ligand gives AuNPs a positive charge, which may cause binding to culture plastic, which has a negative charge. α Gal:PEGamine 50:50 AuNPs were diluted in 500 μ l of serum containing medium, ethanol, water, Hank's buffered saline or 5 M NaCl and were put on 24 well plates to examine their adhesion after 3 hours in the incubator. Ethanol and high molarity NaCl solvent were chosen in order to decrease electrostatic interaction of the AuNPs with the plastic.



Figure 3.14: Silver staining of AuNPs loaded in a) medium + serum, 1 h, b) medium + serum, 3 h, c) distilled water, 3 h, d) ethanol, 3 h, e) 5 M NaCl, 3 h, f) Hank's solution, 3 h.

There is no detectable difference in AuNPs attachment after an hour or 3 hours of incubation in DMEM with serum (Figure 3.14 a, b). Moreover, AuNPs bind to plastic when applied in water or in Hank's buffered saline (0.14 M NaCl) (Figure 3.14 c, f), but the binding decreases when AuNPs were diluted in ethanol or 5 M NaCl (Figure 3.14 d, e). These data are consistent with the hypothesis of an electrostatic interaction.

3.6.2. Effect on AuNP attachment of washing after loading.

After incubation of AuNPs in culture plates for 3 hours, the plates were washed for 3 hours or 24 hours with medium.

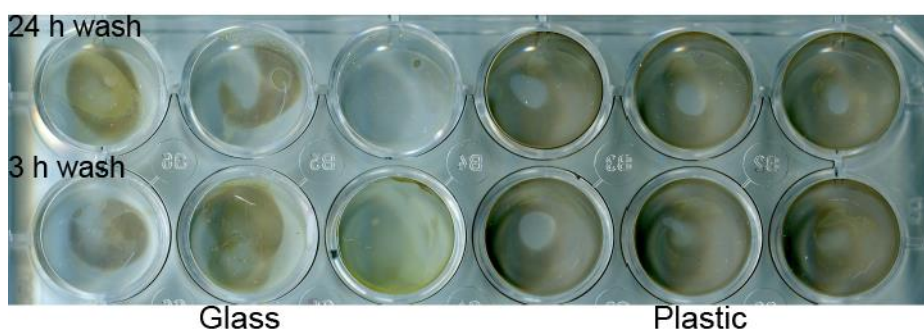


Figure 3.15: Silver staining observation of AuNPs loading for 3 h in 50 µl (glass) or 500 µl (plastic) of medium.

Here again, the staining seemed to be the same for both the time washes (Figure 3.15 a, b). AuNPs sticking seemed to be rapid and, once bound, they were difficult to remove with washes.

Finally, after testing different conditions of AuNPs exposure on plates, another type of surface loading was explored. Falcon tubes could be an alternative to expose the cells, therefore, the AuNPs adhesion was also tested on Falcon tubes. The AuNPs were loaded in 15ml Falcon tubes at a concentration of 10 µg/ml, in a volume of 500 µL, for 3 hours in medium. These AuNPs do not seem to adhere to Falcon tubes (Figure 3.16) as very little silver staining is observed, compared to the staining seen on plastic plates. Cultivating and exposure of floating cells in

Falcon tubes would therefore help to verify the toxic effect of 50:50 α Gal:PEGamine AuNPs on cells, in the absence of AuNP plastic sticking.

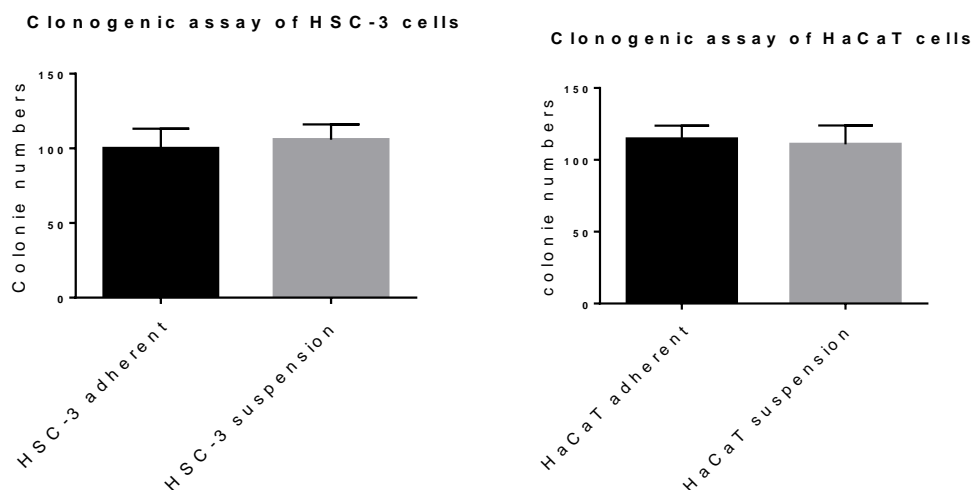


Figure 3.16: Silver staining observations, after 3h of AuNPs diluted in medium with serum and loaded in 15 ml falcon tubes.

3.7. Attachment of AuNPs to substrates and their toxicity under cell culture conditions

Cells were loaded with AuNPs in suspension culture, washed and then seeded on culture plastic for clonogenic assays.

The first experiment focused on comparing the AuNP loading of adherent cells with suspension culture cells.



a)

b)

Figure 3.17: Clonogenic assay of cells loaded in adherent conditions or in suspension. a) HSC-3 cells, B) HaCaT cells. The data are expressed in colony numbers with the standard deviation and a paired t-test with two-tail p value was used to determine any significant difference.

By comparing the number of colonies after loading the cells directly on plates or first in suspension and then adherently, the colony development is not significantly different between these two conditions ($p=0.82$ for HSC-3 and $p=0.36$ for HaCaT) (Figure 3.17). Therefore, the effect of different AuNP ligand ratios on clonogenic survival was determined following cell loading for 3 hrs in suspension culture, then plating the cells at clonogenic density. This experiment can provide information on the potential toxic role of the AuNPs attachment to the plastic surface.

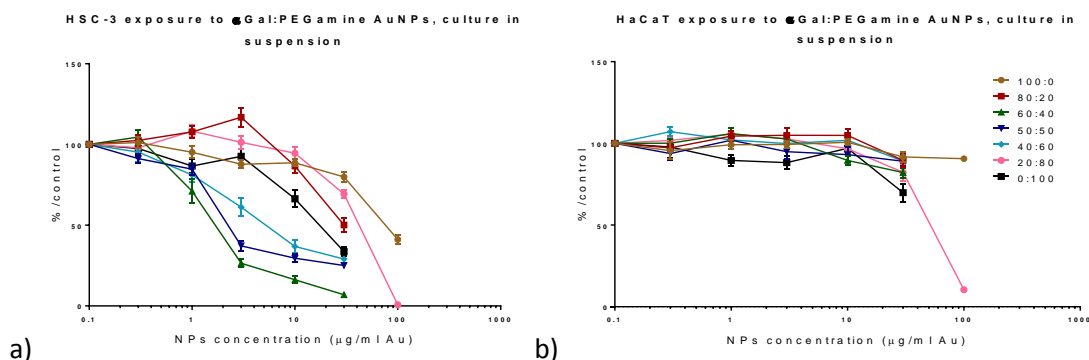


Figure 3.18: Clonogenic assay after AuNPs exposure on cells in suspension at different concentrations and different ratios of α Gal:PEGamine. a) HSC-3 cells exposure, b) HaCaT cells exposure. The graphs represent the percentage colonies at various AuNP concentrations, compared to the control without AuNPs. The data are presented as mean percentage colonies \pm standard deviation. Statistical differences in dose responses for each AuNPs on each cell line was analysed by one two Anova followed by a Dunnett's multiple comparisons test.

Table 3.4: Toxicity of different AuNPs on HSC-3 loaded in suspension culture. As a reminder, the IC50 concentrations of cells exposed adherently are also mentioned.

HSC-3 exposure for 3 hours to the different AuNPs	100:0	80:20	60:40	50:50	40:60	20:80	0:100
IC50 (μ g/ml) suspension cultures	>100	23 \pm 1.10	1.8 \pm 1.10	3.4 \pm 1.12	6.2 \pm 1.14	45.5 \pm 1.21	17.4 \pm 1.12
IC50 (μ g/ml) adherent cultures	>100	23 \pm 1.10	4.2 \pm 1.13	0.8 \pm 1.03	6.8 \pm 1.13	20 \pm 1.07	13 \pm 1.10

When studying the dose response of HSC-3 and HaCaT exposed to different AuNPs on floating conditions, it was found that the toxicity is similar to when cells were exposed under adherent conditions. Indeed, when estimating the IC50 values for cells exposed in suspension, these values are equivalent to the ones obtained with adherent cultures (Table 3.3 and 3.4), apart for the ratio 20:80 where the IC50 is higher when the cells were exposed in suspension. This is unexpected as all the AuNPs were more toxic to the cells when exposed in suspension. These specific AuNPs might interact specifically with the plastic surface and therefore give a lower response to the cells in suspension due to lower uptake. Moreover, 60:40 α Gal:PEGamine is the ratio responsible for the highest toxicity on HSC-3 cells on floating conditions ($p < 0.0001$ at 1 μ g/ml exposure), compared to the 50:50 on adherent conditions (Figure 3.18) (Annex 3.3).

Comparison of IC 50 concentrations toward HSC-3 cells

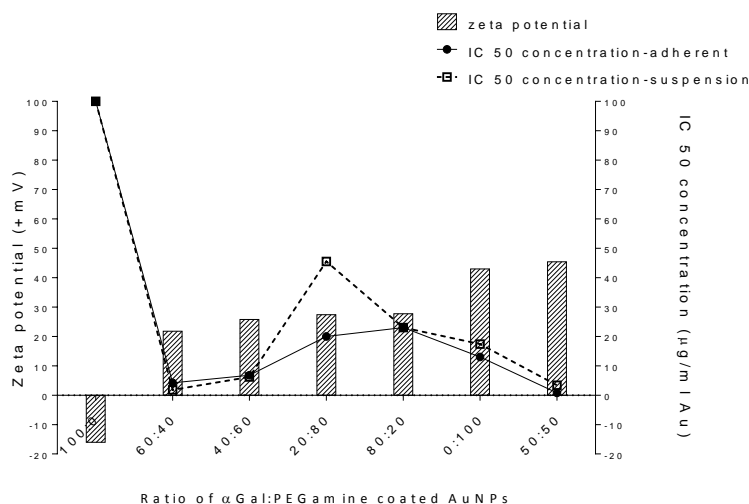


Figure 3.19: IC50 values for HSC-3 cultivated on plates or in suspension arranged is ascending order of zeta potential.

In representing the relationship between AuNPs toxicity and its charge, there is no linear relationship between these two factors (Figure 3.19). However, positively charged AuNPs seem to have a toxic effect on cells and the 50:50 α Gal:PEGamine AuNPs, which give the strongest toxicity, have the highest zeta potential, while negatively charged AuNPs seem to be non-toxic as the 100:0 α Gal:PEGamine AuNPs, which have the lowest zeta potential and negatively charged, give the lowest toxicity.

3.8. AuNP toxicity is related to cellular uptake

3.8.1. Amount of gold per cell

50:50 α Gal:PEGamine AuNPs were found to be selectively toxic for HSC-3 cancer cells, and the AuNPs sticking to the culture plastic is not involved in this effect. So, how does this toxicity occur? A simple hypothesis would be that the toxicity for each AuNP is linked to its cellular uptake. If the hypothesis is true, therefore, cells loaded with equitoxic concentrations of different AuNPs (e.g. each AuNP at its IC 50 concentration) would show an identical intracellular concentration.

Cells were loaded with the IC50 concentration of each AuNP under suspension culture conditions, to minimise sticking to plastic. The experiment protocol is detailed in Section 2.13.

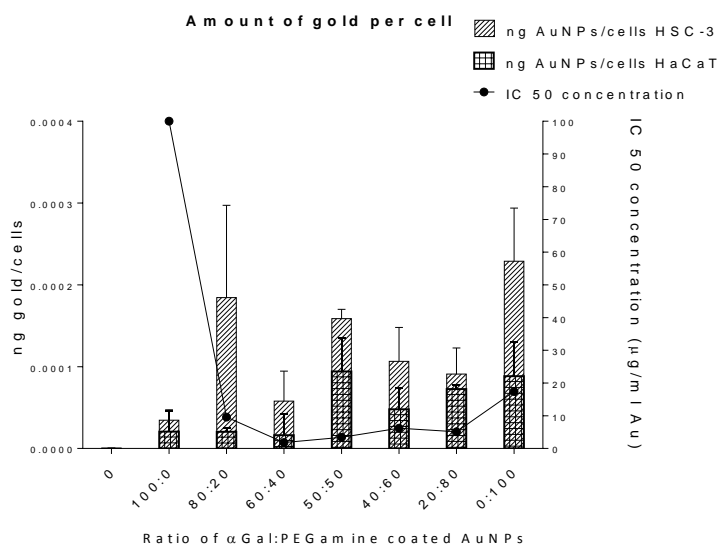


Figure 3.20: Amount of gold per cells. IC50 plotted as a line. The data are presented as mean percentage survival with the standard deviation.

The amount of AuNPs per cells was explored by measuring the total amount of gold present in the total number of cells. Figure 3.20 shows that of the amount seems to be higher inside cancer cells as compared to the normal ones. This uptake inside cells depends also of the AuNPs coating. AuNPs coated with 50:50, 80:20 or 0:100 α Gal:PEGamine show the highest concentration of AuNPs inside HSC-3 cells. These AuNPs are the one also characterised by the highest zeta potential, and thus, with the highest positive charge. The charge is known to have an influence on toxicity and uptake. In the particular case of α Galactose:PEGamine coated AuNPs, negative charged AuNPs did not enter in the cells, while high positively charged AuNPs did enter in cells and caused a strong toxicity (Table 3.2, Figure 3.20). One possible reason for lack of uptake of these negative charged AuNPs, coated with α Galactose, is their instability in solution. Indeed, when looking at their size on TEM, these AuNPs particularly, appear to show substantial aggregation in culture media which would lower their bioavailability for cellular uptake (Figure 3.7). Moreover, Hauck *et al* (2008) reported a possible electrostatic interaction between the negative charge membrane of the cells and positive charged of the NPs which would favours their uptake (Hauck T.S *et al.*, 2008).

The average quantity of gold per cell measured was between 1 and 2 pg/ml. This concentration is smaller than in previous experiments (Cui *et al.*, 2017, Jain *et al.*, 2014). However, the concentration used in our case was also much smaller. Indeed, while Jain *et al* showed a concentration of 4 μ g/ml inside cells, while they used a concentration of 12 μ M on MDA-MB-231 cells (Jain *et al.*, 2014), and a concentration of 40 pg/cell was shown after a exposure at a concentration of 0.5 mg/ml for Cui *et al* (Cui *et al.*, 2017) compared to 1-10 μ g in our case. Finally, although there is a trend, the amount of gold per cell is not directly linked to

the toxic concentration, as the 50:50 α Gal:PEGamine AuNPs is the most toxic toward cancer cells but does not lead to the highest concentration inside cells (Figure 3.19).

Previous works have mentioned the importance of the AuNPs size for cellular uptake and its potential toxic effect (Zarschler *et al.*, 2016). In this case, the combination of α Gal:PEGamine molecules is more likely to be responsible for this toxic effect. It has been suggested that the serum containing medium has an impact on the AuNPs surface and may have an impact on the uptake of these AuNPs by cells (Hauck T.S *et al.*, 2008). Indeed, this hypothesis is tested in the laboratory and the preliminary results show that without serum, the AuNPs have a lower uptake. The protein corona on the AuNPs seems to play a strong role in the cellular uptake (Deng *et al.*, 2015). Moreover, the charge seems to strongly play a role in the cellular uptake. It could also play a role of the AuNPs localisation in the cells. The next experiment focused on the localisation of the two 50:50 and 0:100 α Gal:PEGamine AuNPs inside the cells, as they both show the highest uptake on cells using ICPMS.

3.8.2. Where do AuNPs accumulate inside cells?

To explore the intracellular localisation of the 50:50 and 0:100 α Gal:PEGamine AuNPs, TEM analysis was used. This experiment is detailed in Section 2.14. A constant loading concentration of 10 μ g/ml was used to better visualise the AuNPs in the cells. TEM shows that AuNPs accumulate preferentially in HSC-3 cells (Figure 3.21 b, e) mainly within vesicles that may be lysosomes (Figure 3.21 c, f). It is possible to notice some accumulation close to the nucleus. However, AuNPs were not seen within the nucleus or the mitochondria (Table 3.5).

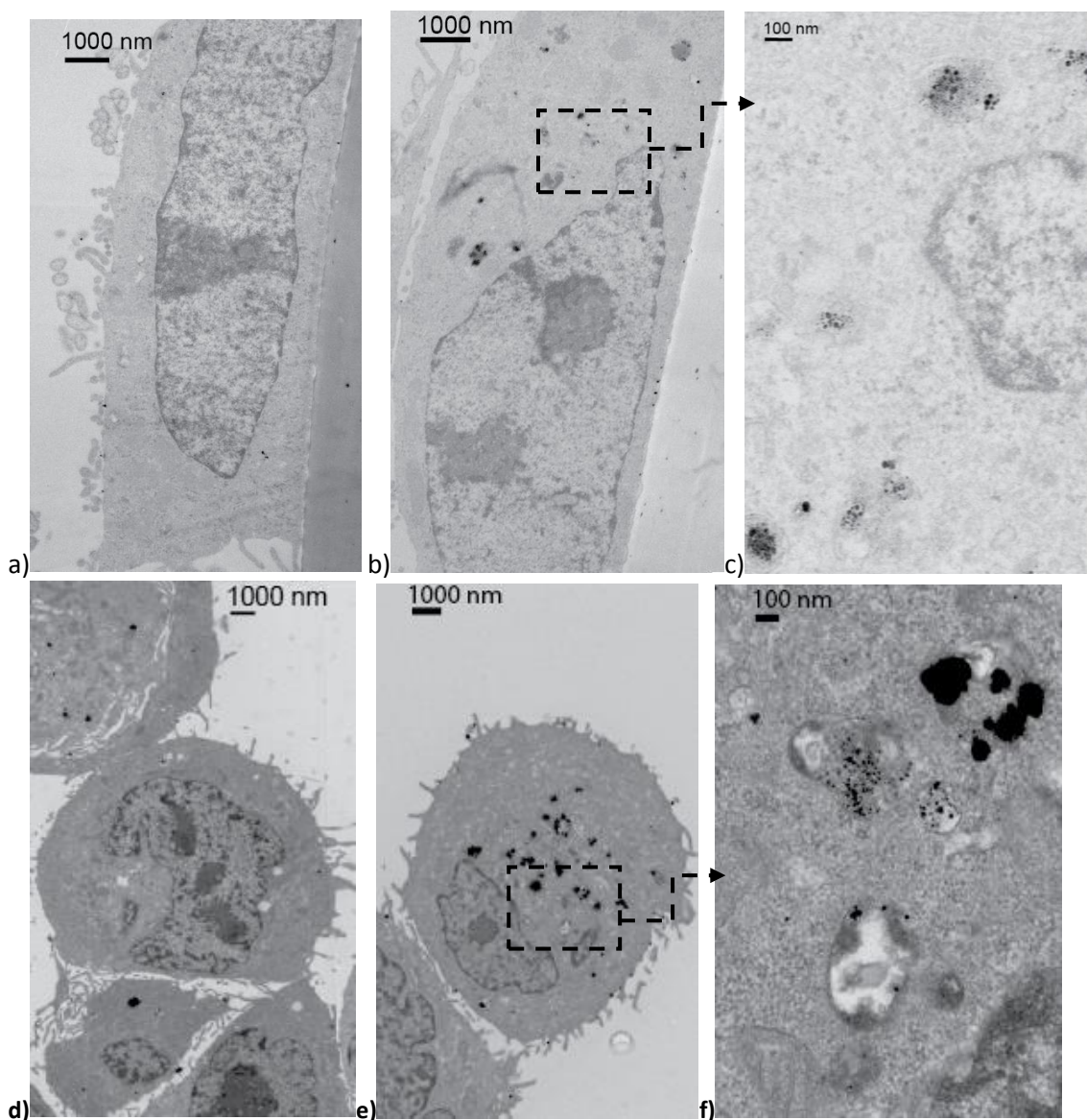


Figure 3.21: Observation by transmission electron microscopy (TEM) of both a;d) HaCaT and b,c,e,f) HSC-3 exposed for 3 h to 10 $\mu\text{g/ml}$ of either 50:50 αGal :PEGamine on top line or 0:100 αGal :PEGamine AuNPs on bottom line. The dotted boxes represent a 10-times zoom of this specific area.

Table 3.5a: Approximation of the number of AuNPs per region of the cell, measured from TEM images of cells exposed to the AuNPs for 3 hours at 10 $\mu\text{g/ml}$ concentration

	50:50 αGal :PEGamine		0:100 αGal :PEGamine	
	HSC-3	HaCaT	HSC-3	HaCaT
Cytoplasm (NP/nm²)	$170 \cdot 10^{-5}$	$26 \cdot 10^{-5}$	$100 \cdot 10^{-5}$	$19 \cdot 10^{-5}$
Nucleus (NP/nm²)	0	0	0	0
Surface (NP/nm)	$17 \cdot 10^{-5}$	$5.8 \cdot 10^{-5}$	$5.2 \cdot 10^{-5}$	$1.9 \cdot 10^{-5}$

Table 3.5b: Average surface area of the cell, its nucleus and its cytoplasm. An unpaired t-test was performed to analyse the statistical difference for each surface area between the two types of cells.

	HSC-3	HaCaT
Cytoplasm (10⁵ nm²)	1.06 ± 0.1	0.98 ± 0.1
Nucleus (10⁵ nm²)	0.56 ± 0.12	0.5 ± 0.1
Entire cell (10⁵ nm²)	1.62 ± 0.2	1.5 ± 0.2

From 10 images taken of each cell exposure, it was possible to measure the amount of AuNP in the different cell organelles. Since the cells were fixed just after exposure, no toxicity will be observed. The highest number of AuNPs is found in the cytoplasm, including vesicles and is 10 times more in cancer cells than in normal cells (Table 3.5a). In addition, some AuNPs are seen on the surface of the cell, and again more are seen on cancer cells than normal cells. This could indicate that AuNPs are interacting more with the membrane of cancer cells than normal cells, improving the cellular uptake, as suggested in the introduction. It is important to note that from the mass spectrometry studies, the 0:100 α Gal:PEGamine AuNPs seems to be responsible for more gold inside the cells compared to the 50:50 α Gal:PEGamine AuNPs (2 pg/cell compared to 1 pg/cell) but less NPs/nm² using TEM (100 NP/nm² compared to 170 nm²). It is important to mention that these experiments have been done only and give indication on the NPs uptake but no affirmative conclusion on the relative uptake. Moreover, a hypothesis from these experiment might be that 50:50 α Gal:PEGamine AuNPs accumulate in specific part of the cells and in bigger quantity while 0:100 α Gal:PEGamine AuNPs could be more spread around the different cells.

From the TEM images, it was also possible to approximate the surface area of skin cancer and normal cells (Table 3.5b). It is possible to note that both cells have similar average cell surface area and similar nucleus and cytoplasm area, with no statistical difference between the two cell lines. Therefore, the surface area of the cells does not seem to be playing a role in the difference in uptake observed in this case.

The AuNPs surface also plays a role on the localisation of AuNPs in the cells, and has a strong impact on its further toxicity (Connor *et al.*, 2005, Hauck T.S *et al.*, 2008, Mironava *et al.*, 2010). The AuNPs localisation for the 50:50 α Gal:PEGamine AuNPs was seen mainly in vesicles after 3h of exposure (Figure 3.21). It will be interesting to explore if this localisation differs between the different ratios of α Gal:PEGamine. However, at this stage, it is not known whether the coating and the charge on the AuNPs remained unchanged, as this can have a further impact on the final destination of the AuNPs in the cells (Connor *et al.*, 2005, Mironava *et al.*, 2010).

Indeed, for example, Hauck *et al.* (2008) showed that positively charged AuNPs accumulate in vesicles (Hauck T.S *et al.*, 2008). Wang *et al.* (2013) showed in addition that Glucose coated AuNPs accumulate in endosomes-lysosomes, which is the final degrading destination of the molecules taken up via endocytosis (Wang *et al.*, 2013). Moreover, strong positively charged AuNPs would likely be found in the mitochondria (Orosz *et al.*, 2017), which is not seen in the case of α Gal:PEGamine AuNPs. Finally, the possibility of an exchange reaction with GSH molecules inside the cells have already been mentioned, and could explain a specific localisation in the cells (Gromnicova, 2017, McCully *et al.*, 2015). For example, Sousa *et al.* (2008) showed that ultrasmall AuNPs coated with GSH accumulated in the cytoplasm of Hela cells (Sousa *et al.*, 2012).

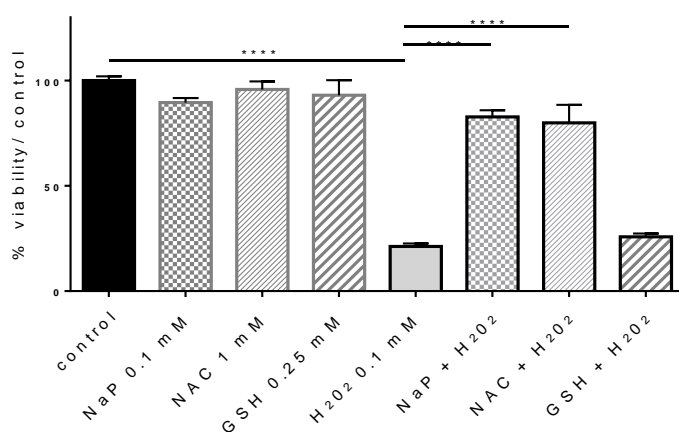
3.9. AuNPs toxicity on cells, role of oxidative stress and caspase dependent apoptosis

3.9.1. Role of oxidative stress in AuNP toxicity

AuNPs could increase intracellular oxidative stress either by inhibiting antioxidant pathways, or by promoting pro-oxidant pathways. Indeed, inside the cells, AuNPs can increase the amount of radicals due to their chemical reactive surface (Cui *et al.*, 2013). This has been described in Section 1.5. AuNPs can also induce apoptosis or inflammation which will then engender ROS production (Fu *et al.*, 2014).

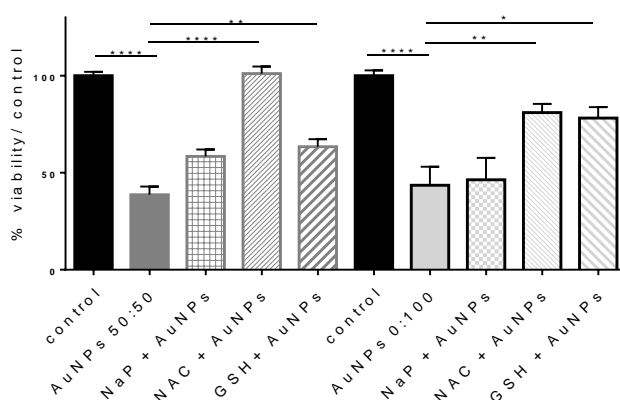
HSC-3 cells were exposed to 1 μ g/ml of 50:50 α Gal:PEGamine AuNPs in the presence or absence of different antioxidants. This AuNP concentration was chosen so as to achieve a baseline ~50% toxicity. The antioxidants used were reduced glutathione (GSH), or sodium pyruvate (NaP), or N-Acetylcysteine (NAC). While GSH and NAC can detoxify different ROS species inside the cells, sodium pyruvate is responsible for the detoxification of H₂O₂, particularly outside the cells (Kelts *et al.*, 2015, Lord-Fontaine and Averill-Bates, 2002, Franco *et al.*, 2007). All three cover different antioxidant pathways and therefore can give an indication of which of them is inhibited/interacting with the AuNPs, as detailed below. The following experiment is described in Section 2.15.1.

HSC-3 exposure +/- antioxidants



a)

HSC-3 exposure +/- antioxidants



b)

Figure 3.22: a) Clonogenic assay of HSC-3 cells exposed to H₂O₂ in presence or in absence of antioxidants (1 mM NAC, or 0.25 mM GSH, or 0.1 mM NaP). b) Clonogenic assay of HSC-3 cells exposed to AuNPs in presence or in absence of antioxidants (1 mM NAC, or 0.25 mM GSH, or 0.1 mM NaP). The data are expressed in percentage colonies with the standard deviation and a one-way ANOVA, followed by Bonferroni post-test was used to quantify any significant differences between each condition.

Figure 3.22a shows the effect of three different antioxidants, in the presence or absence of H₂O₂, as a positive control for ROS-mediated cell death. None of the antioxidants are toxic for HSC-3 cells at the concentration chosen as the number of cell colonies remains similar to the control. H₂O₂ alone decreases the number of colonies after 6 days of culture. It is responsible for 78 % decrease of viability compared to the control ($p < 0.0001$), while AuNPs are responsible for a 60% decrease ($p < 0.0001$). However, when the cells were incubated with H₂O₂ in combination with either NaP or NAC, the toxic effect of H₂O₂ was entirely inhibited, with a cell viability not significantly different to the control. However, GSH did not inhibit the toxicity from H₂O₂ as the viability remained the same with or without the antioxidant.

The same three antioxidants were used in the presence of AuNPs to determine if they could decrease the cell toxicity after AuNPs exposure. Sodium pyruvate was used to study the possible amount of ROS outside the cells while NAC and GSH are effective inside the cells. Indeed, knowing where ROS are produced can give indication on the AuNPs toxicity. (Kelts *et al.*, 2015). Figure 3.22 b shows that the toxicity from either 50:50 or 0:100 C AuNPs is decrease by 59% when using NAC and by 21% when using GSH. For of 50:50 α Gal:PEGamine, the combination with NAC inhibits entirely the toxicity from the AuNPs ($p < 0.0001$). However, NaP did not inhibit the toxicity after AuNPs exposure ($p > 0.05$).

NAC, GSH and NaP do not have the same mechanism of effect, suggesting a particular pathway for the oxidative stress. NaP is able to neutralize peroxides, due to its α -keto-carboxylate structure (Wang *et al.*, 2007) and acts as a peroxide scavenger, mainly outside the cells (Gupta S.K *et al.*, 2000). Pyruvate molecule can be transported inside the cells via proton-monocarboxylate cotransporter. Predominantly extracellular antioxidant, it can also act intracellular (Lord-Fontaine and Averill-Bates, 2002). NAC, due to its structure, can act as a direct antioxidant via its free thiol group, and as a synthetic precursor of reduced glutathione (GSH), a well-known molecule involved in detoxification (Van Zandwijk, 1995, Dekhuijzen, 2004). GSH is the most highly concentrated antioxidant in cells and is responsible for the detoxification of many reactive oxygen species such as hydroxyl radicals, superoxide anion and nitric oxide, however GSH requires the presence of the glutathione peroxidase for the detoxification of H_2O_2 (Lushchak, 2012).

GSH is not able to prevent the cellular toxicity from H_2O_2 but is able, similarly to NAC, to decrease the toxicity due to AuNPs, with a statistically significant difference. It suggests that the oxidative stress induced by the presence of AuNPs does not depend entirely on H_2O_2 species but also on formation of other radical species such as $\cdot O_2$ or singlet oxygen (1O_2) (Zhang *et al.*, 2013). In addition, as NaP does prevent the toxicity from the AuNPs, suggesting that the ROS formed and responsible for the toxicity are more likely inside the cells.

Cells have developed antioxidant defences to fight against oxidative stress and regulate their physiological balance. Xia *et al.* described in 2008 a hierarchical oxidative stress model after NPs exposure (Xia *et al.*, 2008). The cell will fight the oxidative stress differently depending on the amount of ROS produced. During the first stage, where the amount of ROS produced is low, the cells activate radical scavengers and enzymatic enzymes which are controlled by the nuclear factor (erythroid-derived 2)-like 2 (Nrf2) (Havaki *et al.*, 2015, Xia *et al.*, 2008). When the ROS production increases, the cells activate preferentially pro-inflammatory pathways, rather than antioxidants, through the activation of MAP kinases and NF- κ b pathways.

Interestingly, Yang *et al* (2007) have shown that the antioxidant NAC up regulates apoptosis (78 % after a concentration of 10 mM NAC) in melanoma cells through a decrease of the NF- κ B-mediated event, which decreases the expression of anti-apoptotic genes such as Bcl-2. NAC also affected the mitochondria by lowering their membrane potential (Yang *et al.*, 2007). Indeed, at high levels of ROS, a perturbation of the mitochondrial membrane permeability occurs, inducing apoptosis (Xia *et al.*, 2008). NF- κ B plays an important role in the cell survival. Indeed, it is part of a family which is activated by different signals such as ROS or tumor necrosis factor (TNF), thus increasing the expression of anti-apoptotic proteins, decreasing cell death, and increasing the antioxidant defences (Yang *et al.*, 2007). One possible toxic mechanism of AuNPs in the cells is to interact with the NF- κ B system, by binding to the NF- κ B transcription factor and preventing its translocation to the nucleus and the transcription of cell factors, and therefore dysregulate the antioxidant defences (Pujalté *et al.*, 2015).

3.9.2. ROS measurement in cells

The general intracellular ROS probe carboxy DCFH-DA was used in FACS analysis to quantify reactive oxygen species in cells after exposure to AuNPs or positive control TBHP oxidant. This experiment is detailed in Section 2.15.2. DCFH-DA is well known to detect diverse ROS, such as H₂O₂, HO[•], ONOO[•].

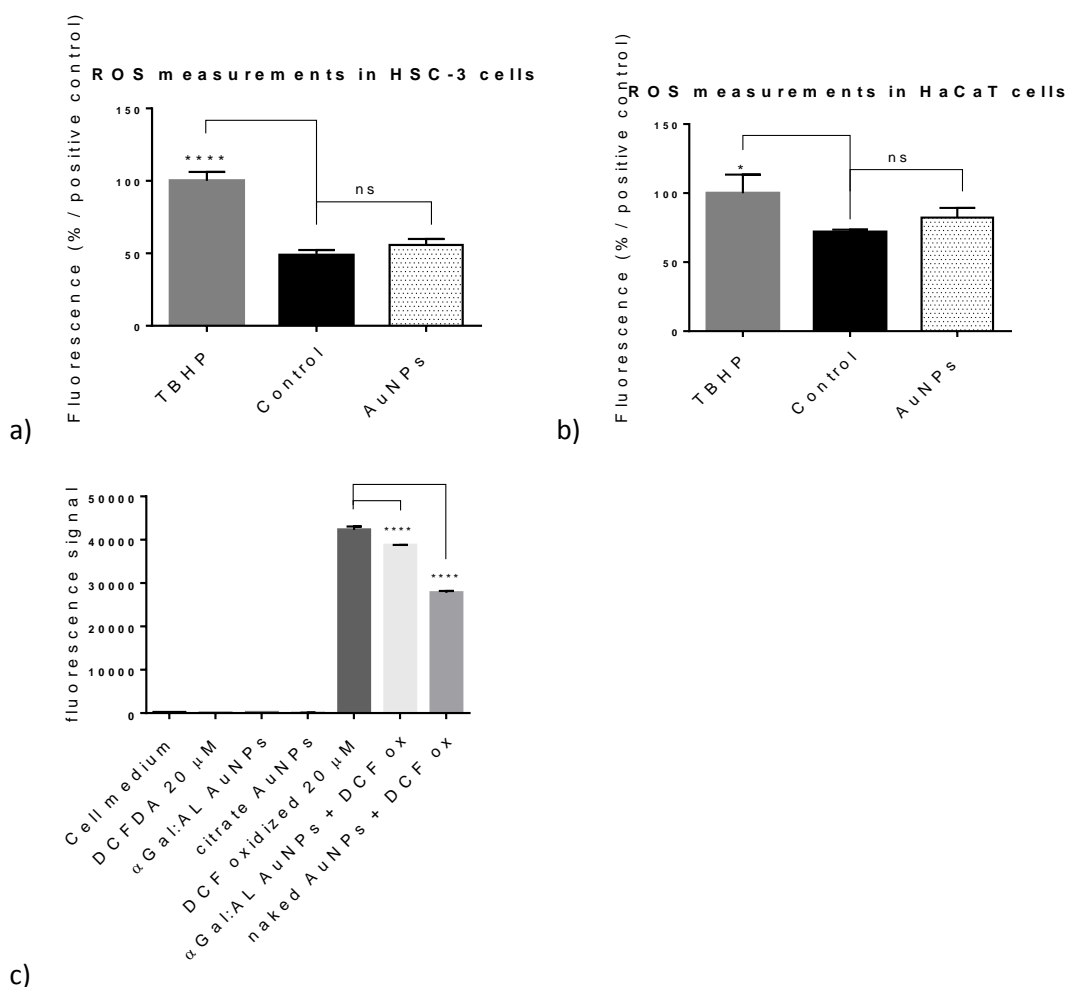


Figure 3.23: Fluorescence measurement of DCFH-DA or its oxidised form DCF, diluted in medium in presence or absence of AuNPs. a) Measurements in HSC-3 cells, b) measurements in HaCaT cells, c) measurements of AuNPs interaction without any cells. The data are expressed with their standard deviation values and a one way Anova followed by a Tukey post-test was used to compare the different conditions. The different asterisks show a significant difference compared to the control or to different conditions.

In order to measure the potential ROS production inside cells after AuNPs exposure, DCFDA probe was used. Figure 3.23 a, b, c does not show any statistical difference compared to the control (Figure 3.23 a, b, c), therefore, 50:50 αGal:PEGamine AuNPs do not seem to increase the radical production inside the cells.

However, AuNPs are known to interact with fluorescent probes and quench their fluorescence. In order to explore if this phenomenon happened with the αGal:PEGamine coated AuNPs, they were incubated with the oxidised, fluorescent probe, but without cells. In the presence of AuNPs probe fluorescence was decreased by around 10% (Figure 3.23 c). Assuming a similar effect within cells, the fluorescence values in the presence of AuNPs in Fig 3.23 a and b

would rise to about 70% and 90% respectively and may have shown significance compared with the control.

AuNPs were responsible for an oxidative stress inside the cells, which did not depend entirely on radical production such as $\cdot\text{OH}$ and H_2O_2 . Indeed, the DCFHDA probe used in order to detect radicals such as $\cdot\text{OH}$ and H_2O_2 did not show any increase of oxidative stress after AuNPs exposure for 3 h. The oxidative stress caused by the AuNPs might be a late or cumulative process and it will be interesting to look at another time point, such as 24h after AuNPs exposure (Thakor *et al.*, 2011). AuNPs could have an impact on the amount of antioxidant, increasing other types of radical levels.

3.9.3. Is caspase dependent death involved in AuNPs toxicity?

Apoptosis is a physiological cell death that can happen after a stress and is characterised by an absence of inflammation (Egger *et al.*, 2003). Caspase dependant apoptosis involves a cascade of caspase activation, culminating in caspase 3 activation. To explore if the caspase dependant pathway was involved in AuNPs toxicity, a pan-caspase inhibitor (Z-VAD.fmk) was used to explore if this would inhibit AuNPs toxicity, inhibiting particularly caspase 3. The experiment is described in Section 2.12.

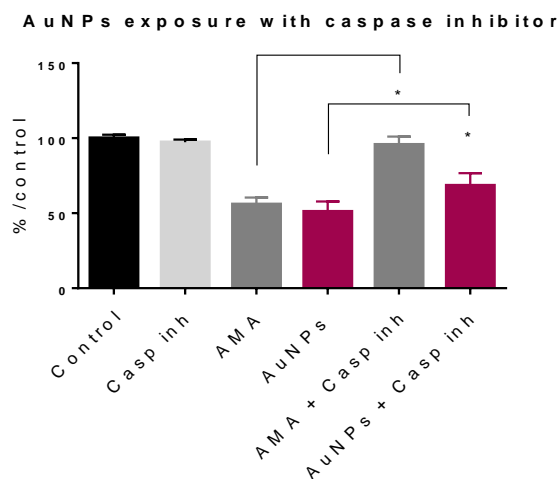


Figure 3.24: Response of HSC-3 exposed to 50:50 αGal :PEGamine AuNPs at a concentration of $1 \mu\text{g}/\text{ml}$, with or without caspase inhibitor. Antimycin A (AMA) was used as a positive control. The graphs represent the number of cell colonies depending on the cell exposure. The data are expressed in percentage with the standard deviation and a one way Anova, followed by a Dunnett post-test was realised to study the difference between numbers of colonies, compared to the control.

Z-VAD.fmk can inhibit caspase activity by crosslinking the fmk group to the cysteine on their active site, with different specificity for each caspase (Egger *et al.*, 2003). In this experiment, Z-

VAD.fmk rescues HSC-3 cells from death due to AMA (Figure 3.24). AMA is a positive control here as it can induce caspase dependant apoptosis (Park *et al.*, 2007). The caspase inhibitor also partially rescues HSC-3 cells from cell death due to AuNPs ($p < 0.05$) (Figure 3.24). In contrast, when HSC-3 cells were incubated with caspase inhibitor only, there was no change in cell colony numbers, compared to the untreated control ($p > 0.05$). These data indicate that AuNP-induced cell death is partially caspase-dependant. It is important to mention that the caspase inhibitor was added to the cells exposed to AuNPs up to 24h after exposure. Apoptosis cell death could increase with time after exposure and therefore the timing of the caspase inhibitor might be critical for the cell death rescue due to caspase dependant apoptosis. Other caspase-independent types of cell death, such as necrosis-like programmed cell death, can be associated with ROS increase (Kögel and Prehn, 2013). Such mechanisms may also be operating here.

3.10. AuNPs interaction with irradiation

3.10.1. Intrinsic properties of AuNPs to interact with irradiation

The 50:50 and 0:100 α Gal:PEGamine AuNPs were selected for radiosensitisation experiments based on their selective chemotoxicity and high uptake per cancer cell. Radiosensitisation is improved by having a high amount of AuNPs inside cells (Arvizo *et al.*), therefore these two AuNPs should be good candidates for radiotherapy studies. The intrinsic radiosensitisation potential of the two different AuNPs was explored by developing a novel coumarin assay to measure the amount of \cdot OH radical produced in solution after X-irradiation

The first experiments were focused on optimising the assay by exploring different concentrations of 3-carboxy-coumarin carboxylic acid (3-CCA) in order to obtain the optimum response. The effect of buffer to dilute the 3-CCA, as well as the concentration of AuNPs used were also explored. Finally, it appeared that when AuNPs were added in the solution, they quenched the fluorescence of the hydroxylated product 7-hydroxy coumarin carboxylic acid (7-OHCCA) and thus the solution needed to be cleared from the AuNPs before being measured using 3 KDa cutoff spin filter plates. Here again, optimisation was required, as the 7-OHCCA interacted with the plate surface and did not pass the filter. Adding pure EtOH in the solution before centrifugation improved 7-OHCCA solubility and passage through the filter. Finally, the optimum protocol for measuring the fluorescence of the 7-OHCCA in presence of AuNPs was used in subsequent experiments. The optimum protocol for the coumarin assay is described in Section 2.15.3.

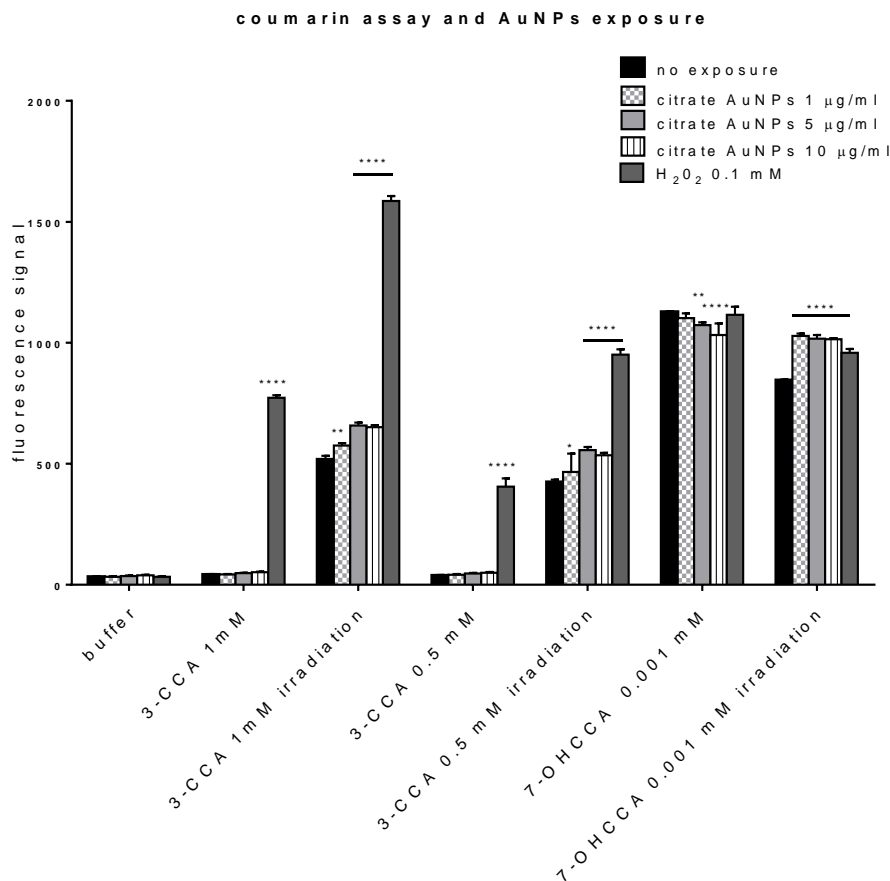


Figure 3.25: Coumarin assay in PBS after AuNPs incubation. 3-CCA was used at a concentration of 1 mM and 0.5 mM and was irradiated with 10 Gy of 6MeV X-rays. The hydroxylated (fluorescent) form of 7-OHCCA was used to explore possible interaction with the fluorescent product, at a concentration of 0.001 mM. The data are expressed in percentage with the standard deviation and a two-way ANOVA followed by a Dunnett's multiple comparisons test was used to study the difference, for each group, between the exposure and the control.

The first coumarin assay, seen in Figure 3.25 was set up to test the validity of the assay. An increase of the 3-CCA fluorescence at both 10 Gy of 6 MeV irradiation and in the presence of hydrogen peroxide was noticed, confirming the presence of 7-OHCCA due to $\cdot\text{OH}$ reaction. The first statement when investigating the AuNPs in PBS is that they do not emit a fluorescence by themselves at this wavelength. They do interact with 3-CCA and increase the production of 7-OHCCA when irradiated, especially at 5 and 10 $\mu\text{g}/\text{ml}$ where the effect is significantly different to 3-CCA alone ($p < 0.0001$). This increase demonstrates the formation of $\cdot\text{OH}$ when AuNPs interact with radiation.

The increase of 7-OHCCA production from the irradiation of 3-CCA is more pronounced when 3-CCA was used at a concentration of 1 mM than of 0.5 mM, therefore, this concentration has been adopted in subsequent experiments. Moreover, AuNPs concentrations of 5 and 10

$\mu\text{g/ml}$ significantly increase 7-OHCCA production; thus, a concentration of $10 \mu\text{g/ml}$ was chosen as a standard AuNPs concentration in order to explore their radiosensitisation effect.

Finally, when exploring the interaction between AuNPs and 7-OH-CCA, an interaction between the fluorescence molecule and the AuNPs was noticed, with a decrease in fluorescence at an AuNPs concentration of $5 \mu\text{g/ml}$ ($p < 0.01$) and of $10 \mu\text{g/ml}$ ($p < 0.0001$). It seems that AuNPs can quench the fluorescence of 7-OHCCA, and therefore decrease the apparent response with radiation.

Filter plates were used in order to clear the AuNPs from the irradiated solution. Figure 3.26 represents the different solutions containing 3-CCA and 7-OHCCA, irradiated and non-irradiated, and using spin filter plates.

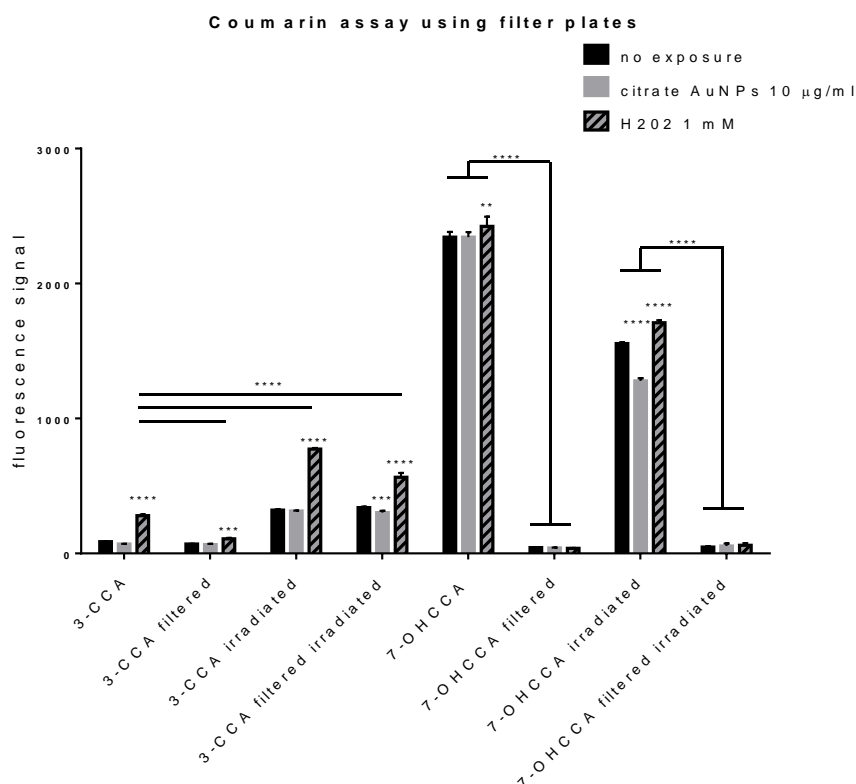


Figure 3.26: Coumarin assay in PBS. 3-CCA was used at a concentration of 1 mM and the samples were irradiated with 10 Gy of 6MeV X-ray photon and without. The hydroxylated form of 7-OHCCA was used at a concentration of 0.001 mM to explore possible interaction with the fluorescent product. The different products were filtered or not using a spin filter plate in order to explore and potential interaction. The data are expressed in percentage with the standard deviation and a two way ANOVA followed by a Dunnett's multiple comparisons test was used to study the difference, for each group, between the exposure and the control, while a Tukey's multiple comparisons test was used to study the difference between groups.

The conclusion from these experiments are that the spin filter plates have an interaction on the fluorescence of the 7-OHCCA as a strong decrease of fluorescence is observed, before

and after spin-filtration of 7-OHCCA ($p < 0.001$, Figure 25) for each exposure and after spin filtration of 3-CCA ($p < 0.001$, Figure 26) after H_2O_2 exposure.

The concentration of 3-CCA was increased up to 5 mM for better quantification after filtration. Citrate AuNPs were used in order to explore $\cdot OH$ production, as explained in the Section 2. 15. Moreover, in order to help the 7-OHCCA to pass through the filter, pure EtOH (100 %) was added onto the wells, just before centrifugation, in order to recover more of the 7-OHCCA formed (Figure 3.27). Indeed, the addition of pure EtOH just before centrifugation helps filtering the 7-OHCCA through the filter plate and improves the measurement of the fluorescence of this compound.

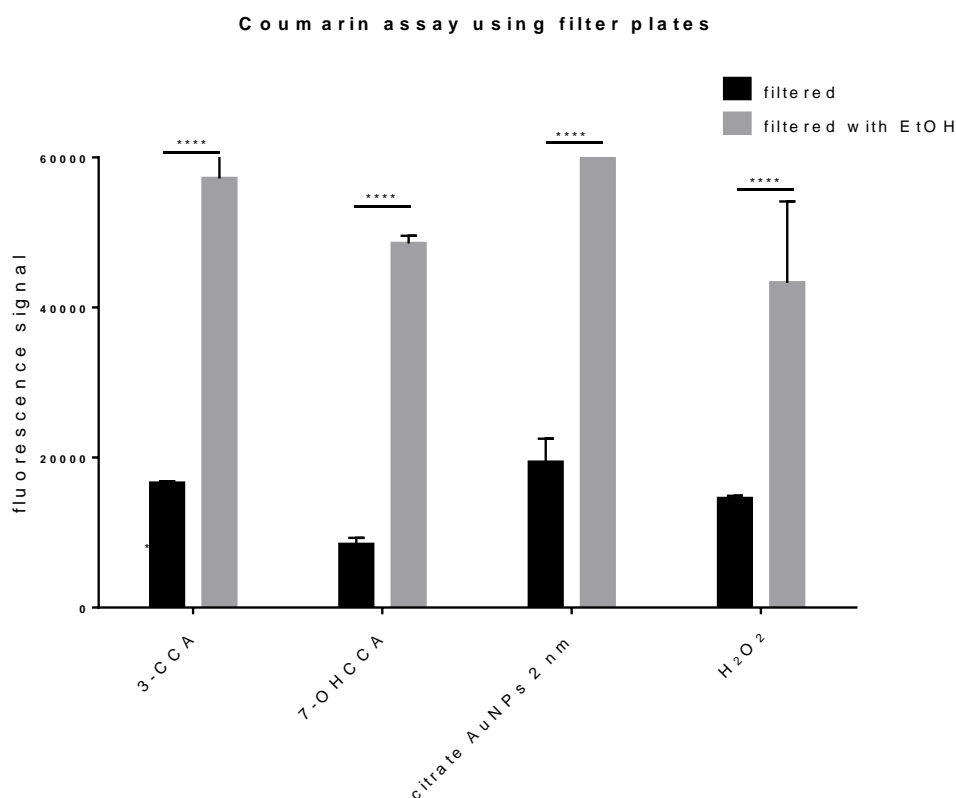


Figure 3.27: Coumarin assay in PBS after citrate AuNPs incubation. 3-CCA was used at a concentration of 1 mM and 7-OHCCA at a concentration of 0.001 mM to explore possible interaction with the fluorescent product. The different products were filtered with or without pure EtOH (100%), in order to explore and potential interaction. The data are expressed in percentage with the standard deviation and a two way ANOVA followed by a Dunnett's multiple comparisons test was used to study the difference, for each groups, between the exposure and the control.

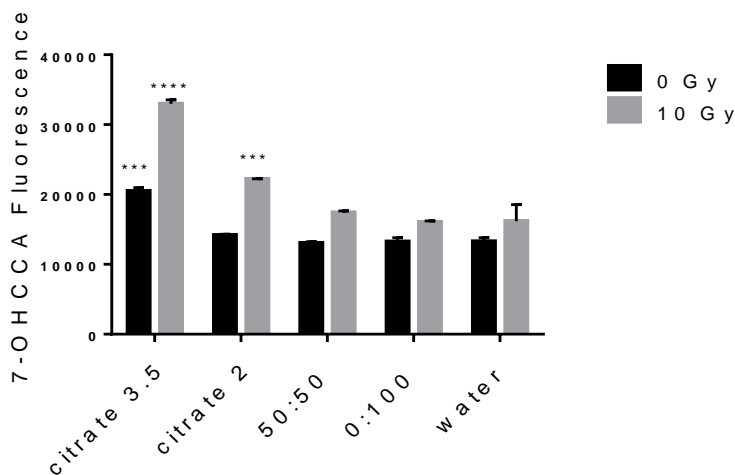


Figure 3.28: Coumarin assay with or without irradiation, with different AuNPs. The graph shows the fluorescence of the 7-OHCCA on different condition. A significant difference in fluorescence of 7-OHCCA probe following irradiation, compared to irradiated water only are indicated as $P < 0.05$ *, $P < 0.01$ ***, $P < 0.0001$ **** (one-way ANOVA with Dunnett's multiple comparisons post-test).

When exploring the effect of the different AuNPs interacting with radiation via the coumarin assay, non-coated AuNPs increase significantly the 3-CCA fluorescence and therefore the $\cdot\text{OH}$ production ($p < 0.01$) (Figure 3.28). However, when looking at the two AuNPs coated with 50:50 and 0:100 αGal :PEGamine, it is not clear if they can enhance the $\cdot\text{OH}$ production as the difference in fluorescence production is not significantly different to the samples with 3-CCA alone. The coumarin assay indicates that these two AuNPs do not significantly increase the $\cdot\text{OH}$ production when interacting with radiation.

3.10.2. Radiosensitisation of AuNPs on skin cells

Following these results, the potential radiosensitisation effect of the two types of AuNPs directly on cells was explored, using both cancer and normal cells irradiated over a range of X-ray doses, from 2 Gy to 8 Gy, with or without AuNPs.

Here again, some experiments were performed to optimise the cellular concentration for clonogenic assays before any exposure. After determining optimal cell seeding density for each dose of radiation, which will lead to well separated colonies, skin cells were exposed to both AuNPs and radiation. AuNPs were used at their IC50 in order to explore the effect of both chemo and radiotoxicity. These experiments are described in Section 2.16.

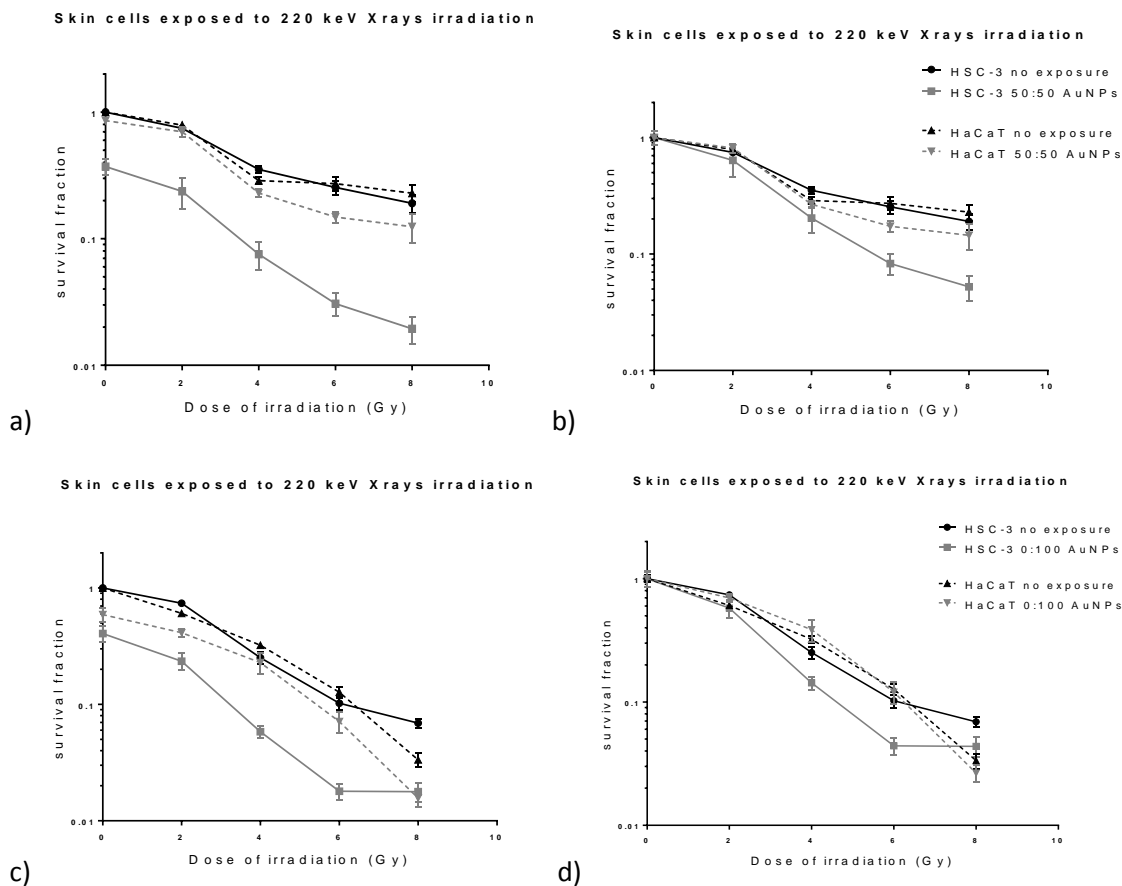


Figure 3.29: HSC-3 and HaCaT cells irradiated with 220 kV X-ray irradiation and exposed to a, b) 50:50 α Gal:PEGamine and c, d) 0:100 α Gal:PEGamine AuNPs. a and c show raw survival fraction data. b and d show survival fraction data corrected for chemotoxicity (normalised based on zero Gy values).

Both HSC-3 and HaCaT show a response after irradiation with 220 kV X-rays. The survival fraction is similar for the normal and cancer cells at the level of 80% after 2 Gy irradiation down to 20% after 8 Gy. Interestingly, when the cells were incubated with 50:50 α Gal:PEGamine AuNPs prior to irradiation, the survival fraction decreased even more than for irradiation only, for both cell lines and the cancer cells do show a higher decrease than the normal cells (Figure 3.29 a).

When looking at the effect of the 0:100 α Gal:PEGamine AuNPs in addition to radiation, the same effect was observed. The survival fraction for both cancer and normal cells decrease when radiation is combined with AuNPs and a higher decrease is observed for the cancer cells. However, this survival decrease for the cancer cells was much more pronounced when incubating the cells with 50:50 α Gal:PEGamine AuNPs than with 0:100 α Gal:PEGamine AuNPs (Figure 3.29 c).

Figure 3.29 a and Figure 3.29 c both show toxicity from AuNPs and irradiation. In Figure 3.29 b and Figure 3.28 d, after normalising the data, it was possible to observe the toxicity arising from the interaction between AuNPs and irradiation. It is clear that there is still a strong decrease in toxicity for skin cancer cells exposed to 50:50 AuNPs or 0:100 AuNPs and irradiation, while the

dose response curve for normal cells are almost equal when irradiating, with or without AuNPs. Figures 3.29 b and Figure 3.29 d indicate therefore a potential additive effect of these two AuNPs with radiation. Not only selectively toxic for the cancer cells, these AuNPs can improve radiotherapy efficiency on skin cells and are therefore very interesting as chemoradiotherapeutics.

It is important to note that the AuNPs were used both at their IC50 concentration. Another factor seems to be responsible to this radiosensitisation effect than concentration. Indeed, the 0:100 AuNPs have a higher IC50, meaning that a higher concentration of AuNP was added to cells than the 50:50 AuNPs. The ICP-MS studies demonstrated that under these conditions 0.0018 ng/cell 50:50 and 0.0023 ng/cell 0:100 AuNPs are loaded in HSC-3 cells. Therefore, it was expected that similar radiosensitisation would be seen or slightly better one with 0:100 AuNPs. However, this was not the case and instead 50:50 AuNPs give better radiosensitisation (after removing the effects of chemotoxicity) (compare Figure 3.29 b and d).

Interestingly, Kong *et al.*, have seen the same tendency when using glucose and cysteamine coating AuNPs (Kong *et al.*, 2008). They have shown that AET-AuNPs were responsible for a fourfold increase of AuNPs uptake inside cells compared to Glu-AuNPs, but Glu-AuNPs were responsible for more than 65% of toxicity with radiotherapy compared to 31.7 % for AET-AuNPs (Kong *et al.*, 2008).

A mechanism for this radiosensitisation effect could be that the AuNPs interact with the cell cycle regulation, blocking the cell into a specific phase of the cell cycle, particularly the S to G2/M phase engender toxicity to the cells but also sensitise them to radiation. Roa *et al.* in 2009 have shown that glucose coated AuNPs decreased the expression of cyclin A by 97.7 % compared to the control, in combination with radiotherapy (Cs-137) after 24h, a kinase responsible for the transition from G2 to M phase, and increased the expression of cyclin E by a 4.2 increase in combination with radiotherapy after 48 h, kinase responsible for the G1 to S transition phase. In consequence, the AuNPs cause acceleration through G1/S (40 % change compared to the control) and slowing through G2/M (30 % change compared to the control) (Roa *et al.*, 2009).

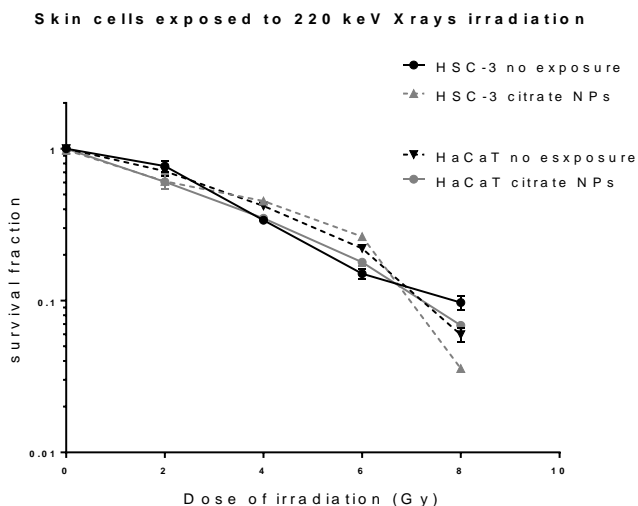


Figure 3.30: HSC-3 and HaCaT cells irradiated to 220 kV X-ray irradiation and exposed to citrate AuNPs. The data represent the survival fraction data corrected for chemotoxicity (normalised based on zero Gy values).

When testing the different AuNPs with the coumarin assay, the non-coated (citrate) AuNPs show a statistically significant increase of 7-OHCCA, representing a significant increase of $\cdot\text{OH}$ radicals upon radiation, better than the $\alpha\text{Gal}:\text{PEGamine}$ coated ones. However, when exploring their radiosensitisation effect on skin cells, these AuNPs do not increase the effect of radiation (Figure 3.30). Indeed, the toxicity of radiation with or without AuNPs remained the same. The coating on the AuNPs seem to play an important role on the cellular uptake and the coating might be affected when the AuNPs are in medium or inside the cells, allowing further electron release.

Interestingly, the coumarin assay informs on the $\cdot\text{OH}$ upon radiation showed a better effect with citrate AuNPs, which appear to have much less effect on cells. This assay indicates that these specific AuNPs do not seem to improve the $\cdot\text{OH}$ production in PBS.

Retif *et al.* in 2015 used various fluorescence probes to look at different ROS species produced during NP irradiation (Retif *et al.*, 2015). It might be of interest to explore other types of ROS potentially produced upon radiation. Even though $\cdot\text{OH}$ radicals are known to be the main ROS produced, other types of radicals, for example singlet oxygen, might play an important role on the radiosensitisation effect and better predict the effect of these AuNPs in cells. For example, Gara *et al.* have shown using furfuryl alcohol, histidine and singlet oxygen sensor green (SOSG) more than a fivefold increase of the production of singlet oxygen after irradiation with 4 MeV X-rays in the presence of silicon NPs in aqueous solution compared to the control (Gara *et al.*, 2012).

The coating of the AuNPs, which seem to interact with the $\cdot\text{OH}$ radical production and their effect with the environment, seems however to be essential for the AuNPs, once inside the

cells, to target a specific part in the cell and have a stronger effect with radiation (Gilles *et al.*, 2014). It is well-known that the coating is changed when being in contact with other molecules, such as proteins. This change must affect the further electron release and radiosensitisation effect of these AuNPs. Here again, the hypothesis that the coating is exchanged by other molecules such as GSH could explain the difference in radiosensitisation effect observed in and outside the cells. Moreover, the localisation of the AuNPs in high amount could locally improve the radiosensitisation by releasing some toxic contents in the environment (Kenzaoui *et al.*, 2012).

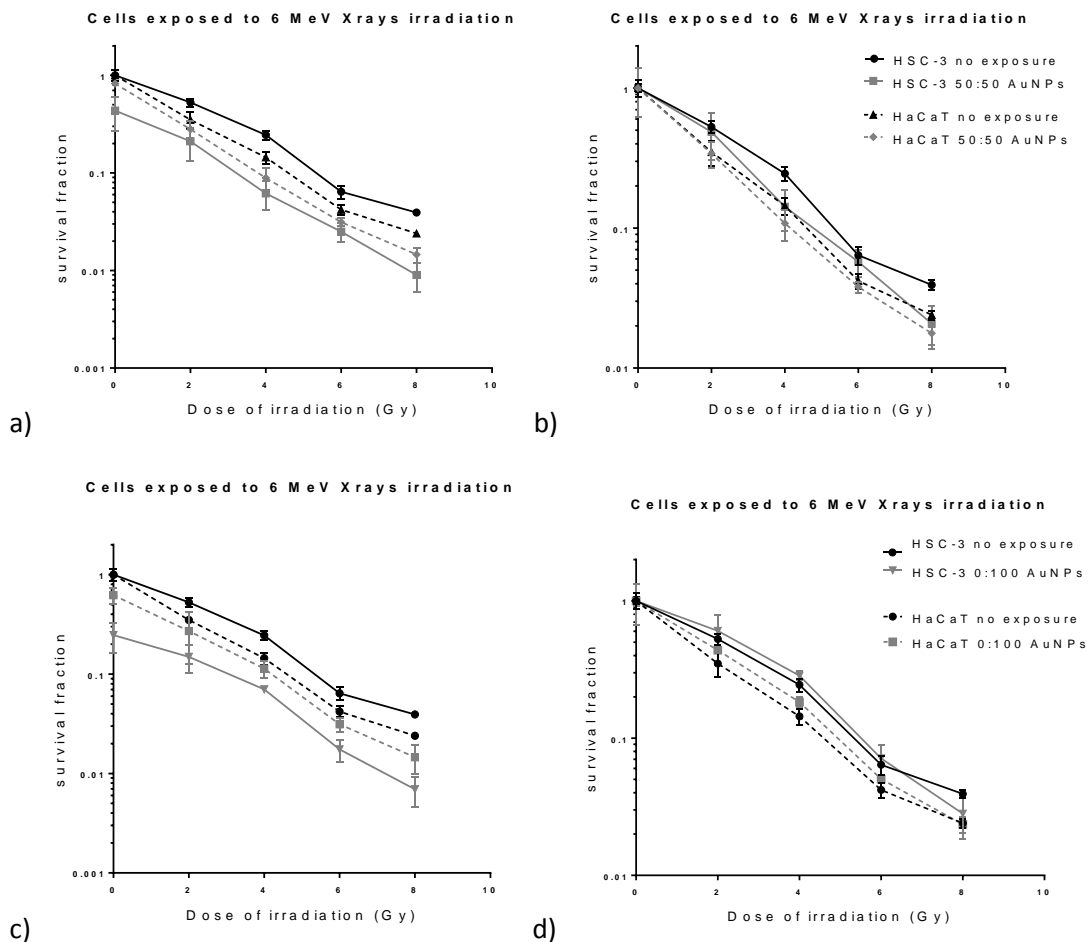


Figure 3.31: HSC-3 and HaCaT cells irradiated to 6 MeV X-ray irradiation and exposed to a, b) 50:50 α Gal:PEGamine AuNPs and c, d) 0:100 α Gal:PEGamine AuNPs AuNPs. a and c show raw survival fraction data. b and d show survival fraction data corrected for chemotoxicity (normalised based on zero Gy values).

The effect of the two types of AuNPs was then explored in combination with MeV X-ray radiation. Figure 3.31 a and c show that both coated AuNPs give a decrease in cell toxicity with radiation, compared to radiation only. However, the effect is clearly different when the cells were irradiated with the different energies of radiation. A stronger decrease is observed in level of 63% survival fraction when the AuNPs were combined with kilovoltage energies than with megavoltage (in the level of 75%) (Figure 3.31 a and c).

When the toxicity from AuNPs is subtracted, the dose response curve after irradiation with or without AuNPs became almost equal, especially for the 0:100 AuNPs. The investigated AuNPs have a very slight additive effect with radiation at Megavoltage energies, which has been the case reported in several publications (Figure 3.31 b and d) (Chithrani *et al.*, 2010, Hainfeld *et al.*, 2008, Jain *et al.*, 2011, Jaynes *et al.*, 2014).

Table 3.6a: Sensitivity Enhancement Ratios and Dose Enhancement Factors calculated for skin cells

Cell line (AuNP)	SER _{4Gy}		DEF _{0.3}	
	6 MV	220 kV	6 MV	220 kV
HSC-3 (50:50)	1.40 ± 0,3	1.73 ± 0,3	1.10 ± 0,76	1.52 ± 0,97
HSC-3 (0:100)	1.02 ± 0,3	1.63 ± 0,5	0.98 ± 0,35	1.16 ± 0,79
HSC-3 (citrate)	N/D	0.97 ± 0,3	N/D	1.03 ± 0,05
HaCaT (50:50)	1.10 ± 0,2	1.08 ± 0,05	1.18 ± 1,00	1.40 ± 0,32
HaCaT (0:100)	0.91 ± 0,2	0.99 ± 0,2	0.99 ± 0,31	0.99 ± 0,39
HaCaT (citrate)	N/D	0.93 ± 0,1	N/D	1.01 ± 0,44

Table 3.6b: linear quadratic factor for skin cells

Cell line (AuNP)	Linear quadratic parameters kV (220 kV)			Linear quadratic parameters MV (6 MV)		
	a	b	a/b	a	b	a/b
HSC-3 control	0,1808 ± 0,0267	0,00728 ± 0.00516	24,8	0,1957 ± 0.0732	0,0251 ± 0.0185	7,8
HSC-3 (50:50)	0,1116 ± 0,2142	0,06197 ± 0.07125	1,8	0,2316 ± 0.1735	0,0226 ± 0.045	10,2
HSC-3 (0:100)	0,1788 ± 0.1686	0,0337 ± 0.0437	5,3	0,1394 ± 0.1228	0,02499 ± 0.0289	5,6
HSC-3 (citrate)	0,2224 ± 0.0339	0,01176 ± 0.0075	18,9	ND	ND	ND
HaCaT control	0,1522 ± 0.0385	0,01111 ± 0.00795	13,7	0,4364 ± 0.694	(-)0,0044 ± 0.0168	-99,2
HaCaT (50:50)	(-) 0,08009 ± 0.0637	0,0945 ± 0.0225	-0,8	0,4665 ± 0.062	(-)0,0076 ± 0.015	-61,4
HaCaT (0:100)	0,03166 ± 0.0689	0,0404 ± 0.0173	0,8	0,278 ± 0.0766	0,0197 ± 0.0205	14,1
HaCaT (citrate)	0,1703 ± 0.0561	0,0138 ± 0.0117	12,3	ND	ND	ND

Table 3.6 a shows the results of the calculation of both the SER and DEF for the two different types of AuNPs with radiation. These two parameters give slightly different information, the DEF gives information on the dose absorbed inside the cells, while the SER gives information about the potential of the AuNPs to act as additive effect (Joiner and Van der Kogel, 2009, Muddineti O.S *et al.*, 2015). In other words, the DEF gives indication on the difference in doses of radiation to observe the same effect, while the SER is defined as the difference of effect for a same dose. The DEF is observed for a survival fraction of 0.3 while the SER is observed for

a dose of 4Gy, which is responsible for a survival fraction of approximately 0.1-0.2. Between these two survival rates, a different effect can happen. The determination of these factors is described in Section 2.16. A linear-quadratic function applied to the normalised toxicity after radiation data gave a good fit up to around 4 Gy dose of irradiation, which is why the SER was calculated for a dose of 4 Gy and the DEF for a survival fraction of 0.3, which corresponds to around 4 Gy. It can be noted here that the SER are associated with small SD, while the DEF have much bigger SD. This is likely to be linked to the linear quadratic model, which needs to be applied to in order to calculate the radiotherapy enhancement and with only 5 points (0-2-4-6-8 Gy), it is difficult to obtain statistically significant data. The DEF gives only in indication of a potential effect but the SER seems to be more accurate to predict the effect of the AuNPs on radiotherapy.

A substantially high SER (1.73) at 4 Gy of 220 kV irradiation was observed for HSC-3 exposed to 50:50 α Gal:PEGamine AuNPs, and exposed to 0:100 α Gal:PEGamine AuNPs (SER of 1.63). When HSC-3 were irradiated with 6MV radiation, lower SERs (1.40 for 50:50 α Gal:PEGamine AuNPs and 1.02 for 0:100 α Gal:PEGamine AuNPs) were seen. The radiosensitisation effect, is well-known and often observed for AuNPs combined with kilovoltage energies of X-rays. The additive effect with radiation observed here is higher than the one reported in many publications, particularly with the 50:50 α Gal:PEGamine AuNPs (SER of 1.73). As already mentioned, a radiosensitisation effect have been shown with a SER = 1.43 after an irradiation of 220 kV X-rays using 50 nm AuNPs (Chithrani *et al.*, 2010), a DEF = 1.39 after 225 kV X-ray irradiation using 5.81 nm AuNPs (Cui *et al.*, 2017), a SER = 1.41 after 160 kV using 1.9 nm AuNPs compared to 1.29 after 6 MV Xrays (Jain *et al.*, 2011). It is important to note as well that the SER obtained in our study is linked to a small amount of AuNPs. Indeed, a concentration of 1 μ g/ml was used, which lead to a concentration inside the cells of around 2 pg/ml, which is smaller than in the three experiment cited previously (Chithrani *et al.*, 2010, Cui *et al.*, 2017, Jain *et al.*, 2011). Indeed, using high concentration of 12 μ M or 0.5 mg/ml for 24 h, a concentration inside MDA-MB-231 cells of 4 μ g/ml (Jain *et al.*, 2011) and 40 pg/ml (Cui *et al.*, 2017) was seen respectively. With a smaller concentration inside cells, our AuNPs are responsible for a higher SER. As mentioned before, other parameters than the NP concentration inside cells seem to affect the radiosensitisation effect, such as the cell type, the cell-cycle, the ROS production (Kwatra *et al.*, 2013, Roa *et al.*, 2009).

The strong radiosensitisation when combining AuNPs with kilovoltage radiation, but smaller radiosensitisation when combining with megavoltage radiation is in accordance with the literature (Jain *et al.*, 2011). Yet, the SER of 1.40 indicates a strong radiosensitisation for the 50:50 AuNPs even at megavoltage energies using 6MV X-rays compared to the literature where radiosensitisation of 1.29 (SER after 24 h exposure with 12 μ M of 1.9 nm NPs) (Jain *et al.*, 2011,

Burger *et al.*, 2014b), 1.15 (SER after 24 exposure with 0.197 mg/ml of 1.9 nm NPs) (Rashid *et al.*, 2018), 1.49 (SER after 24 h exposure with 20 nm of 13 nm NPs) (Wang *et al.*, 2013).

Table 3.6 b was also presented to introduce the different values of α and β parameters obtained from the linear quadratic model used. As mentioned before, the LQ model here is not conclusive and very informative on the radiosensitisation effect as few data points were available. In order to get more accurate data, more data point would be needed from different doses of radiation. Thus, a high uncertainty is obtained for the different parameters. Yet, we can notice that in general, α parameter is bigger than β . α/β parameter is often calculated in order to have indication on the response of a tissue to radiation as it is linked to the dose where single doses and accumulated doses are responsible for the same effect (Joiner and Van der Kogel, 2009, Podgorsak, 2003). A high ratio (superior to 7) would indicate an early response of the tissue and a high impact of low doses. As mentioned before, it is difficult here to make any conclusion on this last effect. The linear quadratic model might not be the best suited model as it does not fit exactly all the data points, especially due to the fact that for *most in vitro* cell lines where the curve flatten to become linear at high doses. The linear quadratic linear model have been proposed as an alternative to better represent this particular effect (Joiner and Van der Kogel, 2009, Podgorsak, 2003).

In conclusion, 50:50 AuNPs give a higher radiosensitisation effect with kilovoltage X-rays than with megavoltage X-rays.

It is important to mention that the SER for the different molecules and the two types of radiation are close to 1 in all conditions with HaCaT cells. Not much radiosensitisation is occurring with this cell line.

3.10.3. Toxicity and radiosensitisation of AuNPs on breast cells

The effect of the 50:50 and 0:100 α Gal:PEGamine AuNPs was explored in cancer and normal breast cells, in order to determine the IC50 concentration for irradiation experiments.

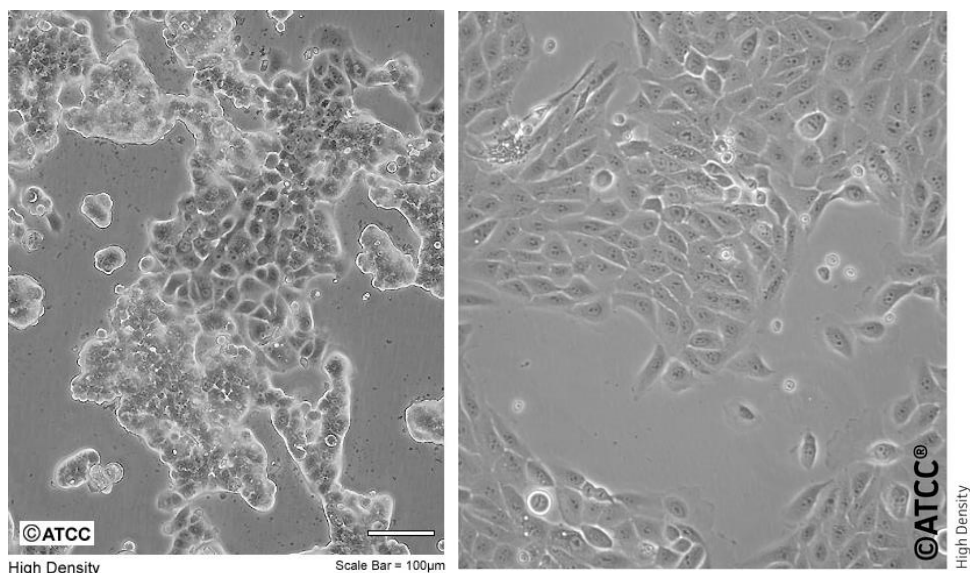


Figure 3.32: Bright field images of a) MCF-7; b) MCF-10.

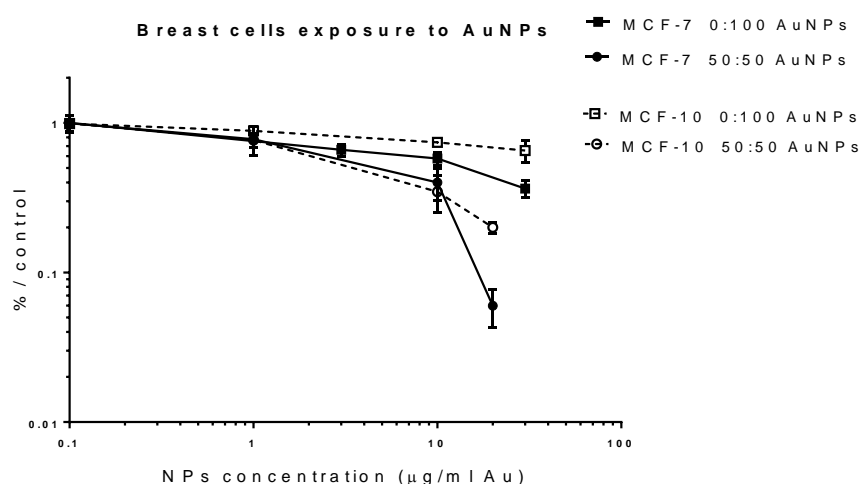


Figure 3.33: Clonogenic assay after AuNPs exposure on breast cells. The graphs represent the percentage of viability compared to the control, regarding AuNPs concentration. The data are presented as mean percentage survival \pm standard deviation.

MCF-7 and MCF-10A are represented on the Figure 3.32. Due to lack of time, TEM images of the cells could not be taken for these particular cell lines and therefore, the cell surface could not be compared to the one for the skin cells. However, it is possible to note from the work published by Geltmeier *et al* in 2015 that MCF-7 cells are bigger than MCF-10 cells (cell volume of 3375-16873 μm^3 for MCF-7 compared to 678-1317 μm^3 for MCF-10) (Geltmeier *et al.*, 2015)

Figure 3.33 shows the toxicity response of both cancer and normal breast cells exposed to the two AuNPs of interest. Both the AuNPs are more toxic toward breast cancer cells (MCF-7) than normal cells (MCF-10), but this toxicity is not as selective as on skin cells as there is also

a toxicity for normal cells already at 10 $\mu\text{g}/\text{ml}$. The IC₅₀ on MCF-7 are 4 $\mu\text{g}/\text{ml}$ for 50:50 $\alpha\text{Gal}:\text{PEGamine AuNPs}$ and 10 $\mu\text{g}/\text{ml}$ for 0:100 $\alpha\text{Gal}:\text{PEGamine}$.

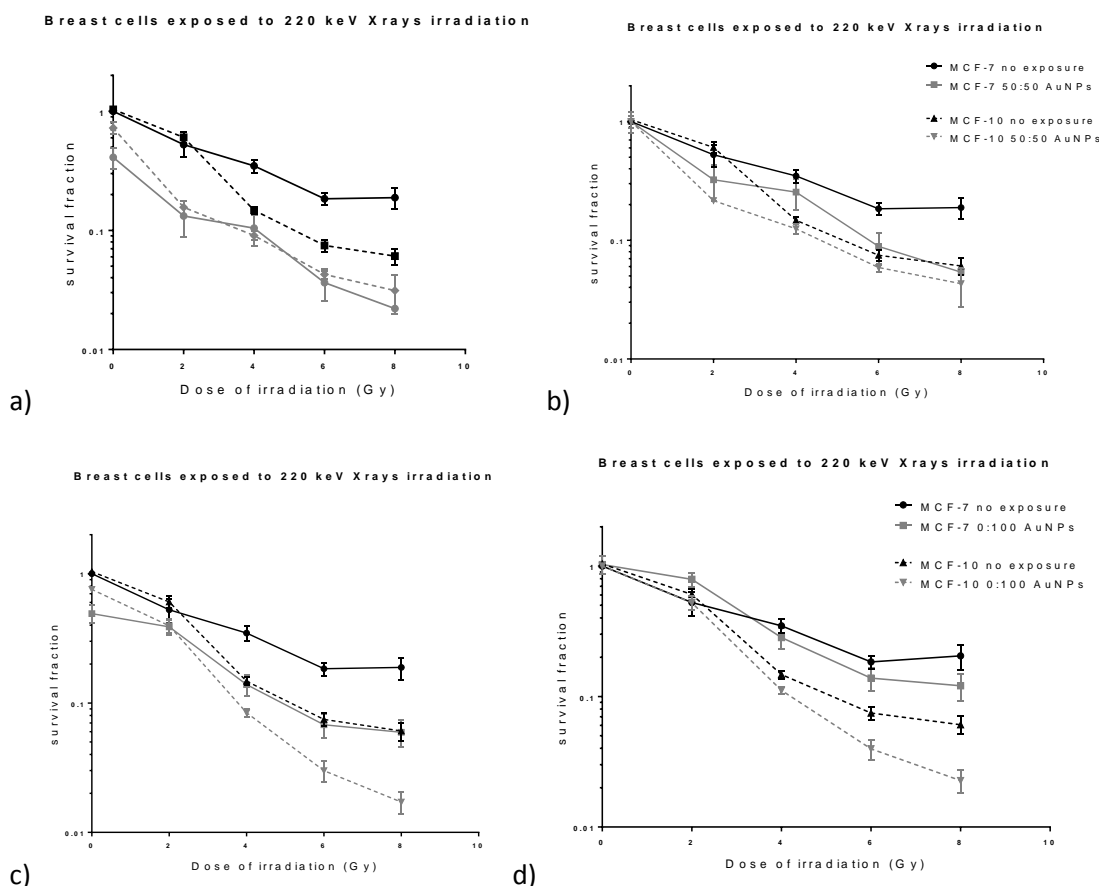


Figure 3.34: MCF-7 and MCF-10 cells irradiated to 220 kV Xray irradiation and exposed to a, b) 50:50 $\alpha\text{Gal}:\text{PEGamine AuNPs}$ and c, d) 0:100 $\alpha\text{Gal}:\text{PEGamine AuNPs}$. a and c show raw survival fraction data. b and d show survival fraction data corrected for chemotoxicity (normalised based on zero Gy values).

When looking at the radiosensitisation effect at kilovoltage energy, radiotherapy only is responsible for a strong decrease of viability for normal breast cells, at the level of 65% survival fraction after 2 Gy irradiation, more substantially than for the cancer ones, where the survival fraction after 2 Gy of irradiation is 85%. MCF10A breast cells are more radiosensitive than MCF-7 cancer ones. This result is controversial to previous work which showed a toxicity for MCF-7 compared to no change for MCF-10 cells after kilovoltage irradiation (Kong *et al.*, 2008, Nicol *et al.*, 2018). Figure 3.34 a shows that 50:50 $\alpha\text{Gal}:\text{PEGamine AuNPs}$ gave a decrease in toxicity for both cancer and normal cells. Figure 3.34 b indicates that 50:50 $\alpha\text{Gal}:\text{PEGamine AuNPs}$ give an additive effect with radiation, both in cancer and normal cells. Additionally, the exposure of 0:100 $\alpha\text{Gal}:\text{PEGamine AuNPs}$, shows a substantial decrease in viability with radiation for normal breast cells, while the toxicity is less obvious for cancer cells (Figure 3.34 c). Moreover, the 0:100 $\alpha\text{Gal}:\text{PEGamine AuNPs}$ shows an additive effect with radiation, only for normal cells, while the toxicity remains equal for cancer cells, with or without AuNPs (Figure 3.34 d).

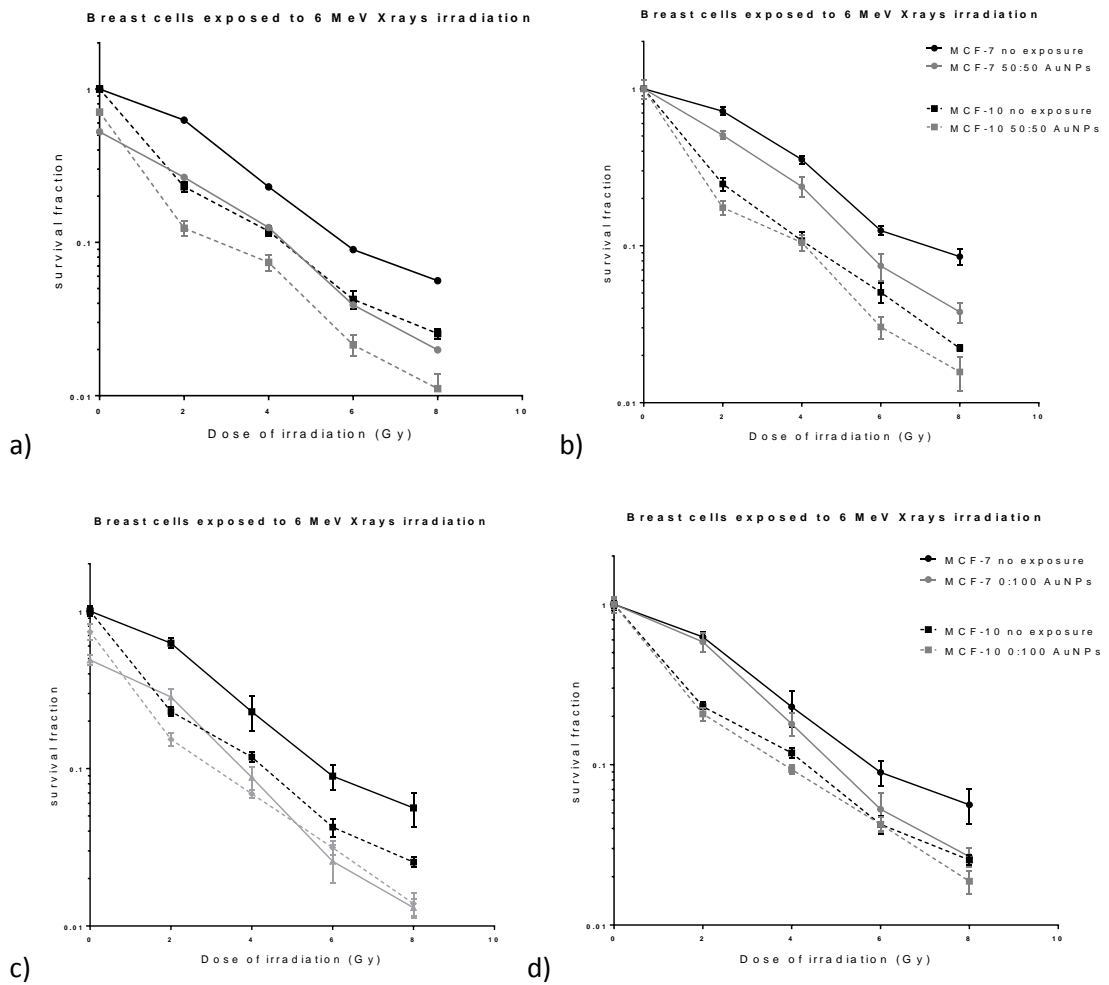


Figure 3.35: MCF-7 and MCF-10 cells irradiated to 6MeV Xray irradiation and exposed to a, b) 50:50 α Gal:PEGamine AuNPs and c, d) 0:100 α Gal:PEGamine AuNPs. a and c show raw survival fraction data. b and d show survival fraction data corrected for chemotoxicity (normalised based on zero Gy values).

When investigating breast cells irradiated with radiotherapy at megavoltage energies, the toxicity after radiation with AuNPs is more pronounced than with kilovoltage energies (Figure 3.35 a, b). Moreover, megavoltage energy X-ray irradiation is more toxic for normal breast cells than for the cancer ones (Figure 3.35). Both AuNPs have a stronger effect on normal breast cells than on breast cancer cells.

Table 3.7a: Sensitivity Enhancement Ratios and Dose Enhancement Factors calculated for breast cells

Cell line (AuNP)	SER _{4Gy}		DEF _{0.3}	
	6 MV	220 kV	6 MV	220 kV
MCF7 (50:50)	1.11 ± 0,15	0.97 ± 0,15	1.15 ± 0,36	1.20 ± 0,16
MCF7 (0:100)	1.21 ± 0,15	0.90 ± 0,15	1.10 ± 0,13	0.99 ± 0,36
MCF10 (50:50)	1.12 ± 0,10	1.20 ± 0,10	1.20 ± 0,42	1.04 ± 0,56
MCF10 (0:100)	1.27 ± 0,10	1.39 ± 0,10	1.10 ± 0,38	1.06 ± 0,36

Table 3.7b: Linear quadratic parameters for breast cells

Cell line (AuNP)	Linear quadratic parameters kV (220 kV)			Linear quadratic parameters MV (6 MV)		
	a	b	a/b	a	b	a/b
MCF-7 control	0,25 ± 0.03	(-)0,0029 ± 0.0044	85,4	0,1509 ± 0.0709	0,0471 ± 0.0212	3,2
MCF-7 (50:50)	0,28 ± 0.12	(-)0,00105 ± 0.025	-267,8	0,3034 ± 0.0955	0,0167 ± 0.025	18,2
MCF-7 (0:100)	0,2182 ± 0.0407	(-)0,00145 ± 0.0073	-150,5	0,135 ± 0.0905	0,0695 ± 0.031	1,9
MCF-10 control	0,3354 ± 0.0441	-0,00232 ± 0.0095	-138	0,8002 ± 0.065	(-)0,0479 ± 0.014	-16,7
MCF-10 (50:50)	0,3265 ± 0.0775	0,0081 ± 0.018	-40,3	0,05 ± 0.080	(-)0,06354 ± 0.017	-14,9
MCF-10 (0:100)	0,3621 ± 0.0619	0,00055 ± 0.0143	658,3	0,8715 ± 0.16	(-)0,0542 ± 0.036	-16,1

The SER and DEF values were calculated when breast cells were irradiated in presence of AuNPs. The SER is higher for MCF10 cells than for MCF-7 cells, which indicates that the radiosensitisation effect is more pronounced with normal cells than with cancer cells. This may be because MCF-10 cells are more sensitive to radiation, as shown in Figure 3.35, although not described in the literature before (Kong *et al.*, 2008, Nicol *et al.*, 2018). Indeed, Nicol *et al* showed a SER of 2.57 for MCF-7 compared to 1.19 for MCF-10A after peptide-AuNPs exposure at 25µg/ml with kilovoltage radiotherapy (160 kV X-rays) (Nicol *et al.*, 2018). Moreover, the difference in cell surface area might have an effect on the AuNPs uptake as the MCF-10 cells are bigger than the MCF-7 (Geltmeier *et al.*, 2015), which may concentrate the AuNPs in the cells and may improve the probability of interaction with the beam of radiation.

Moreover, a difference can be seen between 50:50 and 0:100 α Gal:PEGamine AuNPs, with the 0:100 α Gal:PEGamine AuNPs having a stronger effect with radiation (SER of 1.21 and 1.27 for 6MV radiation on both MCF-7 and MCF-10, compared to 1.12 and 1.11 for 50:50 AuNPs) (Table 3.7a). The AuNPs have less radiosensitising potential on breast cells than on skin cells. Here again, the different parameters explored by the Linear quadratic model are associated with substantial errors which makes difficult to draw a conclusion on the DEF values or the α and β parameters, although it is possible to note that here again, α is in general bigger than β .

After exploring the potential effect of AuNPs on skin cells and breast cells, it is possible to note that 50:50 α Gal:PEGamine AuNPs have a stronger radiosensitising potential with skin cells, particularly at kilovoltage energies, damaging specifically cancer cells, whereas it has a far more limited effect for megavoltage energies and for breast cells, where the radiosensitisation is seen more in normal cells than cancer cells.

3.11. Conclusion of Chapter 3: α Galactose:PEGamine coated AuNPs

In this chapter, the results of many experiments are presented, revealing that AuNPs coated with various ratios of α Galactose and PEGamine have different characteristics and behaviour. The coating influences their size, their aggregation potential, their charge, and all of these characteristics influence their effect on cells (Alkilany and Murphy, 2010b, Pavlin and Bregar, 2012, Zarschler et al., 2016). It was shown that, depending on the coating on the AuNPs, the uptake and toxicity on skin models is different. Indeed, the first conclusion from this work indicates that α Galactose and PEGamine coating the AuNPs improve their uptake and selective toxicity toward HSC-3 cancer cells. However, the mechanism of uptake is still unclear. It is possible that the positively charge AuNPs interact with the negatively charged cellular membrane (He *et al.*, 2010), improving cell interaction and uptake (Beddoes et al., 2015a, Goodman et al., 2004). It seems that a positive charge improves the cellular uptake, but a high positively charge seems to decrease the uptake and the stability of the AuNPs. Some effort in the laboratory are being made trying to understand the mechanism of uptake (active pathways seem to be more involved than passive ones) and the role of cell surface structures such as filopodia.

Regarding the mechanisms of toxicity, it seems that oxidative stress is involved, as antioxidants were able to rescue the AuNPs toxicity on cancer cells, but it is not clear if the AuNPs were disrupting the antioxidant defence, were responsible for lysosomes toxicity, or cell cycle disruption, as, by themselves, the AuNPs did not seem to increase the ROS production. It is important to mention that only a single time point, directly after AuNPs exposure was explored. The production of ROS might be a cumulative process and an increase might appear after a longer period, such as 24h. It will therefore be interesting to look at possible protein dysregulated and implicated in these specific pathways, such as NF- κ B for antioxidant properties or cyclin A, B1 and E for cell cycle dysregulation (Manke *et al.*, 2013, Bajak *et al.*, 2015). All these proteins can be explored using western blot analysis or qRT-PCR for mRNA expression.

It was also found that caspase dependant death is involved in AuNPs toxicity. A further way to explore this death pathway is to look at the subG1 population of the cell cycle, as well as western blots to examine the activation of specific caspases (Caspases 8, 9) and their regulators (Bcl, Bax, Bid) (Wang *et al.*, 2005).

These specific AuNPs coatings also improves the radiosensitisation effect. Indeed, the SER observed for AuNPs in combination with radiotherapy was higher than in many earlier publications. The radiosensitisation effect observed was higher with the 50:50 α Gal:PEGamine AuNPs than with the 0:100 α Gal:PEGamine AuNPs. These two specific AuNPs were chosen

because they gave the highest amount of gold inside the cancer cells. The amount of AuNPs uptake might not be the only factor on the radiosensitisation effect as the two AuNPs gave different responses. Some of the other AuNPs might also be of interest in the radiosensitisation effect and might give some clue on the mechanism behind it, such as the cellular localisation.

The coumarin assay was not able to detect the potential radiosensitisation effect here, as the different coating onto the AuNP were probably interacting with the electron release. Moreover, the coumarin assay explores only the hydroxyl production, which is, with solvated electrons, the main radical produced upon radiation but other radicals such as H_2O_2 and $\text{O}_2^{\cdot-}$ could help to predict the effect of the AuNPs. Different probes have been developed over the years: coumarin assay looking at $^{\cdot}\text{OH}$; DCFHDA looking at H_2O_2 , ONOO^- $\text{O}_2^{\cdot-}$; SOSG looking at $^1\text{O}_2$, but they have been rarely used all together to look at a broad range of radicals, after irradiation (Lukyanov and Belousov, 2014, Roesslein *et al.*, 2013).

The exchange of the coating on the AuNPs with molecules in the cell environment seems to play an important role in the radiosensitisation effect. Glutathione is one of the most present molecule in the cells and is composed of thiol group which can easily interact with the thiol on the AuNP. An exchange between thiolated α Galactose molecule or thiolated PEGamine and the glutathione molecule may occur within the cells. It will be interesting to test this hypothesis by measuring the amount of glutathione inside the cells, and also by looking at the potential AuNP change in coating after incubation with glutathione molecule with ICP-MS or high-performance liquid chromatography (HPLC).

In the next chapter, new types of AuNPs are investigated, which are slightly bigger in size and coated with oligonucleotides, bearing a strongly negatively charge. These AuNPs are designed to target the promoter sequence of the *c-myc* gene, decreasing its transcription. The hypothesis is that these new AuNPs, slightly bigger in order to visualise them due to their plasmon resonance for characterisation, and with their potential to target and inhibit *c-myc* protein, could improve the interaction with radiation, and thus, better act as radiosensitisers its optimised position near the DNA of the cells.

CHAPTER 4: OLIGONUCLEOTIDES COATED AuNPs

Triplex structure, described in Section 1.9, is designed to target a specific DNA sequence of a gene, and the consequence is the prevention of interaction between the gene and its transcription factor or RNA and DNA polymerase. This way, TFOs can inhibit the transcription of specific genes or cell proliferation (Carbone *et al.*, 2004, Wu *et al.*, 2007). In Chapter 4, AuNPs coated with this structure were designed, in order to achieve sequence-specific targeting of AuNPs for radiotherapy, and improve the radiosensitisation effect. Chapter 3 showed that specific coating could improve the uptake of AuNPs in cells and increase their radiosensitisation, thus encouraging the exploration of TFOs coated AuNPs.

Here, the 3.5 nm AuNPs were first coated with 4,4'-(Phenylphosphinidene)bis(benzenesulfonic acid) dipotassium salt hydrate (PN) to limit the number of oligonucleotides per AuNP, and later with specific oligonucleotides capable of targeting the *c-myc* promoter.

C-myc was thought to be a sensible gene to target as it is up regulated in many types of cancer and particularly in most of the head and neck squamous cell carcinoma (HNSCC), when compared to normal tissues (Chen *et al.*, 2004).

The design and testing of the above mentioned are the focus of this chapter, where the formation of the triplex structure was explored *ex vivo* using single stranded oligonucleotides and plasmid DNA. Moreover, the AuNPs size, charge and distribution have been characterised, and the effect (toxicity and radiosensitisation) of these AuNPs were examined on skin cells. All the conducted experiments are summarised in Table 4.1.

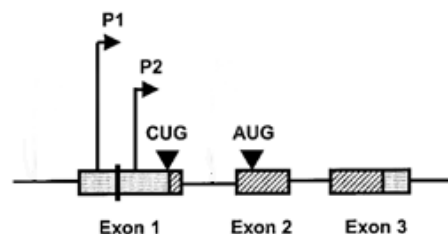
Table 4.1: Summary of the experiments done in Chapter 4.

EXPERIMENTS	RESULTS	CONCLUSION
Duplex and triplex formation with simple DNA sequences, gel electrophoresis	Polyacrylamide electrophoresis exploring the different DNA sequences shows that incubating the two complementary strands of DNA creates easily a duplex, both with a length of 23 bp or 70. The triplex formation is seen with the two TFOs dY3 and PR, and the reaction does not depend on the temperature (4°C, 25°C) and on the time of incubation.	The triplex formation is non-temperature dependant and non-incubation time dependent. The two different TFOs dY3 and PR are able to form a triplex.
Triplex formation with the plasmid	The plasmid interaction was explored using both agarose and polyacrylamide gel. No difference is seen when using relaxed plasmid, whereas a disappearance of the TFO using polyacrylamide gel is seen when incubated with nicked plasmid.	The nicked plasmid may facilitate the accessibility of the triplex. Polyacrylamide gel is more informative than agarose to explore triplex formation.
AuNPs reaction with the TFO coating, TEM characterisation	The AuNPs with various coatings have a similar average size between 4.6 and 5.34 nm observed on TEM but have different aggregation profiles	The different coated AuNPs with various coatings seem to have different surface charges, which may explain their different aggregation.
Characterisation of the oligonucleotide attachment using DLS, XPS and EMSA, looking at the interaction between the TFO and its complementary probe	The DLS experiments did not show differences in hydrodynamic size (between 8.3 and 9.8 nm) but slight difference in charges, especially with PN-dY3 and PN-PR coating. XPs is not conclusive on the AuNPs coating as the concentration of AuNPs is low, especially regarding the gold signal which is very different between the AuNPs. EMSA technique shows an interaction between the probe and the AuNPs, indicating that TFOs most likely are attached on the AuNPs	DLS and XPS techniques were not informative on TFOs attachment to the AuNPs. EMSA technique showed that the oligo probe, complementary to the TFO sequence interact with the AuNPs, indicating the presence of TFOs on these AuNPs
Effect of the Oligo-coated AuNPs with irradiation outside of the cells using coumarin assay and Plasmid DNA	Citrate AuNPs were able to increase the 7-OHCCA fluorescence, more than the other coated AuNPs. The effect of the different AuNPs on the plasmid in combination with radiation and explored by gel electrophoresis and PCR did not indicate any radiosensitisation of the different AuNPs.	The coatings of the AuNPs may prevent *OH production upon radiation. Irradiation affect the plasmid integrity, however, the different AuNPs did not show any difference relative to the non-irradiated plasmid.
Effect of the Oligo-coated AuNPs inside the cells using clonogenic assay and TEM	The different coating on the AuNPs have different impact on the cell toxicity. The TFO seem to lower the cell viability. Moreover, the TFOs coated AuNPs are able to enter in the cells cytoplasm and the cell nucleus, as explored with TEM.	TFO-AuNPs increase cell toxicity, particularly on HSC-3 cells and increase the uptake.
Effect of the Oligo-coated AuNPs with irradiation inside the cells	The oligo-coated AuNPs improve the effect of radiotherapy, even more than the citrate AuNPs, showing an SER of 1.39 for dY3 TFO AuNPs, 1.43 for PR TFO AuNPs and 1.13 for GFP oligo AuNPs, compared to 0.79 for citrate AuNPs.	TFO-AuNPs have a radiosensitisation effect, improving the radiotherapy efficiency, and this effect is TFO dependant as the neutral GFP sequence does not show a SER as large as PR or dY3 sequence.

4.1. Oligonucleotide binding with its target

4.1.1. Oligonucleotide sequence selection

C-myc gene encodes a transcription factor responsible for continued cell division. Under normal conditions, without cancer, it is responsible for the regulation of numerous genes, such as the ones involved in cell proliferation or glycolysis (Miller *et al.*, 2012). It is a well-known pro-oncogene that is dysregulated in many types of cancer (at least 40%), allowing them to divide uncontrollably (McGuffie *et al.*, 2000). An oligonucleotide targeting this sequence would make an interesting cancer therapeutic. McGuffie *et al.*, 2000 and Huo *et al.* in 2014, described a TFO targeting a part of the *c-myc* P2 promoter, which is its major promoter (Figure 4.1.a) (Huo *et al.*, 2014, McGuffie *et al.*, 2000). Indeed, promoter regions in a gene are often rich in purine, which favours the formation of the triplex structure (McGuffie *et al.*, 2000). McGuffie and Huo demonstrated that their TFO sequence dY3 could target and knock-down *c-myc* protein expression in cells. The dY3 TFO was therefore chosen as a proof of principle with the pBV-Luc/Del-6 plasmid, which contains the P2 promoter sequence of the *c-myc* gene. This plasmid is about 5 kb long but the entire sequence is not accessible from Addgene, only a 730 bp long sequence of the plasmid that is shown in the Figure 4.1.b. The P2 promoter sequence of the *c-myc* gene is highlighted in grey (Figure 4.1.b) (Huo *et al.*, 2014, McGuffie *et al.*, 2000).



a) TFO target site 5' -TCCCTCCCTCCGTTCTTTTCC-3'
3' -AGGGAGGGAGGCAAGAAAAAGGG-5'

1	TTTGGCGTCT	TCCATGGGTG	GCTTTACCAA	CAGTACCGGA	ATGCCAAGCT	50
51	TACTTAGATC	GCAGATCTCG	ATACCGGATC	CATTATATAC	CCGAATTCGA	100
101	TATCGACGTC	CAGCTGCAAG	GAGAGCCTTT	CAGAGAAGCG	GGTCTGGCA	150
151	GCGGCGGGGA	AGTGTCCCA	AATGGGCAGA	ATAGCCTCCC	CGCGTCGGGA	200
201	GAGTCGCGTC	CTTGCTCGGG	TGTTGTAAGT	TCCAGTCAA	AGTGCCCGCC	250
251	CGCTGCTATG	GGCAAAGTTT	CGTGGATGCG	GCAAGGGTTG	CGGACCGCTG	300
301	GCTGGGGGAT	CAGCGGGAGG	GCTGGGCCAG	AGGCGAAGCC	CCCTATTGCG	350
351	TCCGGATCTC	CCTTCCAGG	ACGCCCGCAG	CGCAGCTCTG	CTCGCCCGGC	400
401	TCTTCCACCC	TAGCCGGCCG	CCCCTCGCT	CCCTCTGCCT	CTCGCTGGAA	450
451	TTACTACAGC	GAGTTAGATA	AAGCCCCGAA	AACCGGCTTT	TATACTCAGC	500
501	GCGATCCCTC	CCTCCGTTCT	TTTTCCGCCC	AAGCCTCTGA	GAAGCCCTGC	550
551	CCTTCTCGAC	TATCGATAGA	GAAATGTTCT	GGCACCTGCA	CTTGCACTGG	600
601	GGACAGCCTA	TTTTGCTAGT	TTGTTTTGTT	TCGTTTTGTT	TTGATGGAGA	650
651	GCGTATGTTA	GTA CTATCGA	TTCACACAAA	AAACCAACAC	ACAGATGTAA	700
b) 701	TGAAAATAAA	GATATTTTAT	TGCGGCCGCT			730

Figure 4.1: Plasmid pBV-Luc/Del-6, a) map of the plasmid (from: www.addgene.com), b) nucleotide sequence of the *c-myc* P2 promoter region of the plasmid. The TFO binding site is highlighted.

The dY3 sequence designed by McGuffie *et al.* in 2000 was chosen to be used with TFO, along with similar TFO (PR) that was designed in house. These two sequences should be able to interact with the *c-myc* promoter via two different triplex conformations. The dY3 sequence contains guanine and cytosine and is designed to form a reverse Hoogsteen pairing via guanosine-guanosine-cytosine (G(GC)) and thymine-adenine-thymine (T(AT)) structure (Figure 4.2.a). The PR sequence is the newly designed one that contains adenine and guanine and forming the same structure, where G pairs to G (G(GC)), while A to A, forming adenine-adenine-thymine (A(AT)) structure (Figure 4.2.b). This type of oligonucleotide-containing G and A is supposed to form stronger interactions with the DNA double helix (Malvy *et al.*, 1999). All the DNA sequences used in this work are listed in Table 4.2, as well as their melting temperature and GC percentage. The different sequences are also presented in Section 2.1.5.

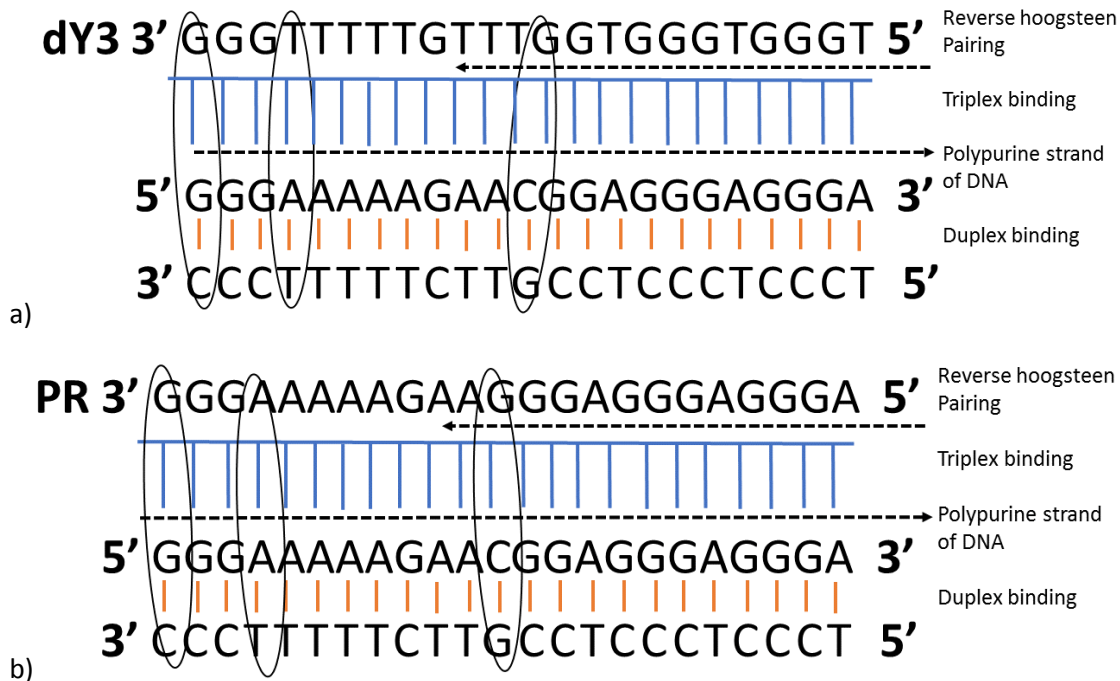


Figure 4.2: Triplex binding between the TFO and the DNA duplex. a) dY3 pairing, b) PR pairing. The loops highlight the triplex structure G(CG), T(AT), A(AT) and G(CG) as examples.

Table 4.2: Different DNA sequences used in the Chapter 4.

Sequence name	Sequence composition 5'-3'	Melting Temperature	% G-C
dR1 23	TCCCTCCCTCCGTTCTTTTCCC	75	57
dY2 23	GGGAAAAGAACGGAGGGAGGGA	75	57
dR1 70	AACCGGCTTTTATACTCAGCGGATCCCTCCCTC CGTTCTTTTCCCAGCAAGCCTCTGAGAAGCCCT GC	94.11	57.1
dY2 70	GCAGGGCTTCTCAGAGGCTTGGCGGGAAAAAG AACGGAGGGAGGGATCGCGCTGAGTATAAAAAG CCGGTT	94.11	57.1
dY3	TGGGTGGGTGGTTTGT TTTTGGG	73.9	52.1
Thio-dY3	[ThioC ₆]TGGGTGGGTGGTTTGT TTTTGGG	73.9	52.1
PR	AGGGAGGGAGGGAAGAAAAGGG	71.7	56.5
Thio-PR	[ThioC ₆]AGGGAGGGAGGGAAGAAAAGGG	71.7	56.5
dY3 complementary	CCCAAAAACAAACCACCCACCCA	73.9	52.1
PR complementary	CCTTTTTCTTGCCTCCCTCCCT	71.7	56.5
Thio-GFP	[ThioC ₆]AATATCGCGGACAGAAGACG	64	50

Table 4.3 indicates the two different ratios described above for each sample. It is possible to note that almost all the samples have a purity ratio around 1.8 (between 1.7 and 2),

apart from the samples dR1 23 (1.21), dR1 70 (1.57), PR (2.22), which could indicate the presence of contaminants. Moreover, almost all the samples have a turbidity ratio above 1.5, instead of dR1 23 (1.19), which indicate that the impurity present might be salt in the solution.

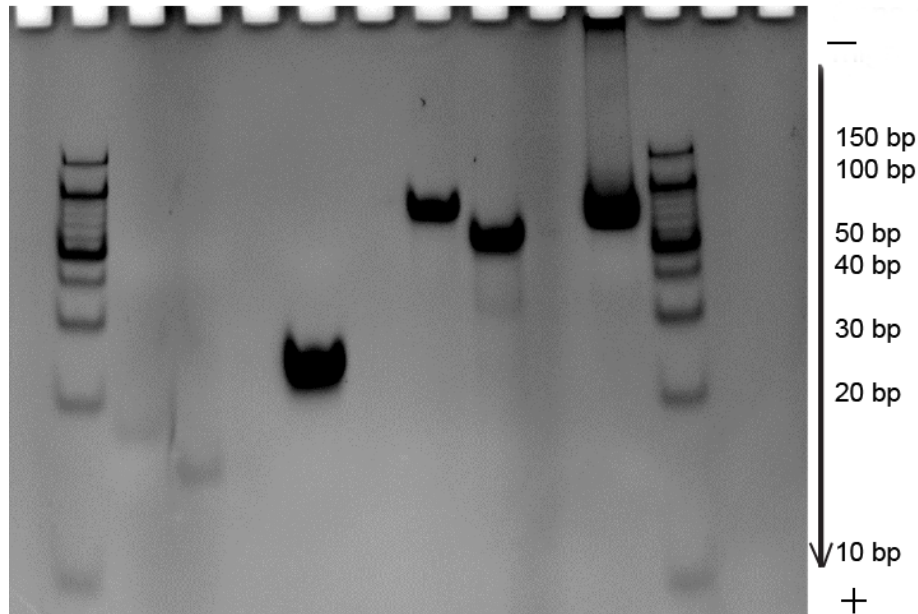
Table 4.3: UV-VIS absorption characteristics of the different oligonucleotide samples.

	Concentration (ng/ μ l)	A260/280	A260/230
dR1 23	963.8	1.21	1.19
dY2 23	1166.3	2.18	2.23
dR1 70	969	1.57	1.81
dY2 70	1104.5	1.94	2.24
D23	2833.5	1.86	2.04
D70	1651.6	1.85	1.70
DY3	1121.4	1.67	2.70
PR	994.9	2.22	2.19
[ThioC₆] dY3	68.2	1.65	2.71
[ThioC₆] PR	100.2	2.18	2.83
[ThioC₆] GFP	144.5	2.13	2.70
Plasmid relaxed	114.5	1.92	2.27

4.1.2. Duplex formation

All the oligonucleotide sequences were supplied by Sigma as single stranded DNA. In order to explore the triplex formation with the sequence of interest, a duplex target sequence was first prepared. Briefly, two complementary strands of DNA, dR1 and dY2, either of 23 bp or 70 bp were incubated in order to form double stranded DNA (Table 4.2).

The details of the incubation can be found in Section 2.14. After 5 min incubation of both sequences at 94°C in order to open the structure and then 1h at RT, the DNA duplex was formed. The samples were then kept in the fridge. The exploration of the *c-myc* duplex formation was done using polyacrylamide gel electrophoresis.



lane	1	2	3	4	5	6	7	8	9	10	11
sample	Ladder	dR1	dY2	X	dR1	X	dR1	dY2	X	dR1	Ladder
sample				X	+dY2	X			X	+dY2	
Size (bp)		23	23		23		70	70		70	

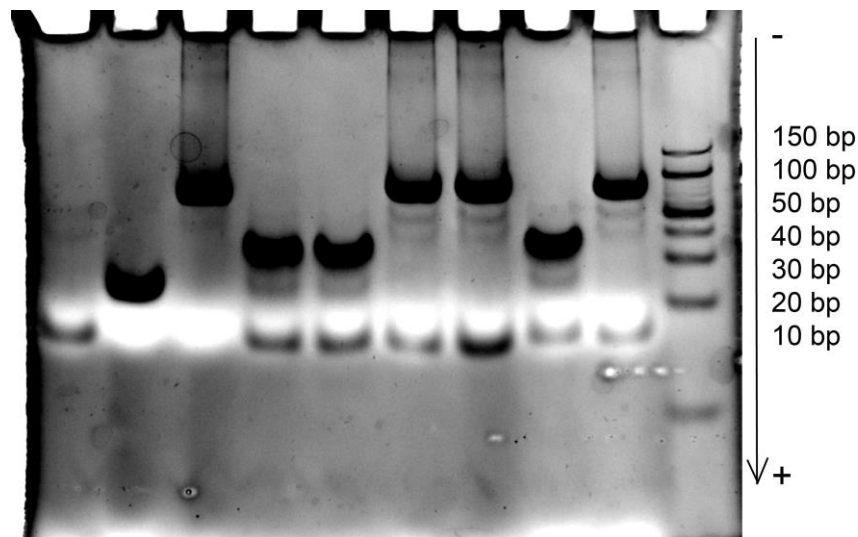
Figure 4.3: 20% PAGE representing the duplex formation. The gel was run in 1xTBE for 1h at $8 \text{ V} \times \text{cm}^{-1}$.

Single stranded and double stranded DNA migrate with different rates on a gel, due to their conformation. Single stranded DNA is lighter and therefore migrates further on a gel. From this statement, on Figure 4.3, the duplex formation is noticed on lane 5, where two complementary single strands of 23 bases each were incubated. This result is confirmed when looking at the DNA ladder, on the right side of the gel (lane 11), which reflects the size of double stranded DNA. The band in lane 5, containing the two complementary strands, supposedly representing a duplex of 23 bp, migrate comparatively to the ladder, between 20 and 30 bp, whereas the single strand migrates between 10 and 20 bp. Single stranded DNA in lane 2 and 3 migrate faster and have a band signal much lighter due to half the amount of DNA, and due to their single strand conformation. The same migration is seen for the sequence of the length of 70 bp, where the band containing the DNA duplex is brighter than single stranded DNA, and migrates less rapidly on the gel, although it is not as clear as for the sequence of 23 nucleotides due to less efficient separation with the high percentage polyacrylamide gel. However, the increase of brightness for the band on lane 10 compared to the two single strands of 70 bp, suggests a possible binding (Annex 3.1).

4.1.3. Triplex formation

After preparing the duplex sequence of interest, the triplex formation between the duplex and each TFOs was investigated. Two sizes of duplexes were used in order to explore the specificity in triplex formation depending on the oligo size, since the triplex binding might be different when the TFO recognises its specific target among a long sequence of DNA. Different conditions were used, such as varying temperatures and incubation times required to find the optimum condition for triplex formation. Figure 4.4 shows the triplex formation with dY3 sequence while Figure 4.5 shows the triplex formation with PR TFO sequence.

During the initial experiments, the samples were run in 1xTBE, the standard buffer used to explore DNA sequences. However, triplex formation requires the presence of positive ions such as magnesium. Therefore, the presence of EDTA in the TBE would interfere with this reaction (Carbone *et al.*, 2004, McGuffie *et al.*, 2000). Accordingly, all the triplex-related electrophoreses were run in tris-borate-magnesium (TBM) buffer. The protocol is shown in Section 2.3.



lane	1	2	3	4	5	6	7	8	9	10
sample	dY3	D23	D70	D23	D23	D70	D70	D23	D70	Ladder
sample				+dY3	+dY3	+dY3	+dY3	+dY3	+dY3	
temperature				RT	4°C	RT	4°C	NI	NI	

Figure 4.4: 20% PAGE representing the triplex formation between the duplex of DNA and the dY3 sequence incubated overnight at different conditions. The gel was run in 1xTBM for 2.5 h at $8 \text{ V} \times \text{cm}^{-1}$ and at 4 °C. dY3 TFO was added in excess of 10/1 to the duplex; NI=- no incubation

In Figure 4.4, the duplexes of 23 bp (lane 2) and 70 bp (lane 3) can be clearly noticed, when compared to the ladder (Annex 3.2.1). Lanes 4 and 5 represent the duplex incubated with TFO-dY3 and a band shift is noticed when comparing to the duplex only. The triplex structure is heavier than the duplex and therefore migrates less far in the gel. Incubating the triplex overnight at different temperatures (4°C, 25°C) does not change the reaction. When looking at lanes 6 and 7, it is not clear whether the TFO is able to bind to the duplex of 70 bp (D70) or not. Finally, when looking at lane 8, which represents the duplex of 23 bp (D23) in presence of the TFO but with an incubation of less than 30 min, a band shift is again noticed, indicating that triplex formation happens very quickly.

Figure 4.5 describes the results of triplex formation, as before, but using the PR TFO. A band shift is noticed when D23 is incubated with PR TFO. This band shift appears clearly as well when PR TFO was incubated with D70. PR and dY3 sequences have two different mechanism of triplex formation and therefore, PR might have a stronger binding probability to the duplex sequence than dY3 (Vasquez and Glazer, 2002). Once again, no difference between the various incubation parameters was observed (Annex 3.2.2), indicating that triplex formation occurs rapidly.

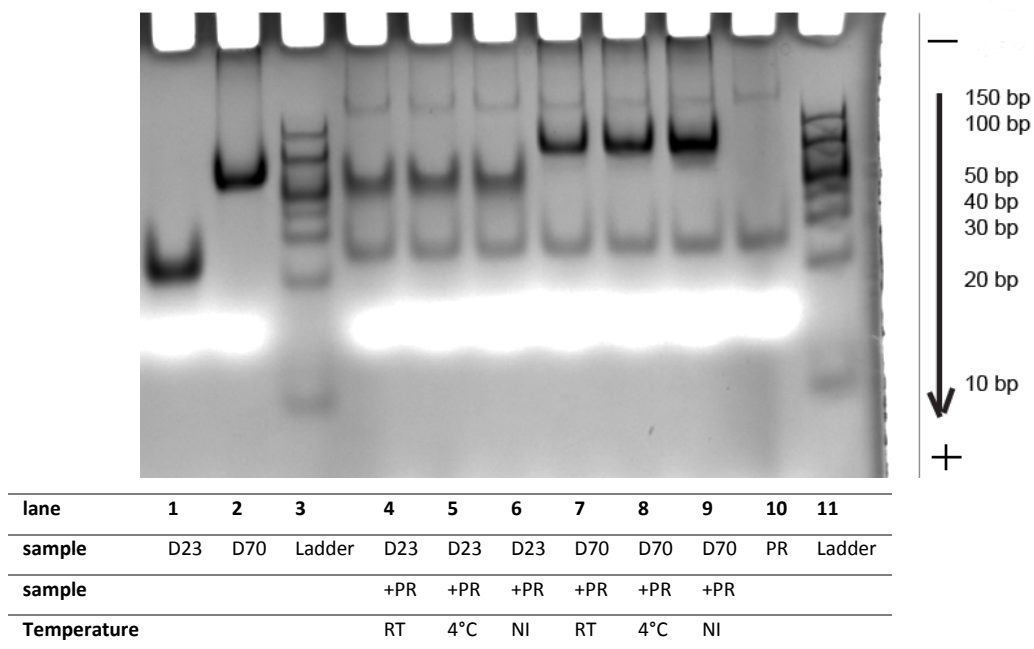
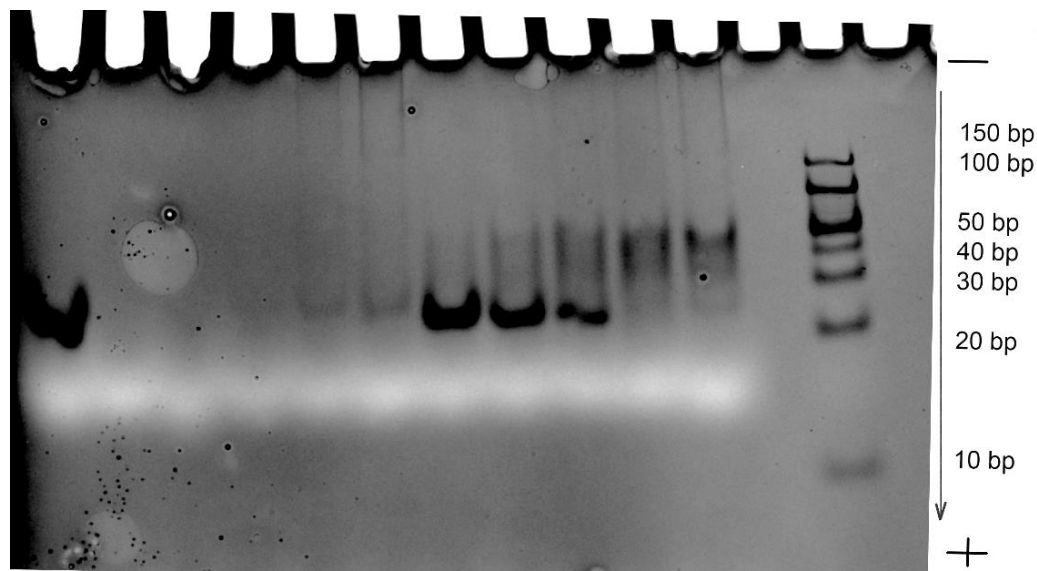


Figure 4.5: 20% PAGE representing the triplex formation with PR sequence incubated overnight at different conditions. The gel has been run in 1xTBM for 2h30 at 8 V×cm⁻¹ and at 4°C. PR TFO was added in excess of 10/1 to the duplex.

After testing different protocols in order to explore the triplex formation, it was possible to observe clearly the triplex structure formed between a double stranded DNA and the designed TFO. As mentioned in Section 1.9., this structure requires divalent cations (such as Mg²⁺) for triplex stabilisation and formation due to electrostatic interaction with the phosphate anions present (Carbone *et al.*, 2004).

Triplex formation can occur when TFO is used at a concentration of 10/1 TFO/Duplex (TFO/D). Thereafter, different ratios of TFO/D were incubated in order to investigate the optimum concentration of TFO required for the reaction to occur. A minimum amount of oligonucleotide will be favoured in order to further coat AuNPs with these sequences. Indeed, too many oligonucleotides on the AuNPs may cause steric hindrance and could form a dense coating that restricts secondary electron release upon irradiation, and therefore lowers the potential radiosensitisation effect.

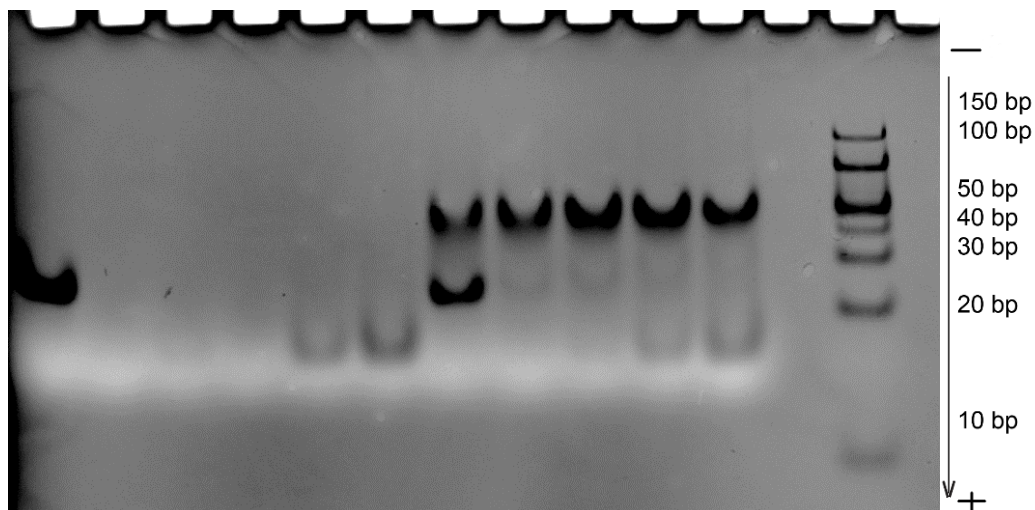
Only the duplex D23 was used for these experiments, as the band shift representing the triplex formation is easier to observe with this length of DNA.



lane	1	2	3	4	5	6	7	8	9	10	11	12	13
sample	D23	dY3	dY3	dY3	dY3	dY3	dY3	dY3	dY3	dY3	dY3	x	Ladder
sample							+D23	+D23	+D23	+D23	+D23	x	
ratio		0.5	1	2	5	10	0.5/1	1/1	2/1	5/1	10/1		
%							2.2%	14.9%	40.7%	86.7%	93.3%		
triplex formed (annexe 3.2.3)													

Figure 4.6: 20% PAGE representing the triplex formation with dY3 sequence incubated overnight at RT. The gel has been run in 1xTBM for 2h30 at $8 \text{ V} \times \text{cm}^{-1}$ and at 4°C .

Figure 4.6 shows the triplex formation after incubating D23 with different concentrations of dY3 TFO. Lane 1 shows D23, while lane 7 to 11 represent D23 incubated with the TFO at various ratios. At a ratio of 0.5 /1 of TFO/D, almost no triplex is formed (2.2%) while at a ratio of 10 /1 of TFO/D, almost all the duplex has reacted with the TFO to form a triplex (93.3%) (Annex 3.2.3., gel analysis). It is possible to note a concentration dependence between the ratio of TFO/D and the triplex formation. Indeed, the duplex band intensity decreases when increasing the amount of TFO and proportionally an increase of band intensity for the triplex signature is seen.

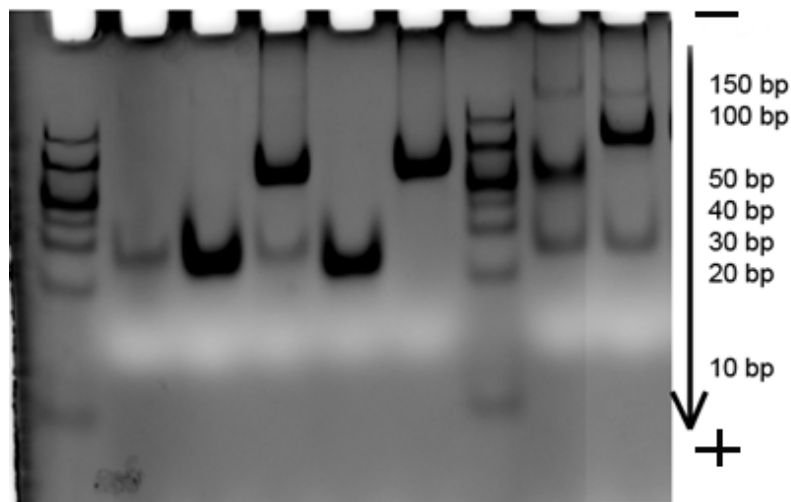


lane	1	2	3	4	5	6	7	8	9	10	11	12	13
sample	D23	PR	PR	PR	PR	PR	PR	PR	PR	PR	PR	x	Ladder
sample							+D23	+D23	+D23	D23	+D23	x	
ratio		0.5	1	2	5	10	0.5/1	1/1	2/1	5/1	10/1		
% triplex formed							53.8	91%	94%	94.7	98.5		
(annexe 3.2.4)							%			%	%		

Figure 4.7: 20% PAGE representing the triplex formation with PR sequence incubated overnight at RT. The gel has been run in 1xTBM for 2h30 at $8 \text{ V} \times \text{cm}^{-1}$ and at 4°C .

A similar experiment on the exploration of triplex formation and ratio of TFO/D, with PR TFO, was performed. At a ratio of 0.5/1 of TFO/D, already 53.8% of D23 has reacted to form a triplex. The triplex formation goes up to 98.5% for a ratio of 10 /1 TFO/D (Figure 4.7, Annex 3.2.4, gel analysis). As previously mentioned, PR TFO has a different triplex binding complex with the purine strand of DNA (Figure 4.2). This TFO can react and form a triplex with the sequence of interest more rapidly and more efficiently than the TFO dY3 (53.8% compared to 2.2% at a ratio of 0.5 /1 of TFO/D) (Figure 4.6, 4.7).

In order to explore the specificity of the triplex formation with the sequence of interest, the duplex of 23 bp was incubated with a non-specific sequence (dY2) of 23 bp, which is not supposed to form a triplex. Indeed, it is important to look at the specificity of the triplex reaction, if considering creating such structure in cells. Only the sequence designed would be able to interact with the targeted gene.



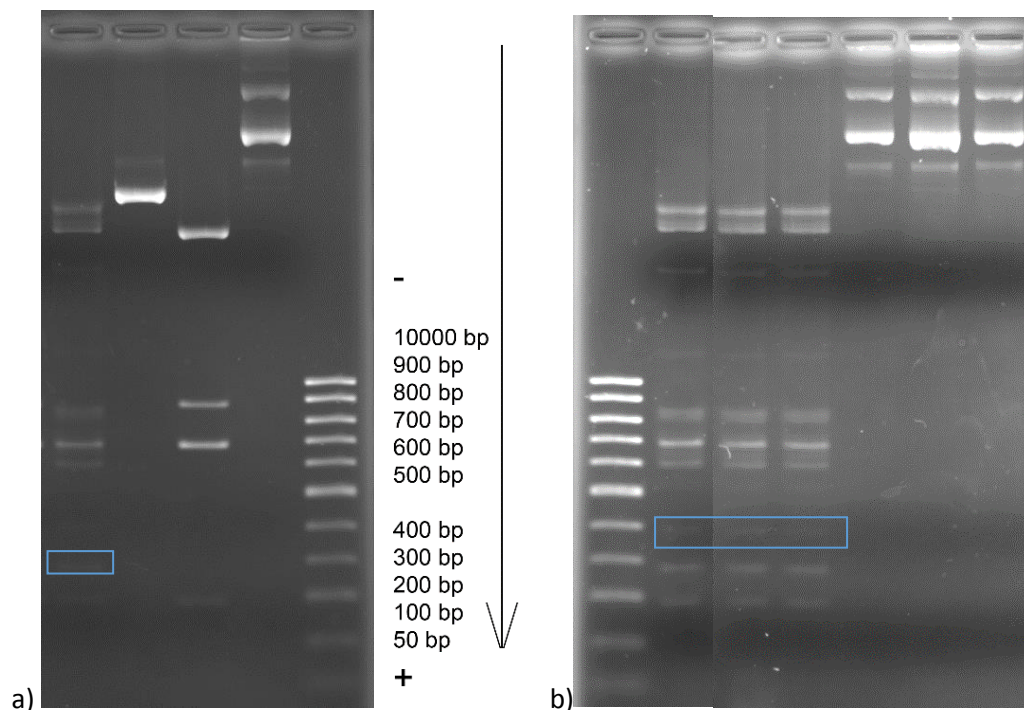
line	1	2	3	4	5	6	7	8	9
sample	Ladder	DY2	D23	D70	D23	D70	Ladder	D23	D70
sample			+dY2	+dY2				+PR	+PR
ratio		10	10/1	10/1				10/1	10/1

Figure 4.8: 20% PAGE representing triplex formation with PR and dY2 sequence incubated overnight at RT. The gel was run in 1xTBM for 2.5 h at $8 \text{ V} \times \text{cm}^{-1}$ and at 4°C .

In Figure 4.8, triplex formation is shown with the TFO-PR sequence on lanes 8 and 9. When a neutral sequence of 23 bp (dY2) was incubated with either D23 or D70, no interaction with the duplexes were observed (lanes 3 and 4). The dY2 sequence is part of the duplex sequence of DNA. It was chosen as very similar in nucleotides to the d23 TFO sequence. The triplex formation seems to be very specific to the sequence of interest.

4.1.4. Triplex formation with plasmid

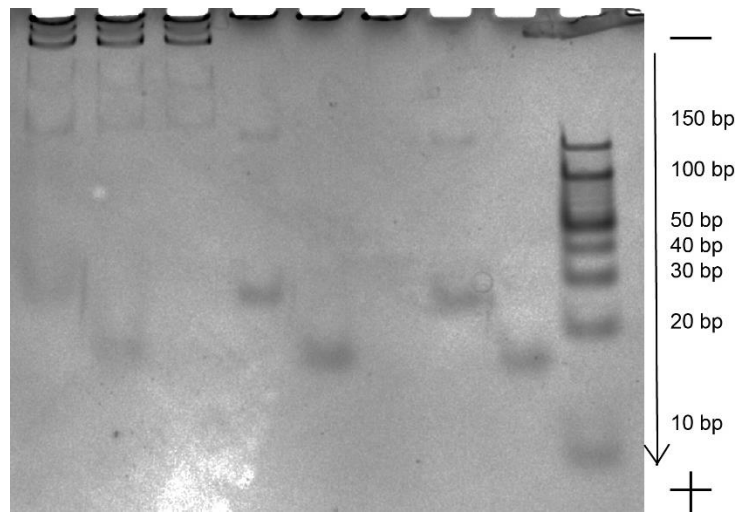
The plasmid pBV-Luc/Del 6 was used in order to explore the sequence targeting with the TFOs of interest on a more complex model. The plasmid was incubated with the two TFOs in order to explore triplex formation. Plasmid DNA was tested either in its relaxed form, or was double cut with *BfmI* and *NotI* restriction enzymes in order to generate a c.a. ~300 bp long sequence containing the *c-myc* promoter region of interest. Restriction enzymes are bacterial enzymes that recognize specifically 4 to 8 bp sequences, called restriction sites, and then cleave both DNA strands at this site.



lane	1	2	3	4	5	lane	1	2	3	4	5	6	7
sample	PI	PI	PI	PI	L	sample	L	PI	PI	PI	PI	PI	PI
form	L	L	L	R		form	L	L	L	R	R	R	R
Enzyme	<i>BfmI</i>	<i>NotI</i>	<i>BfmI</i>			Enzyme	<i>BfmI</i>	<i>BfmI</i>	<i>BfmI</i>				
	<i>+NotI</i>						<i>+NotI</i>	<i>+NotI</i>	<i>+NotI</i>				
sample						sample		dY3	PR		dY3	PR	

Figure 4.9: 1.2% AGE showing a) Incubation of plasmid pBV-Luc/Del6 with 2 endonucleases; b) mixtures of plasmid pBV-Luc/Del6 with PR or dY3 TFO sequences at a 10/1 ratio of TFO/plasmid incubated overnight at RT. The gels have been run in 0.5xTB for 2h at 8 Vxcm⁻¹; R - relaxed, L – linear; L-ladder. The blue rectangles indicate a 300 bp fragment.

In Figure 4.9, two different forms of the plasmid can be observed. Indeed, the two different endonucleases are responsible for cleavage in the relaxed plasmid, thus increasing its linear form. The enzyme *BfmI* seems to recognise and cut different sites in the plasmid (Figure 4.9 a). As mentioned before, the full sequence of the plasmid is not available from the supplier and the restriction enzymes might be responsible for different DNA fragments than expected. The combination of both enzyme together produces various breaks and various bands in the plasmid (Figure 4.9 a). Interestingly, according to the ladder, a band of about 300 bp is seen and could be our sequence of interest (*c-myc* promoter), which will be able to form a triplex with the TFOs. When looking at the triplex formation, it is difficult to note any changes in the plasmid and its different forms (Figure 4.9 b). The agarose gel is not conclusive on whether the triplex formation is happening with the plasmid or not. The agarose gel is able to separate rather large sequences, but for smaller sequences (like the TFO), polyacrylamide gel is preferred. Therefore, plasmid DNA incubated with the TFO of interest was investigated with polyacrylamide gel.



lane	1	2	3	4	5	6	7	8	9
sample	PI	PI	PI	PI	PI	PI	PR	Dy3	Ladder
form	nicked		relaxed						
sample	PR	dY3		PR	dY3				
TFO signal	40.	51.5		95.	105%		100	100	
%/control	3%	%		7%			%	%	

(Annex 3.3)

Figure 4.10: 20% PAGE showing mixtures of plasmid pBV-Luc/Del6 with PR or dY3 TFO sequences incubated overnight at RT. The gel was run in 1xTBM for 2h at $8 \text{ V} \times \text{cm}^{-1}$.

In Figure 4.10, the plasmid was incubated with the different TFOs. The samples were loaded and run this time on a polyacrylamide gel, which does not allow the plasmid to enter due to its large size, but still this could be informative on the possible interaction between the TFO and its target sequence within the plasmid. Indeed, if the band showing the TFO alone is disappearing from the gel when loaded with the plasmid, it will indicate that an interaction between plasmid and TFO took place. From the Figure 4.10, it is possible to notice clearly the two TFOs in lanes 7 and 8. These bands are much less pronounced when TFO were incubated with the nicked plasmid (Lane 2, 51.5% of the original signal for dY3 and Lane 1, 40% for PR, Annex 3.3), indicating a possible interaction with the nicked plasmid. No changes in TFO signal intensity were noticed when the TFOs were incubated with the unprocessed plasmid.

Interestingly, Luigi *et al.* observed triplex formation when incubating their sequence of interest with the nicked form of the plasmid Bluescript KS+ on agarose gel (XODO *et al.*, 1993). Moreover, Hampel *et al.* in 1993 showed a triplex structure on agarose takes place for plasmid at pH 4 and in the presence of supercoiled and nicked form (Hampel *et al.*, 1993). The pH4 could modify the supercoiled form of the plasmid by creating breaks in the structure, relaxing the DNA and therefore aid the triplex structure to happen (Hampel *et al.*, 1993). It is not clear why the relaxed form of the plasmid explored in this work on agarose gel does not give indication on

triplex formation. It may be interesting to try this experiment with a different pH. Moreover, different restriction enzymes could be used to obtain different fragments of plasmid DNA.

Two TFOs were explored as targets of the *c-myc* gene, one designed by Mc Guffie *et al.*, in 2004 and already shown to enter the cell nucleus and form a triplex, another one designed at the Open University laboratory, similar in binding but rich in purine, which is supposed to be more stable and bind more easily to its target sequence. From the *ex vivo* experiments performed on the double stranded DNA and the plasmid, it seems that the sequence designed at the OU (PR) rich in purine binds more substantially to the double stranded target DNA, as more triplex is seen by electrophoresis or a greater disappearance of oligonucleotide when incubated with plasmid. The next experiment explored the possibility to coat AuNPs with these two TFOs and explore their effect on biological models, in order to improve the radiosensitisation effect of AuNPs.

4.2. Oligonucleotide coated AuNPs characterization

4.2.1. AuNPs size characterised by TEM analysis

In order to stabilise the AuNPs and try to regulate the number of the oligonucleotides attached, AuNPs were coated with PN molecule. PN is characterised by two sulphurs which can interact with gold via covalent binding. Moreover, it is known that a ligand exchange reaction can easily happen between the PN-stabilised AuNP and another thiol molecule, making it an interesting coating for further oligonucleotide functionalisation (Muramatsu and Miyashita, 2009).

The coating brings stability to the NPs by avoiding NP-NP interaction, making the AuNPs more soluble in water. Interestingly, AuNPs seem to be more stable and more resistant when the ligand possesses more than one thiol (Kang *et al.*, 2010).

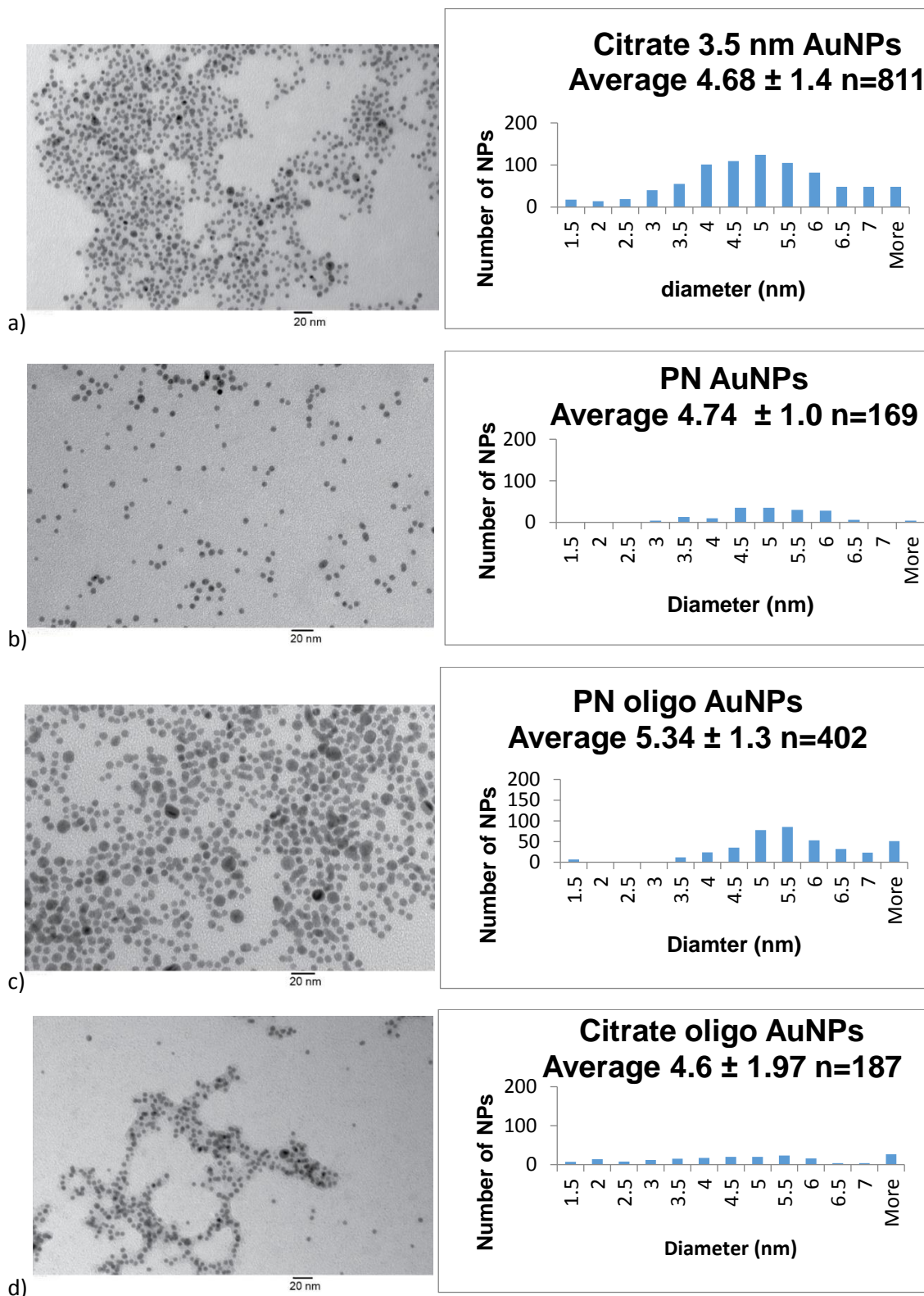


Figure 4.11: Observation of the core size of the different AuNPs under the TEM. a) citrate AuNPs; b) PN AuNPs; c) oligonucleotides -PN-AuNPs; d) citrate-oligonucleotides-AuNPs. Values \pm SD.

From the TEM images on the Figure 4.11, it is possible to conclude about the average size and the aggregation potential of the AuNPs. All the AuNPs seem to have the same average size between 4.6 and 5.34 nm, but the distribution is broad and standard deviation is large for some AuNPs (e.g. citrate oligo AuNPs). Looking at the aggregation, AuNPs coated with citrate

only or PN molecule seem to be well-separated while the AuNPs coated with DNA seem to be more clustered together. The DNA molecules could affect the stability of the AuNPs.

4.2.2. AuNPs concentration measurements

The concentration of the different AuNPs was measured using UV-Vis spectrometry (Nanodrop) and gold measurement (Aqua regia, methods explained in section 2.1.2). Two methods were used in order to explore if the nanodrop could give accurate data on the gold content when a coating on the AuNPs was present, compared to the Aqua regia, which measure only the amount of gold in the sample. These two data were converted to $\mu\text{g/ml}$ using the molecular weight of the AuNPs.

Table 4.4: Concentration of the different AuNPs.

NPs	Nanodrop (Conc in μM)	Nanodrop (Conc in $\mu\text{g/ml}$) $m=n \times M$	Aqua regia (Conc in $\mu\text{g/ml}$)	% difference Nanodrop/Aqua regia
Citrate NPs	8.9	2.7	4.3	159
PN NPs	13.2	4	6.5	163
Citrate-dY3 NPs	9.9	3	3.06	102
Citrate-PR NPs	9.6	2.96	2.49	84
Citrate-GFP NPs	6.38	1.96		
PN-dY3 NPs	7	2.1	2.46	117
PN-PR NPs	5.75	1.7	1.96	115
PN-GFP NPs	8.72	2.68		

For more than half of the AuNPs, the Aqua regia and Nanodrop measurements gave a similar concentration of gold in $\mu\text{g/ml}$, however, for the AuNPs which are the most concentrated, the difference between the two methods became larger (Table 4.4). For further experiments, only the concentration measured by the Nanodrop was used as it was also used for the measurement of DNA, and it was easier and cheaper to perform on a day to day basis.

4.2.3. Oligonucleotide attachment to AuNPs and characterisation

Characterization by Dynamic light scattering (DLS)

The hydrodynamic size of the AuNPs was explored using DLS in UHP water.

Table 4.5: Dynamic Light scattering analysis

NPs	TEM (nm)	Hydrodynamic size (nm)	Zeta potential (mV)
Citrate NPs	4.68 ± 1.40	9.2 ± 3.0	- 41.9 ± 9.52
PN NPs	4.74 ± 1.00	8.9 ± 3.2	- 38.8 ± 6.85
Citrate-DY3 NPs	4.6 ± 1.97	9.8 ± 4.3	- 43.4 ± 25.3
Citrate-PR NPs	n/a	8.7 ± 3.2	- 37.0 ± 32.2
PN-DY3 NPs	5.34 ± 1.25	9.0 ± 3.3	- 27.3 ± 9.45
PN-PR NPs	n/a	8.3 ± 3.2	- 55.7 ± 16.2

The hydrodynamic diameters explored by DLS are higher than those observed with TEM (Figure 4.11; Table 4.5). This is expected as the DLS gives information on the size of AuNPs with their coating in solution. However, no difference was observed between the different coated AuNPs. It is not clear, at this stage, whether the attachment between the TFOs and AuNPs has happen or not. Zeta potential measurements revealed that all the AuNPs have the same average negative charge. Only PN-dY3 AuNPs seemed to have a slight increase in negative charge but this difference is not significant.

Characterization by X-ray photoelectron spectroscopy

In order to explore the coating of the AuNPs and make sure that the dY3 TFO is attached to their surface, X-ray photoelectron spectroscopy (XPS) was used. This ultra-high vacuum technique allows determining the number of photoelectrons emitted from the sample, as well as their binding energy. This information is specific to the interactions between various chemical elements in the sample.

Three different elements were considered, sulphur, phosphorous and gold, and specifically the atomic orbitals: S2p, P2p and Au4f, which can be found respectively in the coating or the core of the AuNPs. The protocol for this technique is described in Section 2.1.4.

Table 4.6: XPS analysis, characteristics of the different peaks, such as their binding energies and their intensities in counts per second (CPS) observed for each element, on the different samples measured (Annex 3.4).

	P(2p)		S(2p)	Au(4f)		P/Au ratio	S/Au ratio
Citrate AuNPs							
Peak (eV)	140	133	166	87	83	1.45	2
Intensity (cps)	30	29	40	20	20		
Citrate-TFO -AuNPs							
Peak (eV)	140	133	167.5	89.5	83	17	26.6
Intensity (cps)	52	51	80	3	2		
PN-AuNPs							
Peak (eV)	140	133	167	89	82.5	1.66	2.29
Intensity (cps)	42	40	55	24	22		
PN-TFO-AuNPs							
Peak (eV)	140	133	167	87	83	0.98	1.62
Intensity (cps)	51	49	81	50	51		

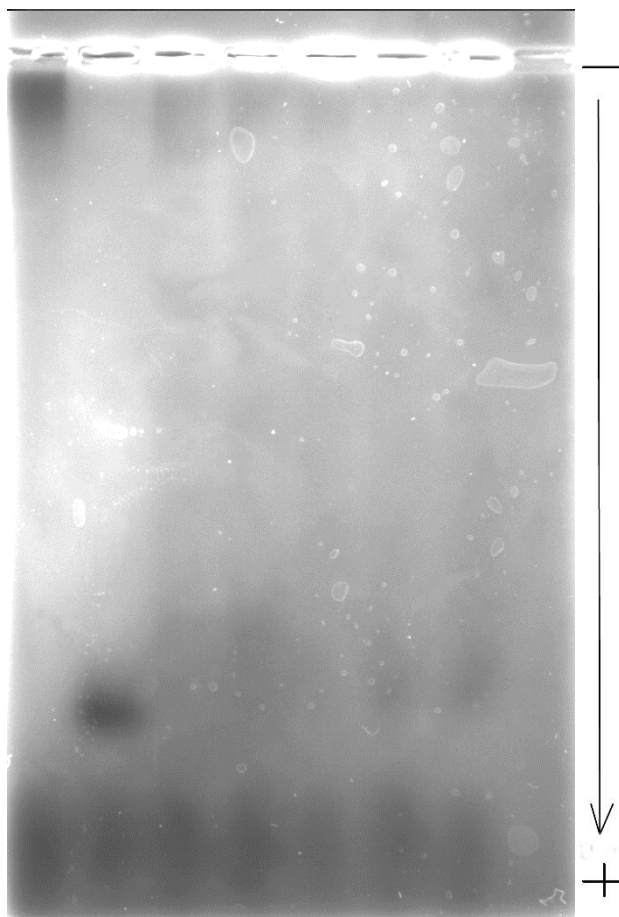
The differences in electrons spectra from XPS technique can be used to analyse the presence of surface coating on the AuNPs (Wang *et al.*, 2016). In all cases, the two characteristic peaks of the gold element, Au4f_{7/2} and Au4f_{5/2} are observed, for some cases very small, at 83 eV for Au4f_{7/2} and between 87 and 89.5 eV for Au4f_{5/2} (Table 4.6, Annex 3.4). The standard energy positions for bulk metallic gold of these two peaks are 84 eV and 87.3 eV for Au4f_{7/2} and Au4f_{5/2} respectively (Wang *et al.*, 2016). The intensities are very different for each sample and could be explained by an interaction with the coating of the AuNPs. However, the highest count levels were obtained with the AuNPs coated with PN and TFOs, therefore, these differences in intensities could be explain by a difference in gold concentration. Although an equivalent concentration (gold amount) of AuNPs was used for these experiments, it will be interesting to repeat the XPS counts with the exact same amount of gold.

Interestingly, analysis of the sulphur element give rise to one single peak, at 166 eV for

the citrate AuNPs and at 167 eV for the other coated AuNPs. A peak around 164 eV would be characteristic for a thiol group, while a peak at 162.5 eV would be characteristic for the Au-S bond (scientific, 2013-2017). In this case, the sulphur analysis is not conclusive whether the Au-S bond is present in the system or not. It is also possible that the PN and the TFO bind via P-S bond (Orthaber *et al.*, 2015). Interestingly, Zhuge *et al.* found three peaks when exploring the interaction between triphenylphosphine molecule and a gold surface, attributing a peak of 132.8 eV to the oxidation of the phosphorous of the molecule and one at 134.32 eV, attributed to the adsorption of phosphorous on the gold surface (Zhuge *et al.*, 2017). In this case, the phosphorous analysis gave rise to two peaks, at 133 eV and at 140 eV (Table 4.6, Annex 3.4). The peak at 133 eV most likely represents the P-O bond. It is possible to note also that the intensity of the peak at 133 eV is increased in all the samples, compared to the citrate AuNPs, which could indicate the presence of the coating as the two different molecules PN and TFOs contains phosphorous groups.

When incubating the AuNPs with the different coatings, the AuNPs were washed and all the unbound molecules should have been removed from the solution. However, it will be interesting to test whether unbound molecules are still present in solution using ICPMS of the supernatant after filtering the AuNPs. In order to observe the possible presence of the coating on the AuNPs, ratios of P/Au and S/Au were calculated. Because the amount of gold in each sample is different, it is difficult to compare the ratio and to conclude on the possible increase of phosphorous and sulphur elements.

Different information arise from the element analysis of the various AuNPs, but due to insufficient amount of each samples, it was not possible to draw quantitative conclusions



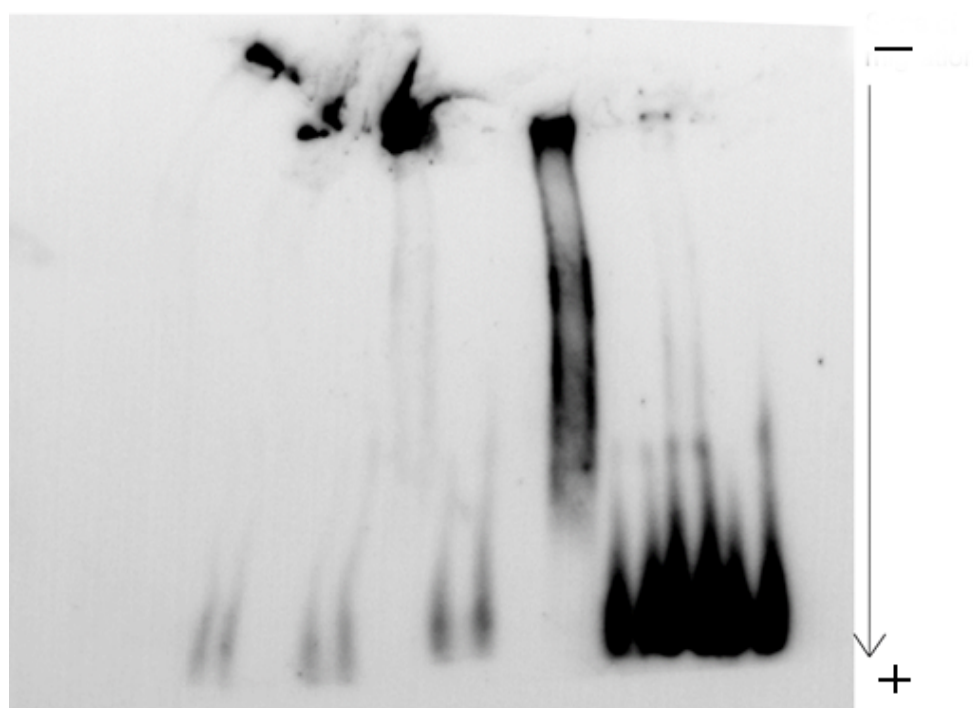
lane	1	2	3	4	5	6	7	8
AuNPs	citrate	PN	PN	PN	PN	PN	PN	x
coating			oligo	oligo	oligo	oligo	oligo	
(ratio			1/1	1.5/1	2/1	5/1	10/1	
of oligo								
/AuNP								

Figure 4.12: 1% AGE representing the AuNPs coated with different molecules. The gel was run in 0.5xTB for 2h at $8 \text{ V} \times \text{cm}^{-1}$.

From the Figure 4.12, it is possible to note that the AuNPs have different migration on the gel regarding their coating. They all have the same size, but their coatings are different. The citrate AuNPs did not migrate in the gel. A possible explanation could be that the citrate capping is easily removed from the AuNPs when entering the gel, and the charge distribution uneven. Indeed, we have seen that citrate AuNPs in water are negatively charge, but as soon as they are in contact with another buffer, the citrate capping might become too weak and fall apart (Kalimuthu and John, 2010). Another possibility would be that they aggregate in salt solution. One way to test this hypothesis would be to look at their behaviour under TEM when the citrate AuNPs are diluted in such a solution, e.g. PBS.

The opposite behaviour is observed for the AuNPs coated with PN, which migrate quite far on the gel and confirm that the AuNPs are negatively charge. PN coating seems to be stronger than the citrate one. Finally, when looking at the AuNPs with different ratio of dY3 oligos attached to their surface, the band is less clear and more diffuse. Moreover, a band near the origin decreases when increasing the amount of oligo, while another band at the end is seen for the AuNPs coated with ratios of 5/1 and 10/1. It is most likely that these AuNPs have different populations and different numbers of oligonucleotides.

AuNPs interaction with its complementary sequence



lane	1	2	3	4	5	6	7	8	9	10
oligo	1	1	1.5	1.5	2	2	5	5	10	10
AuNPs (Yes (Y)/ No (N))	Y	N	Y	N	Y	N	Y	N	Y	N

Figure 4.13: 15% PAGE representing the interaction between the TFO coating the AuNPs and its complementary sequence incubated overnight at RT, followed by an EMSA. The gel has been run in 0.5xTB for 2h at 8 V \times cm⁻¹. The concentration of oligo represents the ratio of oligo/AuNP.

Figure 4.13 represents the dY3 oligonucleotide attachment to its complementary sequence, forming a duplex. The attachment between the two sequences is designed to form a duplex, which is more likely to happen than a triplex, and thus increase the sensitivity of the reaction. For example, there is no limitation in the presence or absence of Mg²⁺ or no limitation in the amount of probe to use. Indeed, the duplex was shown in the section 4.1.2 to happen at a ratio of 1/1 DNA sequences. The complementary sequence attachment will give information

on the number of oligonucleotides attached to the AuNPs as the complementary sequence contains a biotin probe which is very sensitive. Since the AuNPs are not able to enter in the gel, even at a low percentage, it is very difficult to conclude on the number of TFOs on each AuNPs. However, this technique can give information whether the TFOs are indeed attached to the AuNPs. Particularly, as the fluorescent probe recognises the TFO and as the AuNPs cannot enter the gel, if the TFOs are coating the AuNPs, the probe should be retained at the entrance of the gel. This is indeed what can be observed in Figure 4.13.

The fluorescence signal of the biotin probe alone, which is the complementary sequence to the TFO, can be seen at the bottom of the gel on lanes 2, 4, 6, 8, 9 and 10. Different concentrations were used to correlate the different amount of TFOs added on the AuNPs. It is possible to see on lanes 9 and 10 a saturation of the fluorescence. Moreover, a disappearance of the fluorescence of the biotin probe is noticed when this complementary sequence is incubated with the TFO-coated AuNPs (lanes 1, 3, 5, 7). The fluorescence of the probe is not seen on the bottom of the gel anymore but at the top and in a much brighter signal. The AuNPs which seem to react the most are the ones coated with a ratio of 2/1 and 5/1 TFO/NP as a complete disappearance of the biotin signal on the bottom of the gel is observed, representing the complementary sequence unbound. From the Figure 4.13, it is possible to conclude that AuNPs coated with a ratio of 2/1 and 5/1 TFOs/NP seem to have bound with the oligonucleotides and seem to react easily with their complementary sequence to form a duplex. Coated AuNPs with 2/1 or 5/1 TFO/NP have a chance to enter the cells and possibly to react with the sequence of interest and form a triplex.

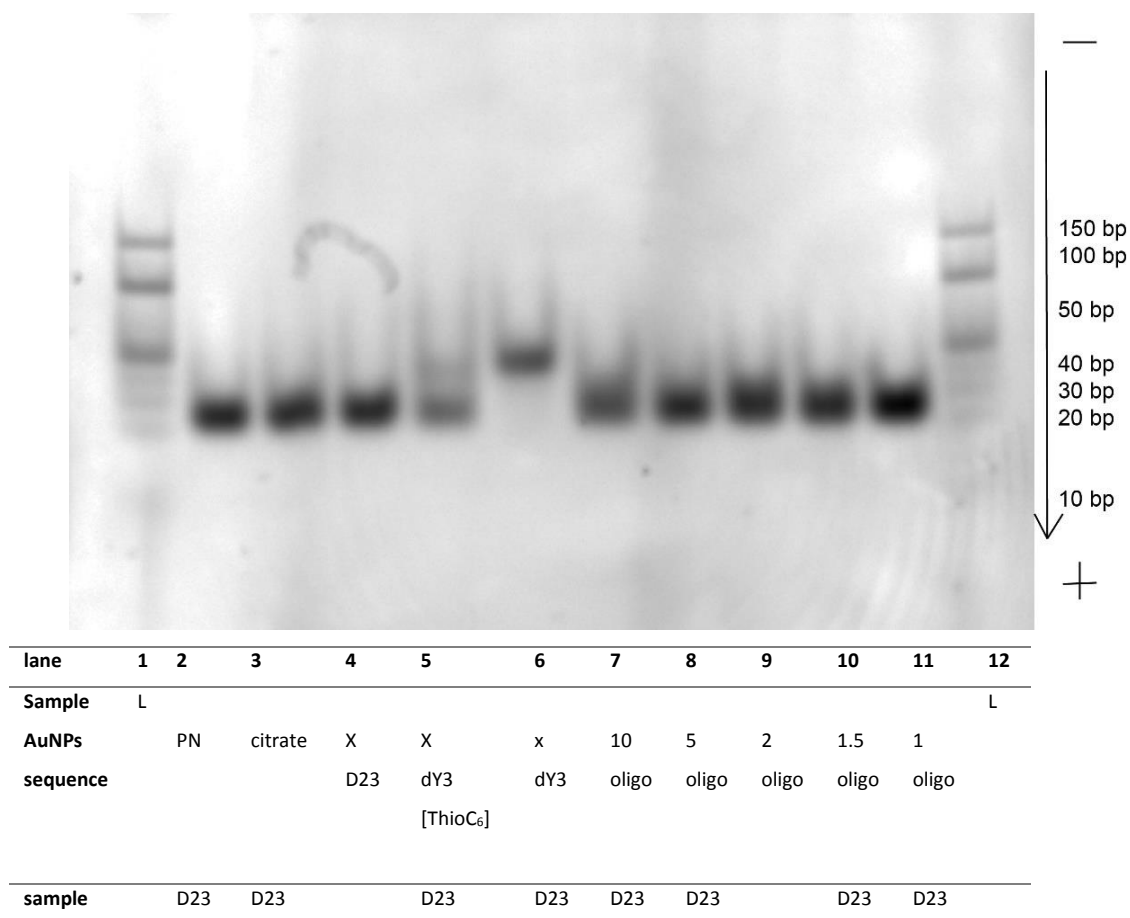


Figure 4.14: 20% PAGE showing mixtures of D23 with PR or dY3 TFO coated AuNPs incubated overnight at RT. The gel was run in 0.5xTB for 2h at 8 Vxcm⁻¹.

The Figure 4.14 shows the migration of the duplex of 23 nucleotides, incubated with the different AuNPs. The AuNPs coated with oligonucleotides should be able to form a triplex with the duplex of DNA. From the Figure 4.14, the triplex formation with the dY3 sequence is clearly seen, while with the thiol-dY3, it is less clear, but a band shift can still be observed. It seems that the thiol group affects the triplex formation. It will be interesting to explore different thiol spacers in order to find the best steric conformation for the triplex formation to happen. However, when looking at the triplex formation with the AuNPs coated with oligonucleotides, the band shift is not observed. A diffuse band is observed with the AuNPs coated with a ratio of 10/1 oligonucleotides, possibly indicating a minor reaction.

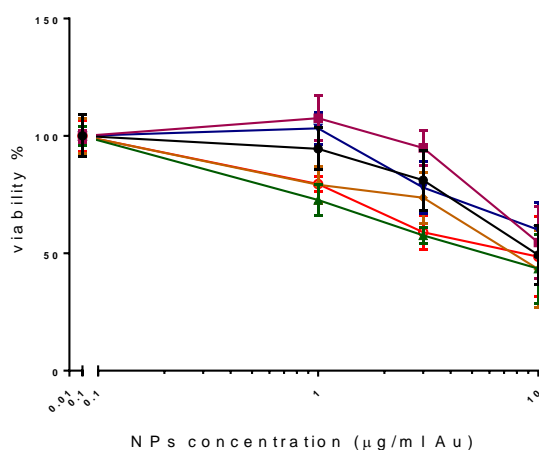
Following these results, it was difficult to make a decision on which ratio of TFO/AuNPs to use for cell analysis and radiosensitisation. The 5/1 TFO coated AuNPs gave the best duplex formation in Figure 4.14 and was taken forwards for possible triplex formation and in the next experiments.

4.3. Oligonucleotide coated AuNPs effect on cell survival

4.3.1. Cell proliferation and survival

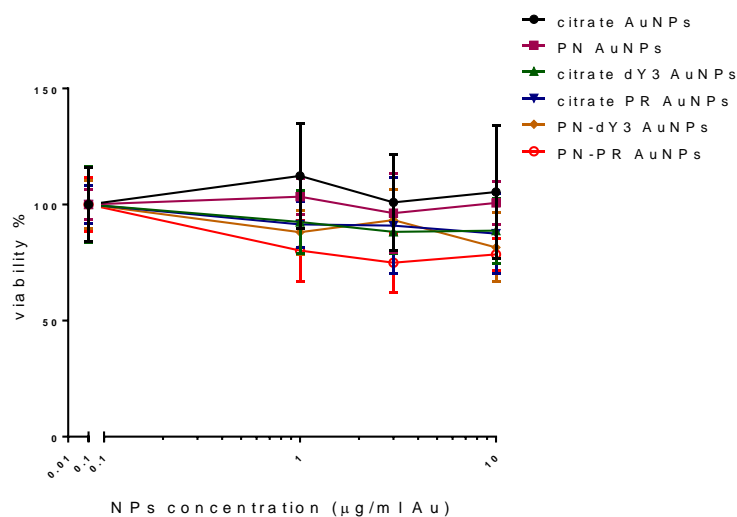
The effect of AuNPs coated with different oligos at a 5/1 ratio of oligo/AuNP was explored on skin cells. In order to investigate the possible toxicity of the different AuNPs, the clonogenic assay was used, which gives information on the cell proliferation and the cell viability.

HSC-3 exposed to oligonucleotides coated AuNPs



a)

HaCaT exposed to oligonucleotides coated AuNPs



b)

Figure 4.15: Clonogenic assay after AuNPs exposure at different concentrations. The graphs represent the percentage of viability compared to the control for a) HSC-3 cells; b) HaCaT cells. Data are presented as mean percentage survival \pm standard deviation. Statistical differences in dose responses for each AuNPs on each cell line was analysed by two-way Anova followed by a Dunnett's multiple comparisons test.

All the AuNPs start to show a toxicity at a concentration of 10 µg/ml on HSC-3 cells (Figure 4.15 a, Annex 3.5.1). Citrate dY3, PN-dY3 and PN-PR AuNPs seem to be the most toxic as they are responsible for a statistically significant effect compared to the control already at 3 µg/ml (Annex 3.5.1). However, none of the AuNPs seem to show a strong toxicity on HaCaT cells (Figure 4.15 b, Annex 3.5.2). Indeed, the viability compared to the control only decreases up to 25% when HaCaT cells were exposed to PN-PR AuNPs. From these experiments, it is possible to notice that the coated AuNPs, especially with TFO present, give a small but selective toxicity toward cancer cells. This toxicity is seen particularly at 10 µg/ml and is statistically significant for all the AuNPs (Annex 3.5.1).

4.3.2. Cell proliferation

Figure 4.16 shows the number of cells after AuNPs exposure, at different time points after an exposure for 3 hours. The CyQuant assay quantifies the amount of duplex DNA in the cells and in a population of unsynchronised cells, this is assumed to be proportional to the number of cells present. Not only TFOs coated AuNPs but also AuNPs coated with non-triplex forming oligos were explored for these experiments and for the further ones. The oligo GFP is not present in the human cells and is moreover not designed to form a triplex. This sequence coating the AuNPs was used to explore the specific effect of the TFO inside the cells, compared to the effect of a DNA sequence. It is possible to note that all AuNPs decrease significantly the cell number compared to the control, without AuNP exposure. However, the number of cells has doubled from 48 h to 96 h in all conditions. Moreover, the difference between the number of cells without AuNPs exposure and the exposed samples is not statistically different after 96 h. It seems that the cell cycle was not impacted by the AuNPs as the cell growth remained unaffected in all condition. Moreover, the slope of the curve representing the cell growth for each condition is similar, indicating no specific effect on the cell proliferation rate.

HSC-3 exposed to oligonucleotides coated AuNPs

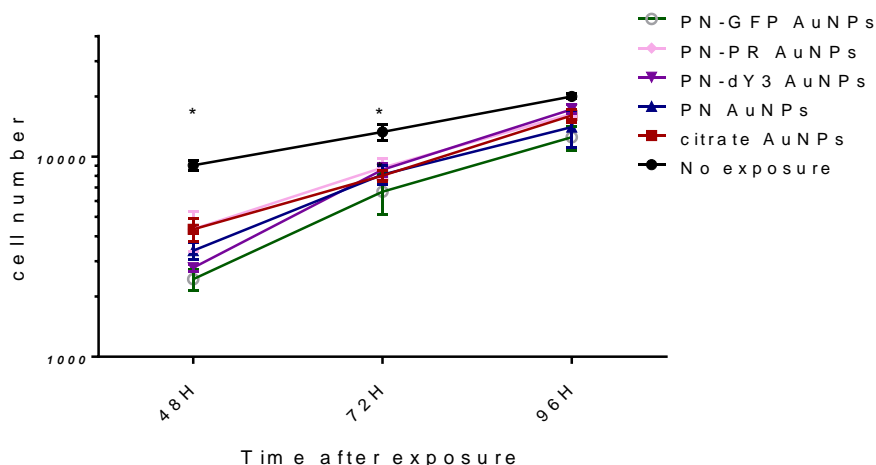


Figure 4.16: Effect of the different AuNPs on the cell proliferation and survival. CyQuant assay. The data are expressed as mean cell number \pm SEM. A two-way Anova followed by a Dunnett's post-test was done to explore the difference between the different exposures and the control for each time point.

At this point there is no evidence that the TFO is binding the *c-myc* promoter sequence in the cells. There is no evidence that the cell cycle or the cell growth is dysregulated. The next experiment was designed to explore if the AuNPs can enter the cells. Indeed, the effect of the TFO will depend on the AuNPs localisations in the cell. In order to explore the effect of these AuNPs on both cell lines, their uptake and localisation were evaluated using TEM.

4.4. Oligonucleotides coated AuNPs and cellular uptake

Figure 4.17 and 4.18 represent the coated AuNPs observed in HSC-3 (Figure 4.17) and HaCaT cells (Figure. 4.18) after 3 hr exposure. From several different TEM images, it was possible to quantify the number of AuNPs within each cell compartment (cytoplasm, nucleus) per nm^2 ; and on the cell surface per nm. These quantitative data are shown in Figure 4.19.

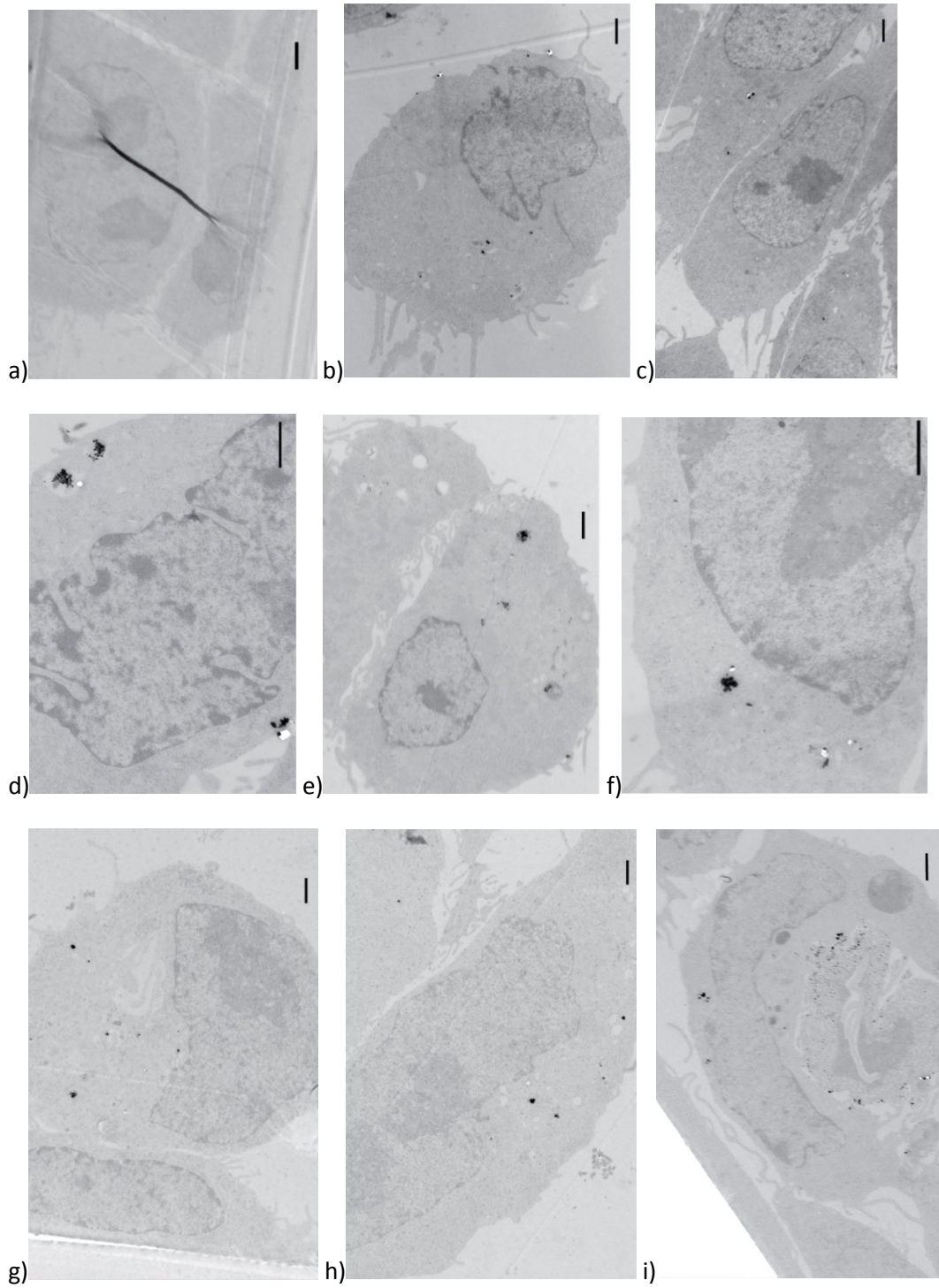


Figure 4.17: Observation by TEM of HSC-3 cells exposed to a) no AuNPs, b) citrate AuNPs, c) PN AuNPs, d) citrate dY3 AuNPs, e) citrate PR AuNPs, f) citrate GFP AuNPs, g) PN-dY3 AuNPs, h) PN-PR AuNPs, i) PN-GFP AuNPs. The scale is 1000 nm for all the images.

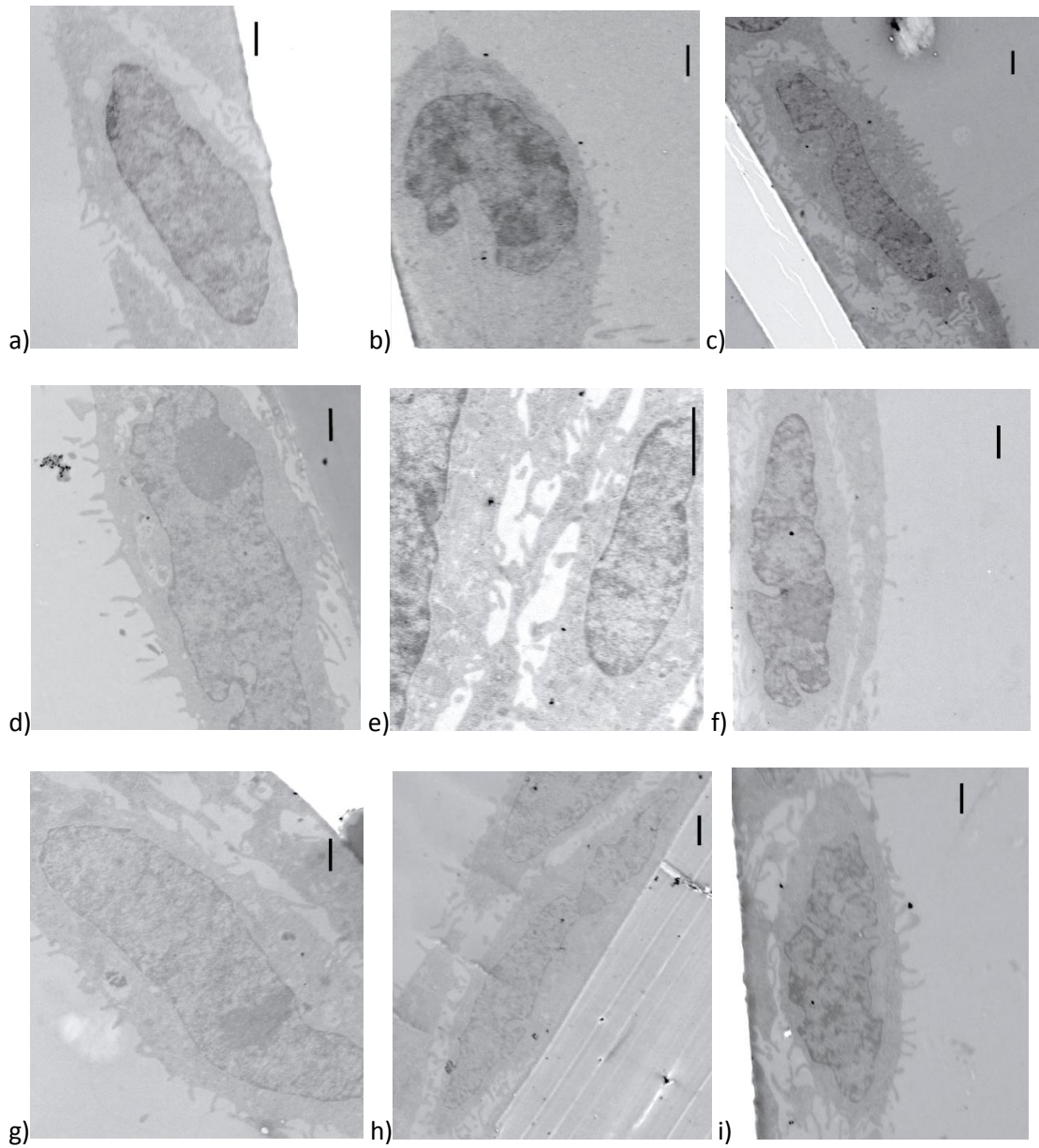


Figure 4.18: Observation by TEM of HaCaT cells exposed to a) no AuNPs, b) citrate AuNPs, c) PN AuNPs, d) citrate dY3 AuNPs, e) citrate PR AuNPs, f) citrate GFP AuNPs, g) PN-Y3 AuNPs, h) PN-PR AuNPs, i) PN-GFP AuNPs. The scale is 1000 nm for all the images.

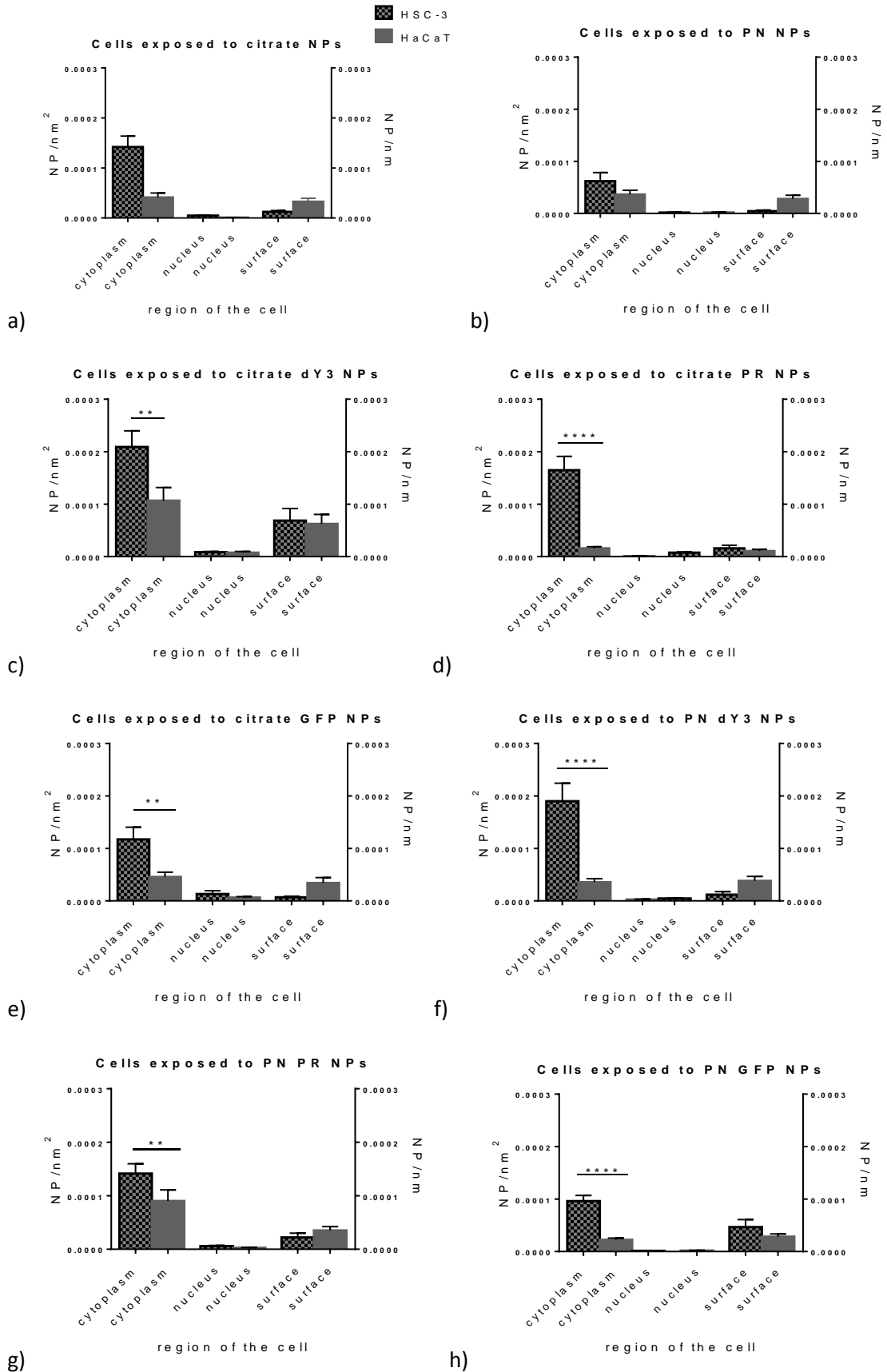


Figure 4.19: TEM analysis of AuNPs/area of the cells after exposure. The data represent mean \pm SEM of a minimum of 20 images, representing 20 cells. Cytoplasm and nucleus uptake are visualised on the y left axis (NP/nm²) while surface uptake is visualised on the y right axis (NP/nm).

a) citrate AuNPs, b) PN AuNPs, c) citrate dY3 AuNPs, d) citrate PR AuNPs, e) citrate GFP AuNPs, f) PN dY3 AuNPs, g) PN PR AuNPs, h) PN GFP AuNPs. The data are presented as mean number of AuNPs \pm SD. A two way Anova, followed by a Tukey post-test was used to explore any statistical difference between the uptake of the different AuNPs for each cell line, while a two-way Anova followed by a Sidak post-test was used to explore any statistical difference in uptake between the two cell lines for each AuNPs. Detailed values of the number of AuNPs for each condition can be found in Annex 3.6.

Interestingly, having an oligonucleotide coating the AuNPs seems to improve the nuclear uptake, compared to citrate coated AuNPs, although this result is only statistically significant for the citrate dY3 AuNPs (Figure 4.19). This result is in accordance with the literature where Cui *et al* found an increase of cellular uptake of AuNPs coated with a peptide compared to PEG alone with a fourfold increase inside MDA-MB-231 cells (Cui *et al.*, 2017), while Burger *et al* used a DNA transfection agent and showed an increase of uptake inside Hela cells (Burger *et al.*, 2014b). Moreover, PN coated AuNPs are responsible for a statistically smaller uptake on HSC-3 cells compared to citrate AuNPs ($p < 0.05$). The PN coating seems to prevent the AuNPs uptake. This effect might be due to the negative charge on the AuNPs which decreases the interaction with the cell membrane due to charge repulsion. It is clearly noticeable that all the AuNPs are found in higher quantity in the cytoplasm of the cells than in the nucleus. Moreover, they all give a higher uptake on HSC-3 cells than on HaCaT. Indeed, a statistical difference in uptake is observed for all the AuNPs coated with oligo between HSC-3 and HaCaT cells. AuNPs coated with citrate dY3 and PN-dY3 seem to give the best cellular uptake (Figure 4.17 d, g) (Figure 4.19 c, f), followed by citrate PR and PN-PR coated AuNPs (Figure 4.19 d, g). However, only citrate dY3 AuNPs show a statistical difference in uptake compared to the other AuNPs ($p < 0.05$).

Here again, as mentioned with the AuNPs coated with α Gal:PEGamine from Chapter 3, the AuNPs are responsible in average for a cellular uptake much smaller than the one described in the literature. Indeed in our case, the NPs concentration found is around 0.002 NP/nm² while Hanžić *et al* found a concentration of $1 \cdot 10^6$ NP/cell after an exposure with 50 μ M of 30 nm AuNPs inside MDA-MB-231 cells (Hanžić *et al.*, 2018), Wang *et al* a concentration of $11.8 \cdot 10^4$ NP/cell after an exposure with 20 nm of 13 nm AuNPs in A549 cells (Wang *et al.*, 2013) and Geng *et al* found a concentration of $9.3 \cdot 10^6$ NP/cell after an exposure with 5 nM of 14.3 nm AuNPs in SK-OV-3 cells (Geng *et al.*, 2011).

The cellular uptake seems to be linked with cellular toxicity. Indeed, the citrate dY3 AuNPs seem to be the ones responsible for the higher uptake on HSC-3 cells and for the highest toxicity on this same cell line (Figure 4.17, 4.23). On the other hand, PN AuNPs show the lowest uptake on cancer cells but also the lowest toxicity (Figure 4.19). AuNPs coated with GFP were used as a control to observe if AuNPs targeting a sequence non-present in the cell could also

improve the uptake. It is also important to mention that the GFP is not a TFO sequence. AuNPs coated with citrate GFP show a non-significant trend to improve the nucleus uptake, compared to simple citrate AuNPs, but neither citrate GFP or PN-GFP AuNPs seem to increase the amount of AuNPs found in the cytoplasm. It is important to note here that these experiments were done only once and will need to be repeated in order to conclude of any link between the coating and the uptake.

When entering the cells, the oligonucleotide attached to the AuNPs should be able to target the sequence of the *c-myc* promoter via triplex formation process, decreasing the transcription of the gene and therefore, the protein activity. A decrease of cell proliferation after TFO coated AuNPs exposure would be expected, especially if the AuNPs were able to enter the cell nucleus. Indeed, Huo *et al.* showed a nuclear uptake of dY3 coated AuNPs in the nucleus of MCF-7 cells, associated with a decrease of *c-myc* mRNA level as well as decrease of *c-myc* protein level (Huo *et al.*, 2014). In this study, the TFO coated AuNPs were able to enter the cell nucleus, however, a potential decrease of *c-myc* protein, indicated by a decrease of cell proliferation was not observed. Because of lack of time, it was not possible to explore the expression of *c-myc* protein, but this experiment is planned in the laboratory. It was shown in the Figure 4.18 that a triplex formation between the TFO and *c-myc* sequence was not observed when the TFO was attached to the AuNPs. The distance between the ligand on the AuNP and its target is critical to define its target affinity (Trapani *et al.*, 2012). Therefore, it is possible that the TFOs might not have enough space in order to interact with the *c-myc* sequence.

Following these experiments and because the AuNPs are localised in the cell nucleus, a potential radiosensitisation with these AuNPs might be observed. The next experiment was focused on exploring the radiosensitisation effect of these AuNPs.

4.5. Oligonucleotide coated AuNPs and their effect with radiotherapy

4.5.1. Coumarin assay

The coumarin assay, whose protocol was already implemented and used in Section 3.10.1 of the thesis, was used once again in this chapter. As mentioned in Chapter 3, the coumarin assay detects $\cdot\text{OH}$ radicals, produced by interaction between the AuNPs, water and the beam of radiation.

For these next experiments, only kilovoltage energy of X-rays was used as it was shown to be the one responsible for the best radiosensitisation in combination with AuNPs in Chapter 3.

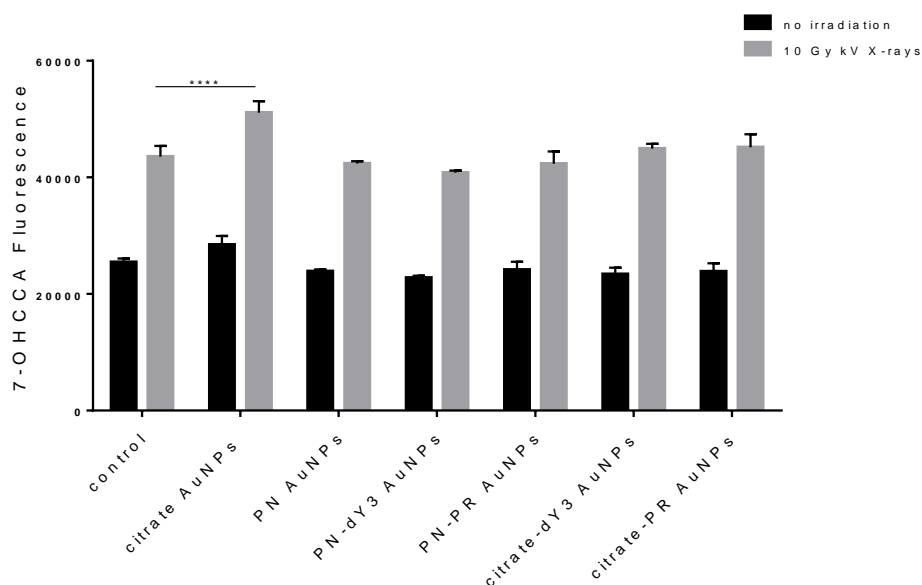
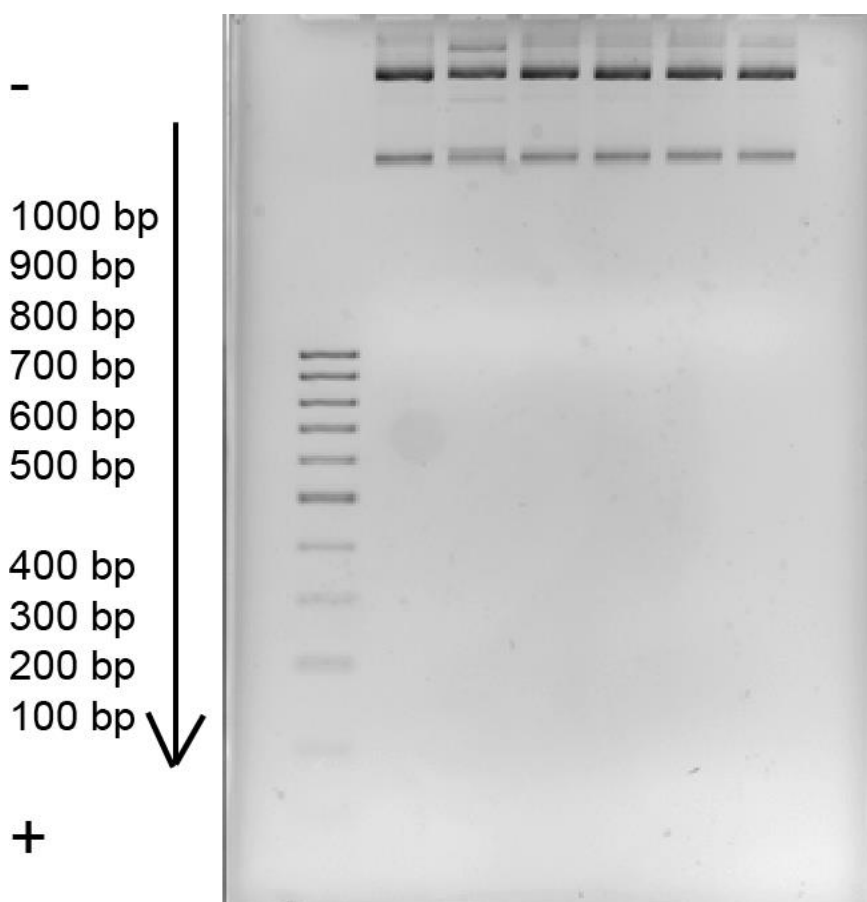


Figure 4.20: Coumarin assay of the different citrate, PN or oligo coated AuNPs in PBS, with or without irradiation. The graph shows the fluorescence of the 7-OHCCA for each AuNP, with or without irradiation. A significant difference in fluorescence of 7-OHCCA probe following irradiation compared to no irradiation is seen for each condition ($P < 0.0001$ ****, two way ANOVA with Sidak's multiple comparisons post-test), while a significant difference in fluorescence compared to irradiated water only is seen for the citrate 3.5 nm sample (two way ANOVA with Tukey multiple comparisons post-test).

Figure 4.20 shows the coumarin assay, exploring the intrinsic radiosensitisation effect of the different AuNPs. By following the increase of fluorescence, it is possible to follow the production of 7-OHCCA and therefore $\cdot\text{OH}$ radical production. A statistically significant increase of the 7-OHCCA production after irradiation is seen compared to the control, without irradiation. Particularly, a statistically significant increase after irradiation in the presence of citrate AuNPs is noticed compared to irradiation without AuNPs. However, when looking at the different coated AuNPs, it is possible to notice an increase of the 7-OHCCA fluorescence with radiation, but not significantly higher than with no AuNPs. The TFOs coating the AuNPs seem to prevent the secondary electron release when AuNPs interact with the beam of radiation. As observed before in Chapter 3, it seems that the coated AuNPs are not able to increase the $\cdot\text{OH}$ radical production upon irradiation.

It will be interesting to see if a similar effect was observed on cells and therefore further models (first plasmid, then cells) were exposed with the different AuNPs combined with radiation.

4.5.2. Radiosensitisation effect on plasmid DNA



lane	1	2	3	4	5	6	7
sample	L	Plasmid	Plasmid	Plasmid	Plasmid	Plasmid	Plasmid
sample		x	x	Citrate AuNPs	dY3 oligo AuNPs	PR oligo AuNPs	GFP oligo AuNPs
irradiation			irr	irr	irr	irr	irr
Signal band 1		144	1629	348	320	355	429
Signal band 2		14037	11234	13078	13363	12229	12279
Signal band 3		6718	5276	5561	5582	5542	5218

Figure 4.21: 2% AGE showing the relaxed plasmid pBV-Luc/Del6 incubated with different AuNPs for 3 hours and then irradiated with 220 kV X-rays at 20 Gy. The gel was run in 1xTBE for 1h at $8 \text{ V}\times\text{cm}^{-1}$; irr - irradiated

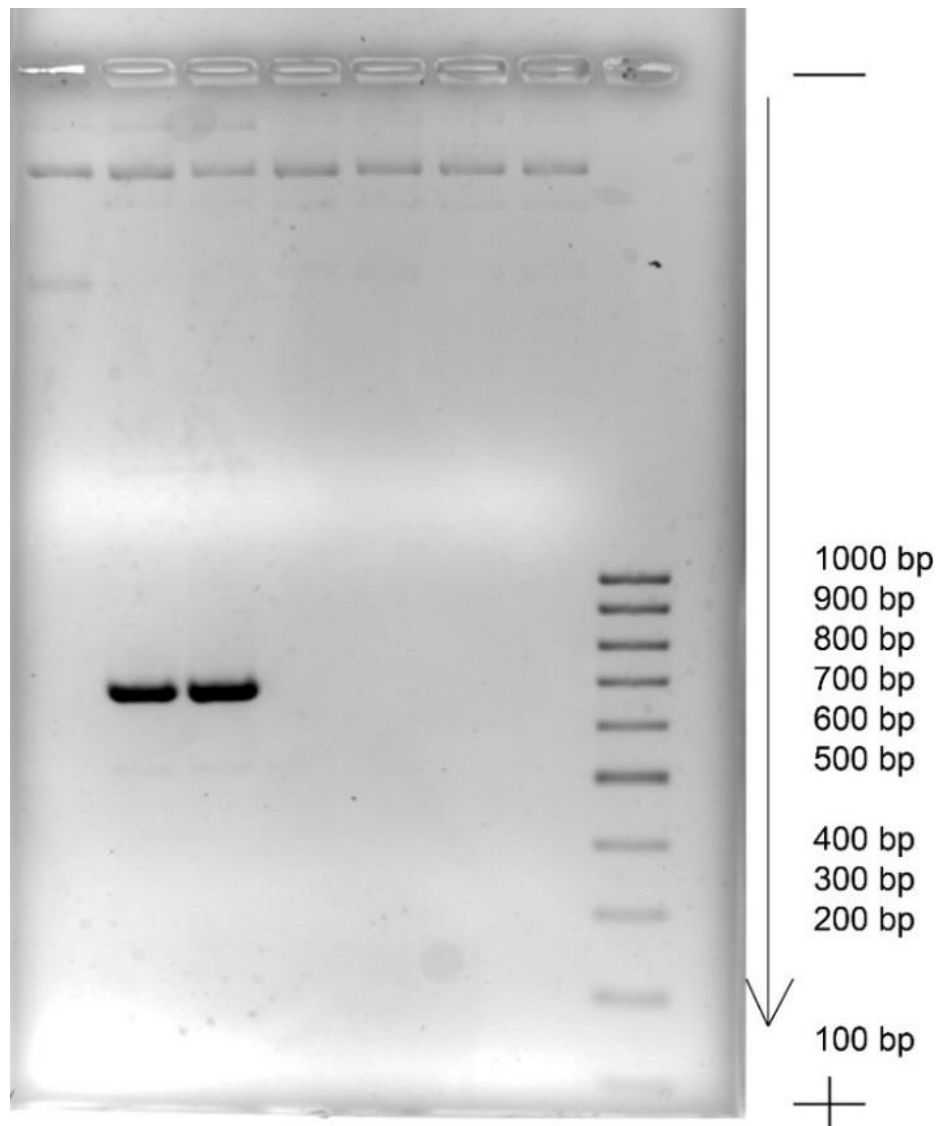
Figure 4.21 shows the plasmid which was irradiated with or without the different AuNPs. Lane 1 shows the control plasmid with no irradiation and no AuNPs. The bands representing the relaxed form (band 2) of the plasmid, as well as the linear one (band 3, Annexe 3.8) can be seen on the gel. It is possible to see a difference when the plasmid was irradiated compared to no irradiation. Indeed, a very bright band is observed at the top of the gel (Figure 4.21, lanes 1 and 2, band 1, Annexe 3.7), which could indicate an increase of DNA damage in the plasmid.

Interestingly, this band appears to be increased in all the samples irradiated, but is more pronounced in the sample without AuNPs (Annex 3.7). Moreover, the band signals representing both the relaxed and linear form of the plasmid (bands 2 and 3, Figure 4.21) appear to be decreased in the samples irradiated.

A possible explanation for the appearance of bands on top of the gel, migrating slower than the relaxed plasmid, could be some DNA rearrangements in the plasmid with intermolecular connection and dimer formation between duplexes of DNA. Indeed, the dose of radiation given here is very high and is expected to cause damage and changes in the plasmid. It is important to note here that this experiment has been done once and gives only an indication of a potential effect of plasmid irradiation.

X-ray irradiation seems to affect the plasmid by decreasing both its relaxed and its linear form, indicating potential DSBs. Indeed, having multiple DNA damage within the plasmid would possible create short fragment of DNA which will migrate faster in the gel and therefore will be representing by a decrease of DNA amount. The hypothesis that the coating of the AuNPs prevents the production of radicals seems to be confirmed, especially $\cdot\text{OH}$ and therefore are not able to radiosensitise the breaks in the plasmid. However, even the citrate AuNPs, which were able to increase radical production, are not able to radiosensitise the plasmid. This result is surprising and indicates that other factors are linked to the radiosensitisation effect in this case. It could be related to the solution, or the concentration of plasmid and AuNPs.

Moreover, the part of the plasmid containing the sequence of interest should be targeted by the TFOs coating the AuNPs and in theory, should be a specific part sensitive to radiotherapy. In order to analyse specifically the c-myc promoter sequence contained in the plasmid, PCR was done to look at this amplified sequence by electrophoresis. This amplified sequence should be about 700 bp.



lane	1	2	3	4	5	6	7	8
sample	Plasmid	PI	PI	PI	PI	PI	PI	L
sample				Citrate AuNPs	dY3 oligo AuNPs	PR oligo AuNPs	GFP oligo AuNPs	x
irradiation		PCR	PCR irr	PCR irr	PCR irr	PCR irr	PCR irr	
Signal	49	160	188	0	32	27	6	
band 1								
Signal	1155	1189	771	1108	1066	1043	1023	
band 2		100 %	64.8 %	93.2 %	89.6 %	87.7 %	86.0 %	
Signal	530	0	0	99	146	97	70	
band 3								
Signal	0	13167	14607	0	0	72	0	
band 4								

Figure 4.22: 2% AGE showing a 700 bp PCR amplicon, derived from the c-myc promoter region of plasmid pBV-Luc/Del6. The plasmid was incubated with the different AuNPs for 3 hours and then irradiated with 220 kV X-rays at 20 Gy, and then subjected to PCR, with 15 cycles. The gel was run in 1xTB for 1h at 8 V \times cm⁻¹.

The effect of both irradiation and AuNPs exposure on the plasmid was explored, as before, but this time, with the sequence of interest amplified. The amplification of the sequence allows measuring whether DNA damages have occurred in the specific sequence of interest or not. Indeed, if the triplex has successfully targeted the sequence of interest, which contains the *c-myc* promoter, DNA damage upon radiation would be observed and therefore, a decrease or absence of amplification will occur. However, to confirm this effect, an amplification of a different region of the promoter should be done, in order to compare the intensities of the different regions and therefore the DNA damages. It could however give an idea on whether a change is occurring in this region or not. When amplifying the fragment containing the sequence of interest, a difference in band intensity will give information on the possible DNA damage. The Figure 4.22 shows migration on the gel of the different samples. The amplified fragment is very bright on the gel and appears only for the samples with no AuNPs present (Figure 4.22, lane 1, 2, Annex 3.8). The different coated AuNPs seem to have an interaction with the DNA polymerase responsible for the amplified fragment reaction. Moreover, the intensities of the two bands representing the amplified fragments are similar, indicating no damage to this precise region. It is important to note that the number of cycles performed was decreased to 15, as compared to the 25 advised by the supplier in order to observe potential difference and not to saturate the band signal. Details of the protocol can be found in the section 2.6.2. Even after reducing the number of cycles of the PCR, the band signal is very bright, indicating either no damage in this region, or possibly still a saturation of the signal. A qPCR, looking at the amount of DNA during each cycle, would be an interesting method to confirm one of the other hypothesis here. Finally, when looking at the samples exposed to AuNPs, it is not possible to conclude whether the sequence of interest was targeted or not. However, the relaxed form of the plasmid seems to be slightly decreased after irradiation, as the band signal is decreased (between 35.2 and 7.8 % decrease of signal) for each sample compared to the non-irradiated ones.

4.5.3. Radiosensitisation effect on cells

After exploring the effect of the different coated AuNPs in addition to radiotherapy on plasmid DNA, the potential radiosensitisation effect was also studied on skin cells.

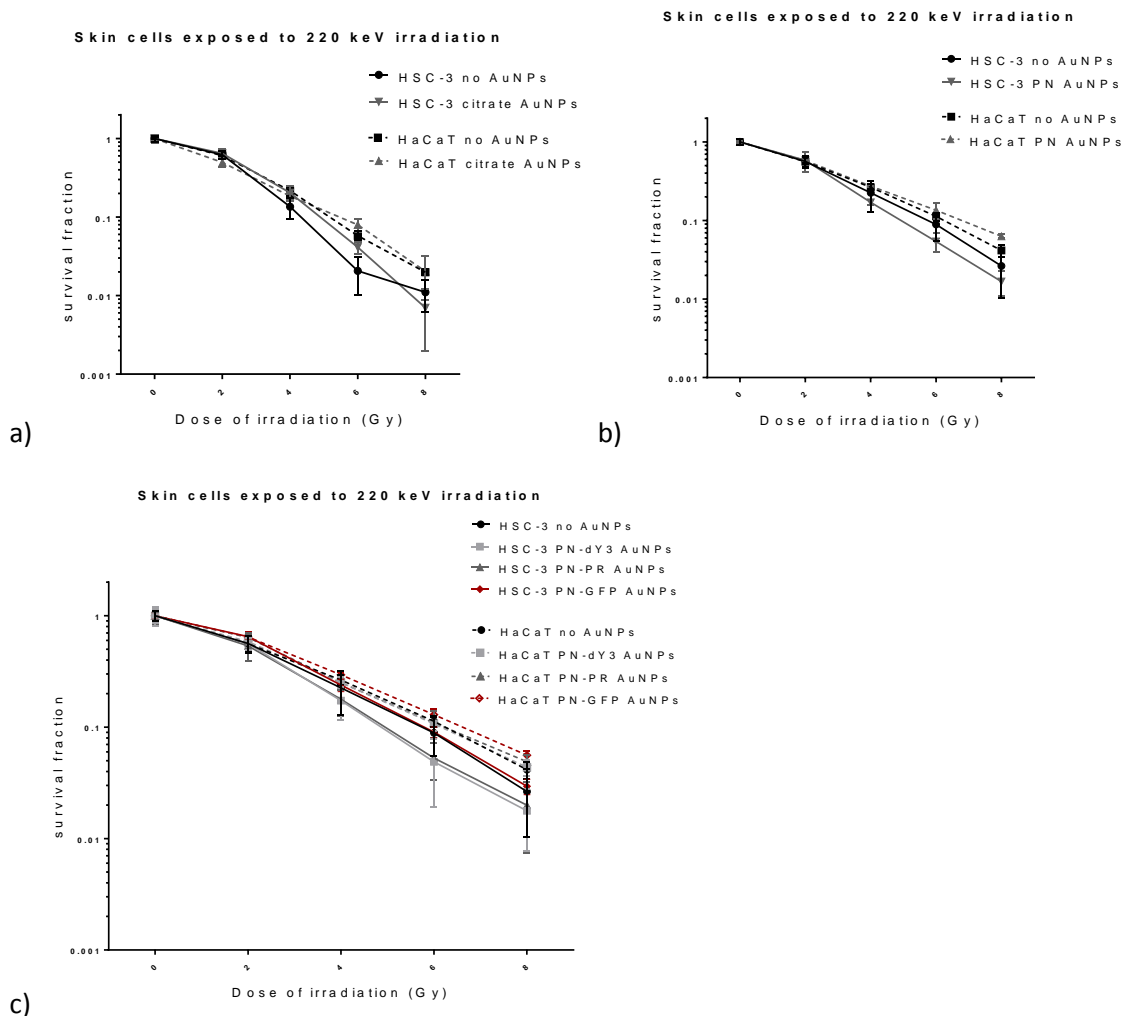


Figure 4.23: HSC-3 and HaCaT cells irradiated with 220 kV X-ray irradiation and exposed to a) citrate AuNPs, b) PN AuNPs or c) oligonucleotide coated AuNPs. The data show survival fraction corrected for chemotoxicity (normalised to zero Gy values).

When the cells were irradiated with the AuNPs, it was possible to see a small decrease of the survival fraction after AuNPs exposure (Figure 4.23 a). Interestingly, the citrate AuNPs are not the ones giving the best effect on cells, but were the ones showing the highest increase of $\cdot\text{OH}$ radical formation with the coumarin assay (Figure 4.24). Within the cells, AuNPs coated with oligonucleotide sequence are able to better radiosensitise the cells, and especially the cancer cells (Figure 4.23). Moreover, the specific TFO dY3 and PR used here radiosensitise the cells, more than the neutral GFP sequence. This result suggests that the TFO might have a specific effect in the cells and increase the radiotherapy efficiency. Particularly, if the TFO-coated AuNPs were able to increase the cellular uptake, they would increase the probability of interaction with radiation and therefore the radiosensitisation effect. Several publications have found a similar tendency where an active targeting toward cancer cells using peptide/DNA, improved the uptake and cancer cells and furthermore the radiosensitisation (Cui *et al.*, 2017, Nicol *et al.*, 2018). Indeed, Cui *et al* have shown a fourfold increase of NP uptake in MDA-MB-231 cells with

peptide coated AuNPs compared to PEG coating and this was linked to a better radiosensitisation effect using 225 kV X-rays (Cui *et al.*, 2017). Moreover, Nicol *et al* showed 10 times more increase of uptake in MDA-MB-231 cells with peptide coating compared to PEG coating and this was link to an increase in radiosensitisation effect using 160 kV X-rays (Nicol *et al.*, 2018).

This appears to be what is happening here, as shown in the Figures 17-19, where using electron microscopy, it is shown that dY3-coated AuNPs showed the best cellular uptake in cancer cells. Indeed, with a concentration inside the cytoplasm of about 0.0002 NP/nm², PN-dY3 AuNPs are responsible for the most additive effect in combination with radiotherapy. However, other characteristics might play a role in the radiosensitisation effect. Indeed, PN-PR-AuNPs give a similar uptake in cancer cells compared to citrate AuNPs, both in cytoplasm, nucleus and cell surface, but still shows a substantial radiosensitisation effect compared to citrate AuNPs.

Interestingly, there is no evidence in this work that the two TFOs did interact with the sequence of interest within cells or were able to knock-down the *c-myc* gene and reduce proliferation. It might be interesting to explore a longer exposure time, as the TFOs might be able to form a triplex and target the sequence of interest but the AuNPs might not have enough time to realise this process. In addition, as mentioned before, the possibility of the TFO to form a triplex when attached to the AuNPs is most likely limited due to the steric limitation, which could be solved by using longer spacers.

Table 4.7a: Sensitivity Enhancement Ratios and Dose Enhancement Factors calculated for skin cells

Cell line (AuNP)	SER _{4Gy}	DEF _{0.3}
	220 kV	220 kV
HSC-3 (citrate)	0.79 ± 0,10	0.90 ± 0,18
HSC-3 (PN)	1.29 ± 0,08	1.07 ± 0,18
HSC-3 (PN DY3)	1.39 ± 0,09	1.09 ± 0,23
HSC-3 (PN PR)	1.43 ± 0,09	1.10 ± 0,26
HSC-3 (PN GFP)	1.13 ± 0,05	0.94 ± 0,12
HaCaT (citrate)	1.36 ± 0,02	1.11 ± 0,26
HaCaT (PN)	1.13 ± 0,02	0.95 ± 0,09
HaCaT (PN DY3)	1.20 ± 0,03	0.99 ± 0,23
HaCaT (PN PR)	1.25 ± 0,03	0.96 ± 0,20
HaCaT (PN GFP)	1.11 ± 0,02	0.90 ± 0,20

Table 4.7b: Linear quadratic parameters of oligonucleotides AuNPs calculated for skin cells irradiated with 220 kV X-rays.

Cell line (AuNP)	HSC-3 cells			HaCaT Cells		
	a	b	a/b	a	b	a/b
control	0,23 ± 0.03 (-0,015 for BBi control)	0,0331 ± 0.005 (0,0076 for BBi control)	6,94 and -1,97	0,1305 ± 0.03	0,06095 ± 0.01	2,14
citrate	0,05101 ± 0,06247	0,08547 ± 0,0205	0,60	0,3096 ± 0,0459	0,0236 ± 0,01468	13,12
PN						
PN	0,1211 ± 0,0798	0,07593 ± 0,0283	1,59	0,253 ± 0,01663	0,0142 ± 0,00396	17,82
PN DY3	0,1567 ± 0,0592	0,06697 ± 0,0205	2,34	0,2209 ± 0,0548	0,02699 ± 0,0147	8,18
PN PR	0,211 ± 0,0618	0,05188 ± 0,0204	4,07	0,1563 ± 0,04622	0,04029 ± 0,0131	3,88
PN GFP	0,111 ± 0,0325	0,05624 ± 0,01003	1,97	0,1695 ± 0,04628	0,02978 ± 0,0119	5,69

The SER and DEF ratio were calculated in order to explore any additive effect of the different AuNPs with radiation. Table 4.7 a confirms the effect observed in Figure 4.27, showing the highest SER for cancer cells of 1.39 and 1.43 for dY3 and PR coated AuNPs respectively, followed by a SER of 1.13 for GFP coated AuNPs and 0.79 for the citrate AuNPs. The SER value of 0.79 is very surprising as it would indicate that citrate AuNPs have a protective effect with radiotherapy. The standard error is higher in this condition and it would be necessary to repeat this experiment in the future to explore any significant changes. Moreover, it was shown that TFO dY3 seemed to improve the cell cytoplasm uptake, more than the PR and GFP oligonucleotides. However, the SER is similar between dY3 and PR TFO. Interestingly, the SER value obtained for the AuNPs coated with TFO are smaller than the one obtained with α Gal:PEGamine coated AuNPs presented in Chapter 3. Indeed, while we showed previously an SER of 1.73, the highest SER showed in this case if 1.43. This might be due to the AuNPs uptake, which is 10 times higher for α Gal:PEGamine AuNPs compared to the TFO coated ones. Moreover, this SER value of 1.43 is in the same range as what has been shown previously in the literature using KV X-rays (Jain *et al* 1.41 using 160 kV X-rays, Cui *et al* 1.39 using 225 kV X-rays, Nicol *et al* 1.54 using 4 Gy of 160 kV X-rays) (Cui *et al.*, 2017, Jain *et al.*, 2011, Nicol *et al.*, 2018). As mentioned before, the organelle localisation might play a role in the radiosensitisation effect, such as localisation in lysosomes or in the nucleus. It will be interesting to repeat the uptake

experiments in order to confirm whether the uptake is indeed linked to the radiosensitisation effect, and whether the localisation of the AuNPs in the cells is having an impact on this radiosensitisation effect (here the difference in nucleus concentration between the different AuNPs are not significant).

Due to time limitations, it was not possible to explore the radiosensitisation effect of citrate dY3 AuNPs in cells, but this experiment will be explored in the future as this particular AuNPs exhibited a statistically significant uptake into cell nucleus.

Although it was shown in Section 4.1 that PR TFO seemed to form more stable triplex with the *c-myc* sequence of interest *ex vivo*, this effect was not seen *in vitro* and dY3 TFO showed actually more uptake and more radiosensitisation inside the cells

Finally, PN AuNPs are responsible for an additive effect with radiation, more than the citrate AuNPs. It is surprising as these AuNPs did not give a strong uptake on the cancer cells. Effectively, it is shown that an SER of 0.79 is seen with citrate AuNPs at a concentration inside the cytoplasm of 0.00015 NP/nm² while an SER of 1.29 is seen with PN-AuNPs and at a concentration of less than 0.0001 NP/nm². PN-AuNPs might be responsible for different reactions inside the cells, such as cell cycle or oxidative stress, which may not show an effect on cell viability by itself but could be responsible for an additive effect with radiation.

The SER is generally lower for HaCaT cells exposed to all the AuNPs, except the citrate AuNPs, which surprisingly show the highest SER on this particular cell line.

When looking at the DEF, this parameter is close to 1 for all the NPs. The highest DEF is seen for PN-PR AuNPs, which were responsible for the highest SER. As a reminder, the DEF is defined as the dose of radiation needed to cause the same biological effect. A DEF smaller than the SER could indicate that the toxic effect observed on cells here may be due to the AuNPs in larger proportion, rather than the dose of radiation. This effect was calculated only for a toxic effect with a 30 % decrease of viability. It needs to be pointed out once again that the linear quadratic model (Table 4.7b) is still linked with high errors, and therefore it is difficult to make any affirmative conclusion on the DEF value obtained or on the α and β parameters. Once again, it is possible to note a trend that α parameter is in general higher than β , however, it may be interesting in the future to explore the linear quadratic linear model to analyze these specific parameters (Joiner and Van der Kogel, 2009, Podgorsak, 2003).

4.6. Conclusions of Chapter 4: oligonucleotide-coated AuNPs

The second type of AuNP used in this thesis has a bigger size core, of 3.5 nm compared to 1.9 nm. This was chosen mainly to make the AuNPs visible, due to plasmon resonance, during the stages of TFO attachment and gel characterisation. The AuNP size is also known to have an impact on the interaction with radiation. 2 nm AuNPs have been explored for radiosensitisation in several studies (Butterworth *et al.*, 2010, Grellet *et al.*, 2017, Jain *et al.*, 2011). A size below 5 nm was also chosen in order for the AuNPs to enter the cell nucleus passively via the nuclear pores. Larger AuNPs could also possibly enter the nucleus but different processes will have to take place, such as a membrane disruption and dilatation of the pores, as occurs with nuclear-localising chaperone proteins (Setua *et al.*, 2014) or the disappearance of the nuclear envelope which happens just before cell division (Worman and Courvalin, 2000).

Oligonucleotide-coated AuNPs are an interesting tool but challenging to purify and to characterise due to the sensitivity of oligonucleotides to change with pH and temperature. Moreover, their uptake into cells and travel to their target can be compromised by their biocompatibility (Herdt *et al.*, 2006).

Trying to characterise and explore the number of TFOs attached to the AuNP was not an easy task. Electrophoresis on the agarose gel gave information on the different coatings but was not able to separate the potentially different populations. XPS, using X-ray photons and electron release was used, trying to identify the density of the coating. The AuNPs being in small quantities made it difficult to obtain a good signal of each element and to fully characterise the coating of the AuNPs. Fast protein liquid chromatography (FPLC) could be useful to look at the different population of AuNPs and will be the next step to characterise these AuNPs. Depending on the number of TFOs attached to the AuNPs, different effect can be observed, with or without radiation, as numerous TFOs can help the AuNPs to enter in the cell and nucleus but can limit the accessibility of the TFOs to its target sequence, and the electron release upon radiation, as mentioned before.

In general, it is observed that having an oligonucleotide coating the AuNPs does not necessarily improve the general uptake of the AuNPs, compared to the α Gal:PEGamine coated ones for example, but seems to increase their relative accumulation in the cell nucleus. Moreover, oligonucleotides coating the AuNPs do not seem to be responsible for a strong effect on cell cycle. As mentioned before, it is not clear whether the TFOs coating the AuNPs have formed a triplex inside the cells. Indeed, it was successfully shown in the thesis that TFOs were able to form a triplex with the double stranded DNA *ex vivo* when considering simple double stranded DNA (up to 70 bp). A possible interaction with plasmid DNA (up to 5000 bp) was seen,

with a disappearance of the TFO band, especially when the plasmid was on a nicked form. However, it seems more challenging to observe the triplex formation process *in vitro* when skin cells were incubated with these same AuNPs. Moreover, the AuNPs being of a size bigger than 200 kDa (308kDa), do not enter the polyacrylamide gel, therefore their characterisation and interaction with the sequence of interest was difficult to achieve.

It was challenging to explore the triplex formation in the plasmid, as well as the potential DSBs upon radiation. First, the restriction enzyme cut the plasmid differently than expected, forming a nicked plasmid with various fragments. Moreover, the relaxed plasmid did not seem to react with the TFOs coated AuNPs. The map of the plasmid is only partially communicated. It will be interesting to realise a full sequencing of the plasmid in order to understand the role of the restriction enzymes and the probability of the TFOs to recognise the targeted sequence.

Some work is still required in order to improve and characterise the triplex formation *in vitro*. One way to improve TFOs affinity is to use ribose oligonucleotides which should decrease the possible degradation from nucleases. Interestingly, Lacroix *et al.* showed in 1999 that replacing tyrosine by 5-(1-propynyl)-2'-deoxyuridine in TFOs could overcome the dependence of magnesium to form the triplex structure (Lacroix *et al.*, 1999). Moreover, a spacer between the AuNPs and the oligonucleotide sequence, such as polyethylene glycol polymer or different oligonucleotides, seem to help the recognition with the sequence of interest (Kang *et al.*, 2010, Suzuki *et al.*, 2009). Suzuki *et al.* in 2009 proposed a new method to control this coating. They used phosphine molecules to coat the AuNPs and block the non-specific sites for oligonucleotide coating. Then, a neutral oligonucleotide was used in order to form a complex of DNA and allow a separation between the different oligonucleotides on the AuNPs. In the final step, this neutral oligonucleotide complex was removed from the AuNPs (Suzuki *et al.*, 2009).

When considering the effect of the AuNPs coated with the two different TFOs, the coumarin assay did not show any statistical difference in 7-OHCCA production. Only the citrate AuNPs showed an increase of $\cdot\text{OH}$ radical when irradiated. However, oligonucleotides coated AuNPs did show a radiosensitisation effect in the cells with a maximum SER of 1.43 with the specific PR TFO coating. These AuNPs were able to enter the cell and particularly the nucleus. This specific localisation should improve the radiosensitisation effect when combined with X-ray radiotherapy. Indeed, as mentioned before, Fan *et al.* were able to radiosensitise MCF-7 cells using mesoporous silica NPs coated with tat protein and encapsulating mitomycin C (Fan W *et al.*, 2015). Their treatment was particularly of interest as mitomycin is specific to hypoxic tumours as it can inhibit DNA synthesis under hypoxic conditions. They have successfully shown an improvement of the radiosensitisation effect with nuclear targeted NPs. They have shown more than 50 % decrease of cell number using comet assay after X-ray irradiation (5Gy) in the

presence of 10 $\mu\text{g}/\text{ml}$ of NPs for 24h compared to irradiation alone (Fan W *et al.*, 2015) and an increase of apoptosis and decrease cell proliferation for MCF-7 multidrug resistance cells exposed to NPs and radiotherapy by measuring the expression of caspase-3 and p27 protein (no quantitative data).

As mentioned before, AuNPs coated with $\alpha\text{Gal}:\text{PEGamine}$ presented in Chapter 3 were able to better radiosensitise the cells with the same dose of irradiation with a SER of 1.73. Moreover, the additional effect of the TFO to target *c-myc* inside the cells and therefore potentially amplify the radiosensitisation effect was not seen here. Other criteria might affect the radiosensitisation effect and will be discussed in Chapter 6.

Before concluding this thesis, a small chapter will be dedicated to, cerium oxide NPs, which were mentioned in the Introduction and could be of interest in combination with radiotherapy due to their capacity to adsorb oxygen.

CHAPTER 5: PRELIMINARY WORK WITH METAL OXIDE NPs

As discussed in Sections 1.3 and 1.6 of the introduction, other metal or even non-metallic NPs have shown promise as radiosensitisers. Taupin *et al.* in 2015 demonstrated a radiosensitisation effect using gadolinium NPs in a concentration range of 2-10 mg/ml on glioma cells irradiated with X-rays at different energies (31 keV-1.25 MeV) (Taupin *et al.*, 2015). They have shown that the sensitiser enhancement ratio (SER) increases both with NPs concentration and X-ray dose. The highest SER was obtained when cells were irradiated with 65 keV.

Metallic oxide NPs, such as cerium oxide, are of interest due to their catalytic ability to form radicals. Such NPs can act either as radiosensitiser or as radioprotector depending on pH and oxidation state. Indeed, previous studies reported that cerium oxide NPs can scavenge radicals such as H_2O_2 , by acting like catalyse enzyme. However, when in an acidic environment, their ability to scavenge H_2O_2 is much reduced and therefore addition of CeO_2 can increase the amount of ROS. The explanation for these contradictory effects is probably the oxidation state of the cerium, either Ce^{3+} which is characterised by an oxygen vacancy and acts as radiosensitiser (Sun *et al.*, 2012) or Ce^{4+} , which forms a superposition lattice with oxygen in the centre of the structure, decreasing the oxidative stress and therefore acts as radioprotector (Figure 5.1) (Wason *et al.*, 2013).

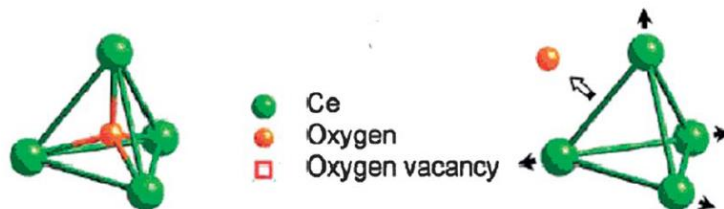


Figure 5.1: Geometrical form of a) Ce^{4+} and b) Ce^{3+} (Sun *et al.*, 2012).

As discussed in Section 1.6, cerium oxide could be interesting due to its cubic fluorite-type oxide conformation, where each cerium site is surrounded by 8 oxygen sites, allowing it to adsorb oxygen and thus, could help in radiosensitising hypoxic tumours. Combining cerium oxide with another high atomic element such as gold, or bismuth could change this radioprotector vs radiosensitiser effect and is already on-going work within the laboratory. In this Chapter, some preliminary results are reported. Commercially available CeO_2 NPs of 5 nm size from Sigma were used. Two NPs were tested. They were prepared at two different pH, one being in an acidic environment (pH 4) and the other one in a basic environment (pH 8). This difference in preparation will lead to a difference in oxidative state, which is known to play a role on the radiosensitisation potential (Briggs *et al.*, 2013, Cheng *et al.*, 2013, Park *et al.*, 2008) or radioprotection (Arya *et al.*, 2016).

5.1. EM microscopy of commercial cerium oxide NPs

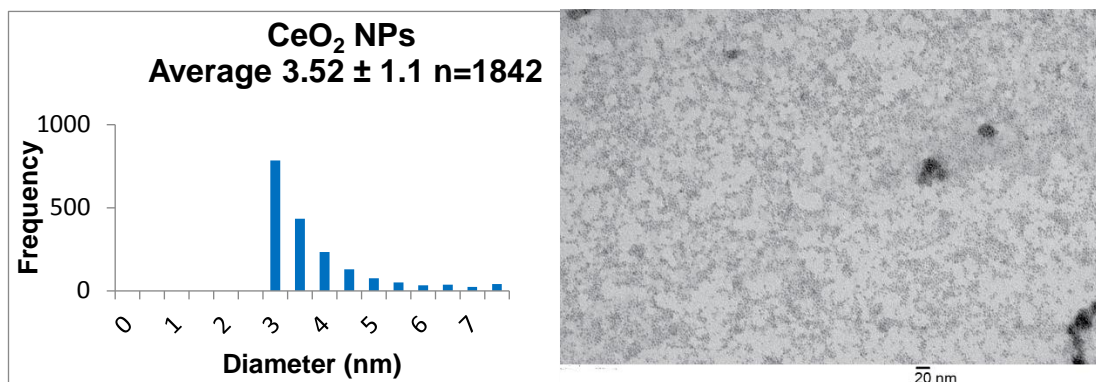


Figure 5.2: Size histogram and TEM image of CeO₂ NPs pH 8. The data are presented as mean NP diameter ± standard deviation.

The NPs have an average size of 3.52 nm, and seem quite homogeneously distributed, which make them good candidate for entering in cells.

5.2. SEM-EDX composition

In order to understand their future role when combined with radiotherapy and cells, their chemical element analysis has been performed by SEM-EDX.

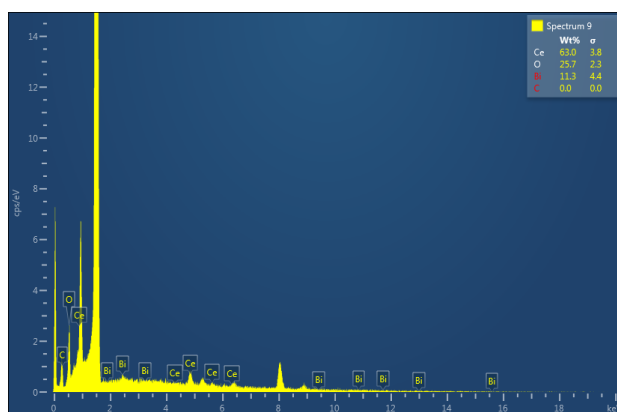


Figure 5.3: SEM-EDX spectrum of CeO₂ NPs showing their elemental composition. Inset: The data are presented as mean NP diameter ± standard deviation.

The SEM-EDX analysis used for these experiments allows measuring the average elemental composition of the NPs solution but not of the individual NPs. SEM-EDX confirms the presence of Cerium. Interestingly, it seems that Bismuth (4.4 %) is found in the solution, which could come from the reaction process to form the NPs, although the manufacturer communicated not using bismuth in the reaction and could be of interest for radiosensitisation.

Indeed, Bismuth is a high atomic number element which can interact with X-rays. However, Bismuth is known to be toxic and needs to be carefully handled.

Therefore, the toxicity of these NPs were tested on the main cells used in this project, HSC-3 and HaCaT.

5.3. Cell exposure to commercial cerium oxide

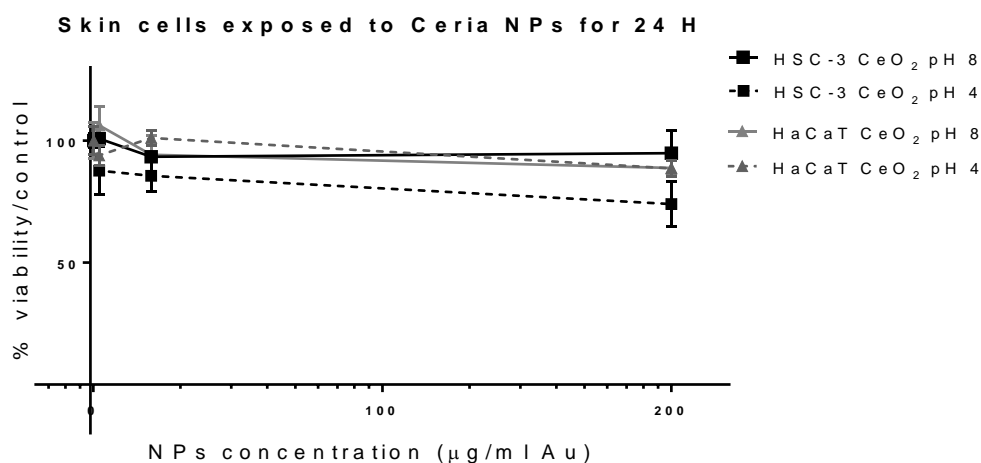


Figure 5.4: Toxicity of CeO₂ NPs on HSC-3 and HaCaT cells. The data represent the viability compared to the control and are expressed as mean \pm standard deviation. A two-way Anova followed by a Dunnett post-test was performed to explore any statistical differences between the exposed groups and the control.

The toxicity of the different CeO₂ appears to change with NPs prepared at different pH. CeO₂ NPs prepared at pH 8 do not seem to change the viability of the cells as no statistical difference is observed compared to the control either for the different concentration of CeO₂ NPs or in both cell lines. However, when HSC-3 cells were exposed to CeO₂ NPs prepared at pH 4, a toxic effect was observed at the highest concentration of 200 µg/ml, which is statistically significant ($p < 0.01$) while this effect is not observed for HaCaT, suggesting this is not simply due to the pH of the medium. The pH which the NPs were made seems to have an effect on the CeO₂ mechanism of action, and one possible reason for this increase of toxicity could be because of an increase of environmental ROS levels.

After exploring the toxicity of the NPs, their radiosensitisation effect was evaluated, using kilovoltage X-rays.

5.4. Cell exposure to ceria and interaction with radiation

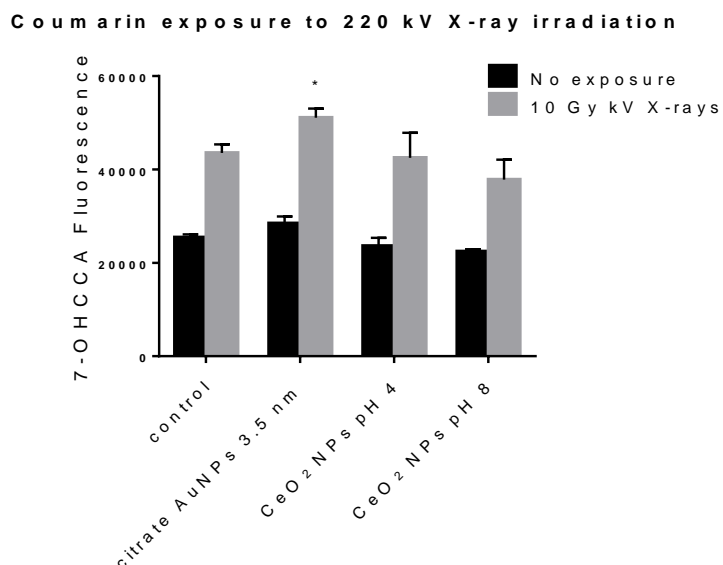


Figure 5.5: Coumarin assay with or without irradiation, with different CeO₂ NPs. The graph shows the fluorescence of 7-OHCCA on different condition. A significant difference in fluorescence of 7-OHCCA probe following irradiation compared to no irradiation is seen for each condition ($P < 0.0001$ ****, two-way ANOVA with Sidak's multiple comparisons post-test) while a significant difference in fluorescence compared to irradiated water only is seen only for the citrate 3.5 nm sample (two way ANOVA with Tukey multiple comparisons post-test).

Figure 5.5 shows the effect of the NPs to interact with X-ray irradiation using the coumarin assay. This assay was used in the chapter 3 & 4 and was showing an increase of 7-OHCCA, representing an increase of $\cdot\text{OH}$ radical production in the presence of non-coated AuNPs, but no effect was seen in the presence of coated ones. Once again, irradiation of non-coated AuNPs with radiation show an increase of 7-OHCCA fluorescence, higher than without the AuNPs. interestingly, both ceria NPs made at pH 4 and pH 8 do not show an increase of this 7-OHCCA fluorescence, and this fluorescence was not significantly different than the control (without NPs). The ceria NPs therefore do not seem to be able to increase the $\cdot\text{OH}$ production. However, other ROS species, such as $\text{O}_2^{\cdot-}$ and $^1\text{O}_2$ would be interesting to measure for better evaluation of the intrinsic radiosensitisation effect of these NPs (Gara *et al.*, 2012). Following these experiments, the NPs were tested in cells, in combination with radiation.

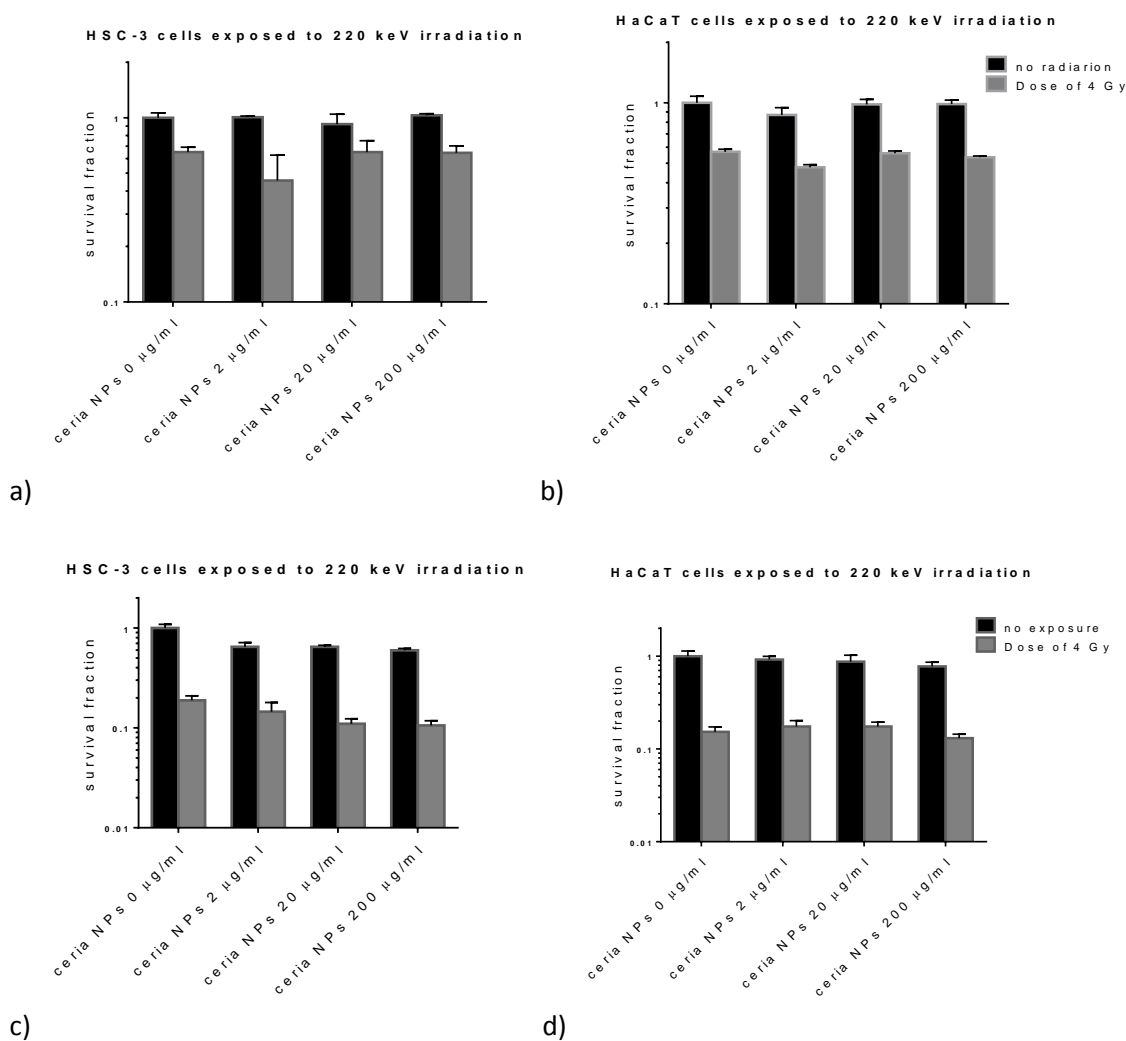


Figure 5.6: Radiosensitisation of CeO₂ NPs on HSC-3 and HaCaT cells exposed to kilovoltage radiotherapy. a) HSC-3 exposed to CeO₂ pH 8; b) HaCaT exposed to CeO₂ pH 8; c) HSC-3 exposed to CeO₂ pH 4; d) HaCaT exposed to CeO₂ pH4. The data represent the survival fraction compared to the control and are expressed as mean ± standard deviation. A two-way Anova followed by a Dunnett post-test has been performed to explore the statistical difference between the exposed groups and the control.

No obvious effect with radiotherapy was observed when using X-ray irradiation at a dose of 4 Gy. However, a small decrease of cell viability seems to occur when the cells were exposed to high concentration of pH 4 CeO₂ NPs compared to the control (Figure 5.6 c and d). However, this result is not statistically significant. It seems that the concentration influences the radiosensitisation. It is not clear whether NPs were able to enter the cells, therefore, the next experiment will be to look at the cellular uptake using ICP-MS as a function of the concentration of CeO₂ NPs, to explore if an increase of concentration is associated with an increase of uptake. Cerium oxide NPs might be able to dysregulate the amount of oxygen and radicals, but it may not be electron dense enough to interact strongly with radiation and give secondary electrons. One way to improve their radiosensitisation effect might be to combine the metallic oxide with

a high atomic weight element such as gold, silver or bismuth and this is now ongoing in the OU labs.

Combination of different treatment could be a key to improve the radiosensitisation effect. Indeed, it has been shown that a combination of AuNPs with radiotherapy gives an additive effect. Using a third therapy such as the use of cerium oxide NPs could enhance the radiotherapy and at the same time, increase the amount of oxygen, which could increase the amount of radicals (Wason *et al.*, 2013). It has not been shown in these experiments whether or not CeO₂ NPs were able to absorb oxygen. In the near future, different techniques to explore this phenomenon will be considered, such as molecular beam where the oxygen uptake and release can be followed by measurement of CO₂ production after introduction of O₂ in the system (Schalow *et al.*, 2005). Thermogravimetry could be another technique used and is detailed in the paper by Imagawa *et al.* (Imagawa *et al.*, 2011). Briefly, it consists on the introduction of O₂/N₂ in the system, followed by H₂/N₂ and the measurement of the weight change of the NPs.

CHAPTER 6: CONCLUSION AND FUTURE WORK

6.1. General conclusion

Cancer is one of the leading causes of non-communicable death in developed countries worldwide (McMullin, 2016). Considerable efforts are being made to improve cancer treatment, including development of new types of radiotherapy, such as the use of nanoparticles, presented in this thesis. About 50% of the treatment plans now include radiotherapy (Burger *et al.*, 2014a) and one of the major limitations of X-ray radiotherapy is the damage to surrounding healthy tissue whilst simultaneously maximising the dose to the tumour (Chauhan *et al.*, 2011). In the field of cancer research treatment, different strategies are being developed in order to fulfil this goal (Kwatra *et al.*, 2013); either by (1) radioprotecting the healthy tissues surrounding the tumour, (2) by suppressing radioresistance, or (3) radiosensitising the tumour to radiotherapy.

The focus of the work presented in this thesis is radiosensitising the tumour using AuNPs.

The main aims of this project were:

- 1) To explore the relationship between the different AuNPs characteristics, such as charge, cellular uptake, intracellular localisation, and toxicity for a range of AuNPs with different types of coatings, in cancer and normal cell lines.
- 2) To explore and try to improve the radiosensitisation potential of these AuNPs using clinical X-ray sources at different energies.

NPs made of gold were chosen in this thesis work because of their high atomic number, their large potential for surface modification, and their well-defined characteristics (Kwatra *et al.*, 2013). Indeed, during this work, and as part of the larger ARGENT (Advanced Radiotherapy, Generated by Exploiting Nanoprocesses and Technologies) project, within which this framework was conducted, research was undertaken to explore the effect of new coatings on the radiosensitisation properties of AuNPs.

The concentration of AuNPs in the cancer tissue also plays an important role in the effectiveness of radiotherapy (Babaei and Ganjalikhani, 2014a, Mesbahi *et al.*, 2013). Many different strategies have been used to increase the concentration of AuNPs inside cells and one of them includes the application of a coating to the AuNPs improving their biocompatibility and uptake (Babaei and Ganjalikhani, 2014b, Retif *et al.*, 2015). With the proper coating, it may be possible to increase the uptake, without reducing the number of electrons released (which

drives the subsequent chemistry) thus, improving the radiosensitisation effect (Gilles *et al.*, 2014, Zhu *et al.*, 2015).

In this thesis, two AuNPs of different sizes and with different coatings were explored as possible radiotherapeutics. This work showed that α Gal:PEGamine coating improves the uptake in the cytoplasm and lysosomes and the triplex forming oligonucleotides (TFOs) in the cell nucleus. 50:50 α Gal:PEGamine coating on AuNPs was shown to have a selective toxicity for cancer cells, like the different oligonucleotides coated AuNPs, and they both give a better uptake in cancer cells compared to normal cells.

However, electron microscopy studies showed that the uptake of 50:50 α Gal:PEGamine AuNPs in the cells is 10 times higher than with oligonucleotides coated AuNPs, and thus using 10 times less concentration. Indeed a concentration of 0.002 NP/nm² was seen in skin cancer cells after 50:50 α Gal:PEGamine AuNPs exposure using electron microscopy while a concentration of 0.0002 NP/nm² was seen after TFO AuNPs exposure. These published results are described in Sections 3.8.2 (Grellet *et al.*, 2017) and are compared with the one in Section 4.4.

As shown in Sections 3.10.1 (Grellet *et al.*, 2017) and 4.5.1, the coatings used in this project were shown to lower the amount of \cdot OH radical produced from the coated AuNPs when irradiated using the coumarin assay, however, both of the coated AuNPs are still able to radiosensitise the cells. Further studies on the coating modification within the medium and the cell could help to understand how AuNPs with specific coatings act as radiosensitisers inside the cells but not outside the cells.

Several previous studies have focused on improving the cell nucleus' uptake of NPs to improve the radiosensitisation effect. It was difficult, as described in Section 4.4, to conclude whether the nucleus uptake had an impact on the radiotherapy efficiency as the amount of gold observed in the cell nucleus with the TFOs coated AuNPs tested was very low (10⁻⁵ NP/nm²), and was not significantly different from that obtained using non-coated AuNPs, although a 50 % increase is seen in the presence of oligonucleotides. These results are in preparation for publishing.

Further optimisation of the AuNP coatings could improve this nuclear uptake. Moreover, while many studies have shown a high AuNPs uptake after 24h of exposure, a longer exposure time will be considered in the future (Chithrani *et al.*, 2010, Cui *et al.*, 2017, Geng *et al.*, 2011, Wang *et al.*, 2013, Zhu *et al.*, 2015). Nevertheless, the nucleus might not be the critical organelle to target. Indeed, several teams have already observed a selective uptake of NPs in the lysosomes, which, if damaged, are capable of releasing acidic contents and enzymes in the cytoplasm, thereby damaging the cell. Several groups have shown that the main target of NPs uptake (silica

and superparamagnetic NPs) were the lysosome and lead to an increase of ROS production (Ma *et al.*, 2011, He *et al.*, 2015, Kenzaoui *et al.*, 2012).

It is important to point out that although using a smaller concentration of AuNPs (1 µg/ml for αGal:PEGamine AuNPs compared to 10 µg/ml for TFO AuNPs), the AuNPs presented in Chapter 3 and designed in collaboration with Midatech give a better radiosensitisation effect on skin cancer cells after 3 hours of exposure. In this particular case, having a TFO does not improve the general uptake of AuNPs in cell and does not improve the toxicity as TFO AuNPs did not show a strong toxicity while αGal:PEGamine AuNPs showed an IC 50 for skin cancer cells of less than 1 µg/ml.

In conclusion, active cellular targeting was not able to improve the cellular uptake with the particular AuNPs tested and the AuNPs concentration in cell does not always predict on the radiosensitisation effect as the uptake for both AuNPs was much slower than in previous studies, with a SER equal or above these same explorations (Burger *et al.*, 2014b, Cui *et al.*, 2017, Jain *et al.*, 2011, Rashid *et al.*, 2018, Wang *et al.*, 2013).

When considering radiotherapy treatment, the 4Rs defined by Withers in 1975 should be taken into account (Mayles *et al.*, 2007). They correspond to different mechanisms occurring within the cells after irradiation, such as *repair*, which happens a few hours after exposure; *reassortment*, which corresponds to the cell cycle progression; *repopulation*, where the cancer cells which survive the first weeks course of radiotherapy treatment can survive and proliferate; and *reoxygenation*, where the hypoxic cells forming a cancer tumour survive the first dose of radiation but thereafter, their oxygen level will increase, as well as their *radiosensitivity*. Radiosensitivity is the fifth R which is now defined as a difference of radioresponse between different tissues (Mayles *et al.*, 2007). The repair and repopulation processes will be responsible for a radioresistance of these tissues to further doses of radiation, while the reoxygenation and reassortment will tend more to make it radiosensitive.

As discussed in the introduction, different strategies can be used to limit the repair and repopulation of the cancer tissues, such as inhibitors of PARP (Shelton *et al.*, 2013) or inhibitors of EGFR pathways (Small Jr, 2008). These two strategies could be used in combination with AuNPs to radiosensitise even more the cancer cells. Reoxygenation is also an important factor to radiosensitise the cancer cells. Indeed, cancer cells are generally associated with an acidic environment, which is characterised by a lower basal level of H₂O₂ inside the cells, and is therefore linked to more resistance to radiotherapy (Wason *et al.*, 2013).

Hypoxic conditions are not favourable for radiosensitisation as oxygen is an important factor in radiotherapy efficiency (Retif *et al.*, 2015). Several studies have tried to improve ROS production during irradiation by using catalytic materials such as ceria (Wason *et al.*, 2013) which, due to its valence state, can capture molecules of oxygen, depending on their oxidative

state, and can act as antioxidants, radioprotectors or radiosensitisers (Sun *et al.*, 2012, Colon *et al.*, 2010, Wason *et al.*, 2013). Previous work has shown ceria based NPs potential as adjuvants with radiotherapy (Shcherbakov *et al.*, 2014). In this area, cerium oxide could be of interest in order to reoxygenate the tumour quickly and make it radiosensitive. In this thesis, preliminary work looking at the characterisation of simple CeO₂ NPs have been done and showed that these NPs are not able to radiosensitise the cells.

Another parameter used to understand and improve the radiosensitisation effect is the use of different energies of radiation, including kilovoltage X-rays, and now megavoltage energies of X-rays, which is widely used nowadays and require a selective and more efficient toxicity.

As previously discussed in Section 1.2.1, AuNPs can improve radiotherapy efficiency at kilovoltage energy, but are less efficient with megavoltage energies (Butterworth *et al.*, 2012, Rahman *et al.*, 2009). Indeed, using higher energies, such as those produced by a linear accelerator (LINAC), the photoelectric effect no longer dominates and much lower DEFs are expected (Taupin *et al.*, 2015).

Nonetheless, Jain *et al.* among other teams, showed a radiosensitisation effect of AuNPs in combination with Megavoltage X-ray radiotherapy (Jain *et al.*, 2011). Indeed, in Section 3.10.2 of the thesis, it is shown that AuNPs could improve radiotherapy efficiency, both with kilovoltage, but also megavoltage energies (Grellet *et al.*, 2017).

Moreover, NPs have shown great interest with new strategies of cancer treatment including radiation delivery by charged particles such as proton and heavy ions (e.g. carbon) (Mayles *et al.*, 2007). Both protons and heavy ions confer improvement of dose delivery to the tumour by controlling the dose distribution and are now being used in the clinic.

Kim *et al.* have shown a radiosensitisation effect using AuNPs in combination with proton therapy both *in vivo* and *in vitro* (Kim *et al.*, 2010), while Porcel *et al.* showed an improvement of carbon ion therapy efficiency using platinum NPs on plasmid DNA (Porcel *et al.*, 2010a).

A challenging task when looking at the interaction between AuNPs and radiation is to be able to compare and analyse different radiosensitisation effects. Indeed, as observed during this work in Section 3.10 and 4.5, different energies of radiation, as well as different coating on the AuNPs and different cell lines can show very different radiosensitisation effects. To be able to fully characterise the effect of NPs with radiation, experimental studies using similar characteristics of cells, NPs size or charge, and radiation energies are needed, especially when considering collaborative works between different laboratories. Moreover, the comparison of different parameters to analyse the radiosensitisation effect can also be limited by the model

used, such as the linear quadratic model which does not always fit the *in vitro* measurements, as mentioned previously in this thesis. And where the linear quadratic linear model might be of interest (Joiner and Van der Kogel, 2009, Podgorsak, 2003).

In conclusion, optimisation of AuNPs requires still more characterisation and understanding of the radiosensitisation effect, such as the impact of the coating on the AuNPs uptake and intrinsic effect when interacting with radiotherapy, and the key organelles targeted by the AuNPs.

6.2. Future works

In this section, future work to build upon the results described in this thesis is presented, some of which is being performed by new students.

6.2.1. Oligonucleotide coated AuNPs

As mentioned in the chapter 4, dY3 and PR TFO were able to form a triplex with their target c-myc sequence but this structure was perturbed when adding a thiol group to the TFOs and when the TFO was attached to the AuNPs. Two different strategies may be developed in the future, modifying the size of the gold core or using different spacers between the TFO and the thiol group in order to find the best conformation for the TFO to recognise and binds to its target. Indeed, molecules such as polyethylene glycol polymer or different oligonucleotides, could help the recognition and target of the sequence of interest (Kang *et al.*, 2010, Suzuki *et al.*, 2009). A range of spacers between the TFO and the AuNPs will be explored at the Open University in a continuation of this project. In addition, trying a range of different AuNPs sizes could modify the cellular uptake and improve gene targeting. It would therefore be interesting to compare different coatings on comparable and smaller core size AuNPs, such as the α Gal:PEGamine coated AuNPs which gave a better uptake in skin cells than the uncoated 3.5 nm size AuNPs. This experimental programme could be part of a collaboration with the commercial company Midatech. In the rest of this section a few specific experiments are proposed.

6.4.2. Radiosensitisation effects of the NPs

To measure the intrinsic radiosensitisation effect of the NPs, the coumarin assay, measuring the \cdot OH production upon radiation was used in this project. However, the interaction between AuNPs and radiation may lead to the production of other types of radicals and

therefore, in the near future, studies using different probes such as DCFHDA to monitor H_2O_2 , ONOO⁻ to monitor $\text{O}_2^{\bullet-}$; and SOSG to probe $^1\text{O}_2$ is planned.

The amount of radicals produced inside the cells is a good indicator of the radiosensitisation effect and therefore quantifying the type and amount of radicals in the cells after irradiation is critical. Due to lack of appropriate in situ facilities and the long travel time between the hospital and the OU laboratory (> 1 hour), quantifying radical production immediately after radiation was not possible in the studies reported in the thesis. A collaboration with Queen's University Belfast has therefore been designed in order to explore the radical production with DCFHDA probe, immediately after irradiation.

6.4.3. Theoretical work and simulations

Understanding the radiosensitisation effect of NPs requires a multidisciplinary approach as this process involves biology, atomic physics and material engineering (Haume *et al.*, 2016a). Relating the uptake and toxicity of the AuNPs presented in chapters 3 & 4 with theoretical work, by approximating how the coating is linked to the metallic NP, and how it can change with the environment (e.g. surrounded by water molecules or proteins) is therefore of high importance, if a better understanding of how the characteristics of the AuNPs influence the radiosensitisation effect is to be achieved. Moreover, a collaboration between biology and theoretical modelling will provide feedbacks on both experiments and simulation codes.

In order to explore the coating behaviour on the AuNPs, a collaborative project involving theoretical modelling has begun, with Kaspar Haume (ARGENT PhD student) and Kurt Stokbro at Synopsis/QuantumWise, Denmark, where the AuNPs were designed using the VNL platform following the protocol from Haume *et al.* 2016 (Haume *et al.*, 2016a). Initial results show that the presence of a coating reduced the amount of water near the NP and hence reduces the number of OH radicals produced during irradiation. A presentation of multiscale models of the irradiation process in collaboration with MBN Explorer and has been described in the chapter 12 of the book *Nanoscale Insights into ion beam cancer therapy* (Bolsa Ferruz *et al.*, 2017).

6.4.3. Cerium oxide NPs

As discussed in chapter 5, CeO_2 NPs might not have sufficient electron density to give a radiosensitisation effect, although they are of interest due to their oxygen adsorbing properties. One way to improve CeO_2 NPs radiosensitisation effect might be to combine this metallic oxide with a high atomic weight element such as gold, silver or bismuth. Some work has already been performed on this area in the OU labs. Moreover, different techniques to explore the capacity

of CeO₂ NPs to absorb oxygen are being explored, such as the measure of oxygen uptake and release after introduction of O₂ in the system (Schalow *et al.*, 2005) or thermogravimetry. (Imagawa *et al.*, 2011).

6.4.4. Alternative strategies

Not only the use of NPs but also different molecules such as inhibitors of DNA repair (Inhibitors of topoisomerase II) (Zhu *et al.*, 2015), antioxidant inhibitors (N-acetyl cysteine) would be interesting and be the key in developing a synergistic effect with radiotherapy and increasing its efficiency (Lushchak, 2012, Yang *et al.*, 2007).

For example, Inhibitors of topoisomerase, such as doxorubicin (Zhu *et al.*, 2015), have shown promising results in combination with NPs and radiotherapy. Moreover, inhibitors of PARP, are already used clinically to increase the DNA damage upon radiation, and could also be of interest in combination with the AuNPs currently tested (Kouvaris *et al.*, 2007).

Thus there are many experiments to be done before the role and potential of NPs in radiotherapy is known. The results presented in this thesis and the wider work of the ARGENT Network has created a consortium capable of developing this work and is expected to lead to many exciting results in the next decade.

LIST OF PUBLICATIONS AND POSTER/ORAL CONFERENCE PRESENTATIONS

Journal publications

1. [Grellet, S.](#); Tzelepi, K.; Roskamp, M.; Williams, P.; Sharif, A.; Slade-Carter, R.; Goldie, P.; Whilde, N.; Śmialek, M. A. Mason, N. J.; Golding, J. P., *PLoS One* 2017, 12, 7.




RESEARCH ARTICLE

Cancer-selective, single agent chemoradiosensitising gold nanoparticles

Sophie Grellet¹, Konstantina Tzelepi¹, Meike Roskamp², Phil Williams², Aquila Shari², Richard Slade-Carter³, Peter Goldie⁴, Nicky Whilde⁴, Malgorzata A. Śmialek^{5,6}, Nigel J. Mason⁵, Jon P. Golding^{1*}

1 School of Life, Health & Chemical Sciences, The Open University, Walton Hall, Milton Keynes, United Kingdom, 2 Midatech Pharma, Milton Park, Abingdon, United Kingdom, 3 GenesisCare, Milton Keynes Medical Centre, Milton Keynes, United Kingdom, 4 Radiotherapy Department, Northampton General Hospital NHS Trust, Northampton, United Kingdom, 5 Department of Control and Power Engineering, Faculty of Ocean Engineering and Ship Technology, Gdansk University of Technology, Gdansk, Poland, 6 School of Physical Sciences, The Open University, Walton Hall, Milton Keynes, United Kingdom

* Jon.Golding@open.ac.uk

 Check for updates

Abstract

Two nanometre gold nanoparticles (AuNPs), bearing sugar moieties and/or thiol-polyethylene glycol-amine (PEG-amine), were synthesised and evaluated for their *in vitro* toxicity and ability to radiosensitise cells with 220 kV and 6 MV X-rays, using four cell lines representing normal and cancerous skin and breast tissues. Acute 3 h exposure of cells to AuNPs, bearing PEG-amine only or a 50:50 ratio of alpha-galactose derivative and PEG-amine resulted in selective uptake and toxicity towards cancer cells at unprecedentedly low nanomolar concentrations. Chemotoxicity was prevented by co-administration of N-acetyl cysteine antioxidant, or partially prevented by the caspase inhibitor Z-VAD-FMK. In addition to their intrinsic cancer-selective chemotoxicity, these AuNPs acted as radiosensitisers in combination with 220 kV or 6 MV X-rays. The ability of AuNPs bearing simple ligands to act as cancer-selective chemoradiosensitisers at low concentrations is a novel discovery that holds great promise in developing low-cost cancer nanotherapeutics.

OPEN ACCESS

Citation: Grellet S, Tzelepi K, Roskamp M, Williams P, Sharif A, Slade-Carter R, et al. (2017) Cancer-selective, single agent chemoradiosensitising gold nanoparticles. *PLoS ONE* 12(7): e0181103. <https://doi.org/10.1371/journal.pone.0181103>

Editor: Ying-lan Wang, National Cheng Kung University, TAIWAN

Received: March 7, 2017

Accepted: June 25, 2017

Published: July 10, 2017

2. Bolsa Ferruz, M.; Ivošev, V.; Haume, K.; Ellis-Gibbings, L.; Traore, A.; Thakare, V.; Rosa, S.; de Vera, P.; Tran, V. L.; Mika, A.; Boscolo, D.; [Grellet, S.](#); Verkhovtsev, A.; Huber, B. A.; Butterworth, K. T.; Prise, K. M.; Currell, F. J.; Mason, N. J.; Golding, J.; Scifoni, E.; García, G.; Boschetti, F.; Lux, F.; Tillement, O.; Louis, C.; Stokbro, K.; Solov'yov, A. V.; Lacombe, S., *New Research in Ionizing Radiation and Nanoparticles: The ARGENT Project*. In *Nanoscale Insights into Ion-Beam Cancer Therapy*, Solov'yov, A. V., Ed. Springer International Publishing: Cham, 2017; pp 379-434.

CHAPTER 12

Nanoscale Insights into Ion-Beam Cancer Therapy

New Research in Ionizing Radiation and Nanoparticles: The ARGENT Project

Authors: S. Lacombe · Andrey V. Solov'yov · K. Stokbro · C. Louis · O. Tillement · F. Lux · F. Boschetti · Gustavo Garcia · E. Scifoni · J. Golding · Nigel J. Mason · F. J. Currell · K. M. Prise · K. T. Butterworth · Bernd A. Huber · Alexey Verkhovtsev · S. Grellet · D. Boscolo · A. Mika · V.-L. Tran · Pablo de Vera · S. Rosa · V. Thakare · A. Traore · L. Ellis-Gibbings · K. Haume · V. Ivošev · M. Bolsa Ferruz

This Bolsa Ferruz, M. chapter Ivošev, V. gives Haume, K. an Ellis-Gibbings, L. overview Traore, A. of Thakare, V. " ARGENT Rosa, S. " ("Advanced Radiotherapy De Vera, Pablo , Generated Tran, V.-L. by Exploiting Mika, A. Nanoprocesses Boscolo, D.... [Read more](#)

- Haume, K.; Rosa, S.; Grellet, S.; Śmiałek, M. A.; Butterworth, K. T.; Solov'yov, A. V.; Prise, K. M.; Golding, J. P.; Mason, N. J. **Cancer Nanotechnology** 2016, 7, (1), 8.

Haume et al. *Cancer Nano* (2016) 7:8
DOI 10.1186/s12645-016-0021-x

 Cancer Nanotechnology

REVIEW

Open Access



Gold nanoparticles for cancer radiotherapy: a review

Kaspar Haume^{1*}, Soraia Rosa², Sophie Grellet³, Małgorzata A. Śmiałek⁴, Karl T. Butterworth², Andrey V. Solov'yov², Kevin M. Prise², Jon Golding³ and Nigel J. Mason¹

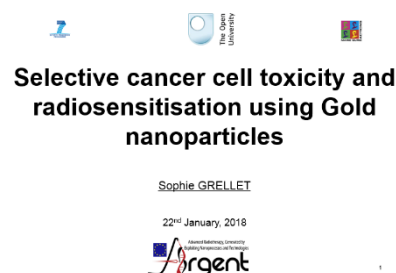
*Correspondence:
kaspar.haume@open.ac.uk
¹ Department of Physical Sciences, The Open University, Walton Hall, Milton Keynes MK7 6AA, UK
Full list of author information is available at the end of the article

Abstract

Radiotherapy is currently used in around 50% of cancer treatments and relies on the deposition of energy directly into tumour tissue. Although it is generally effective, some of the deposited energy can adversely affect healthy tissue outside the tumour volume, especially in the case of photon radiation (gamma and X-rays). Improved radiotherapy outcomes can be achieved by employing ion beams due to the charac-

Poster and oral conference presentations

- Selective cancer cell toxicity and radiosensitization of Gold nanoparticles, S. Grellet, M.A. Smialek, N.J. Mason, J.P. Golding, Advanced radiotherapy generated by exploiting nanoprocesses and technologies, 01/2018, U Paris Saclay, Paris, France



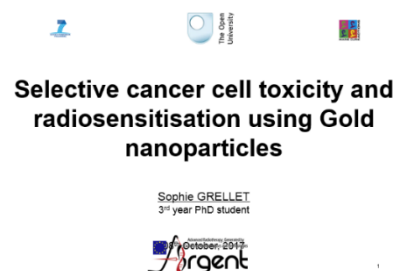
Selective cancer cell toxicity and radiosensitisation using Gold nanoparticles

Sophie GRELLET

22nd January, 2018

Argent

- Selective cancer cell toxicity and radiosensitization of Gold nanoparticles, S. Grellet, M.A. Smialek, N.J. Mason, J.P. Golding, Baltic conference series, 10/2017, IAAM, Stockholm, Sweden



Selective cancer cell toxicity and radiosensitisation using Gold nanoparticles

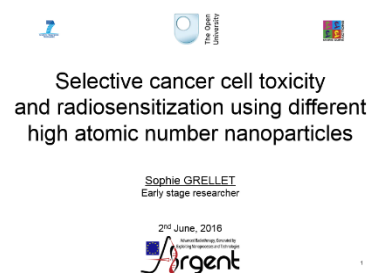
Sophie GRELLET

3rd year PHD student

October 2017

Argent

- S. Grellet, M.A. Smialek, N.J. Mason, J. Golding, Characterisation of coated-gold nanoparticles: its potential as radiosensitizers, DYSON (Dynamics of systems on the nanoscale), 10/2016, Bad Ems, Germany



Selective cancer cell toxicity and radiosensitization using different high atomic number nanoparticles

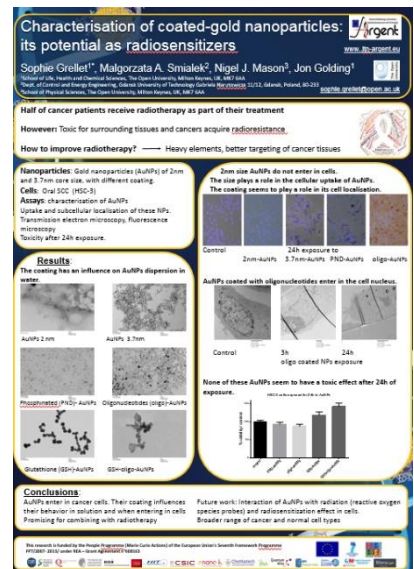
Sophie GRELLET

Early stage researcher

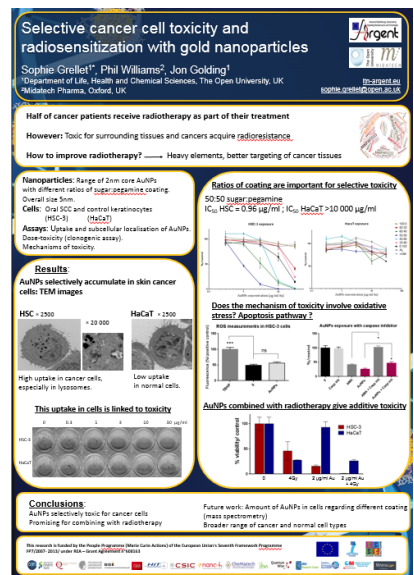
2nd June, 2016

Argent

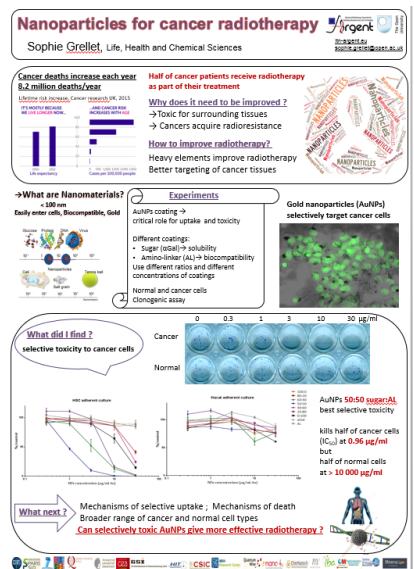
4. Selective cancer cell toxicity and radiosensitization using different high atomic number nanoparticles, S. Grellet, S. Kaas, E. Craab, S. Allman and J. Golding, Nanotech, 06/2016, Paris, France



5. S. Grellet, Phil Williams, N.J. Mason, J. Golding, Confnano, 10/2015, Paris, France,



6. S. Grellet, Phil Williams, N.J. Mason, J. Golding, Nanoparticles for cancer radiotherapy, Poster competition, 06/2015, Open University, UK,



BIBLIOGRAPHY

2001. *The cancer handbook*, Nature publishing group.
2014. *American Cancer Society* [Online]. Available: <https://www.cancer.org/cancer/cancer-basics/history-of-cancer/what-is-cancer.html>.
2015. Nanobiotix Secures Approval to Initiate Phase I/II Clinical Trial for NBTXR3. *Wireless News*.
- ADLER, D. C., HUANG, S.-W., HUBER, R. & FUJIMOTO, J. G. 2008. Photothermal detection of gold nanoparticles using phase-sensitive optical coherence tomography. *Optics express*, 16, 4376.
- ALKILANY, A. M. & MURPHY, C. J. 2010a. Toxicity and cellular uptake of gold nanoparticles: what we have learned so far? *Journal of nanoparticles respiration*, 12.
- ALKILANY, A. M. & MURPHY, C. J. 2010b. Toxicity and cellular uptake of gold nanoparticles: what we have learned so far? *Journal of nanoparticles respiration*, 12, 2313-2333.
- ALKILANY, A. M., NAGARIA, P. K., HEXEL, C. R., SHAW, T. J., MURPHY, C. J. & WYATT, M. D. 2009. Cellular uptake and cytotoxicity of gold nanorods: molecular origin of cytotoxicity and surface effects. *Small*, 5, 701-708.
- ALRIC, C., MILADI, I., KRYZA, D., TALEB, J., LUX, F., BAZZI, R., BILLOTEY, C., JANIER, M., PERRIAT, P., ROUX, S. & TILLEMENT, O. 2013. The biodistribution of gold nanoparticles designed for renal clearance. *Nanoscale*, 5, 5930-5939.
- ARVIZO, R. R., BHATTACHARYYA, S., KUDGUS, R. A., GIRI, K., BHATTACHARYA, R. & MUKHERJEE, P. 2012. Intrinsic therapeutic applications of noble metal nanoparticles: past, present and future. *Chemical Society Reviews*, 41, 2943-2970.
- ARYA, A., GANGWAR, A., SINGH, S. K., ROY, M., DAS, M., SETHY, N. K. & BHARGAVA, K. 2016. Cerium oxide nanoparticles promote neurogenesis and abrogate hypoxia-induced memory impairment through AMPK–PKC–CBP signaling cascade. *International journal of nanomedicine*, 11, 1159.
- ASTHANA, G. S., ASTHANA, A., KOHLI, D. V. & VYAS, S. P. 2014. Mannosylated chitosan nanoparticles for delivery of antisense oligonucleotides for macrophage targeting. *BioMed Research International*, 2014.
- AZZAM, E. I., DE TOLEDO, S. & LITTLE, J. B. 2003. Oxidative metabolism, gap junctions and the ionizing radiation-induced bystander effect. *Oncogene*, 22, 7050.
- BABAEI, M. & GANJALIKHANI, M. 2014a. The potential effectiveness of nanoparticles as radio sensitizers for radiotherapy. *Bioimpacts*, 1.
- BABAEI, M. & GANJALIKHANI, M. 2014b. The potential effectiveness of nanoparticles as radio sensitizers for radiotherapy. *Bioimpacts*, 4, 15-20.
- BAJAK, E., FABBRI, M., PONTI, J., GIORIA, S., OJEA-JIMÉNEZ, I., COLLOTTA, A., MARIANI, V., GILLILAND, D., ROSSI, F. & GRIBALDO, L. 2015. Changes in Caco-2 cells transcriptome profiles upon exposure to gold nanoparticles. *Toxicology Letters*, 233, 187-199.
- BANNUNAH, A. M., VLLASALIU, D., LORD, J. & STOLNIK, S. 2011a. Mechanisms of nanoparticle internalization and transport across an intestinal epithelial cell model: effect of size and surface charge. *Molecular pharmaceuticals*, 11, 4363-4373.
- BANNUNAH, A. M., VLLASALIU, D., LORD, J. & STOLNIK, S. 2011b. Mechanisms of nanoparticle internalization and transport across an intestinal epithelial cell model: effect of size and surface charge. *Molecular pharmaceuticals*, 11, 4363-4373.
- BARI, W. 1968. Cysteine protection against the morphologic effects of x-irradiation on mouse spleen. *Pathobiology*, 32, 205-218.
- BARKALINA, N., CHARALAMBOUS, C., JONES, C. & KOWARD, K. 2014. Nanotechnology in reproductive medicine: emerging application of nanomaterials. *Nanomedicine: Nanotechnology, Biology and medicine*, 10, 921-938.
- BECKER, D., ADHIKARY, A. & SEVILLA, M. D. 2007. The role of charge and spin migration in DNA radiation damage. *Charge migration in DNA*. Springer.

- BEDDOES, C. M., CASE, C. P. & BRISCOE, W. H. 2015a. Understanding nanoparticle cellular entry: a physicochemical perspective. *Advances in colloid and interface science*, 218, 48-68.
- BEDDOES, C. M., CASE, C. P. & BRISCOE, W. H. 2015b. Understanding nanoparticle cellular entry: a physicochemical perspective. *Advances in colloid and interface science*, 218, 48-68.
- BELOTSEKOVSKII, B. P., DE SILVA, E., TORNALETTI, S., WANG, G., VASQUEZ, K. M. & HANAWALT, P. C. 2007. A triplex-forming sequence from the human c-MYC promoter interferes with DNA transcription. *Journal of Biological Chemistry*, 282, 32433-32441.
- BERTHO, J.-M., FRICK, J., PRAT, M., DEMARQUAY, C., DUDOIGNON, N., TROMPIER, F., GORIN, N.-C., THIERRY, D. & GOURMELON, P. 2005. Comparison of autologous cell therapy and granulocyte-colony stimulating factor (G-CSF) injection vs. G-CSF injection alone for the treatment of acute radiation syndrome in a non-human primate model. *International Journal of Radiation Oncology* Biology* Physics*, 63, 911-920.
- BERTRAND N, WUB J, XU X, NAZILA KAMALY N & O.C, F. 2014. Cancer nanotechnology: The impact of passive and active targeting in the aera of modern cancer biology. *Advanced drug delivery reviews*, 66, 2-25.
- BINDER, M., ROBERTS, C., SPENCER, N., ANTOINE, D. & CARTWRIGHT, C. 2014. On the Antiquity of Cancer: Evidence for Metastatic Carcinoma in a Young Man from Ancient Nubia (c. 1200BC). *PLOS ONE*, 9, e90924.
- BJORNSTI, M.-A. 1999. *DNA Topoisomerase Protocols, Volume 1 : DNA Topology and Enzymes*, Totowa, Totowa : Humana Press.
- BOBYK, L., EDOUARD, M., DEMAN, P., VAUTRIN, M., PERNET-GALLAY, K., DELAROCHE, J., ADAM, J. F., ESTÈVE, F., RAVANAT, J. F. & ELLEAUME, A. 2013. Photoactivation of gold nanoparticles for glioma treatment. *Nanomedicine: Nanotechnology, Biology and medicine*, 9, 1089-1097.
- BOISSELIER, E. & ASTRUC, D. 2009. Gold nanoparticles in nanomedicine: preparations, imaging, diagnostics, therapies and toxicity. *The royal society of chemistry*, 38, 1759-1782.
- BOLSA FERRUZ, M., IVOŠEV, V., HAUME, K., ELLIS-GIBBINGS, L., TRAORE, A., THAKARE, V., ROSA, S., DE VERA, P., TRAN, V. L., MIKA, A., BOSCOLO, D., GRELLET, S., VERKHOVTSEV, A., HUBER, B. A., BUTTERWORTH, K. T., PRISE, K. M., CURRELL, F. J., MASON, N. J., GOLDING, J., SCIFONI, E., GARCÍA, G., BOSCHETTI, F., LUX, F., TILLEMENT, O., LOUIS, C., STOKBRO, K., SOLOV'YOV, A. V. & LACOMBE, S. 2017. New Research in Ionizing Radiation and Nanoparticles: The ARGENT Project. In: SOLOV'YOV, A. V. (ed.) *Nanoscale Insights into Ion-Beam Cancer Therapy*. Cham: Springer International Publishing.
- BOUDAIFFA B, CLOUTIER P, HUNTING D, HUELS M.A & SANCHE L 2000. Resonant Formation of DNA Strand Breaks by Low-Energy (3 to 20 eV) Electrons. *Science*, 287.
- BRIGGS, A., CORDE, S., OKTARIA, S., BROWN, R., ROSENFELD, A., LERCH, M., KONSTANTINOV, K. & TEHEI, M. 2013. Cerium oxide nanoparticles: influence of the high-Z component revealed on radioresistant 9L cell survival under X-ray irradiation. *Nanomedicine: Nanotechnology, Biology and Medicine*, 9, 1098-1105.
- BRIZEL, D. M., MURPHY, B. A., ROSENTHAL, D. I., PANDYA, K. J., GLÜCK, S., BRIZEL, H. E., MEREDITH, R. F., BERGER, D., CHEN, M.-G. & MENDENHALL, W. 2008. Phase II study of palifermin and concurrent chemoradiation in head and neck squamous cell carcinoma. *Journal of clinical oncology*, 26, 2489-2496.
- BRUN, E., SANCHE, L. & SICARD-ROSELLI, C. 2009a. Parameters governing gold nanoparticle X-ray radiosensitization of DNA in solution. *Colloids and Surfaces B: Biointerfaces*, 72, 128-134.
- BRUN, E., SANCHE, L. & SICARD-ROSELLI, C. 2009b. Parameters governing gold nanoparticle X-ray radiosensitization of DNA in solution. *Colloids and Surfaces B: Biointerfaces*, 72, 128-134.
- BURGER, N., BISWAS, A., BARZAN, D., KIRCHNER, A., HOSSER, H., HAUSMANN, M., HILDENBRAND, G., HERSKIND, C., WENZ, F. & VELDWIJK, M. R. 2014a. A method for the efficient cellular uptake and retention of small modified gold nanoparticles for the radiosensitization of cells. *Nanomedicine: Nanotechnology, Biology, and Medicine*, 10, 1365-1373.

- BURGER, N., BISWAS, A., BARZAN, D., KIRCHNER, A., HOSSER, H., HAUSMANN, M., HILDENBRAND, G., HERSKIND, C., WENZ, F. & VELDWIJK, M. R. 2014b. A method for the efficient cellular uptake and retention of small modified gold nanoparticles for the radiosensitization of cells. *Nanomedicine: Nanotechnology, Biology, and Medicine*, 10, 1365-1373.
- BUTTERWORTH K.T, COULTER J.A, JAIN S, FORKER J, MCMAHON S.J, SCHETTINO G, PRISE K.M, CURRELL F.J & HIRST, D. G. 2010. Evaluation of cytotoxicity and radiation enhancement using 1.9 nm gold particles: potential application for cancer therapy. *Nanotechnology*, 21, 295101-295109.
- BUTTERWORTH, K. T., COULTER, J. A., JAIN, S., FORKER, J., MCMAHON, S. J., SCHETTINO, G., PRISE, K. M., CURRELL, F. J. & HIRST, D. G. 2010. Evaluation of cytotoxicity and radiation enhancement using 1.9 nm gold particles: potential application for cancer therapy. *Nanotechnology*, 21, 295101.
- BUTTERWORTH, K. T., MCMAHON, S. J., CURRELL, F. J. & PRISE, K. M. 2012. Physical basis and biological mechanisms of gold nanoparticle radiosensitization. *Nanoscale.*, 4, 4830-4838.
- CALVAREZIA E.C & HERGENROTHER P.J 2013. Glucose conjugation for the specific targeting and treatment of cancer. *Chemical science*, 4, 2319-2333.
- CARBONE, G. M., MCGUFFIE, E., NAPOLI, S., FLANAGAN, C. E., DEMBECH, C., NEGRI, U., ARCAMONE, F., CAPOBIANCO, M. L. & CATAPANO, C. V. 2004. DNA binding and antigene activity of a daunomycin-conjugated triplex-forming oligonucleotide targeting the P2 promoter of the human c-myc gene. *Nucleic acids research*, 32, 2396.
- CARIVEAU, M. J., STACKHOUSE, M. & CUI XIAOLI, E. M. X. S. O. 2008. Clofarabine acts as radiosensitizer in vitro and in vivo by interfering with DNA damage response. *International Journal of Radiation Oncology, Biology and Physics*, 70.
- CHAUHAN, M., MANSHANDA, A., KHURANA, J., JAIN, P., SHARMA, D., JAIN, S. & BANSAL, S. 2011. Nanotechnology: the nano soldiers in the war against cancer. *Journal of Pharmacy research*, 4, 4420-4423.
- CHEN, Y. J., LIN, S. C., KAO, T., CHANG, C. S., HONG, P. S., SHIEH, T. M. & CHANG, K. W. 2004. Genome-wide profiling of oral squamous cell carcinoma. *The Journal of pathology*, 204, 326-332.
- CHENG, G., GUO, W., HAN, L., CHEN, E., KONG, L., WANG, L., AI, W., SONG, N., LI, H. & CHEN, H. 2013. Cerium oxide nanoparticles induce cytotoxicity in human hepatoma SMMC-7721 cells via oxidative stress and the activation of MAPK signaling pathways. *Toxicology in Vitro*, 27, 1082-1088.
- CHHOUR, P., KIM, J., BENARDO, B., TOVAR, A., MIAN, S., LITT, H. I., FERRARI, V. A. & CORMODE, D. P. 2016. Effect of gold nanoparticle size and coating on labeling monocytes for CT tracking. *Bioconjugate chemistry*, 28, 260-269.
- CHITHRANI, B. D., GHAZANI, A. A. & CHAN, W. C. 2006. Determining the size and shape dependence of gold nanoparticle uptake into mammalian cells. *Nano letters*, 6, 662-668.
- CHITHRANI, B. D., STEWART, J., ALLEN, C. & JAFFRAY, D. 2009. Intracellular uptake, transport, and processing of nanostructures in cancer cells. 5, 118-127.
- CHITHRANI, D. B., JELVEH, S., JALALI, F., PROOIJEN, M., ALLEN, C. & BRISTOW, R. G. 2010. Gold nanoparticles as radiation sensitizers in cancer therapy. *Radiat Research*, 173, 719-28.
- CHOU, L. Y., MING, K. & CHAN, W. C. 2011. Strategies for the intracellular delivery of nanoparticles. *Chemical Society Reviews*, 40, 233-245.
- CITRIN, D., COTRIM, A. P., HYODO, F., BAUM, B. J., KRISHNA, M. C. & MITCHELL, J. B. 2010. Radioprotectors and mitigators of radiation-induced normal tissue injury. *The Oncologist*, 15, 360-371.
- CLANCY, S. 2008. DNA damage & repair: mechanisms for maintaining DNA integrity. . *How do DNA repair mechanisms detect and repair damaged DNA, and what happens when they fail*, 10-4.
- COLLINS, A., MAKRIGIORGOS, G. & SVENSSON, G. 1994. Coumarin chemical dosimeter for radiation therapy. *Medical physics*, 21, 1741-1747.

- COLOMBO, M., CARREGAL-ROMERO, S., CASULA, M. F., GUTIRREZ, L., MORALES, M. P., BHM, I. B., HEVERHAGEN, J. T., PROSPERI, D. & PARAK, W. J. 2012. Biological applications of magnetic nanoparticles. *Chemical Society Reviews*, 41, 4306-4334.
- COLON, J., HSIEH, N., FERGUSON, A., KUPELIAN, P., SEAL, S. & JENKINS, D. W. 2010. Cerium oxide nanoparticles protect gastrointestinal epithelium from radiation-induced damage by reduction of reactive oxygen species and upregulation of superoxide dismutase 2. *Nanomedicine*, 6, 698-705.
- CONNOR, E. E., MWAMUKA, J., GOLE, A., MURPHY, C. J. & WYATT, M. D. 2005. Gold nanoparticles are taken up by human cells but do not cause acute cytotoxicity. *Small*, 1, 325-327.
- COOPER, G. M. & GANEM, D. 1997. The cell: A molecular approach. *Nature Medicine*, 3, 1042-1042.
- COOPER, G. M. & HAUSMAN, R. E. 2004. *The cell: Molecular approach*, Medicinska naklada.
- COSTANTINI, D. L., VILLANI, D. F., VALLIS, K. A. & REILLY, R. M. 2010. Methotrexate, paclitaxel, and doxorubicin radiosensitize HER2-amplified human breast cancer cells to the auger electron-emitting radiotherapeutic agent ¹¹¹In-NLS-trastuzumab. *Journal of Nuclear Medicine*, 51, 477-483.
- COULTER J.A, JAIN S, BUTTERWORTH K.T, TAGGART L.E, DICKSON G.R, MCMAHON S.J, HYLAND, W. B., MUIR, M. F., TRAINOR C, HOUNSELL, A. R., O'SULLIVAN J.M, SCHETTINO G, CURRELL F.J, HIRST, D. G. & PRIZE, K. M. 2012. Cell type-dependent uptake, localization, and cytotoxicity of 1.9 nm gold nanoparticles. *International Journal of nanomedicine*, 7, 2673-2685.
- CUI, F.-B., LI, R.-T., LIU, Q., WU, P.-Y., HU, W.-J., YUE, G.-F., DING, H., YU, L.-X., QIAN, X.-P. & LIU, B.-R. 2014. Enhancement of radiotherapy efficacy by docetaxel-loaded gelatinase-stimuli PEG-Pep-PCL nanoparticles in gastric cancer. *Cancer Letters*, 346, 53-62.
- CUI, L., HER, S., DUNNE, M., BORST, G. R., DE SOUZA, R., BRISTOW, R. G., JAFFRAY, D. A. & ALLEN, C. 2017. Significant radiation enhancement effects by gold nanoparticles in combination with cisplatin in triple negative breast cancer cells and tumor xenografts.(RADIATION RESEARCH)(Report). *Radiation Research*, 187, 147.
- CUI, L., ZAHEDI, P., SARACENO, J., BRISTOW, R., JAFFRAY, D. & ALLEN, C. 2013. Neoplastic cell response to tiopronin-coated gold nanoparticles. *Nanomedicine: nanotechnology, biology and medicine*, 9, 264-273.
- DA ROCHA, E. L., CARAMORI, G. F. & RAMBO, C. R. 2013. Nanoparticles translocation through a lipid bilayer tuned by surface chemistry. *Physical chemistry chemical physics*, 15, 2282-2290.
- DAMODARAN, V. B., FEE, C. J. & POPAT, K. C. 2010. Prediction of protein interaction behaviour with PEG-grafted matrices using X-ray photoelectron spectroscopy. *Applied Surface Science*, 256, 4894-4901.
- DAVDA, R., ABDULLAH, A. & RICKETTS, K. 2016. Advances in external beam radiotherapy for prostate cancer. *Trends in Urology & Men's Health*, 7, 13-16.
- DAVIDSON, R. & GUO, T. 2014. Average physical enhancement by nanomaterials under X-ray irradiation. *Journal of physical chemistry*, 118, 30221-30228.
- DAVIS, R. M., SOWERS, A. L., DEGRAFF, W., BERNARDO, M., THETFORD, A., KRISHNA, M. C. & MITCHELL, J. B. 2011. A novel nitroxide is an effective brain redox imaging contrast agent and in vivo radioprotector. *Free Radical Biology and Medicine*, 51, 780-790.
- DE LA FUENTE, J., BERRY, C., RIEHLE, M. & CURTIS, A. 2006. Nanoparticle targeting at cells. *Langmuir*, 22, 3286-3293.
- DEKHUIJZEN, P. N. R. 2004. Antioxidant properties of N-acetylcysteine: their relevance in relation to chronic obstructive pulmonary disease. *European Respiratory Journal*, 23, 629-636.
- DENDY P.P & HEATON B 1999. *Physics for diagnostic radiology*.
- DENDY, P. P. & HEATON, B. 1999. *Physics for diagnostic radiology*.
- DENG, J., ZHENG, H., WU, S., ZHANG, P. & GAO, C. 2015. Protein adsorption and cellular uptake of AuNPs capped with alkyl acids of different length. *RSC Advances*, 5, 22792-22801.

- DRESCHER, D. & KNEIPP, J. 2012. Nanomaterials in complex biological systems: insights from Raman spectroscopy. *Chemical Society Reviews*, 41, 5780-5799.
- EGGER, L., SCHNEIDER, J., RHEME, C., TAPERNOUX, M., HACKI, J. & BORNER, C. 2003. Serine proteases mediate apoptosis-like cell death and phagocytosis under caspase-inhibiting conditions. *Cell Death and Differentiation*, 10, 1188-1203.
- EL-SAYED, I. H., HUANG, X. & EL-SAYED, M. A. 2005. Surface plasmon resonance scattering and absorption of anti-EGFR antibody conjugated gold nanoparticles in cancer diagnostics: applications in oral cancer. *Nano letters*, 5, 829.
- FALABELLA, J. B., CHO, T. J., RIPPLE, D. C., HACKLEY, V. A. & TARLOV, M. J. 2010. Characterization of gold nanoparticles modified with single-stranded DNA using analytical ultracentrifugation and dynamic light scattering. *Langmuir*, 26, 12740.
- FAN W, SHEN B, BU W, ZHENG X, HE Q, CUI Z, ZHAO K, ZHANG S & SHI J 2015. Design of an intelligent sub-50 nm nucleartargeting nanotheranostic system for imaging guided intranuclear radiosensitization†. *Chemical science*, 6, 1747-1753.
- FERLAY, J., AUTIER, P., BONIOL, M., HEANUE, M., COLOMBET, M. & BOYLE, P. 2007. Estimates of the cancer incidence and mortality in Europe in 2006. *Annals of oncology*, 18, 581-592.
- FINCH, P. W. & RUBIN, J. S. 2004. Keratinocyte growth factor/fibroblast growth factor 7, a homeostatic factor with therapeutic potential for epithelial protection and repair. *Advances in cancer research*, 91, 69-136.
- FLEURY, B., CORTES-HUERTO, R., TACHÉ, O., TESTARD, F., MENGUY, N. & SPALLA, O. 2015. Gold nanoparticle internal structure and symmetry probed by unified small-angle X-ray scattering and X-ray diffraction coupled with molecular dynamics analysis. *Nano letters*, 15, 6088.
- FRANCO, R., PANAYIOTIDIS, M. I. & CIDLOWSKI, J. A. 2007. Glutathione depletion is necessary for apoptosis in lymphoid cells independent of reactive oxygen species formation. *Journal of Biological Chemistry*, 282, 30452-30465.
- FRATODDI, I., VENDITTI, I., CAMETTI, C. & RUSSO, M. V. 2015. How toxic are gold nanoparticles? The state-of-the-art. *Nano Research*, 8, 1771-1799.
- FU, P. P., XIA, Q., HWANG, H. M., RAY, P. C. & YU, H. 2014. Mechanisms of nanotoxicity: generation of reactive oxygen species. *Journal of food and drug analysis*, 22, 64-75.
- GARA, P. M. D., GARABANO, N. I., PORTOLES, M. J. L., MORENO, M. S., DODAT, D., CASAS, O. R., GONZALEZ, M. C. & KOTLER, M. L. 2012. ROS enhancement by silicon nanoparticles in X-ray irradiated aqueous suspensions and in glioma C6 cells. *Journal of Nanoparticle Research*, 14, 741.
- GELTMEIER, A., RINNER, B., BADE, D., MEDITZ, K., WITT, R., BICKER, U., BLUDSZUWEIT-PHILIPP, C. & MAIER, P. 2015. Characterization of Dynamic Behaviour of MCF7 and MCF10A Cells in Ultrasonic Field Using Modal and Harmonic Analyses. *PLOS ONE*, 10, e0134999.
- GENG, F., SONG, K., XING, J. Z., YUAN, C., YAN, S. & YANG, Q. 2011. Thio-glucose bound gold nanoparticles enhance radiocytotoxic targeting of ovarian cancer. *Nanotechnology*, 22, 285101-285108.
- GEORGIEVA, J., KALICHARAN, D., COURAUD, P. O., ROMERO, I., WEKSLER, B., HOEKSTRA, D. & ZUHORN, I. 2011. Surface characteristics of nanoparticles determine their intracellular fate in and processing by human blood-brain barrier endothelial cells in vitro. *Molecular therapy*, 19, 318-325.
- GHOSH P, HAN G, DE M, KIM C & ROTELLO V.M 2008. Gold nanoparticles in delivery applications. *Advanced drug delivery reviews*, 60, 1307-1315.
- GILLES, M., BRUN, E. & SICARD-ROSELLI, C. 2014. Gold nanoparticles functionalization notably decreases radiosensitization through hydroxyl radical production under ionizing radiation. *Colloids and Surfaces B: Biointerfaces*, 123, 770-777.
- GOODMAN, C., MCCUSKER, YILMAZ, T. & ROTELLO, V. M. 2004. Toxicity of gold nanoparticles functionalized with cationic and anionic side chains. *Bioconjugate chemicals*, 15, 897-900.

- GRDINA, D., MURLEY, J., MILLER, R. C., MAUCERI, H., SUTTON, H., LI, J., WOLOSCHAK, G. & WEICHSELBAUM, R. 2013. A Survivin-Associated Adaptive Response in Radiation Therapy. *Cancer Research*, 73, 4418-4428.
- GRELLET, S., TZELEPI, K., ROSKAMP, M., WILLIAMS, P., SHARIF, A., SLADE-CARTER, R., GOLDIE, P., WHILDE, N., SMIALEK, M. A., MASON, N. J. & GOLDING, J. P. 2017. Cancer-selective, single agent chemoradiosensitising gold nanoparticles. *PLoS ONE*, 12.
- GROMNICOVA, R. 2017. *Gold Nanoparticles as a Delivery System of Oligonucleotides into the Brain*. PhD, The Open University.
- GROMNICOVA R, DAVIES H.A, SREEKANTHREDDY P, ROMERO I.A, LUND T, ROITT I.M, PHILLIPS J.B & MALE D.K 2013. Glucose-coated gold nanoparticles transfer across human brain endothelium and enter astrocytes in vitro. *Plos One*, 8, e81043.
- GÜLDEN, M., JESS, A., KAMMANN, J., MASER, E. & SEIBERT, H. 2010. Cytotoxic potency of H₂O₂ in cell cultures: impact of cell concentration and exposure time. *Free Radical Biology and Medicine*, 49, 1298-1305.
- GUPTA S.K, RASTOGI S, PRAKASH J, JOSHI S, GUPTA Y.K, AWOR L & S.D, V. 2000. Anti-inflammatory activity of sodium pyruvate-A physiological antioxidant. *Indian Journal of physiology and pharmacology*, 44, 101-104.
- HAHN, S. M., KRISHNA, C. M., SAMUNI, A., DEGRAFF, W., CUSCELA, D. O., JOHNSTONE, P. & MITCHELL, J. B. 1994. Potential use of nitroxides in radiation oncology. *Cancer Research*, 54, 2006s-2010s.
- HAINFELD, J. F., DILMANIAN, F. A., SLATKIN, D. N. & SMILOWITZ, H. M. 2008. Radiotherapy enhancement with gold nanoparticles. *Journal of Pharmacy and Pharmacology*, 60, 977-985.
- HAINFELD, J. F., SLATKIN, D. N. & SMILOWITZ, H. M. 2004. The use of gold nanoparticles to enhance radiotherapy in mice. *Physics in Medicine and Biology*, 49, N309.
- HÄKKINEN, H. 2012. Ligand-protected gold nanoclusters as superatoms: insights from theory and computations. *Frontiers of Nanoscience*, 3, 129-157.
- HAMPEL, K. J., LEE, J. S. & BURKHOLDER, G. D. 1993. Plasmid dimerization mediated by triplex formation between polypyrimidine-polypurine repeats. *Biochemistry*, 32, 1072-1077.
- HANAHAN, D. & WEINBERG, R. A. 2000. The hallmarks of cancer. *cell*, 100, 57-70.
- HANŽIĆ, N., HORVAT, A., BIBIĆ, J., UNFRIED, K., JURKIN, T., DRAŽIĆ, G., MARIJANOVIĆ, I., SLADE, N. & GOTIĆ, M. 2018. Syntheses of gold nanoparticles and their impact on the cell cycle in breast cancer cells subjected to megavoltage X-ray irradiation. *Materials Science and Engineering: C*, 91, 486-495.
- HATANO, Y., KATSUMURA, Y. & MOZUMDER, A. 2010. *Charged particle and photon interactions with matter: recent advances, applications, and interfaces*, CRC Press.
- HAUCK T.S, GHAZANI A.A & W.C, C. 2008. Assessing the effect of surface chemistry on gold nanorod uptake, toxicity, and gene expression in mammalian cells. *Small*, 4, 153-159.
- HAUME, K., MASON, N. J. & SOLOV'YOV, A. V. 2016a. Modeling of nanoparticle coatings for medical applications. *The European Physical Journal D*, 70, 181.
- HAUME, K., ROSA, S., GRELLET, S., ŚMIAŁEK, M. A., BUTTERWORTH, K. T., SOLOV'YOV, A. V., PRISE, K. M., GOLDING, J. P. & MASON, N. J. 2016b. Gold nanoparticles for cancer radiotherapy: a review. *Cancer Nanotechnology*, 7, 8.
- HAVAKI, S., KOTSINAS, A., CHRONOPOULOS, E., KLETSAS, D., GEORGAKILAS, A. & GORGOLIS, V. G. 2015. The role of oxidative DNA damage in radiation induced bystander effect. *Cancer Letters*, 356, 43-51.
- HE, C., HU, Y., YIN, L., TANG, C. & YIN, C. 2010. Effects of particle size and surface charge on cellular uptake and biodistribution of polymeric nanoparticles. *Biomaterials*, 31, 3657-3666.
- HE, L., LAI, H. & CHEN, T. 2015. Dual-function nanosystem for synergetic cancer chemo-/radiotherapy through ROS-mediated signaling pathways. *Biomaterials*, 51, 30-42.
- HEBIĆ, S., KOKOH, B., SERVAT, K. & NAPPORN, T. 2013. Shape-dependant electrocatalytic activity of free gold nanoparticles toward glucose oxidation. *Gold bulletin*, 46, 311-318.

- HEIN, A. L., OUELLETTE, M. M. & YAN, Y. Radiation-induced signaling pathways that promote cancer cell survival. *International Journal of oncology*, 45, 1813-1819.
- HERDT, A. R., DRAWZ, S. M., KANG, Y. & TATON, T. A. 2006. DNA dissociation and degradation at gold nanoparticle surfaces. *Colloids and Surfaces B: Biointerfaces*, 51, 130-139.
- HIRSCH, V., SALAKLANG, J., ROTHEN-RUTISHAUSER, B. & PETRI-FINK, A. 2013a. Influence of serum supplemented cell culture medium on colloidal stability of polymer coated iron oxide and polystyrene nanoparticles with impact on cell interactions in vitro. *IEEE Transactions on magnetics*, 49, 402-407.
- HIRSCH, V., SALAKLANG, J., ROTHEN-RUTISHAUSER, B. & PETRI-FINK, A. 2013b. Influence of serum supplemented cell culture medium on colloidal stability of polymer coated iron oxide and polystyrene nanoparticles with impact on cell interactions in vitro. *IEEE Transactions on magnetics*.
- HOBBIE, R. K. & ROTH, B. J. 2007. *Intermediate physics for medicine and biology*, Springer Science & Business Media.
- HOSSAIN M & SU M 2012. Nanoparticle location and material-dependent dose enhancement in X-ray radiation therapy. *Journal of physical chemistry*, 116, 23047–23052.
- HU C, NIESTROJ M, YUAN D, CHANG S & CHEN J 2015. Treating cancer stem cells and cancer metastasis using glucose-coated gold nanoparticles. *International Journal of nanomedicine*, 10, 2065-2077.
- HUANG, H., YU, N. C., FU, L., WEI, X., SU, W., HUANG, G., WU, Y., HUANG, H., LIU, Q. & XIAO, H. 2008. siRNA directed against c-Myc inhibits proliferation and downregulates human telomerase reverse transcriptase in human colon cancer Colo 320 cells *Journal of experimental and clinical cancer research*, 27.
- HUO, S., JIN, S., MA, X., XUE, X., YANG, K., KUMAR, A., WANG, P. C., ZHANG, J., HU, Z. & LIANG, X.-J. 2014. Ultrasmall gold nanoparticles as carriers for nucleus-based gene therapy due to size-dependent nuclear entry. *ACS Nano*, 8, 5852-5862.
- ILIAKIS, G. & NÜSSE, M. 1983. Evidence that repair and expression of potentially lethal damage cause the variations in cell survival after X-irradiation observed through the cell cycle in ehrlich ascites tumor cells. *Radiation research*, 95, 87-107.
- IMAGAWA, H., SUDA, A., YAMAMURA, K. & SUN, S. 2011. Monodisperse CeO₂ nanoparticles and their oxygen storage and release properties. *The Journal of Physical Chemistry C*, 115, 1740-1745.
- JAIN, S., COULTER, J. A., BUTTERWORTH, K. T., HOUNSELL, A. R., MCMAHON, S. J., HYLAND, W. B., MUIR, M. F., DICKSON, G. R., PRISE, K. M., CURRELL, F. J., HIRST, D. G. & O'SULLIVAN, J. M. 2014. Gold nanoparticle cellular uptake, toxicity and radiosensitisation in hypoxic conditions. *Radiotherapy and Oncology*, 110, 342-347.
- JAIN, S., COULTER, J. A., HOUNSELL, A. R., BUTTERWORTH, K. T., MCMAHON, S. J., HYLAND, W. B., MUIR, M. F., DICKSON, G. R., PRISE, K. M., CURRELL, F. J., O'SULLIVAN, J. M. & HIRST, D. G. 2011. Cell-specific radiosensitization by gold nanoparticles at megavoltage radiation energies. *International Journal of Radiation Oncology*Biophysics*, 79, 531-539.
- JEYNES, J. C. G., MERCHANT, M. J., SPINDLER, A., WERA, A. C. & KIRKBY, K. J. 2014. Investigation of gold nanoparticle radiosensitization mechanisms using a free radical scavenger and protons of different energies. *Physics in Medicine and Biology*, 59, 6431-6443.
- JOH, D., SUN, L., STANGL, M., ZAKI, A. A., MURTY, S., SANTOIEMMA, P. P., DAVIS, J. J., BAUMANN, B. C., ALONSO-BASANTA, M., BHANG, D., KAO, G. D., TSOURKAS, A. & DORSEY, J. 2013. Selective targeting of brain tumors with gold nanoparticle-induced radiosensitization. *Plos One*, 8.
- JOINER, M. & VAN DER KOGEL, A. 2009. *Basic clinical radiobiology*, Hodder Arnold London.
- JOKERST, J. V., LOBOVKINA, T., ZARE, R. N. & GAMBHIR, S. S. 2011. Nanoparticle PEGylation for imaging and therapy. *Nanomedicine*, 6, 715-728.
- JOLIVET, J.-P., CASSAIGNON, S., CHANÉAC, C., CHICHE, D., DURUPHTY, O. & PORTEHAULT, D. 2010. Design of metal oxide nanoparticles: Control of size, shape, crystalline structure and functionalization by aqueous chemistry. *Comptes Rendus Chimie*, 13, 40-51.

- JOSEPH, B., VISHWANATH, L. & VENUGOPAL, B. K. 2014. Radiosensitization in head and neck cancer: do we have an alternative to platins? Role of taxanes. *Oral Surgery, Oral Medicine, Oral Pathology and Oral Radiology*, 117, 324-328.
- KALAY, S., BLANCHET, C. & CULHA, M. 2014. Linear assembly and 3D networks of peptide modified gold nanoparticles. *Turkish journal of chemistry*, 686-700.
- KALIMUTHU, P. & JOHN, S. A. 2010. Studies on ligand exchange reaction of functionalized mercaptothiadiazole compounds onto citrate capped gold nanoparticles. *Materials Chemistry and Physics*, 122, 380-385.
- KANG, B., MACKEY, M. A. & EL-SAYED, M. A. 2010. Nuclear targeting of gold nanoparticles in cancer cells induces DNA damage, causing cytokinesis arrest and apoptosis. *Journal of the American Chemical Society*, 132, 1517.
- KELLY, K., CORONADO, E., ZHAO, L. & SCHATZ, G. 2003. The optical properties of metal nanoparticles: The influence of size, shape, and dielectric environment. *Journal of physical chemistry*, 107, 668-677.
- KELTS, J. L., CALI, J. J., DUELLMAN, S. J. & SHULTZ, J. 2015. Altered cytotoxicity of ROS-inducing compounds by sodium pyruvate in cell culture medium depends on the location of ROS generation. *SpringerPlus*, 4, 269.
- KENZAOU, B. H., BERNASCONI, C. C., GUNEY-AYRA, S. & JUILLERAT-JEANNERET, L. 2012. Induction of oxidative stress, lysosome activation and autophagy by nanoparticles in human brain-derived endothelial cells. *Biochemical Journal*, 441, 813-821.
- KHAN, A. K., RASHID, R., MURTAZA, G. & ZAHRA, A. 2014. Gold nanoparticles : synthesis and applications in drug delivery. *Tropical journal of pharmaceutical research*, 13, 1169-1177.
- KIM, J.-H., YEOM, J.-H., KO, J.-J., HAN, M. S., LEE, K., NA, S.-Y. & BAE, J. 2011. Effective delivery of anti-miRNA DNA oligonucleotides by functionalized gold nanoparticles. *Journal of Biotechnology*, 155, 287-292.
- KIM, J.-K., SEO, S.-J., KIN, K.-H., KIM, T.-J., CHUNG, M. H., KIM, K.-R. & YANG, T.-K. 2010. Therapeutic application of metallic nanoparticles combined with particle-induced x-ray emission effect. *Nanotechnology*, 21, 10.
- KLEEBE, H.-J., LAUTERBACH, S. & MÜLLER, M. M. 2012. *Transmission Electron Microscopy*.
- KLEIN, S., SOMMER, A., DISTEL, L. V. R., HAZEMANN, J.-L., KRÖNER, W., NEUHUBER, W., MÜLLER, P., PROUX, O. & KRYSCHI, C. 2014. Superparamagnetic iron oxide nanoparticles as novel X-ray enhancer for low-dose radiation therapy. *The journal of physical chemistry. B*, 118, 6159.
- KODIHA, M., HUTTER, E., BORIDY, S., JUHAS, M., MAYSINGER, D. & STOCHAJ, U. 2014. Gold nanoparticles induce nuclear damage in breast cancer cells, which is further amplified by hyperthermia. *Cellular and Molecular Life Sciences*, 71, 4259-4273.
- KODIHA, M., WANG, Y., HUTTER, E., MAYSINGER, D. & STOCHAJ, U. 2015. Off to the Organelles - Killing Cancer Cells with Targeted Gold Nanoparticles. *Theranostics*.
- KÖGEL, D. & PREHN, J. H. 2013. *Caspase-independent cell death mechanisms*.
- KONG T, WZHENG J, WANG X, YANG X, YANG J, MCQUARRIE S, MCEWAN A, ROA W, CHEN J & XING J.Z 2008. Enhancement of radiation cytotoxicity in breast-cancer cells by localized attachment of gold nanoparticles. *Small*, 4, 1537-1543.
- KONG, T., ZENG, J., WANG, X. P., YANG, X., YANG, J. & MCQUARRIE, S. 2008. Enhancement of radiation cytotoxicity in breast-cancer cells by localized attachment of gold nanoparticles. *Small*, 4, 1537-1543.
- KOUTCHER, J. A., ALFIERI, A. A., THALER, H., MATEI, C. & MARTIN, D. S. 1997. Radiation enhancement by biochemical modulation and 5-fluorouracil. *International Journal of Radiation Oncology, Biology, Physics*, 39, 1145-1152.
- KOUVARIS, J. R., KOULOULIAS, V. E. & VLAHOS, L. J. 2007. Amifostine: the first selective-target and broad-spectrum radioprotector. *The oncologist*, 12, 738-747.
- KRALJ, S., ROJNIK, M., JAGODIČ, M., KOS, J. & MAKOVEC, D. 2012. Effect of surface charge on the cellular uptake of fluorescent magnetic nanoparticles. *Journal of Nanoparticle Research*, 14, 1151.

- KRYSTON, T. B., GEORGIEV, A. B., PISSIS, P. & GEORGAKILAS, A. G. 2011. Role of oxidative stress and DNA damage in human carcinogenesis. *Mutation Research - Fundamental and Molecular Mechanisms of Mutagenesis*, 711, 193-201.
- KUCINSKA, M., MURIAS, M. & NOWAK-SLIWINSKA, P. 2017. Beyond mouse cancer models: Three-dimensional human-relevant in vitro and non-mammalian in vivo models for photodynamic therapy. *Mutation Research/Reviews in Mutation Research*, 773, 242-262.
- KUMAR A, MA H, ZHANG X, HUANG K, JIN S, LIU J, WEI T, CAO W, ZOU G & X-J, L. 2012. Gold nanoparticles functionalized with therapeutic and targeted peptides for cancer treatment. *Biomaterials*, 33, 1180-1189.
- KUMAR, K. S. 2002. Nutritional approaches to radioprotection: vitamin E. *Military medicine*, 167, 57.
- KUNZ-SCHUGHART, L. A., KREUTZ, M. & KNUECHEL, R. 1998. Multicellular spheroids: a three-dimensional in vitro culture system to study tumour biology. *International journal of experimental pathology*, 79, 1-23.
- KWATRA, D., VENUGOPAL, A. & ANANT, S. 2013. Nanoparticles in radiation therapy: a summary of various approaches to enhance radiosensitization in cancer. *Translational cancer research*, 2, 330-342.
- LACROIX, L., LACOSTE, J., REDDOCH, J. F., MERGNY, J.-L., LEVY, D. D., SEIDMAN, M. M., MATTEUCCI, M. D. & GLAZER, P. M. 1999. Triplex formation by oligonucleotides containing 5-(1-propynyl)-2'-deoxyuridine: Decreased magnesium dependence and improved intracellular gene targeting. *Biochemistry*, 38, 1893-1901.
- LE CAËR, S. 2011. Water radiolysis: influence of oxide surfaces on H₂ production under ionizing radiation. *Water*, 3, 235-253.
- LEE, C.-F., CHANG, C.-L., YANG, J.-C., LAI, H.-Y. & CHEN, C.-H. 2012. Morphological determination of face-centered-cubic metallic nanoparticles by X-ray diffraction. *Journal of colloid and interface science*, 369, 129-133.
- LEHNERT, S. 2014. *Radiosensitizers and radiochemotherapy in the treatment of cancer*, CRC Press.
- LEIST M, SINGLE B, CASTOLDI A.F, KUHNLE S & NICOTERA P 1997. Intracellular adenosine triphosphate (ATP) concentration : a switch in the decision between apoptosis and necrosis. *Journal of experimental medicine*, 185, 1481-1486.
- LEROY C 2009. Radiation interaction in matter and principles of detection. *American institute of physics*, 958, 85-91.
- LEVY, R., SHAHEEN, U., CESBRON, Y. & SEE, V. 2010. Gold nanoparticles delivery in mammalian live cells: a critical review. *Nano reviews*, 1, 1-18.
- LI, J. J., HARTONO, D., ONG, C. N., BAY, B. H. & YUNG, L. Y. 2010. Autophagy and oxidative stress associated with gold nanoparticles. *Biomaterials*, 31, 5996-6003.
- LIN, Y., MCMAHON, S. J., SCARPELLI, M., PAGANETTI, H. & SCHUEMANN, J. 2014. Comparing gold nano-particle enhanced radiotherapy with protons, megavoltage photons and kilovoltage photons: a Monte Carlo simulation. *Physics in medicine and biology*, 59, 7675.
- LIU M, GU X, ZHANG K, DING Y, WEI X, ZHANG X & ZHAO Y 2013. Gold nanoparticles trigger apoptosis and necrosis in lung cancer cells with low intracellular glutathione. *Journal of nanoparticles respiration*, 15, 1-14.
- LONGMIRE, M., CHOYKE, P. L. & KOBAYASHI, H. 2008. Clearance properties of nano-sized particles and molecules as imaging agents: considerations and caveats.
- LORD-FONTAINE, S. & AVERILL-BATES, D. A. 2002. Heat shock inactivates cellular antioxidant defenses against hydrogen peroxide: protection by glucose. *Free Radical Biology and Medicine*, 32, 752-765.
- LOUIS, C. & PLUCHERY, O. 2012. *Gold nanoparticles for physics, chemistry and biology*, World Scientific.

- LUCLETTE, M., KORIDECK, H., MAKRIGIORGOS, M., TILLEMENT, O. & BERBECO, R. 2014. Radiation dose enhancement of gadolinium-based AGuIX nanoparticles on HeLa cells. *Nanomedicine: Nanotechnology, Biology and Medicine*, 10, 1751-1755.
- LUKYANOV, K. A. & BELOUSOV, V. V. 2014. Genetically encoded fluorescent redox sensors. *Biochimica et Biophysica Acta (BBA)-General Subjects*, 1840, 745-756.
- LUND, T., CALLAGHAN, M. F., WILLIAMS, P., TURMAINE, M., BACHMANN, C., RADEMACHER, T., ROITT, I. M. & BAYFORD, R. 2011. The influence of ligand organization on the rate of uptake of gold nanoparticles by colorectal cancer cells. *Biomaterials*, 32, 9776-9784.
- LUSHCHAK, V. I. 2012. Glutathione homeostasis and functions: potential targets for medical interventions. *Journal of Amino Acids*, 2012, 736837.
- LV, S., SONG, W., TANG, Z., LI, M., YU, H., HONG, H. & CHEN, X. 2014. Charge-conversional PEG-polypeptide polyionic complex nanoparticles from simple blending of a pair of oppositely charged block copolymers as an intelligent vehicle for efficient antitumor drug delivery. *Molecular pharmaceuticals*, 11, 1562-1574.
- MA, C. M. C. 2013. *Proton and carbon ion therapy*, Boca Raton, Boca Raton : Taylor & Francis.
- MA, X., WU, Y., JIN, S., TIAN, Y., ZHANG, X., ZHAO, Y., YU, L. & LIANG, X.-J. 2011. Gold nanoparticles induce autophagosome accumulation through size-dependent nanoparticle uptake and lysosome impairment. *ACS nano*, 5, 8629-8639.
- MADHANKUMAR, A., SLAGLE-WEBB, B., MINTZ, A., SHEEHAN, J. M. & CONNOR, J. R. 2006. Interleukin-13 receptor-targeted nanovesicles are a potential therapy for glioblastoma multiforme. *Molecular cancer therapeutics*, 5, 3162-3169.
- MAGGIORELLA, L., BAROUCH, G., DEVAUX, C., POTTIER, A., DEUTSCH, E., BOURHIS, J., BORGHI, E. & LEVY, L. 2012. Nanoscale radiotherapy with hafnium oxide nanoparticles. *Future oncology*, 8, 1167-1181.
- MALVY, C., HAREL-BELLAN, A. & PRITCHARD, L. L. 1999. *Triple helix forming oligonucleotides*, Springer Science & Business Media.
- MANEVICH, Y., HELD, K. D. & BIAGLOW, J. E. 1997. Coumarin-3-carboxylic acid as a detector for hydroxyl radicals generated chemically and by gamma radiation. *Radiation research*, 148, 580-591.
- MANKE, A., WANG, L. & ROJANASAKUL, Y. 2013. Mechanisms of nanoparticle-induced oxidative stress and toxicity. *BioMed research international*, 2013.
- MAO, Z., WANG, B., MA, L., GAO, C. & SHEN, J. 2007. The influence of polycaprolactone coating on the internalization and cytotoxicity of gold nanoparticles. *Nanomedicine: Nanotechnology, Biology, and Medicine*, 3, 215-223.
- MARQUEZ, M., NILSSON, S., LENNARTSSON, L., LIU, Z., TAMMELA, T., RAITANEN, M. & HOLMBERG, A. R. 2004. Charge-dependent targeting: results in six tumor cell lines. *Anticancer research*, 24, 1347-1352.
- MASTERS, J. R. W. & PALSSON B 1998. *Cancer cell lines Part 1* Kluwer Academic Publishers.
- MAYLES, P., NAHUM, A. & ROSENWALD, J.-C. 2007. *Handbook of radiotherapy physics: theory and practice*, CRC Press.
- MCCULLY, M., HERNANDEZ, Y., CONDE, J., BAPTISTA, P., FUENTE, J., HURSTHOUSE, A., STIRLING, D. & BERRY, C. 2015. Significance of the balance between intracellular glutathione and polyethylene glycol for successful release of small interfering RNA from gold nanoparticles. *Nano Research*, 8, 3281-3292.
- MCGUFFIE, E. M., PACHECO, D., CARBONE, G. M. R. & CATAPANO, C. V. 2000. Antigenic and antiproliferative effects of a c-myc-targeting phosphorothioate triple helix-forming oligonucleotide in human leukemia cells. *Cancer Research*, 60, 3790-3799.
- MCMAHON, S. J., HYLAND, W. B., MUIR, M. F., COULTER, J. A., JAIN, S., BUTTERWORTH, K. T., SCHETTINO, G., DICKSON, G. R., HOUNSELL, A. R., O'SULLIVAN, J. M., PRIZE, K. M., HIRST, D. G. & CURRELL, F. J. 2011. Biological consequences of nanoscale energy deposition near irradiated heavy atom nanoparticles. *Scientific reports*, 1.
- MCMAHON, S. J., PAGANETTI, H. & PRISE, K. M. 2015. Optimising element choice for nanoparticle radiosensitisers. *Nanoscale*, 8, 581-589.
- MCMULLIN, J. 2016. Cancer. *Annual review of anthropology*, 45, 251-251.

- MEHMOOD, R. K. 2014. Review of cisplatin and oxaliplatin in current immunogenic and monoclonal antibody treatments. *Oncology reviews*, 8.
- MESBAHI, A. 2010. A review on gold nanoparticles radiosensitization effect in radiation therapy of cancer. *Reports of Practical Oncology & Radiotherapy*, 15, 176-180.
- MESBAHI, A., JAMALI, F. & GHAREHAGHAJI, N. 2013. Effect of photon beam energy, gold nanoparticle size and concentration on the dose enhancement in radiation therapy. *Bioimpacts*, 3, 29-35.
- METRO, G., FABI, A., MIRRI, M., VIDIRI, A., PACE, A., CAROSI, M., RUSSILLO, M., MASCHIO, M., GIANNARELLI, D., PELLEGRINI, D., POMPILI, A., COGNETTI, F. & CARAPPELLA, C. 2010. Phase II study of fixed dose rate gemcitabine as radiosensitizer for newly diagnosed glioblastoma multiforme. *Cancer Chemotherapy and Pharmacology*, 65, 391-397.
- METZ, J. M., SMITH, D., LUSTIG, R., GLATSTEIN, E., HAHN, S. M., MICK, R., MITCHELL, J. & CHERAKURI, M. 2004. A phase I study of topical tempol for the prevention of alopecia induced by whole brain radiotherapy. *Clinical Cancer Research*, 10, 6411-6417.
- MIKKELSEN, R. B. & WARDMAN, P. 2003. Biological chemistry of reactive oxygen and nitrogen and radiation-induced signal transduction mechanisms. *Oncogene*, 22, 5734.
- MILADI, I., ALOY, M.-T., ARMANDY, E., MOWAT, P., KRYZA, D., MAGNÉ, N., TILLEMENT, O., LUX, F., BILLOTEY, C. & JANIER, M. 2015. Combining ultrasmall gadolinium-based nanoparticles with photon irradiation overcomes radioresistance of head and neck squamous cell carcinoma. *Nanomedicine: Nanotechnology, Biology and Medicine*, 11, 247-257.
- MILLER, D. M., THOMAS, S. D., ISLAM, A., MUENCH, D. & SEDORIS, K. 2012. c-Myc and cancer metabolism. *Clinical cancer research*, 18, 5546-53.
- MIRJOLET, C., PAPA, A., CRÉHANGE, G., RAGUIN, O., SEIGNEZ, C., PAUL, C., TRUC, G., MAINGON, P. & MILLOT, N. 2013. The radiosensitization effect of titanate nanotubes as a new tool in radiation therapy for glioblastoma: a proof-of-concept. *Radiotherapy and Oncology*, 108, 136-142.
- MIRONAVA, T., HADIJARGYROU, M., SIMON, M., JURUKOVSKI, V. & RAFAILOVICH, M. H. 2010. Gold nanoparticles cellular toxicity and recovery: effect of size, concentration and exposure time. *Nanotoxicology*, 4, 120-137.
- MISAWA M & TAKAHASHI J 2011. Generation of reactive oxygen species induced by gold nanoparticles under x-ray and UV Irradiations. *Nanomedicine: Nanotechnology, biology and medicine*, 7, 604-614.
- MITSUDOME, T., YAMAMOTO, M., MAENO, Z., MIZUGAKI, T., JITSUKAWA, K. & KANEDA, K. 2015. One-step Synthesis of Core-Gold/Shell-Ceria Nanomaterial and Its Catalysis for Highly Selective Semihydrogenation of Alkynes. *Journal of the American Chemical Society*, 137, 13452.
- MKANDAWIRE, M. M., LAKATOS, M., SPRINGER, A., CLEMENS, A., APPELHANS, D., KRAUSE-BUCHHOLZ, U., POMPE, W., RDEL, G. & MKANDAWIRE, M. 2015. Induction of apoptosis in human cancer cells by targeting mitochondria with gold nanoparticles. *Nanoscale*, 7, 10634-10640.
- MODING, E. J., KASTAN, M. B. & KIRSCH, D. G. 2013. Strategies for optimizing the response of cancer and normal tissues to radiation. *Nature Reviews Drug Discovery*, 12, 528-542.
- MONTAGNANI, F., TURRISI, G., MARINOZZI, C., ALIBERTI, C. & FIORENTINI, G. 2011. Effectiveness and safety of oxaliplatin compared to cisplatin for advanced, unresectable gastric cancer: a systematic review and meta-analysis. *Gastric Cancer*, 14, 50-55.
- MOWAT, P., MIGNOT, A., RIMA, W., LUX, F., TILLEMENT, O., ROULIN, C., DUTREIX, M., BECHET, D., HUGER, S. & HUMBERT, L. 2011. In vitro radiosensitizing effects of ultrasmall gadolinium based particles on tumour cells. *Journal of nanoscience and nanotechnology*, 11, 7833-7839.
- MOZUMDER, A. & HATANO, Y. 2003. *Charged particle and photon interactions with matter: chemical, physicochemical, and biological consequences with applications*, CRC press.

- MRAKOVČIĆ M, MEINDL C, ROBLEGG E & FRÖHLICH E 2014. Reaction of monocytes to polystyrene and silica nanoparticles in short-term and long-term exposures. *Toxicology research*, 3, 86-97.
- MU, X., ZHANG, F., KONG, C., ZHANG, H., ZHANG, W., GE, R., LIU, Y. & JIANG, J. 2017. EGFR-targeted delivery of DOX-loaded Fe₃O₄@polydopamine multifunctional nanocomposites for MRI and antitumor chemo-photothermal therapy. *International journal of nanomedicine*, 12, 2899-2911.
- MUDDINETI O.S, GHOSH B & BISWAS S 2015. Current trends in using polymer coated gold nanoparticles for cancer therapy. *International journal of pharmaceutics*, 484, 252-267.
- MURAMATSU, A. & MIYASHITA, T. 2009. *Nano-hybridization of organic-inorganic materials*, Springer.
- NAZIR S, HUSSAIN T, AYUB A, RASHID U & MACROBERT A.J 2014. Nanomaterials in combating cancer: therapeutic applications and developments. *Nanomedicine: nanotechnology, biology and medicine*, 10, 19-34.
- NEL, A. E., MÄDLER, L., VELEGOL, D., XIA, T., HOEK, E. M., SOMASUNDARAN, P., KLAESSIG, F., CASTRANOVA, V. & THOMPSON, M. 2009. Understanding biophysicochemical interactions at the nano–bio interface. *Nature materials*, 8, 543-557.
- NICOL, J. R., HARRISON, E., O'NEILL, S. M., DIXON, D., MCCARTHY, H. O. & COULTER, J. A. 2018. Unraveling the cell-type dependent radiosensitizing effects of gold through the development of a multifunctional gold nanoparticle. *Nanomedicine: Nanotechnology, Biology and Medicine*, 14, 439-449.
- NIEMANTSVERDIET, M., VAN GOETHEM, M.-J., BRON, R., HOGWERF, W., BRANDENBURG, S., LANGENDIJK, J. A., VAN LUIJK, P. & COPPES, R. P. High and low LET radiation differentially induce normal tissue damage signals. *International Journal of Radiation Oncology • Biology • Physics*, 83, 1291-1297.
- OGAWA, K., ITO, Y., HIROKAWA, N., SHIBUYA, K., KOKUBO, M., OGO, E., SHIBUYA, H., SAITO, T., ONISHI, H. & KARASAWA, K. 2012. Concurrent radiotherapy and gemcitabine for unresectable pancreatic adenocarcinoma: impact of adjuvant chemotherapy on survival. *International Journal of Radiation Oncology* Biology* Physics*, 83, 559-565.
- OGAWA, Y., CHEN, Z.-S. & YANG, D.-H. 2016. Paradigm Shift in Radiation Biology/Radiation Oncology-xploitation of the "H₂O₂ Effect" for radiotherapy using low-LET (Linear Energy Transfer) radiation such as X-rays and high-energy electrons. *Cancers*, 8.
- OROSZ, Á., B?SZE, S., MEZ, G., SZABÓ, I., HERÉNYI, L. & CSÍK, G. 2017. Oligo- and polypeptide conjugates of cationic porphyrins: binding, cellular uptake, and cellular localization. *The forum for amino acid, peptide and protein research*, 49, 1263-1276.
- ORTHABER, A., LÖFÁS, H., ÖBERG, E., GRIGORIEV, A., WALLNER, A., JAFRI, S. H. M., SANTONI, M. P., AHUJA, R., LEIFER, K. & OTTOSSON, H. 2015. Cooperative gold nanoparticle stabilization by acetylenic phosphalkenes. *Angewandte Chemie International Edition*, 54, 10634-10638.
- PAN, Y., LEIFERT, A., RUAU, D., NEUSS, S., BORNEMANN, J., SCHMID, G., BRANDAU, W., SIMON, U. & JAHNEN-DECHENT, W. 2009. Gold nanoparticles of diameter 1.4 nm trigger necrosis by oxidative stress and mitochondrial damage. *Small*, 5, 2067-2076.
- PAN, Y., NEUSS, S., LEIFERT, A., FISCHLER, M., WEN, F., SIMON, U., SCHMID, G., BRANDAU, W. & JAHNEN-DECHENT, W. 2007. Size-dependent cytotoxicity of gold nanoparticles. *Small*, 3, 1941-1949.
- PARK, E.-J., CHOI, J., PARK, Y.-K. & PARK, K. 2008. Oxidative stress induced by cerium oxide nanoparticles in cultured BEAS-2B cells. *Toxicology*, 245, 90-100.
- PARK, W. H., HAN, Y. W., KIM, S. W., KIM, S. H., CHO, K. W. & KIM, S. Z. 2007. Antimycin A induces apoptosis in As4.1 juxtglomerular cells. *Cancer letters*, 251, 68-77.
- PARSHAD, R., GANTT, R., SANFORD, K. K. & JONES, G. M. 1984. Chromosomal radiosensitivity of human tumor cells during the G2 cell cycle period. *Cancer research*, 44, 5577.
- PASZEK M.J, DUFORT C.C, ROSSIER O, BAINER R, MOUW J.K, GODULA K, HUDAK J.E, LAKINS J.N, WIJEKOON A.C, CASSEREAU L, RUBASHKIN M.G, MAGBANUA M, THORN K.S, DAVIDSON M.W, RUGO H.S, PARK J.W, HAMMER D.A, GIANNONE G, BERTOZZI C.R & V.M, W. 2014.

- The cancer glycocalyx mechanically primes integrin-mediated growth and survival. *Nature* 511, 319-324.
- PATEL, S., JUNG, D., YIN, P. T., CARLTON, P., YAMAMOTO, M., BANDO, T., SUGIYAMA, H. & LEE, K. B. 2014. NanoScript: a nanoparticle-based artificial transcription factor for effective gene regulation. *ACS Nano*, 8, 8959-8967.
- PATRA, H. K., BANERJEE, S., CHAUDHURI, U., LAHIRI, P. & DASGUPTA, A. K. 2007. Cell selective response to gold nanoparticles. *Nanomedicine: nanotechnology, biology and medicine*, 3, 111-119.
- PAVLIN, M. & BREGAR, V. B. 2012. Stability of nanoparticle suspensions in different biologically relevant media. *Digest journal of nanomaterials and biostructures*, 7, 1389-1400.
- PERNODET N, FANG X, SUN Y, BAKHTINA A, RAMAKRISHNAN A, SOKOLOV J, ULMAN A & M, R. 2006. Adverse effects of citrate/gold nanoparticles on human dermal fibroblasts. *Small*, 2, 766 – 773.
- PIKTEL, E., NIEMIROWICZ, K., WATEK, M., WOLLNY, T., DEPTUAA, P. & BUCKI, R. 2016. Recent insights in nanotechnology-based drugs and formulations designed for effective anti-cancer therapy.(Report). *Journal of Nanobiotechnology*, 14.
- PISSUWAN, D., NIIDOME, T. & CORTIE, M. B. 2011. The forthcoming applications of gold nanoparticles in drug and gene delivery systems. *Journal of Controlled Release*, 149, 65-71.
- PLUCHERY, O. 2012. Optical properties of gold nanoparticles. In: LOUIS, C. & PLUCHERY, O. (eds.) *Gold Nanoparticles for physics, chemistry and biology*. Imperial College Press.
- PODGORSKAK, E. B. 2003. Review of radiation oncology physics: a handbook for teachers and students. *Vienna, Austria: IAE Agency*.
- PORCEL, E., LIEHN, S., REMITA, H., USAMI, N., KOBAYASHI, K., FURUSAWA, Y., LE SECH, C. & LACOMBE, S. 2010a. Platinum nanoparticles: a promising material for future cancer therapy? *Nanotechnology*, 21, 085103.
- PORCEL, E., LIEHN, S., REMITA, H., USAMI, N., KOBAYASHI, K., FURUSAWA, Y., LE SECH, C. & LACOMBE, S. 2010b. Platinum nanoparticles; a promising material for future cancer therapy ? *Nanotechnology*, 21.
- PORCEL, E., LIEHN, S., REMITA, H., USAMI, N., KOBAYASHI, K., FURUSAWA, Y., SECH, C. L. & LACOMBE, S. 2010c. Platinum nanoparticles: a promising material for future cancer therapy? *Nanotechnology*, 21, 085103.
- POWELL, C., MIKROPOULOS, C., KAYE, S. B., NUTTING, C. M., BHIDE, S. A., NEWBOLD, K. & HARRINGTON, K. J. 2010a. Pre-clinical and clinical evaluation of PARP inhibitors as tumour-specific radiosensitisers. *Cancer Treatment Reviews*, 36, 566-575.
- POWELL, C., MIKROPOULOS, C., KAYE, S. B., NUTTING, C. M., BHIDE, S. A., NEWBOLD, K. & HARRINGTON, K. J. 2010b. Pre-clinical and clinical evaluation of PARP inhibitors as tumour-specific radiosensitisers. *Cancer treatment reviews*, 36, 566-575.
- PRADHAN, A. K., NAHAR, S. N., MONTENEGRO, M., YAN, Y., ZHANG, H. L., SUR, C., MROZIK, M. & PITZER, R. M. 2009. Resonant x-ray enhancement of the Auger effect in high-Z atoms, molecules, and nanoparticles: potential biomedical applications.(Report). *Journal of Physical Chemistry A*, 113, 12356-12363.
- PUJALTÉ, I., PASSAGNE, I., DACULSI, R., DE PORTAL, C., OHAYON-COURTÈS, C. & L'AZOU, B. 2015. Cytotoxic effects and cellular oxidative mechanisms of metallic nanoparticles on renal tubular cells: impact of particle solubility. *Toxicology research*, 4, 409-422.
- RAHMAN, S. 2016. Size and concentration analysis of gold nanoparticles with ultraviolet-visible spectroscopy. *Undergraduate Journal of Mathematical Modeling: One + Two*, 7.
- RAHMAN W.N, BISHARA N, ACKERLY T, HE C.F, JACKSON P, WONG C, DAVIDSON B & GESO M 2009. Enhancement of radiation effects by gold nanoparticles for superficial radiation therapy. *Nanomedicine: nanotechnology, biology, and medicine*, 5, 136-142.
- RAHMAN, W. N., BISHARA, N., ACKERLY, T., HE, C. F., JACKSON, P., WONG, C., DAVIDSON, R. & GESO, M. 2009. Enhancement of radiation effects by gold nanoparticles for superficial radiation therapy. *Nanomedicine: Nanotechnology, Biology and Medicine*, 5, 136-142.
- RAJU, M. 2012. *Heavy particle radiotherapy*, Elsevier.

- RALEIGH, D. R. & HAAS-KOGAN, D. A. 2013. Molecular targets and mechanisms of radiosensitization using DNA damage response pathways. *Future oncology (London, England)*, 9, 219-233.
- RASHID, R. A., RAZAK, K. A., GESO, M., ABDULLAH, R., DOLLAH, N. & RAHMAN, W. 2018. Radiobiological Characterization of the Radiosensitization Effects by Gold Nanoparticles for Megavoltage Clinical Radiotherapy Beams. *BioNanoScience*, 1-10.
- RETIF, P., PINEL, S., TOUSSAINT, M., FROCHOT, C., CHOUIKRAT, R., BASTOGNE, T. & BARBERI-HEYOB, M. 2015. Nanoparticles for Radiation Therapy Enhancement: the Key Parameters. *Theranostics*.
- REZAEI-TAVIRANI, M., DOLAT, E., HASANZADEH, H., SEYYEDI, S. S., SEMNANI, V. & SOBHI, S. 2013. TiO₂ Nanoparticle as a sensitizer drug in radiotherapy: in vitro study. *Iranian Journal of Cancer Prevention*.
- ROA, W., ZHANG, X., GUO, L., SHAW, A., HU, X., XIONG, Y., GULAVITA, S., PATEL, S., SUN, X., CHEN, J., MOORE, R. & XING, J. Z. 2009. Gold nanoparticle sensitize radiotherapy of prostate cancer cells by regulation of the cell cycle. *Nanotechnology*, 20, 375101.
- ROESSLEIN, M., HIRSCH, C., KAISER, J.-P., KRUG, H. F. & WICK, P. 2013. Comparability of in vitro tests for bioactive nanoparticles: a common assay to detect reactive oxygen species as an example. *International journal of molecular sciences*, 14, 24320-24337.
- ROGOSNITZKY, M. & BRANCH, S. 2016. Gadolinium-based contrast agent toxicity: a review of known and proposed mechanisms. *Biometals*, 29, 365-376.
- ROSA, S., CONNOLLY, C., SCETTINO, G., BUTTERWORTH, K. T. & PRISE, K. M. 2017. Biological mechanisms of gold nanoparticle radiosensitization. *Cancer Nanotechnology*, 8, 2.
- S WADAJKAR, A., U MENON, J., KADAPURE, T., T TRAN, R., YANG, J. & T NGUYEN, K. 2013. Design and application of magnetic-based theranostic nanoparticle systems. *Recent patents on biomedical engineering*, 6, 47-57.
- SAIJO, N. 2002. Irinotecan combined with radiation therapy for patients with stage III non-small-cell lung cancer: Current trials. *Clinical Lung Cancer*, 4, S21-S25.
- SANCEY, L., LUX, F., KOTB, S., ROUX, S., DUFORT, S., BIANCHI, A., CRÉMILLIEUX, Y., FRIES, P., COLL, J. L., RODRIGUEZ-LAFRASSE, C., JANIER, M., DUTREIX, M., BARBERI-HEYOB, M., BOSCHETTI, F., DENAT, F., LOUIS, C., PORCEL, E., LACOMBE, S., LE DUC, G., DEUTSCH, E., PERFETTINI, J. L., DETAPPE, A., VERRY, C., BERBECO, R., BUTTERWORTH, K. T., MCMAHON, S. J., PRISE, K. M., PERRIAT, P. & TILLEMENT, O. 2014. The use of theranostic gadolinium-based nanoprobe to improve radiotherapy efficacy. *The British Journal of Radiology*, 87, 20140134.
- SCHAEUBLIN, N. M., BRAYDICH-STOLLE, L. K., SCHRAND, A. M., MILLER, J. M., HUTCHISON, J., SCHLAGER, J. J. & HUSSAIN, S. M. 2011a. Surface charge of gold nanoparticles mediates mechanism of toxicity. *Nanoscale*, 3.
- SCHAEUBLIN, N. M., BRAYDICH-STOLLE, L. K., SCHRAND, A. M., MILLER, J. M., HUTCHISON, J., SCHLAGER, J. J. & HUSSAIN, S. M. 2011b. Surface charge of gold nanoparticles mediates mechanism of toxicity. *Nanoscale*, 3, 410-420.
- SCHALOW, T., LAURIN, M., BRANDT, B., SCHAUERMANN, S., GUIMOND, S., KUHNENBECK, H., STARR, D. E., SHAIKHUTDINOV, S. K., LIBUDA, J. & FREUND, H. J. 2005. Oxygen storage at the metal/oxide interface of catalyst nanoparticles. *Angewandte Chemie International Edition*, 44, 7601-7605.
- SCHLATHÖLTER, T., EUSTACHE, P., PORCEL, E., SALADO, D., STEFANCIKOVA, L., TILLEMENT, O., LUX, F., MOWAT, P., BIEGUN, A. K. & VAN GOETHEM, M.-J. 2016. Improving proton therapy by metal-containing nanoparticles: nanoscale insights. *International journal of nanomedicine*, 11, 1549.
- SCHOLLBACH M, ZHANG F, ROOSEN-RUNGE F, SKODAM.W.A, JACOBS R.M.J & SCHREIBER F 2014. Gold nanoparticles decorated with oligo(ethylene glycol) thiols: surface charges and interactions with proteins in solution. *Journal of colloid and interface science*, 426, 31-38.
- SCHWAB, M. 2008. *Encyclopedia of cancer*, Springer Science & Business Media.

- SCIENTIFIC, T. F. 2013-2017. XPS [Online]. Available: <https://xpssimplified.com/elements/sulfur.php>.
- SEDELNIKOVA, O. A., LUU, A. N., KARAMYCHEV, V. N., PANYUTIN, I. G. & NEUMANN, R. D. 2001. Development of DNA-based radiopharmaceuticals carrying Auger-electron emitters for antigene radiotherapy. *International Journal of Radiation Oncology, Biology, Physics*, 49, 391-396.
- SETUA, S., OUBERAI, M., PICCIRILLO, S. G., WATTS, C. & WELLAND, M. 2014. Cisplatin-tethered gold nanospheres for multimodal chemo-radiotherapy of glioblastoma. *The royal society of chemistry*.
- SHARMA, U., PAL, D. & PRASAD, R. 2014. Alkaline Phosphatase: An Overview. *Indian Journal of Clinical Biochemistry*, 29, 269-278.
- SHCHERBAKOV, A., ZHOLOBAK, N., SPIVAK, N. & IVANOV, V. 2014. Advances and prospects of using nanocrystalline ceria in cancer theranostics. *Russian Journal of Inorganic Chemistry*, 59, 1556-1575.
- SHELTON, J. W., WAXWEILER, T. V., LANDRY, J., GAO, H., XU, Y., WANG, L., EL-RAYES, B. & SHU, H.-K. G. 2013. In vitro and in vivo enhancement of chemoradiation using the oral PARP inhibitor ABT-888 in colorectal cancer cells. *Internation journal of radiation oncology, biology, physics*, 86, 469-476.
- SHEN, W.-J., HSIEH, C.-Y., CHEN, C.-L., YANG, K.-C., MA, C.-T., CHOI, P.-C. & LIN, C.-F. 2013. A modified fixed staining method for the simultaneous measurement of reactive oxygen species and oxidative responses. *Biochemical and biophysical research communications*, 430, 442-447.
- SHUKLA, R., BANSAL, V., CHAUDHARY, M., BASU, A., BHONDE, R. R. & SASTRY, M. 2005. Biocompatibility of gold nanoparticles and their endocytotic fate inside the cellular compartment: a microscopic overview. *Langmuir*, 21, 10644-10654.
- SINGH, V. K., BEATTIE, L. A. & SEED, T. M. 2013. Vitamin E: tocopherols and tocotrienols as potential radiation countermeasures. *Journal of radiation research*, 54, 973-988.
- SMALL JR, W. 2008. *Combining targeted biological agents with radiotherapy: Current status and future directions*, Demos Medical Publishing.
- SMALLA, K., JECHALKE, S. & TOP, E. M. 2015. Plasmid detection, characterization and ecology. *Microbiology spectrum*, 3.
- ŚMIAŁEK, M. 2007. *Damage to DNA induced by low energy electrons and photons : mechanisms and analysis at the molecular level*. Thesis (PhD) - Open University. BLDSC no.DXN116696.
- ŚMIAŁEK, M. A., HOFFMANN, S. V., FOLKARD, M., PRISE, K. M., SHUKER, D. E. G., BRAITHWAITE, N. S. & MASON, N. J. 2008. Vuv irradiation studies of plasmid dna in aqueous solution. *Journal of Physics: Conference Series*, 101, 012020.
- SMITH, L., KUNCIC, Z., OSTRIKOV, K. & KUMAR, S. 2012. Nanoparticles in cancer imaging and therapy. *Journal of Nanomaterials*, 2012, 7.
- SOTTER, E., VILANOVA, X., LLOBET, E., STANKOVA, M. & CORREIG, X. 2005. Niobium-doped titania nanopowders for gas sensor applications. *Journal of Optoelectronic and Advanced Materials*, 7, 1395-1398.
- SOUSA, A. A., MORGAN, J. T., BROWN, P. H., ADAMS, A., JAYASEKARA, M. P. S., ZHANG, G., ACKERSON, C. J., KRUEHLAK, M. J. & LEAPMAN, R. D. 2012. Synthesis, characterization, and direct intracellular imaging of ultrasmall and uniform glutathione-coated gold nanoparticles. *Small*, 8, 2277-2286.
- STORHOFF, J. J., ELGHANIAN, R., MUCIC, R. C., MIRKIN, C. A. & LETSINGER, R. L. 1998. One-pot colorimetric differentiation of polynucleotides with single base imperfections using gold nanoparticle probes. *Journal of the American Chemical Society*, 120, 1959.
- SUN, C., LI, H. & CHEN, L. 2012. Nanostructured ceria-based materials: synthesis, properties, and applications. *Energy & Environmental Science*, 5, 8475-8505.
- SUZUKI, K., HOSOKAWA, K. & MAEDA, M. 2009. Controlling the number and positions of oligonucleotides on gold nanoparticle surfaces. *Journal of the American Chemical Society*, 131, 7518-7519.

- TAN, Y., LI, Y. & ZHU, D. 2004. Noble metal nanoparticles. *Encyclopedia of nanoscience and nanotechnology*, 8, 9-40.
- TATON, T. A. 2001. Preparation of gold nanoparticle–DNA conjugates. *Current Protocols in Nucleic Acid Chemistry*. John Wiley & Sons, Inc.
- TAUPIN, F., FLAENDER, M., DELORME, R., BROCHARD, T., MAYOL, J.-F., ARNAUD, J., PERRIAT, P., SANCEY, L., LUX, F., BARTH, R. F., CARRIÈRE, M., RAVANAT, J.-L. & ELLEAUME, H. 2015. Gadolinium nanoparticles and contrast agent as radiation sensitizers. *Physics in Medicine and Biology*, 60, 4449-4464.
- THAKOR, A. S., PAULMURUGAN, R., KEMPEN, P., ZAVALITA, C., SINCLAIR, R., MASSOUD, T. F. & GAMBHIR, S. S. 2011. Oxidative stress mediates the effects of raman-active gold nanoparticles in human cells. *Small*, 7, 126-136.
- TKACHENKO, A. G., XIE, H., COLEMAN, D., GLOMM, W., RYAN, J., ANDERSON, M., FRANZEN, S. & FELDHEIM, D. L. 2003. Multifunctional gold nanoparticle-peptide complexes for nuclear targeting. *Journal of the American Chemical Society*, 125, 4700-4701.
- TORRE, L. A., BRAY, F., SIEGEL, R. L., FERLAY, J., LORTET-TIEULENT, J. & JEMAL, A. 2015. Global cancer statistics, 2012. *CA: a cancer journal for clinicians*, 65, 87-108.
- TORRES, M. & FORMAN, H. J. 2003. Redox signaling and the MAP kinase pathways. *Biofactors*, 17, 287-296.
- TOWNLEY, H. E., RAPA, E., WAKEFIELD, G. & DOBSON, P. J. 2012. Nanoparticle augmented radiation treatment decreases cancer cell proliferation. *Nanomedicine: Nanotechnology, Biology, and Medicine*, 8, 526-536.
- TRAPANI, G., DENORA, N., TRAPANI, A. & LAQUINTANA, V. 2012. Recent advances in ligand targeted therapy. *Journal of drug targeting*, 20, 1-22.
- TSOLI, M., KUHN, H., BRANDAU, W., ESCHÉ, H. & SCHMID, G. 2005. Cellular uptake and toxicity of Au55 cluster *Small*, 1, 841-844.
- TUBIANA, M., DUTREIX, J. & WAMBERSIE, A. 1990. *Introduction to radiobiology*, CRC Press.
- VAN ZANDWIJK, N. 1995. N-acetylcysteine (NAC) and glutathione (GSH): Antioxidant and chemopreventive properties, with special reference to lung cancer. *Journal of cellular biochemistry*, 58, 24-32.
- VASQUEZ, K. M. & GLAZER, P. M. 2002. Triplex-forming oligonucleotides: principles and applications. *Quarterly reviews of biophysics*, 35, 89-107.
- WAGNER, J. M. 2010. *X-Ray Photoelectron Spectroscopy*, Hauppauge, Hauppauge: Nova Science Publishers, Inc.
- WANG, C., LI, X., WANG, Y., LIU, Z., FU, L. & HU, L. 2013. Enhancement of radiation effect and increase of apoptosis in lung cancer cells by thio-glucose-bound gold nanoparticles at megavoltage radiation energies. *An Interdisciplinary Forum for Nanoscale Science and Technology*, 15, 1-12.
- WANG, X., PEREZ, E., LIU, R., YAN, R. J., MALLET, R. T. & YANG, S. H. 2007. Pyruvate protects mitochondria from oxidative stress in human neuroblastoma SK-N-SH cells. *Brain research*, 1132, 1-9.
- WANG, Y.-C. A., ENGELHARD, M. H., BAER, D. R. & CASTNER, D. G. 2016. Quantifying the impact of nanoparticle coatings and non-uniformities on XPS analysis: gold/silver core-shell nanoparticles. *Analytical Chemistry*, 88.
- WANG, Y. H., SHUANG, L., ZHANG, G., ZHOU, C. Q., ZHU, H. X., ZHOU, X. B., QUAN, L. P., BAI, J. F. & XU, N. Z. 2005. Knockdown of c-Myc expression by RNAi inhibits MCF-7 breast tumor cells growth in vitro and in vivo. *Breast cancer research*, 7, R220-R228.
- WARNER, M. G., REED, S. M. & HUTCHISON, J. E. 2000. Small, water-soluble, ligand-stabilized gold nanoparticles synthesized by interfacial ligand exchange reactions. *Chemistry of Materials*, 12, 3316-3320.
- WASON, M. S., COLON, J., DAS, S., SEAL, S., TURKSON, J., ZHAO, J. & BAKER, C. H. 2013. Sensitization of pancreatic cancer cells to radiation by cerium oxide nanoparticle-induced ROS production. *Nanomedicine: Nanotechnology, Biology and Medicine*, 9, 558-569.
- WATT, T. A., MCCLEERY, R. H. & HART, T. 2007. *Introduction to statistics for biology*, CRC Press.

- WEBER, G. F. 2007. *Molecular mechanisms of cancer*, Springer Science & Business Media.
- WOLFE, T., CHATTERJEE, D., LEE, J., GRANT, J. D., BHATTARAI, S., TAILOR, R., GOODRICH, G., NICOLUCCI, P. & KRISHNAN, S. 2015. Targeted gold nanoparticles enhance sensitization of prostate tumors to megavoltage radiation therapy in vivo. *Nanomedicine: Nanotechnology, Biology, and Medicine*, 11, 1277-1283.
- WORMAN, H. & COURVALIN, J.-C. 2000. The inner nuclear membrane. *Journal of Membrane Biology*, 177, 1-11.
- WU, M. & SWARTZ, M. A. 2014. Modeling tumor microenvironments in vitro. *Journal of biomechanical engineering*, 136, 021011.
- WU, Q., GADDIS, S. S., MACLEOD, M. C., WALBORG, E. F., THAMES, H. D., DIGIOVANNI, J. & VASQUEZ, K. M. 2007. High affinity Triplex-forming oligonucleotide target sequences in mammalian genomes. *Molecular carcinogenesis*, 46, 15-23.
- XAVIER, S., PIEK, E., FUJII, M., JAVELAUD, D., MAUVIEL, A., FLANDERS, K. C., SAMUNI, A. M., FELICI, A., REISS, M. & YARKONI, S. 2004. Amelioration of radiation-induced fibrosis inhibition of transforming growth factor- β signaling by halofuginone. *Journal of Biological Chemistry*, 279, 15167-15176.
- XIA, T., KOVOCHICH, M., LIONG, M., MÄDLER, L., GILBERT, B., SHI, H., YEH, J. I., ZINK, J. I. & NEL, A. E. 2008. Comparison of the mechanism of toxicity of zinc oxide and cerium oxide nanoparticles based on dissolution and oxidative stress properties. *ACS nano*, 2, 2121-2134.
- XODO, L. E., ALUNNI-FABBRONI, M., MANZINI, G. & QUADRIFOGLIO, F. 1993. Sequence-specific DNA-triplex formation at imperfect homopurine-homopyrimidine sequences within a DNA plasmid. *The FEBS Journal*, 212, 395-401.
- YAH, C. S. 2013. The toxicity of gold nanoparticles in relation to their physiochemical properties. *Biochemical research*, 24, 400-413.
- YANG, J., SU, Y. & RICHMOND, A. 2007. Antioxidants tiron and N-acetyl-L-cysteine differentially mediate apoptosis in melanoma cells via a reactive oxygen species-independent NF κ B pathway. *Free Radical Biology and Medicine*, 42, 1369-1380.
- YONAMINE, Y., YOSHIMATSY, K., LEE, S. H., HOSHINO, Y., OKAHATA, Y. & SHEA, K. 2013. Polymer nanoparticle-protein interface. Evaluation of the contribution of positively charged functional groups to protein affinity. *American chemical society Applied materials and interfaces*, 5, 374-379.
- YU, C. H., ODURO, W., TAM, K. & E.S.C., T. 2008. Some Applications of Nanoparticles. In: BLACKMAN, J. (ed.) *Metallic nanoparticles*.
- ZAFFARONI, N., PANNATI, M. & DIADONE, M. G. 2005. Survivin as a target for new anticancer interventions. *Journal of Cellular and Molecular Medicine*, 9, 360-372.
- ZARSCHLER, K., ROCKS, L., LICCIARDELLO, N., BOSELLI, L., POLO, E., GARCIA, K. P., DE COLA, L., STEPHAN, H. & DAWSON, K. A. 2016. Ultrasmall inorganic nanoparticles: State-of-the-art and perspectives for biomedical applications. *Nanomedicine: Nanotechnology, Biology, and Medicine*, 12, 1663-1701.
- ZELLER, K. I., ZHAO, X., LEE, C. W. H., CHIU, K. P., YAO, F., YUSTEIN, J. T., OOI, H. S., ORLOV, Y. L., SHAHAB, A., YONG, H. C., FU, Y., WENG, Z., KUZNETSOV, V. A., SUNG, W.-K., RUAN, Y., DANG, C. V. & WEI, C.-L. 2006. Global mapping of c-myc binding sites and target gene networks in human B cells. *Proceedings of the National Academy of Sciences*, 103, 17834.
- ZHANG, S. X., GAO, J., BUCHHOLZ, T. A., WANG, Z., SALEHPOUR, M. R., DREZEK, R. A. & YU, T. K. 2009. Quantifying tumor-selective radiation dose enhancements using gold nanoparticles: a monte carlo simulation study. *Biomedical microdevices*.
- ZHANG, W., LI, Y., NIU, J. & CHEN, Y. 2013. Photogeneration of reactive oxygen species on uncoated silver, gold, nickel, and silicon nanoparticles and their antibacterial effects. *Langmuir*, 29, 4647-4651.
- ZHANG, X., YANG, H., GU, K., CHEN, J., RUI, M. & JIANG, G.-L. 2011. In vitro and in vivo study of a nanoliposomal cisplatin as a radiosensitizer. *International Journal of Nanomedicine*, 6, 437-444.

- ZHANG, X. D., WU, D., SHEN, X., CHEN, J., SUN, Y. M., LIU, P. X. & LIANG, X. J. 2012. Size-dependent radiosensitization of PEG-coated gold nanoparticles for cancer radiation therapy. *Biomaterials*, 33, 6408-6419.
- ZHENG, M., GONG, P., ZHENG, C., ZHAO, P., LUO, Z., MA, Y. & CAI, L. 2015. Lipid-polymer nanoparticles for folate-receptor targeting delivery of doxorubicin. *Journal of nanoscience and nanotechnology*, 15, 4792-4798.
- ZHU, A. X. & WILLETT, C. G. 2003. Chemotherapeutic and biologic agents as radiosensitizers in rectal cancer. *Seminars in Radiation Oncology*, 13, 454-468.
- ZHU, C.-D., ZHENG, Q., WANG, L.-X., XU, H.-F., TONG, J.-L., ZHANG, Q.-A., WAN, Y. & WU, J.-Q. 2015. Synthesis of novel galactose functionalized gold nanoparticles and its radiosensitizing mechanism. *Journal of Nanobiotechnology*, 13, 1-11.
- ZHU, M., NIE, G., MENG, H., XIA, T., NEL, A. & ZHAO, Y. 2012. Physicochemical properties determine nanomaterial cellular uptake. *Accounts of chemical research*, 46, 622-631.
- ZHUGE, X., BIAN, Z., LUO, Z., MU, Y. & LUO, K. Adsorption and exchange kinetics of hydrophilic and hydrophobic phosphorus ligands on gold surface. IOP Conference Series: Materials Science and Engineering, 2017. IOP Publishing, 012015.
- ZIMBONE, M., CALCAGNO, L., MESSINA, G., BAERI, P. & COMPAGNINI, G. 2011. Dynamic light scattering and UV-vis spectroscopy of gold nanoparticles solution. *Materials Letters*, 65, 2906-2909.
- ZOLOTOYABKO, E. 2014. *Basic concepts of X-ray diffraction*, John Wiley & Sons.

ANNEXES

1. Annexes related to Chapter 2

1.1. α Gal :PEGamine AuNPs concentration

AuNPs	Concentration ($\mu\text{g} / \text{ml}$)
100 :0 α Gal :PEGamine AuNPs	1317
80 :20 α Gal :PEGamine AuNPs	1310
60 :40 α Gal :PEGamine AuNPs	1039
40 :60 α Gal :PEGamine AuNPs	1256
20 :80 α Gal :PEGamine AuNPs	1250
0 :100 α Gal :PEGamine AuNPs	1265
50 :50 α Gal :PEGamine AuNPs	1033
50 :50 β Glc :PEGamine AuNPs	1000
50 :50 NaGlul :PEGamine AuNPs	1000

1.2. Consumables

- 15 ml and 50 ml tubes, sterile, graduation and writing area (Greiner bio one[®], 188261, 227270)
- 0.5 ml Eppendorf (Greiner bio one[®], 667201)
- 1.5 ml Eppendorf (Greiner bio one[®], 676201)
- Pipette 5ml, 10ml, 25ml (Cellstar[®], greiner bio one[®], 606180, 607180, 760 180)
- Dispenser tips non sterile, 2.5ml, (Fisherbrand[®], 13-668-704)
- Dispenser tips sterile, 12.5ml (Fisherbrand[®], 13-668-717)
- Aspiration pipette (Cellstar[®], greiner bio one[®], 710183)
- Graduated filter tips Tip One[®] 10 μl , 20 μl , 200 μl , 1000 μl (Starlab[®], S1121-3810, S1120-1810, S1120-8810, S1126-7810)
- pH fix 0-14 (Fisherbrand[®], AO17986)

2. Annexes related to Chapter 3

2.1. Statistical difference between AuNPs coated with different sugars

2.1.1. Statistical differences in dose responses for each AuNPs on each cell line was analysed by two way Anova followed by a Dunnett's multiple comparisons test. * represents $p < 0.05$, ** represents $p < 0.01$, *** represents $p < 0.001$ and **** represents $p < 0.0001$.

AuNPs α Gal:PEGamine exposure

Dunnett's multiple comparisons test	Mean Diff.	95% CI of diff.	Summary
HSC-3			
0 vs. 0.3	22.19	2.934 to 41.44	*
0 vs. 1	61.56	42.30 to 80.81	****
0 vs. 3	94.99	75.74 to 114.2	****
0 vs. 10	100.0	80.75 to 119.3	****
0 vs. 30	100.0	80.75 to 119.3	****
Hacat			
0 vs. 0.3	19.22	-0.03321 to 38.47	ns
0 vs. 1	14.96	-4.298 to 34.21	ns
0 vs. 3	19.65	0.3926 to 38.90	*
0 vs. 10	19.26	0.004603 to 38.51	*
0 vs. 30	26.84	7.585 to 46.09	**

AuNPs β Glu:PEGamine exposure

Dunnett's multiple comparisons test	Mean Diff.	95% CI of diff.	Summary
HSC-3			
0 vs. 0.3	29.91	15.37 to 44.44	****
0 vs. 1	73.81	59.27 to 88.34	****
0 vs. 3	98.33	83.79 to 112.9	****
0 vs. 10	100.0	85.47 to 114.5	****
0 vs. 30	100.0	85.47 to 114.5	****
Hacat			
0 vs. 0.3	13.10	-1.436 to 27.63	ns
0 vs. 1	13.24	-1.292 to 27.78	ns
0 vs. 3	26.30	11.77 to 40.84	****
0 vs. 10	32.67	18.14 to 47.21	****
0 vs. 30	36.63	22.10 to 51.17	****

AuNPs GlcNac:PEGamine exposure

Dunnett's multiple comparisons test	Mean Diff.	95% CI of diff.	Summary
HSC-3			
0 vs. 0.3	16.24	-9.565 to 42.04	ns
0 vs. 1	31.88	6.078 to 57.68	**
0 vs. 3	56.56	30.76 to 82.36	****
0 vs. 10	83.64	57.84 to 109.4	****
0 vs. 30	100.0	74.20 to 125.8	****
Hacat			
0 vs. 0.3	10.57	-15.23 to 36.37	ns
0 vs. 1	18.93	-6.868 to 44.73	ns
0 vs. 3	14.13	-11.67 to 39.93	ns
0 vs. 10	11.31	-14.49 to 37.11	ns
0 vs. 30	25.60	-0.2005 to 51.40	ns

2.1.2. Statistical differences in dose responses for each AuNPs comparing both cell line was determined by two way Anova followed by a Sidak's multiple comparisons tests.

AuNPs α Gal:PEGamine exposure

Sidak's multiple comparisons test	Mean Diff.	95% CI of diff.	Summary
HSC-3 - Hacat			
0	-7.629e-006	-20.28 to 20.28	ns
0.3	-2.967	-23.25 to 17.32	ns
1	-46.60	-66.88 to -26.32	****
3	-75.34	-95.63 to -55.06	****
10	-80.74	-101.0 to -60.46	****
30	-73.16	-93.44 to -52.88	****

AuNPs β Glu:PEGamine exposure

Sidak's multiple comparisons test	Mean Diff.	95% CI of diff.	Summary
HSC-3 - Hacat			
0	-7.629e-006	-15.31 to 15.31	ns
0.3	-16.81	-32.12 to -1.499	*
1	-60.56	-75.88 to -45.25	****
3	-72.02	-87.34 to -56.71	****
10	-67.33	-82.64 to -52.02	****
30	-63.37	-78.68 to -48.05	****

AuNPs GlcNac:PEGamine exposure

Sidak's multiple comparisons test	Mean Diff.	95% CI of diff.	Summary
HSC-3 - Hacat			
0	-7.629e-006	-27.18 to 27.18	ns
0.3	-5.662	-32.84 to 21.52	ns
1	-12.95	-40.13 to 14.23	ns
3	-42.43	-69.61 to -15.25	***
10	-72.33	-99.51 to -45.15	****
30	-74.40	-101.6 to -47.22	****

2.2. Dose response for each ratio of α Gal:PEGamine AuNP exposed to adherent cells

2.2.1. Statistical differences in dose responses for the different AuNPs exposure on HSC-3 cells was analysed by two way Anova followed by a Dunnett's multiple comparisons test.

Dunnett's multiple comparisons test	Mean Diff.	95% CI of diff.	Summary
100:0			
0 vs. 0.3	-1.552	-14.73 to 11.63	ns
0 vs. 1	0.8618	-12.32 to 14.04	ns
0 vs. 3	2.795	-10.38 to 15.97	ns
0 vs. 10	9.202	-3.976 to 22.38	ns
0 vs. 30	15.21	2.033 to 28.39	*
80:20			
0 vs. 0.3	0.6235	-12.56 to 13.80	ns
0 vs. 1	4.336	-8.843 to 17.51	ns
0 vs. 3	5.765	-7.413 to 18.94	ns
0 vs. 10	14.00	0.8225 to 27.18	*
0 vs. 30	59.10	45.92 to 72.28	****
60:40			
0 vs. 0.3	4.889	-8.290 to 18.07	ns
0 vs. 1	10.55	-2.630 to 23.73	ns
0 vs. 3	47.74	34.56 to 60.91	****
0 vs. 10	81.26	68.08 to 94.44	****
0 vs. 30	99.25	86.07 to 112.4	****
50:50			
0 vs. 0.3	4.227	-8.952 to 17.41	ns
0 vs. 1	53.47	40.29 to 66.65	****
0 vs. 3	90.32	77.14 to 103.5	****
0 vs. 10	99.59	86.41 to 112.8	****
0 vs. 30	100.0	86.82 to 113.2	****
40:60			
0 vs. 0.3	-11.00	-24.17 to 2.183	ns
0 vs. 1	-10.81	-23.99 to 2.372	ns
0 vs. 3	2.744	-10.44 to 15.92	ns
0 vs. 10	84.37	71.19 to 97.55	****
0 vs. 30	97.95	84.77 to 111.1	****
20:80			
0 vs. 0.3	2.184	-10.99 to 15.36	ns
0 vs. 1	5.053	-8.125 to 18.23	ns
0 vs. 3	8.895	-4.284 to 22.07	ns
0 vs. 10	14.18	0.9992 to 27.36	*
0 vs. 30	75.73	62.55 to 88.91	****
0:100			
0 vs. 0.3	8.046	-5.133 to 21.22	ns
0 vs. 1	6.056	-7.123 to 19.23	ns
0 vs. 3	10.62	-2.560 to 23.80	ns
0 vs. 10	35.67	22.49 to 48.85	****
0 vs. 30	85.37	72.19 to 98.55	****

2.2.2. Statistical differences in dose responses for the different AuNPs exposure on HaCaT cells was analysed by two way Anova followed by a Dunnett's multiple comparisons test.

Dunnett's multiple comparisons test	Mean Diff.	95% CI of diff.	Summary
100:0			
0 vs. 0.3	13.60	0.6321 to 26.56	*
0 vs. 1	8.016	-4.950 to 20.98	ns
0 vs. 3	3.263	-9.704 to 16.23	ns
0 vs. 10	24.94	11.97 to 37.90	****
0 vs. 30	16.75	3.783 to 29.72	**
80:20			
0 vs. 0.3	10.87	-2.099 to 23.83	ns
0 vs. 1	6.325	-6.642 to 19.29	ns
0 vs. 3	-4.010	-16.98 to 8.957	ns
0 vs. 10	18.42	5.452 to 31.38	**
0 vs. 30	23.05	10.09 to 36.02	****
60:40			
0 vs. 0.3	1.845	-11.12 to 14.81	ns
0 vs. 1	-2.169	-15.13 to 10.80	ns
0 vs. 3	-2.719	-15.69 to 10.25	ns
0 vs. 10	38.85	25.88 to 51.81	****
0 vs. 30	23.29	10.32 to 36.25	****
50:50			
0 vs. 0.3	8.728	-4.238 to 21.69	ns
0 vs. 1	7.033	-5.934 to 20.00	ns
0 vs. 3	15.90	2.934 to 28.87	**
0 vs. 10	17.68	4.717 to 30.65	**
0 vs. 30	24.01	11.04 to 36.98	****
40:60			
0 vs. 0.3	-9.971	-22.94 to 2.995	ns
0 vs. 1	-16.42	-29.39 to -3.456	**
0 vs. 3	-2.939	-15.91 to 10.03	ns
0 vs. 10	9.736	-3.231 to 22.70	ns
0 vs. 30	14.43	1.460 to 27.39	*
20:80			
0 vs. 0.3	5.370	-7.596 to 18.34	ns
0 vs. 1	2.010	-10.96 to 14.98	ns
0 vs. 3	0.6429	-12.32 to 13.61	ns
0 vs. 10	6.383	-6.583 to 19.35	ns
0 vs. 30	24.05	11.08 to 37.01	****
0:100			
0 vs. 0.3	14.99	2.027 to 27.96	*
0 vs. 1	6.897	-6.069 to 19.86	ns
0 vs. 3	3.318	-9.648 to 16.28	ns
0 vs. 10	18.58	5.616 to 31.55	**
0 vs. 30	39.30	26.34 to 52.27	****

2.3. Dose response for each ratio of α Gal:PEGamine AuNP exposed to floating cells

2.3.1. Statistical differences in dose responses for the different AuNPs exposure on HSC-3 cells was analysed by two way Anova followed by a Dunnett's multiple comparisons test.

Dunnett's multiple comparisons test	Mean Diff.	95% CI of diff.	Summary
100:0			
0 vs. 0.3	-1.167	-13.02 to 10.69	ns
0 vs. 1	4.844	-7.012 to 16.70	ns
0 vs. 3	12.29	0.4358 to 24.15	*
0 vs. 10	11.36	-0.4971 to 23.22	ns
0 vs. 30	20.17	8.312 to 32.03	***
80:20			
0 vs. 0.3	-2.504	-14.36 to 9.352	ns
0 vs. 1	-7.748	-19.60 to 4.108	ns
0 vs. 3	-16.80	-28.66 to -4.946	**
0 vs. 10	13.42	1.568 to 25.28	*
0 vs. 30	49.90	38.05 to 61.76	****
60:40			
0 vs. 0.3	-4.579	-16.43 to 7.278	ns
0 vs. 1	28.96	17.10 to 40.81	****
0 vs. 3	73.56	61.70 to 85.41	****
0 vs. 10	83.81	71.96 to 95.67	****
0 vs. 30	93.09	81.23 to 104.9	****
50:50			
0 vs. 0.3	8.806	-3.050 to 20.66	ns
0 vs. 1	15.30	3.449 to 27.16	**
0 vs. 3	62.79	50.93 to 74.64	****
0 vs. 10	70.47	58.61 to 82.33	****
0 vs. 30	74.96	63.11 to 86.82	****
40:60			
0 vs. 0.3	4.814	-7.042 to 16.67	ns
0 vs. 1	18.88	7.021 to 30.73	***
0 vs. 3	38.83	26.97 to 50.69	****
0 vs. 10	63.16	51.30 to 75.02	****
0 vs. 30	70.97	59.11 to 82.83	****
20:80			
0 vs. 0.3	2.041	-9.816 to 13.90	ns
0 vs. 1	-8.212	-20.07 to 3.645	ns
0 vs. 3	-1.274	-13.13 to 10.58	ns
0 vs. 10	5.417	-6.439 to 17.27	ns
0 vs. 30	30.67	18.81 to 42.52	****
0:100			
0 vs. 0.3	2.535	-9.322 to 14.39	ns
0 vs. 1	13.37	1.510 to 25.22	*
0 vs. 3	7.346	-4.511 to 19.20	ns
0 vs. 10	33.61	21.76 to 45.47	****
0 vs. 30	66.39	54.54 to 78.25	****

2.3.2. Statistical differences in dose responses for the different AuNPs exposure on HaCaT cells

was analysed by two way Anova followed by a Dunnett's multiple comparisons test.

Dunnett's multiple comparisons test	Mean Diff.	95% CI of diff.	Summary
100:0			
0 vs. 0.3	4.418	-6.209 to 15.05	ns
0 vs. 1	0.8283	-9.799 to 11.46	ns
0 vs. 3	0.6959	-9.932 to 11.32	ns
0 vs. 10	-0.6885	-11.32 to 9.939	ns
0 vs. 30	8.307	-2.321 to 18.93	ns
80:20			
0 vs. 0.3	2.774	-7.854 to 13.40	ns
0 vs. 1	-4.433	-15.06 to 6.195	ns
0 vs. 3	-4.924	-15.55 to 5.704	ns
0 vs. 10	-4.910	-15.54 to 5.717	ns
0 vs. 30	10.44	-0.1834 to 21.07	ns
60:40			
0 vs. 0.3	-0.08218	-10.71 to 10.55	ns
0 vs. 1	-5.935	-16.56 to 4.693	ns
0 vs. 3	-2.688	-13.32 to 7.939	ns
0 vs. 10	10.42	-0.2062 to 21.05	ns
0 vs. 30	17.85	7.220 to 28.47	***
50:50			
0 vs. 0.3	6.231	-4.396 to 16.86	ns
0 vs. 1	-1.979	-12.61 to 8.648	ns
0 vs. 3	5.070	-5.557 to 15.70	ns
0 vs. 10	6.882	-3.746 to 17.51	ns
0 vs. 30	10.90	0.2756 to 21.53	*
40:60			
0 vs. 0.3	-7.182	-17.81 to 3.445	ns
0 vs. 1	-2.083	-12.71 to 8.544	ns
0 vs. 3	0.1385	-10.49 to 10.77	ns
0 vs. 10	-1.867	-12.49 to 8.760	ns
0 vs. 30	10.81	0.1838 to 21.44	*
20:80			
0 vs. 0.3	-1.823	-12.45 to 8.805	ns
0 vs. 1	-5.729	-16.36 to 4.898	ns
0 vs. 3	-2.778	-13.41 to 7.850	ns
0 vs. 10	3.299	-7.329 to 13.93	ns
0 vs. 30	17.66	7.037 to 28.29	***
0:100			
0 vs. 0.3	2.217	-8.410 to 12.84	ns
0 vs. 1	10.41	-0.2220 to 21.03	ns
0 vs. 3	11.80	1.170 to 22.43	*
0 vs. 10	3.062	-7.566 to 13.69	ns
0 vs. 30	30.17	19.54 to 40.80	****

3. Annexes related to Chapter 4

3.1. Duplex formation with the DNA sequences of 23 bp and 70 bp

Lane	Samples	Band 1
1	x	
2	dR1 23	1348
3	dY2 23	1185
4	dR1+dY2	27660
5	dR1 70	12790
6	dY2 70	13256
7	dR1+dY2 70	19459

3.2. Triplex formation with the two duplexes of DNA

3.2.1. Triplex formation at different temperature with the TFO dY3.

lane	Samples	Band 1	Band 2	Band 3	Band 4
1	dY3				9114
2	D23			18451	
3	D70	14241			
4	D23+dY3 RT		21277		10038
5	D23+dY3 4°C		26738		10293
6	D70+dY3 RT	21832			5906
7	D70+dY3 4°C	20676			16409
8	D23+dY3 NI		26923		5768
9	D70+dY3 RT	23441			3756

3.2.2. Triplex formation with different temperature with the TFO-PR.

lane	Samples	Band 1	Band 2	Band 3	Band 4
1	D23				19651
2	D70		17296		
3	D23+PR RT		6945		2250
4	D23+PR 4°C		6664		2231
5	D23+PR NI		6141		1915
6	D70+PR RT	8887			2106
7	D70+PR 4°C	12231			2492
8	D70+PR NI	17135			2848
9	PR				3331

3.2.3. Triplex formation with different concentration of dY3-TFO

lane	Samples	Band 1	Band 2	Band 3	Band 4	Band 5	Band 6	Band 7
1	D23	17125.6						
2	DY3 0.5	1444.9						
3	DY3 1	1605.7						
4	DY3 2	2422.4						
5	DY3 5	4652.2						
6	DY3 10	7775.2						
7	DY3 0.5/1 + D23	307.6 2.2%	13937.4 97.8%					
8	DY3 1/1 + D23	1830.4 14.9%	10390.4 85.1%					
9	DY3 2/1 + D23	4795.8 40.7%	6969.9 59.3%					
10	DY3 5/1 + D23	9219.1 86.7%	1419.6 13.3%					
11	DY3 10/1 + D23	120091 93.3%	874.3 6.7%					
12								
13	Ladder	2129.5 8.7%	3894.8 15.9%	5755.8 23.5%	1505.2 6.1%	3910.2 15.9%	6421.5 26.2%	903.6 3.7%

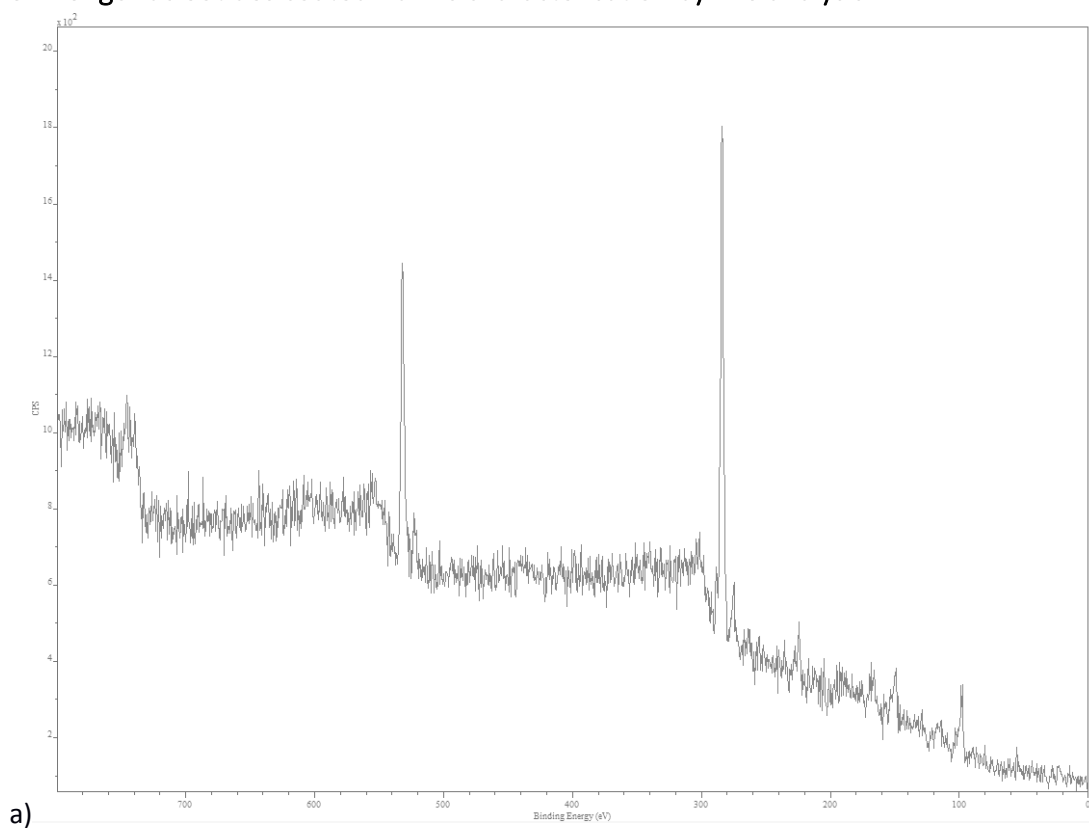
3.2.4. Triplex formation with different concentration of PR-TFO

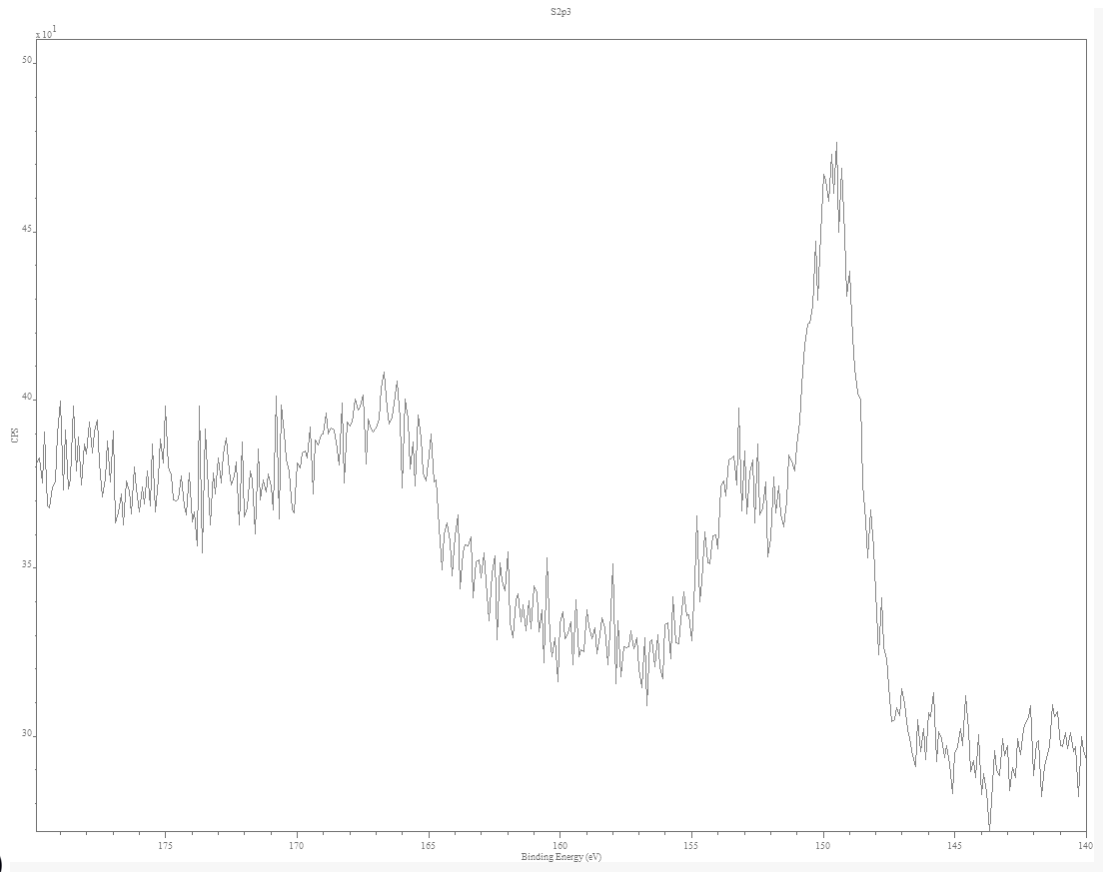
lane	Samples	Band 1	Band 2	Band 3	Band 4	Band 5	Band 6	Band 7
1	D23	19997.1						
2	PR 0.5	1760.9						
3	PR 1	1763.6						
4	PR 2	2654.9						
5	PR 5	4219.6						
6	PR 10	5968.6						
7	PR 0.5/1 + D23	12299.2 53.8%	10565.9 46.2%					
8	PR 1/1 + D23	14950 91%	1471.3 9%					
9	PR 2/1 + D23	16942.64 94%	1070.8 6%					
10	PR 5/1 + D23	16602.23 94.7%	916.9 5.3%	1450.6				
11	PR 10/1 + D23	14737 98.5%	229.5 1.5%	4058.9				
12								
13	Ladder	2554.5 8.3%	4925.916 8.3%	7914.7 25.9%	1597. 5.2%	4902. 16.0%	6930. 22.7%	1769. 5.8%

3.3. Triplex formation within the plasmid and the TFOs DY3 and PR

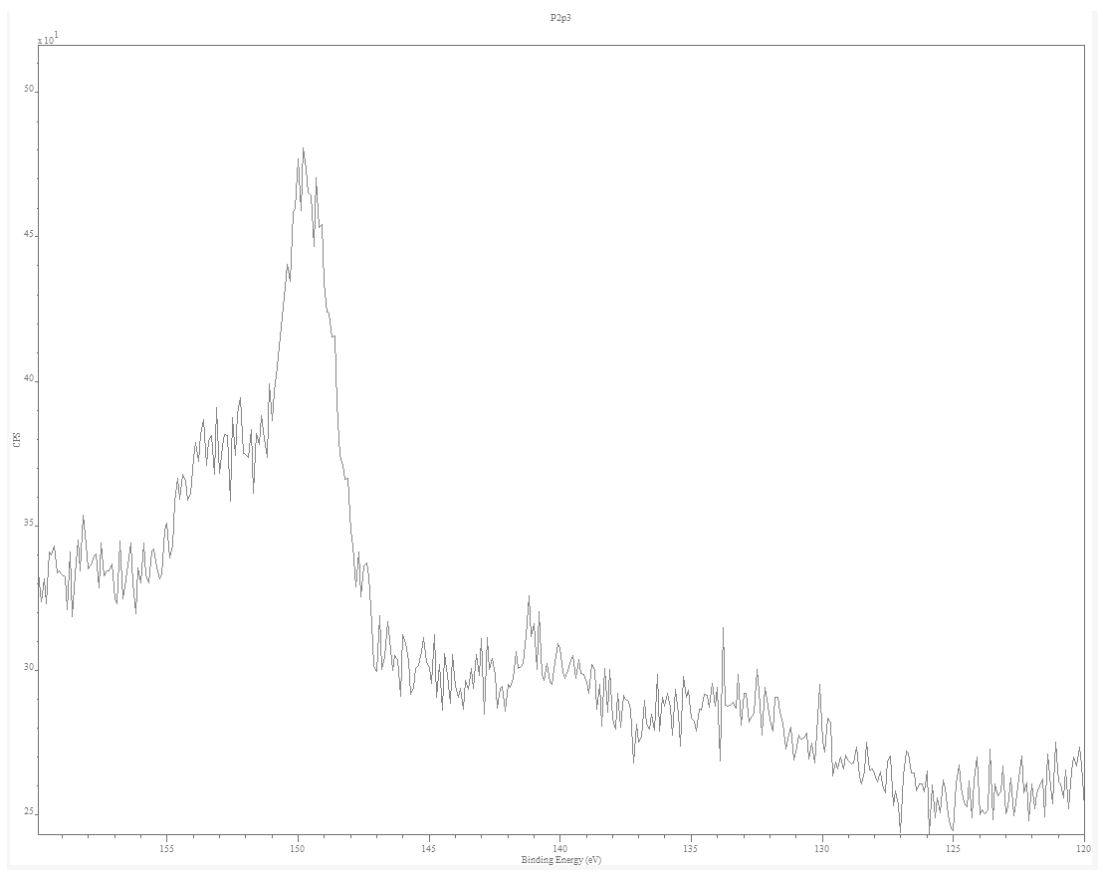
lane	Samples	Band (percentage are compared to PR and DY3 only)
1	PI nicked + PR	5193 (40%)
2	PI nicked + DY3	9251 (51.5%)
3	PI nicked	x
4	PI + PR	12445 (95.7%)
5	PI + DY3	18903 (105%)
6	P	X
7	PR	13010 (100%)
8	DY3	17959 (100%)
9	Ladder	x

3.4. Oligonucleotides coated AuNPs characterisation by XPS analysis

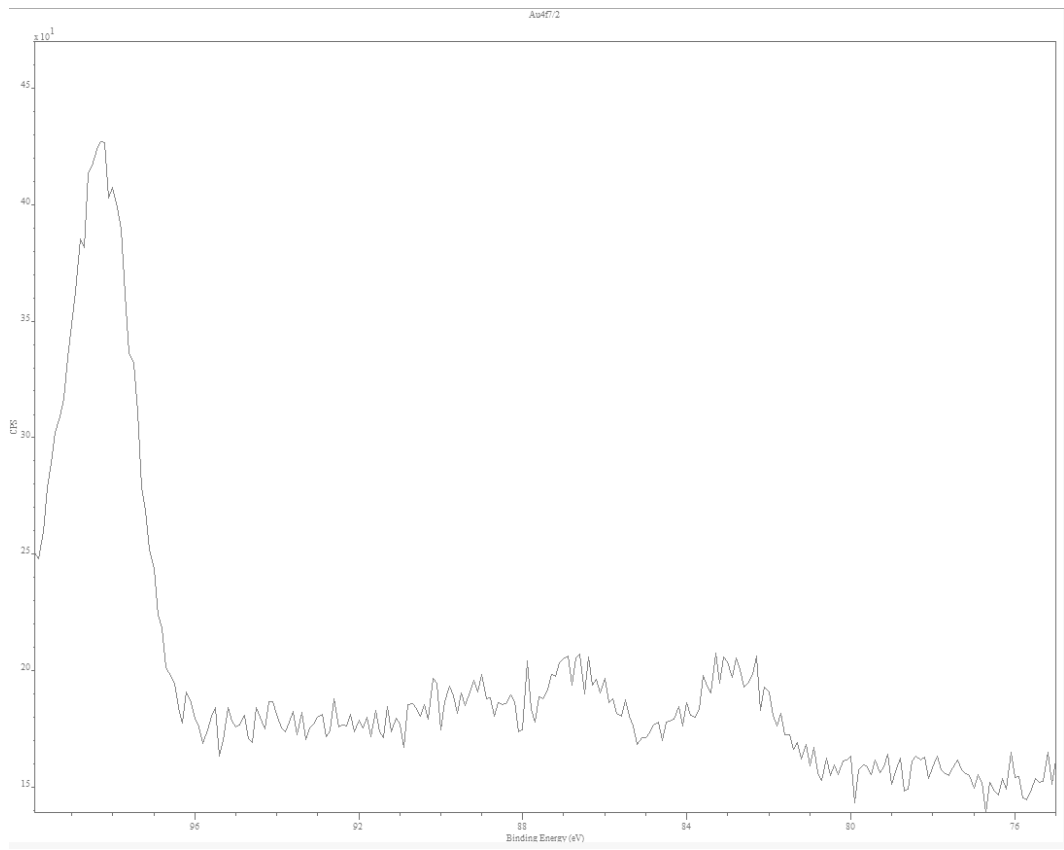




b)

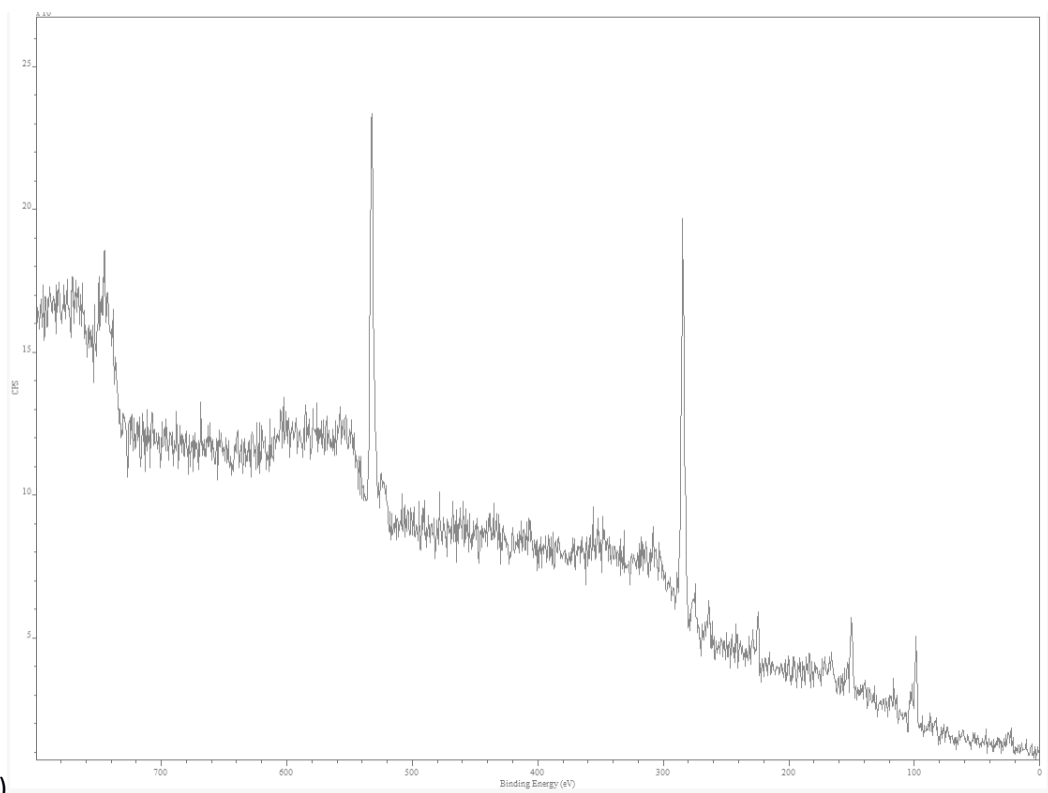


c)

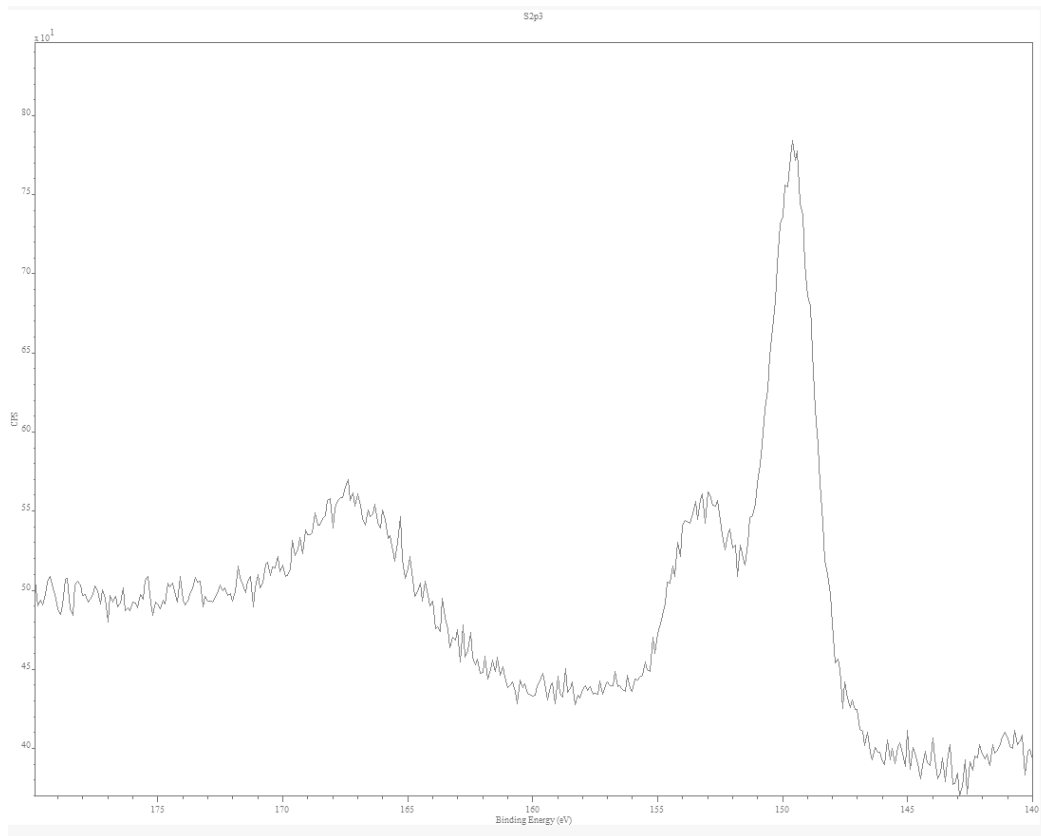


d)

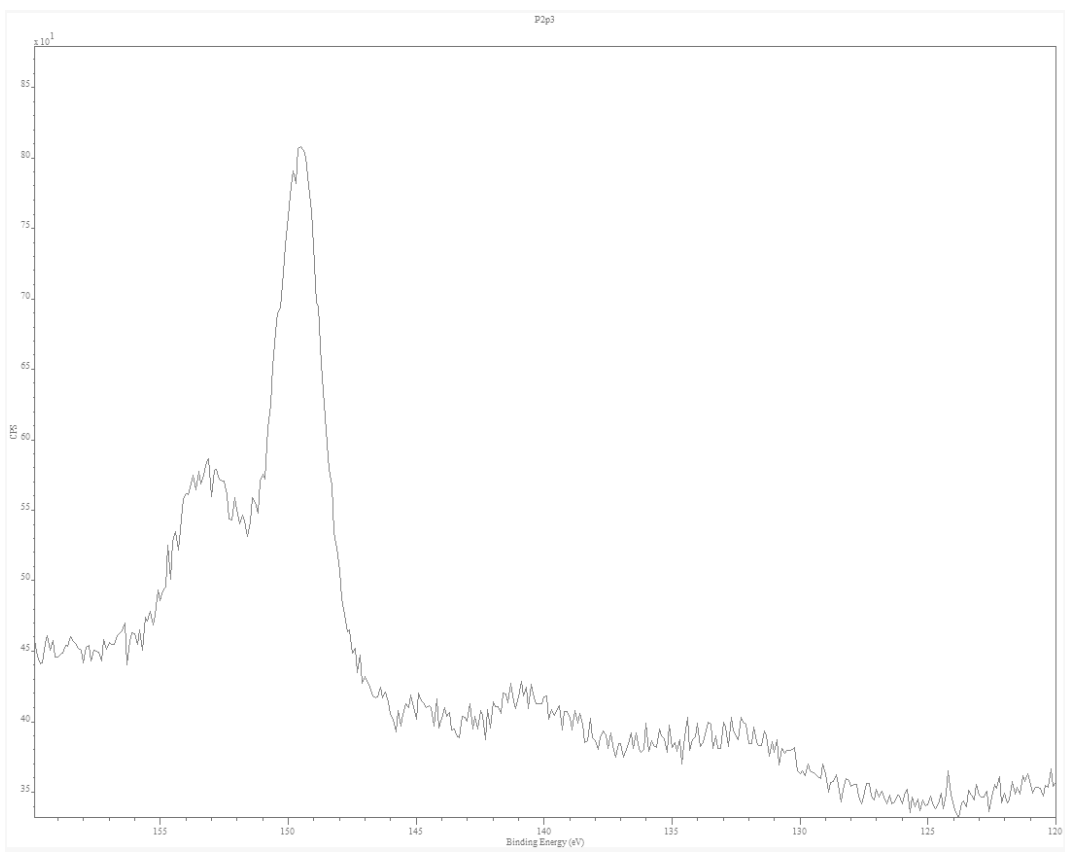
Figure A.1 : XPS analysis of the citrate AuNPs. a) broad spectrum of the AuNPs, b)) S2p, c) P2p, d) Au4f



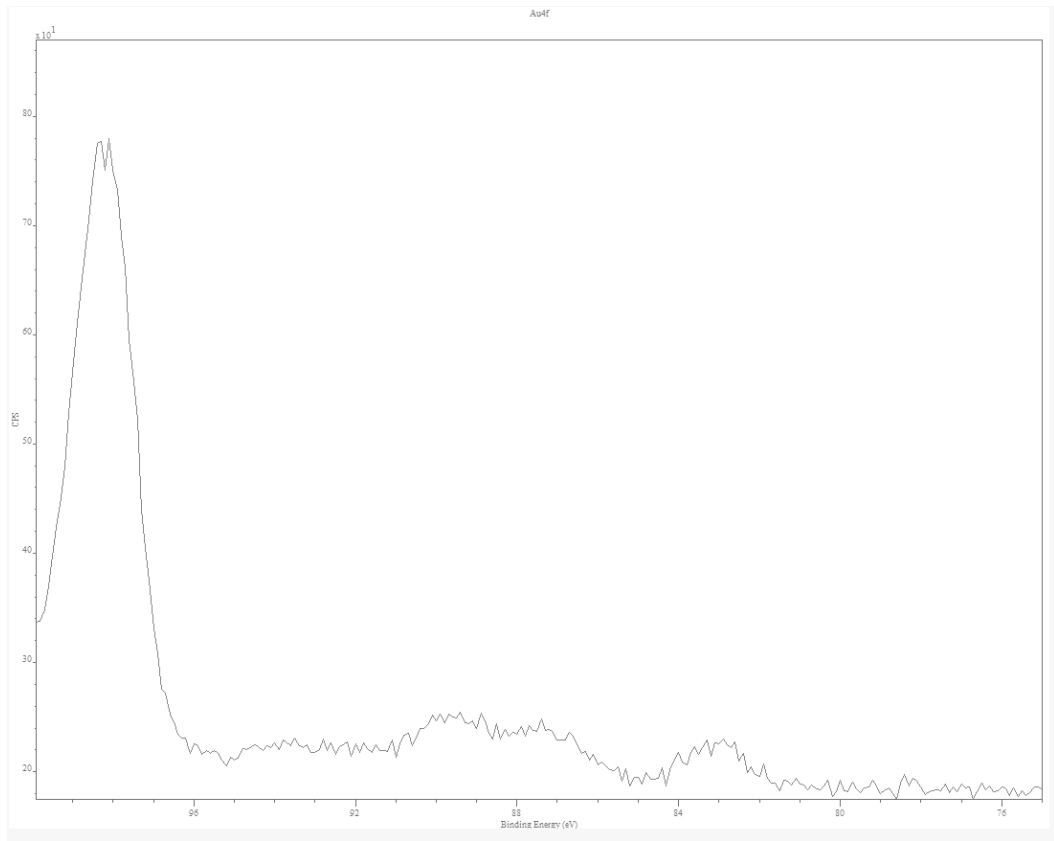
a)



b)

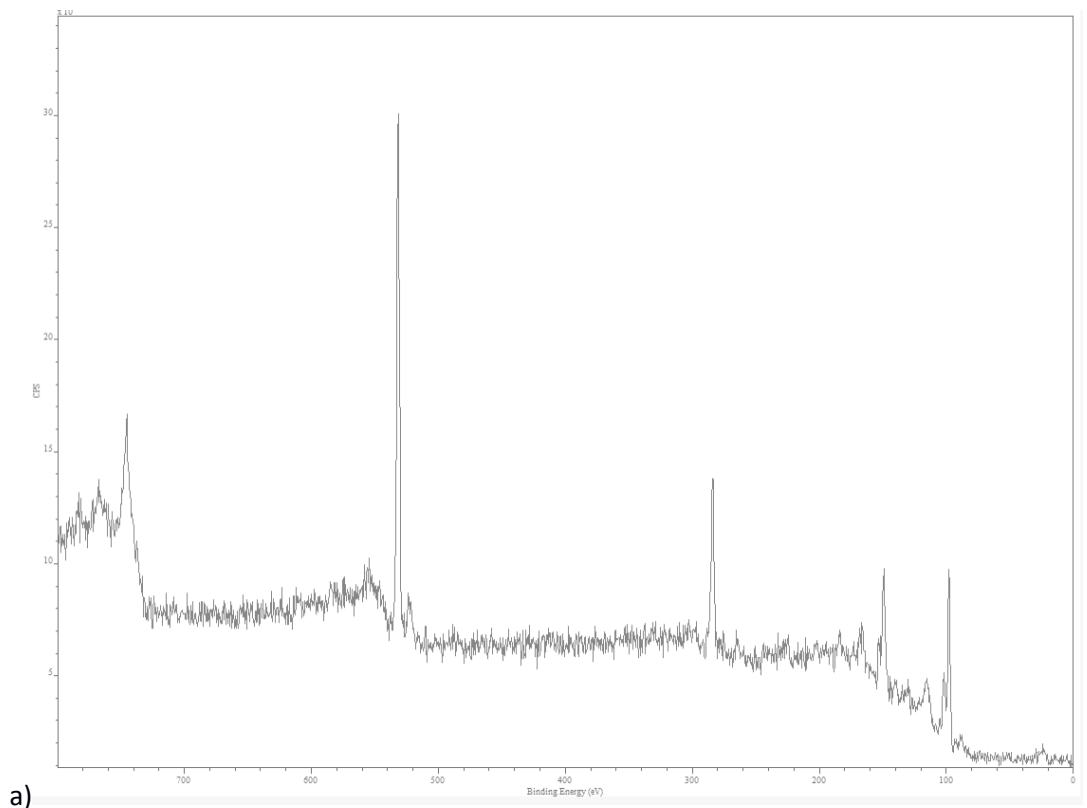


c)

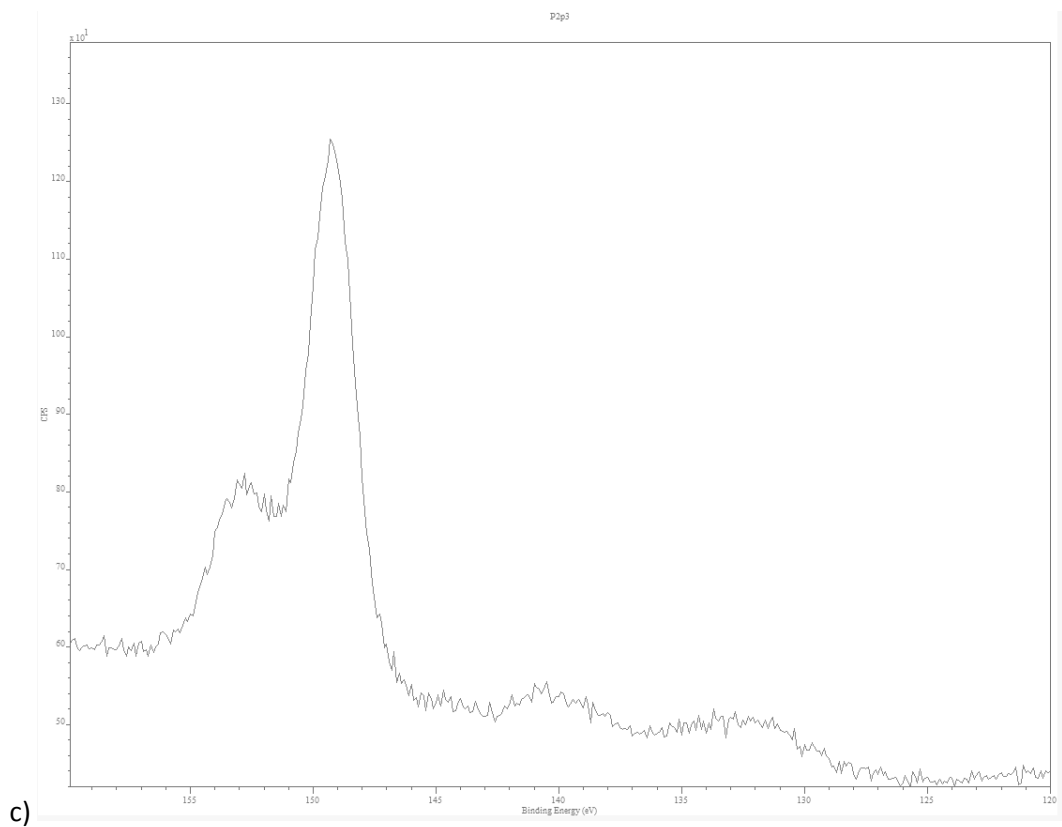
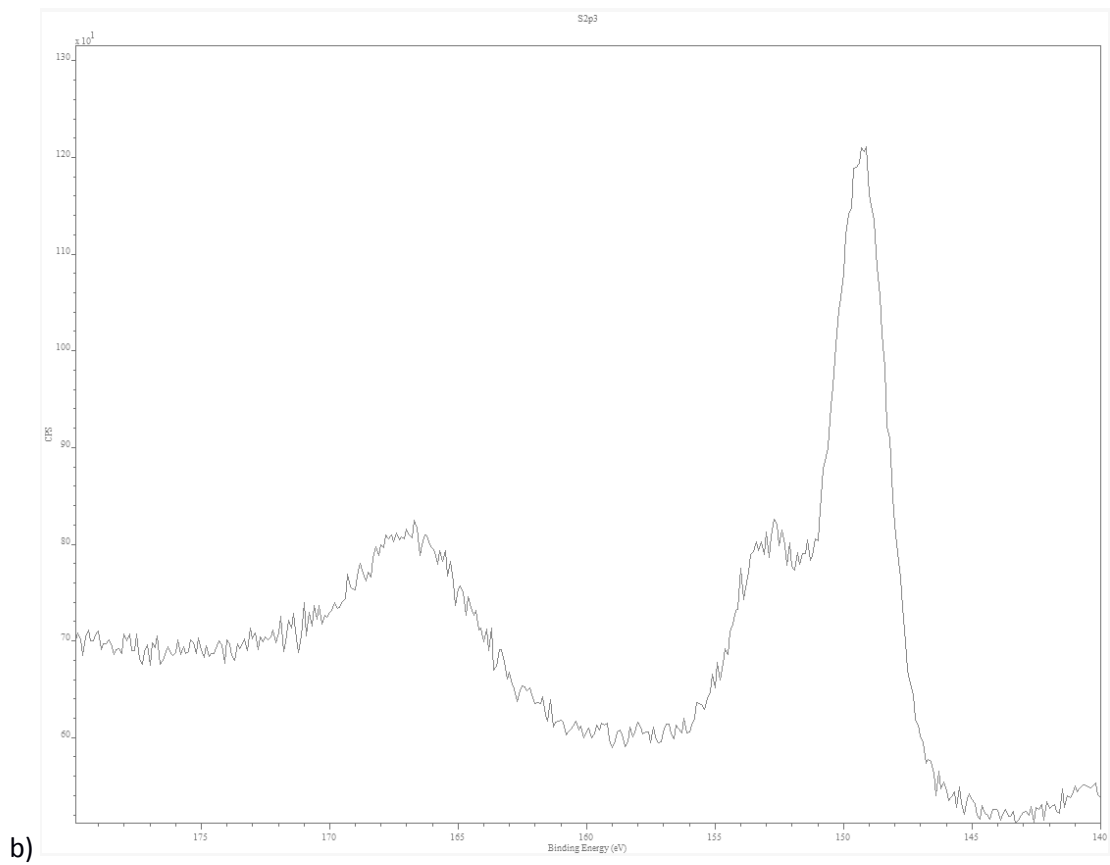


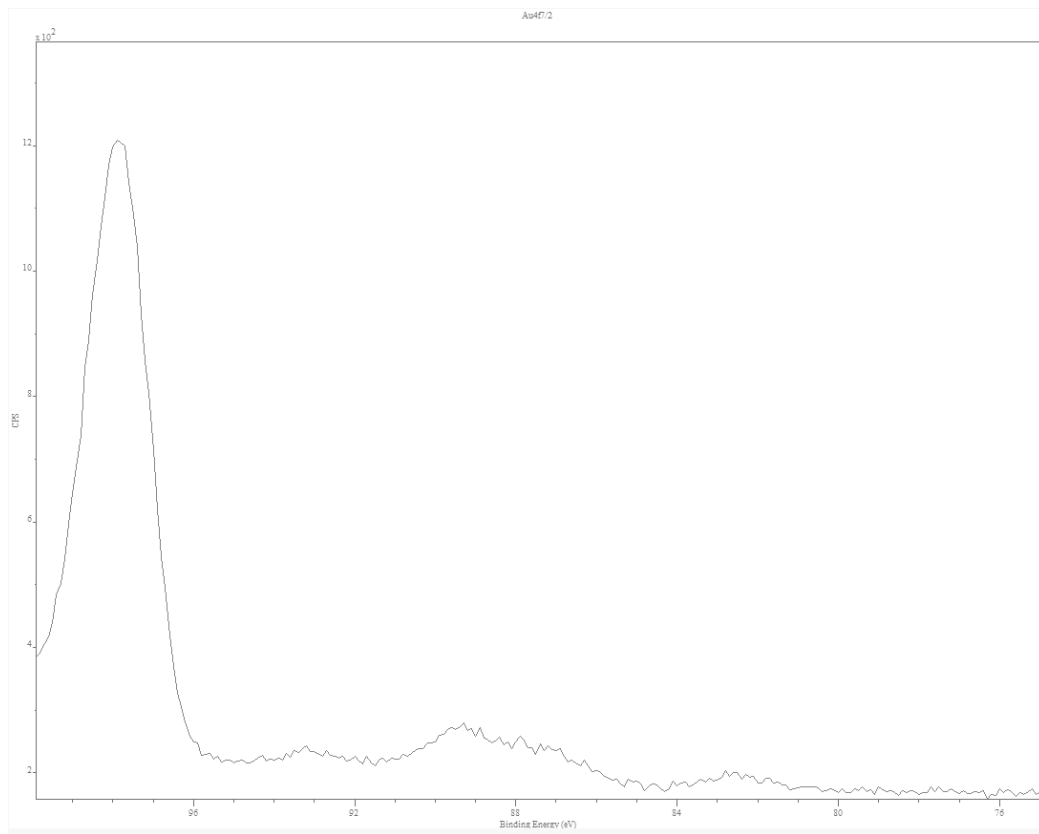
d)

Figure A.2: XPS analysis of the PN AuNPs. a) broad spectrum of the AuNPs, b) S2p, c) P2p, d) Au4f



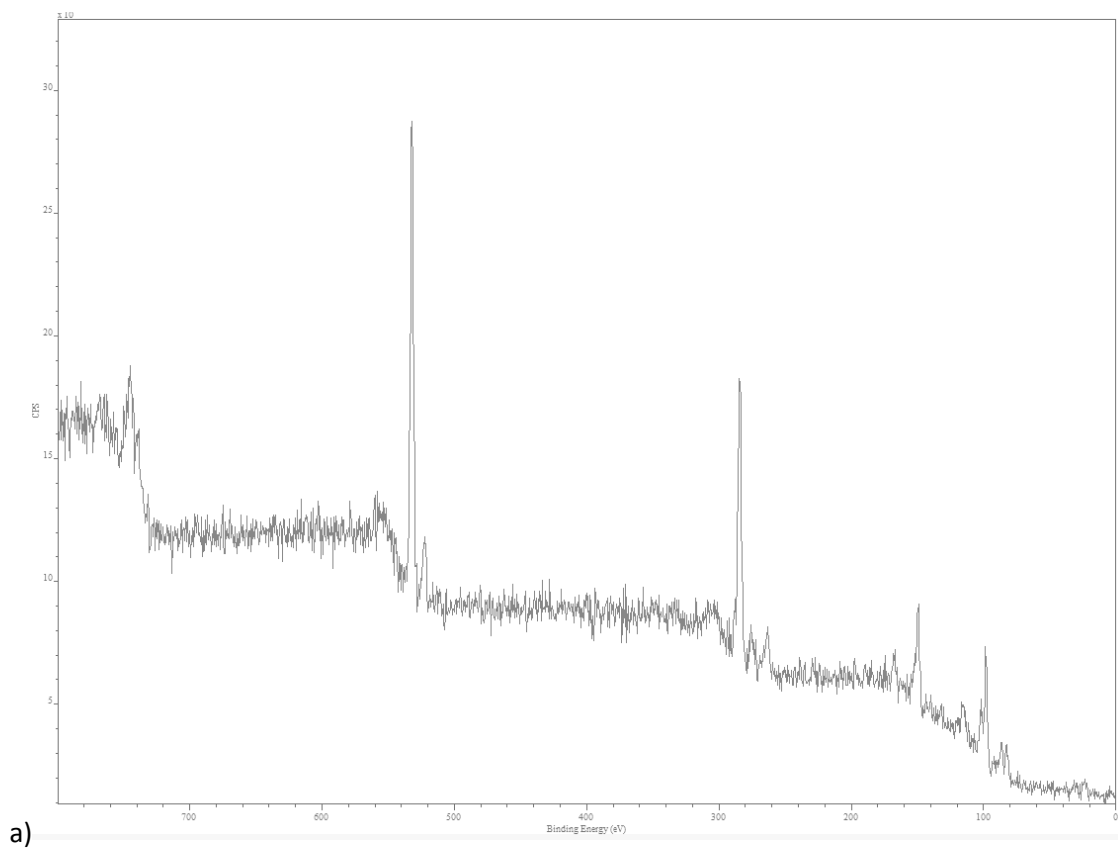
a)



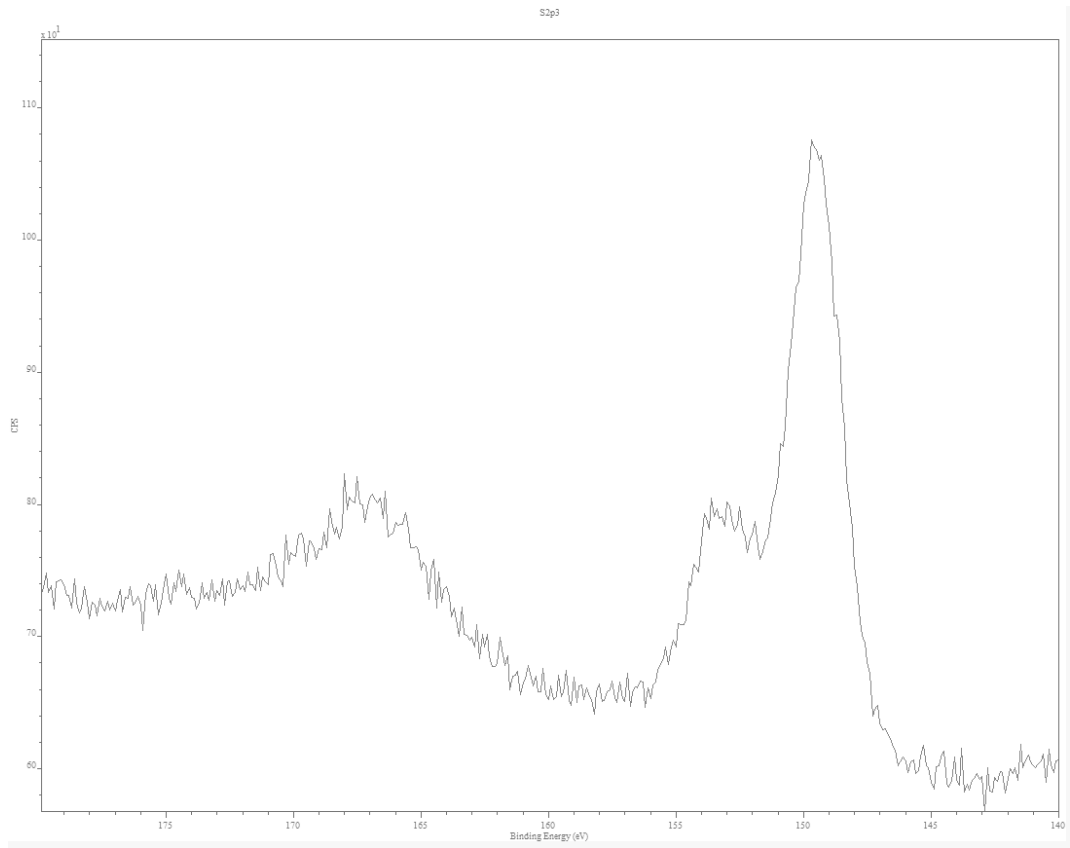


d)

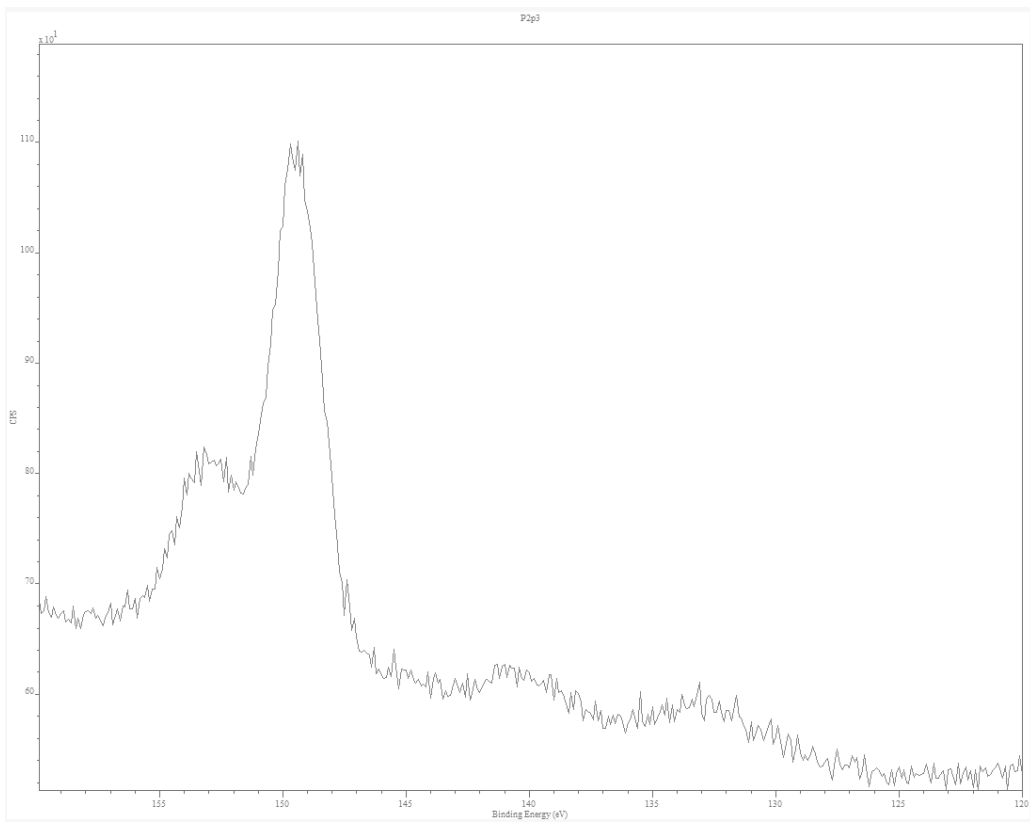
Figure A.3 : XPS analysis of the citrate -TFO-AuNPs. a) broad spectrum of the AuNPs, b) S2p, c) P2p, d) Au4f



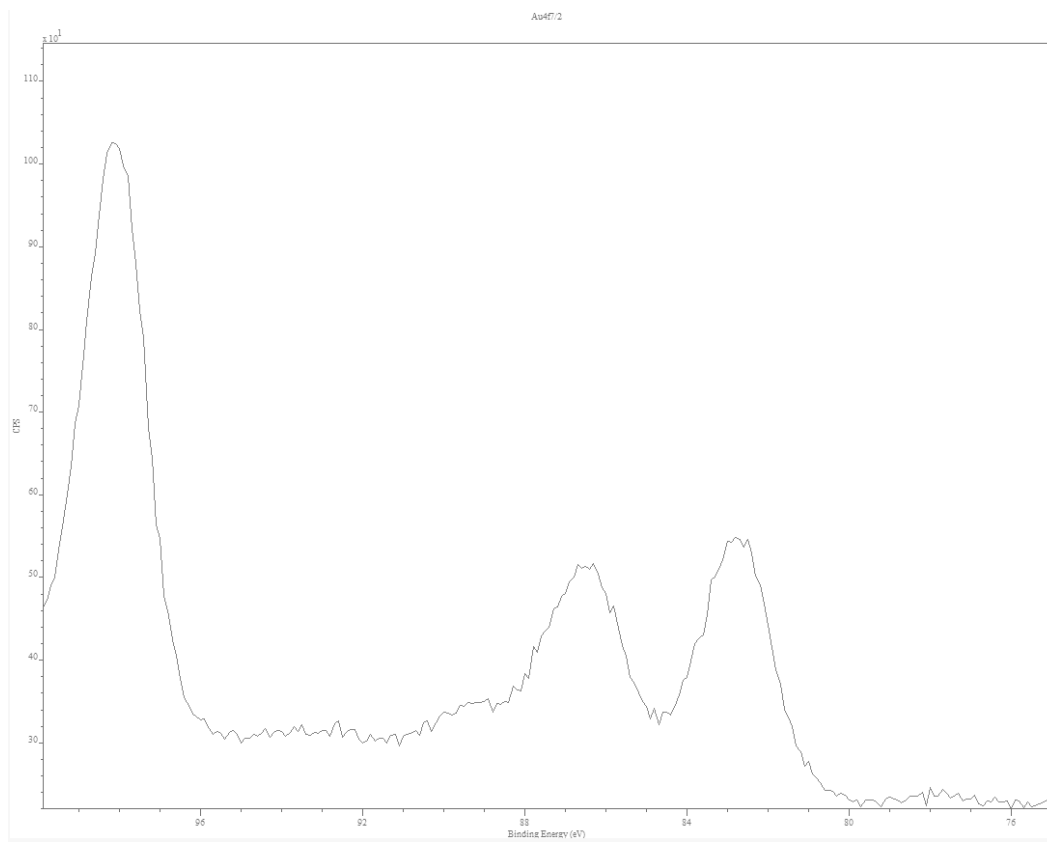
a)



b)



c)



d)

Figure A.4 : XPS analysis of the PN-TFO- AuNPs. a) broad spectrum of the AuNPs, b) S2p, c) P2p, d) Au4f

3.5. Statistical differences in dose responses for the different oligo coated AuNPs exposure on cells analysed by two way Anova followed by a Dunnett's multiple comparisons test.

3.5.1. HSC-3 cells

Dunnett's multiple comparisons test	Mean Diff.	95% CI of diff.	Summary
citrate AuNPs			
0 vs. 1.0	5.498	-21.86 to 32.85	ns
0 vs. 3.0	18.87	-8.481 to 46.23	ns
0 vs. 10.0	50.68	17.18 to 84.19	**
PN AuNPs			
0 vs. 1.0	-7.543	-34.90 to 19.81	ns
0 vs. 3.0	5.118	-22.24 to 32.47	ns
0 vs. 10.0	45.38	11.88 to 78.89	**
citrate DY3 AuNPs			
0 vs. 1.0	27.31	-0.04791 to 54.66	ns
0 vs. 3.0	42.37	15.01 to 69.72	**
0 vs. 10.0	56.55	23.05 to 90.05	***
citrate PR AuNPs			
0 vs. 1.0	-3.225	-30.58 to 24.13	ns
0 vs. 3.0	21.97	-5.389 to 49.32	ns
0 vs. 10.0	40.00	6.498 to 73.50	*
PN-DY3 AuNPs			
0 vs. 1.0	20.77	-6.587 to 48.12	ns
0 vs. 3.0	26.30	-1.054 to 53.66	ns
0 vs. 10.0	56.73	23.23 to 90.23	***
PN-PR AuNPs			
0 vs. 1.0	20.48	-6.871 to 47.84	ns
0 vs. 3.0	40.98	13.62 to 68.33	**
0 vs. 10.0	51.46	17.95 to 84.96	**

3.5.2. HaCaT cells

Dunnett's multiple comparisons test	Mean Diff.	95% CI of diff.	Summary
BBi			
0 vs. 1.0	-12.33	-32.70 to 8.031	ns
0 vs. 3.0	-0.9471	-21.31 to 19.42	ns
0 vs. 10.0	-5.433	-25.80 to 14.93	ns
PN			
0 vs. 1.0	-3.366	-23.73 to 17.00	ns
0 vs. 3.0	3.691	-16.67 to 24.06	ns
0 vs. 10.0	-0.6745	-21.04 to 19.69	ns
BBi DY3			
0 vs. 1.0	7.520	-12.85 to 27.89	ns
0 vs. 3.0	11.74	-8.622 to 32.11	ns
0.1 vs. 10.0	11.22	-9.140 to 31.59	ns
BBi PR			
0 vs. 1.0	8.542	-11.82 to 28.91	ns
0 vs. 3.0	9.063	-11.30 to 29.43	ns
0 vs. 10.0	12.50	-7.865 to 32.87	ns
PN DY3			
0 vs. 1.0	11.89	-8.473 to 32.26	ns
0 vs. 3.0	6.667	-13.70 to 27.03	ns
0 vs. 10.0	18.45	-1.914 to 38.82	ns
PN PR			
0 vs. 1.0	19.83	-0.5306 to 40.20	ns
0 vs. 3.0	25.04	4.676 to 45.41	*
0 vs. 10.0	21.45	1.081 to 41.81	*

3.6. Oligonucleotide coated AuNPs and cellular uptake using TEM

NP/nm ²	Cytoplasm (*10 ⁻⁵)		Nucleus (*10 ⁻⁵)		Surface (*10 ⁻⁵)	
	HSC-3	HaCaT	HSC-3	HaCaT	HSC-3	HaCaT
Citrate AuNPs	14.2 ± 2.17 N=61	11.7 ± 1.0 N=33	0.49 ± 0.07 N=61	0.075 ± 0.04 N=33	1.24 ± 0.23 N=61	0.67 ± 0.10 N=33
PN AuNPs	6.2 ± 2 N=27	3.6 ± 1.0 N=31	0.17 ± 0.10 N=27	0.18 ± 0.07 N=31	0.49 ± 1.03 N=27	2.78 ± 1.00 N=31
Citrate DY3 AuNPs	20.1 ± 3.06 N=52	10.7 ± 2.49 N=34	0.87 ± 0.11 N=52	0.76 ± 0.22 N=34	10.0 ± 0.23 N=52	6.22 ± 1.8 N=34
Citrate PR AuNPs	20.0 ± 2.6 N=32	1.60 ± 0.30 N=34	0.76 ± 0.14 N=32	0.11 ± 0.06 N=34	1.6 ± 0.56 N=32	1.07 ± 0.3 N=34
Citrate GFP AuNPs	11.7 ± 2.31 N=33	4.56 ± 1.00 N=20	1.31 ± 0.64 N=33	0.63 ± 0.19 N=20	0.68 ± 0.21 N=33	3.4 ± 1.0 N=20

PN DY3 AuNPs	18.99 ± 3.4 N=48	3.56 ± 1.00 N=47	0.45 ± 0.088 N=48	0.27 ± 0.07 N=47	1.18 ± 0.57 N=48	3.81 ± 1.00 N=47
PN PR AuNPs	14.15 ± 1.81 N=47	9.02 ± 2.05 N=37	0.59 ± 0.11 N=47	0.25 ± 0.09 N=37	2.22 ± 0.79 N=47	3.50 ± 0.71 N=37
PN GFP AuNPs	9.60 ± 1.0 N=54	2.22 ± 0.31 N=54	0.13 ± 0.05 N=54	0.18 ± 0.05 N=54	4.66 ± 1.0 N=54	2.83 ± 1.00 N=54

3.7. Relaxed plasmid irradiated with or without the different AuNPs

lane	Samples	Band 1	Band 2 (relaxed plasmid)	Band 3	Band 4 (linear plasmid)
1	PI	144	14037	115	6718
2	PI irr	1629	11234	463	5276
3	PI citrate AuNPs irr	348	13078	143	5561
4	PI DY3 AuNPs irr	320	13363	97	5582
5	PI PR AuNPs irr	355	12229	117	5542
6	PI GFP AuNPs irr	429	12279	72	5218

3.8. Relaxed plasmid irradiated with or without the different AuNPs and PCR amplicon of the sequence of interest

line	Samples	Band 1	Band 2	Band 3	Band 4	Band 5
1	PI	49	1155	0	530	0
2	PI PCR	160	1189	77	0	13167
3	PI irr PCR	188	771	34	0	14607
4	PI citrate AuNPs irr PCR	0	1108	92	99	0
5	PI DY3 AuNPs irr PCR	32	1066	95	146	0
6	PI PR AuNPs irr PCR	27	1043	94	97	72
7	PI GFP AuNPs irr PCR	6	1023	74	70	0